

*Appropriately Complex Biomechanical
Modelling of Distance Running*

Niamh Gill

A thesis submitted for the degree of Doctor of Philosophy

University of Salford

School of Health Sciences

[2017]

Contents

Table of Figures.....	vii
Table of Tables	xxii
Acknowledgments	xxviii
Abbreviations	xxix
Abstract.....	xxx
1. General Introduction	1
1.1. Running.....	1
1.1.1. Running as a leisure activity.....	1
1.1.2. The biomechanics of running – what we know	2
1.1.3. The biomechanics of running – what we don’t know	12
1.2. Computer Modelling and Simulation	13
1.2.1. Modelling – what is it?	13
1.2.2. The importance of validating models	14
1.3. Chapter Summary	15
2. Literature Review.....	18
2.1. The Simplest Model of Running.....	18
2.2. Using the Spring Mass Model to Study Running	20
2.2.1. Stiffness as a parameter to describe running	21
2.2.2. Stiffness and its relationship to other running parameters	23
2.3. Accuracy of the Spring Mass Model	24
2.4. Limitations of the Spring Mass Model	29
2.5. Modifications to the Spring Mass Model	29
2.5.1. Variable stiffness	29
2.5.2. Spring-Mass-Damper models	31
2.5.3. Moving centre of pressure	35

2.5.4.	Bipedal models	37
2.5.5.	Limitations of the modified models.....	39
2.6.	Questions Still Unanswered by the Modified Models	40
2.7.	Complex Models of Running.....	40
2.7.1.	Components of complex models	41
2.7.2.	Complex model analysis and simulation	42
2.7.3.	Complex models of running	45
2.7.4.	Limitations of complex models	48
2.8.	Questions Still Unanswered By Complex Models	49
2.9.	Aims and Research Questions	50
3.	Experimental Data.....	52
3.1.	Participants.....	52
3.2.	Data Collection	52
3.3.	Data Processing.....	53
4.	A Simple Model of Running: Force-Length Relationships and Foot Strike Patterns..	56
4.1.	Introduction.....	56
4.1.1.	The spring mass model	56
4.1.2.	Force-length relationships	58
4.1.3.	Definition of foot strike pattern	63
4.1.4.	Aims	66
4.2.	Methods	67
4.2.1.	Experimental data	67
4.2.2.	Foot strike patterns	67
4.2.3.	Force-length relationships	69
4.2.4.	Quantifying the linearity of the force-length curve	71
4.2.5.	Hysteresis	73
4.2.6.	Statistics.....	75

4.3.	Results.....	76
4.3.1.	Force-length relationships	76
4.3.2.	Quantifying the linearity of the force-length curve.....	77
4.3.3.	Hysteresis	79
4.4.	Discussion.....	81
5.	A Critical Analysis of Methods for Calculating Lower Limb Stiffness	92
5.1.	Introduction.....	92
5.1.1.	Stiffness of the human body	92
5.1.2.	Lower limb stiffness	93
5.1.3.	Vertical stiffness	97
5.1.4.	Aims	98
5.2.	Methods	99
5.2.1.	Experimental data.....	99
5.2.2.	Lower-limb length definitions	100
5.2.3.	Lower limb stiffness calculation	101
5.2.4.	Vertical stiffness calculation and comparison.....	103
5.2.5.	Statistics.....	103
5.3.	Results.....	104
5.3.1.	Lower limb length definitions	104
5.3.2.	Lower limb stiffness calculations.....	107
5.3.3.	Lower limb stiffness vs. Vertical stiffness	112
5.4.	Discussion.....	114
6.	Common modelling methods	120
6.1.	Experimental data	120
6.2.	Model parameters	120
6.3.	OpenSim	122
6.4.	Model set up and simulation.....	123

6.5.	Joint angles	124
7.	The Simple Spring Mass Model.....	127
7.1.	Introduction.....	127
	Aims	129
7.2.	Methods	129
7.2.1.	The model.....	129
7.2.2.	OpenSim implementation.....	130
7.2.3.	Model simulation.....	131
7.2.4.	Compare solutions and statistics	131
7.3.	Results.....	132
7.3.1.	Initial conditions vs. Experimental data	132
7.3.2.	CoM trajectories	133
7.3.3.	GRFs.....	135
7.3.4.	Contact time difference	138
7.3.5.	Stiffness values	139
7.4.	Discussion.....	139
8.	... adding a knee joint	146
8.1.	Introduction.....	146
	Aims	151
8.2.	Methods	152
8.2.1.	The Model	152
8.2.2.	Joint angle calculations.....	154
8.2.3.	Initial conditions, optimisation and simulation	156
8.2.4.	Ground reaction force calculations.....	158
8.2.5.	Comparing solutions & Statistics	159
8.3.	Results.....	160
8.3.1.	CoM trajectory curves	160

8.3.2.	Maximum vertical displacement	162
8.3.3.	GRF curves	162
8.3.4.	Hip joint angles.....	166
8.3.5.	Knee kinematics	167
8.3.6.	Initial conditions vs. Experimental data	169
8.3.7.	Linear stiffness vs. experimental limb stiffness	171
8.3.8.	Knee joint stiffness / joint torques.....	171
8.4.	Discussion.....	172
9.	... adding an ankle joint	179
9.1.	Introduction.....	179
	Aims	185
9.2.	Methods	186
9.2.1.	The Model	186
9.2.2.	Joint angle calculations.....	188
9.2.3.	Initial conditions, optimisation and simulation	190
9.2.4.	Ground reaction force calculations.....	192
9.2.5.	Comparing solutions & Statistics	194
9.3.	Results.....	195
9.3.1.	CoM trajectory curves	196
9.3.2.	Maximum vertical displacement	197
9.3.3.	GRF curves	198
9.3.4.	Hip joint angles.....	203
9.3.5.	Knee kinematics	204
9.3.6.	Ankle kinematics	206
9.3.7.	Initial conditions vs. Experimental data	209
9.3.8.	Joint stiffness / joint torques.....	211
9.4.	Discussion.....	213

10.	General Discussion	220
10.1.	Introduction	220
10.2.	Research Question 1	222
10.3.	Research Question 2	222
10.4.	Research Question 3	223
10.5.	General Limitations	226
10.6.	A note on OpenSim	228
10.7.	Future Work	229
10.8.	Conclusions	230
	Appendices	231
AI.	OpenSim Validation	231
AII.	Extra Figures	238
AIII.	Different lower limb length definitions in rearfoot strikers	242
AIV.	Are The Arms and Head Required To Accurately Estimate Centre Of Mass Motion During Running?	243
	Abstract	243
	Introduction	244
	Methods	244
	Results	245
	Discussion	247
	Conflict of Interest	248
	References	248
	References	251

Table of Figures

Figure 1 - Running gait cycle (Adelaar 1986) showing the alternating (right side) stance and swing phases.	3
Figure 2 - CoM mechanical energy fluctuations (J/kg) as a function of the gait cycle (%) (Kehler et al. 2014). Kinetic energy (KE), gravitational potential energy (GPE) and the total mechanical energy (TE) are normalised to body mass. The dotted vertical lines represent the start of the different phases of the gait cycle, i.e. touch down and take off.....	4
Figure 3 – The three planes of movement include the transverse, frontal and sagittal planes. The sagittal plane is perpendicular to the ground and divides the body into left and right. The frontal plane is also perpendicular to the ground, but divides the body into dorsal and ventral portions. Finally, the transverse plane is parallel to the ground and divides the body into superior and inferior portions.	5
Figure 4 – Hip (a-c), knee (d-f), and ankle (g-i) kinematics during overground running at 3.9 m/s. Data is plotted from right initial contact, and the three vertical lines indicate right toe off, left initial contact and left toe off, respectively.	6
Figure 5 - Pelvis movement during running (Preece et al. 2016), where the dashed vertical lines represent right toe off, left initial contact and left toe off, respectively.....	7
Figure 6 - Vertical GRFs for rearfoot and forefoot strikers, highlighting a key difference between the two strike patterns, where the impact peak characteristic of rearfoot strike patterns is generally not seen in forefoot strikers (Lieberman et al. 2010).	9
Figure 7 – Approximate CoP trajectories for rearfoot, midfoot and forefoot strikers (left to right respectively). Rearfoot strikers tend to land on the posterior-lateral edge of the foot and the CoP travels distally to the medial edge of the first metatarsal head. On the other hand, midfoot and forefoot strikers tend to land more distally, with the CoP initially travelling proximally as the heel lowers before moving distally towards the medial edge of the first metatarsal head.....	10
Figure 8 – Individual muscle contributions to the hip, knee and ankle moments during the stance phase of running (Dorn et al. 2012). Shaded region represents the net sagittal plane joint moment, normalised to body mass, with a positive moment indicating hip extension,	

knee flexion and ankle plantar flexion. cFO, contralateral foot-off; cFS, contralateral foot strike; iFO, ipsilateral foot-off; iFS, ipsilateral foot strike. ILPSO, combined iliacus and psoas; GMAX, superior, middle and inferior gluteus maximus; HAMS, combined biceps femoris long head, semimembranosus and semitendinosus; RF, rectus femoris; VAS, combined vastus medialis, vastus intermedius and vastus lateralis; GAS, combined medial and lateral compartments of gastrocnemius; SOL, soleus; TIBANT, tibialis anterior. 12

Figure 9 - Simple spring mass model, where m represents the entire mass of the system, β represents the angle of the landing velocity, v the absolute value of the landing velocity and α the angle of attack of the spring (Blickhan 1989)..... 18

Figure 10 - Example force-length curve for the stance phase of running. Initial contact is indicated by the triangle at 0 m compression, and arrows indicate the direction of loading. Maximum compression is at approximately midstance (black circle), and the spring extension towards the end of stance occurs as the CoM prepares for flight. 22

Figure 11 – Example of the influence of the lower limb length definition when considering different foot strike patterns. 27

Figure 12 - Example of different GRF profiles depending on running strike pattern (Watkins 2014). Note the existence of the characteristic impact peak in the heel-striker that is not evident in the forefoot striker..... 30

Figure 13 - Modified two-body spring mass model used by Derrick et al. (2000) to simulate the vertical ground reaction forces during human running. M_1 and M_2 are the point masses, P_1 and P_2 the vertical positions, and K_1 and K_2 the spring stiffness of the upper and lower elements, respectively, while C is the damping constant. 32

Figure 14 -Three body model used by Kim et al. (1994) to investigate the vertical impact vibrations during running. M represents the mass, k the spring stiffness, c the damping constant and x the vertical positions of the different elements..... 32

Figure 15 - LN model used by Nigg et al. (1999) to simulate the impact dynamics of heel-toe running. This model consisted of four masses, m_{1-4} , five springs, k_{1-5} , and four dampers, c_{1-4} , with x_{1-4} representing the vertical positions of each of the masses, as well as a separate spring-damper ground reaction model..... 33

Figure 16 - Five-body modified spring mass model used by Ly et al. (2010). Springs ($k_{3,5}$), spring–damper units ($k_{2,4,6}, c_{2,4,6}$) connected rigid masses ($m_{1,3}$) and wobbling mass ($m_{2,4}$). Spring–damper unit (k_6, b_6, c_6) connected the lowest rigid mass (m_1) to the shoe rigid mass (m_5) and finally spring (k_s) represents the ground stiffness.34

Figure 17 - Example of CoP movement in rearfoot (left), midfoot (middle) and forefoot (right) strikers.35

Figure 18 - Spring mass model with and without foot translation (Bullimore et al. 2006). Circles represent the point mass and lines the spring. Peak vertical ground reaction force, F , initial spring length, l_0 , contact length, x_c , peak vertical CoM displacement during stance phase, Δy , magnitude of landing and take-off angles, θ_0/ϕ_0 , and the distance of point of force translation, d36

Figure 19 - Passive bipedal running model designed by McGeer (1990). The limbs have arbitrary mass, m_{leg} , and compress telescopically via linear springs, k_{leg} . The point mass at the hip, m_T , approximates the torso, and the torsional spring at the hip, k_{hip} , allows the limbs to swing back and forth. The feet are modelled using massless rigid semicircles, and γ indicates the incline of the surface.38

Figure 20 - Bi-pedal model with compliant limbs used by (Iida et al. 2008) to study the influence of bi-articular muscles during walking and running. The model is comprised of three limb segments connected via hinge joints, and an actuator at the hip. Tension springs are attached across the joints and two ground contact points are located on the foot segment.39

Figure 21 - Schematic diagram of a musculotendon actuator (Pandy 2001). *CE* represents the contractile element, *SEE* the series elastic element and *PEE* the parallel elastic element.42

Figure 22 - Overview of IDA and static optimisation (D. Gordon E. Robertson et al. 2013).43

Figure 23 - Overview of FDA and dynamic optimisation (D. Gordon E. Robertson et al. 2013).44

Figure 24 - Full body musculoskeletal model of running developed by Hamner et al. (2010) to study the muscle contributions to propulsion and support. Muscles coloured in red indicate they are fully activated, while those in blue indicate they are fully deactivated. Forward acceleration of the CoM signifies propulsion, backward acceleration braking, and upward acceleration support.47

Figure 25 – Anatomical marker positions and QTM static trail showing the marker positions.....54

Figure 26 - Simple spring mass model at four phases of the gait cycle: 1) initial contact, 2) midstance, 3) take-off and 4) aerial phase (since a ballistic trajectory is assumed the spring will have no influence during this phase). The initial spring length is denoted by l_0 , approach angle by θ_0 , spring stiffness by k , mass by m56

Figure 27 - Simulations using the spring mass model (Blickhan 1989); x_c and x_a indicate the contact length and hopping distance, t_c and t_a the contact and hopping times, y_{cc} the spring compression at midstance (not equivalent to the total vertical displacement, y_D , which is the sum of the stance phase vertical displacement, y_c , and the hopping phase vertical displacement, y_a) and F_y and F_x the peak vertical and horizontal forces, respectively.....57

Figure 28 - Example force-length relationships. Here the length change is in relative to the resting length of the system, l_0 , and the relative tension is related to the proof load of the system. The proof load of the system represents the greatest load that can be applied before stretching the system beyond its elastic limit.60

Figure 29 - Example hysteresis loop. Hysteresis determines the amount of elastic potential energy lost during each step, assuming no losses during the aerial phase.62

Figure 30 - Foot strike index (SI) calculation (Altman et al. 2012). The SI represents the location of the CoP, at initial contact, as a percentage of the foot length, along the longitudinal axis of the foot coordinate system (A).63

Figure 31 - Example of CoP movement in rearfoot (left), midfoot (middle) and forefoot (right) strikers.65

Figure 32 - Typical vertical GRF profiles from rearfoot (top) and forefoot (bottom) strikers running at 3.5 m/s. Characteristic impact peak and high loading rate associated with rearfoot striking are evident in the rearfoot strike profile, but not in the forefoot strike profile. (Lieberman et al. 2010).....66

Figure 33 – Scatter plot showing the distribution of the foot strike index among (n=28) participants. The black, red, green, and blue markers represent speeds 1 – 4, respectively. The dotted vertical lines show the participants who transitioned from a rearfoot strike pattern at the slower speeds to a forefoot strike pattern at faster speeds.....68

Figure 34 - Definition of the lower limb length.70

Figure 35 – Lower limb force, F_{limb} , determined by projecting the resultant GRF onto the lower limb axis, where θ_d represents the difference between the resultant angle, θ_{GRF} , and the approach angle, θ_071

Figure 36 - Typical force-length curve of a linear spring. The slope of the line can then be used to determine the stiffness of the spring.72

Figure 37 – Example loading (red dots) and unloading (blue dots) force-length data, and the “perfectly elastic line” (solid black line). The “perfectly elastic line” was defined as the straight line between the force-length values at initial contact (IC) and midstance (MS – the point of maximum compression). FF indicates foot flat, EP the endpoint for calculating the RMSr, and toe off is indicated by TO.....73

Figure 38 - Example of the area under the loading and unloading portions of the force length curve.74

Figure 39 - Example of the hysteresis loop calculated for each participant's force-length curve.74

Figure 40 – Mean (solid black line) and standard deviation (grey shaded area) force-length relationships from all participants, separated into the different foot strike groups. Initial contact is indicated by the triangle, while toe off is indicated by the square. Rows (top to bottom) correspond to speeds 1 – 4, respectively.....76

Figure 41 – RMSr [BW] against foot strike index for the loading phase of stance. Grey area indicates the foot strike indexes that were excluded from the analysis.78

Figure 42 – RMSr [BW] against foot strike index for the unloading phase of stance. Grey area indicates the foot strike indexes that were excluded from the analysis.79

Figure 43 – Hysteresis against foot strike index. Grey area indicates the foot strike indexes that were excluded from the analysis.80

Figure 44 – Mean (solid black line) and standard deviation (grey shaded region) force-length curves of forefoot (top) rearfoot (bottom) strikers at the slowest (left: 3.3 m/s) and fastest (right: 5.6 m/s) speeds. The loading and unloading phases of forefoot running are shown in the top plots, whereas three phases of stance apparent during rearfoot running are indicated on the bottom plots.....82

Figure 45 – Values for the energy cost of running collected from previous literature. Black (Mayhew 1977), blue (Williams et al. 1987), red (Svedenhag et al. 1984), green (Svedenhag et al. 1994), magenta (Jones et al. 1996), cyan (Kyrolainen et al. 2001) and yellow (Shaw et al. 2014) dots represent values determine from previously published papers.....87

Figure 46 - Pictorial representation of force and displacement used to calculate stiffness. 93

Figure 47 – Mean force-length curves produced from the different definitions of lower limb length. The definitions are as follows: black - hip to ball of foot at midstance; red - hip to ball of foot at initial contact; blue - hip to average CoP..... 106

Figure 48 - Example of the relationships between the PC method and the other methods of calculating lower limb stiffness at speed 2 (3.9 m/s), n = 12. 110

Figure 49 - Comparison of lower limb stiffness values calculated using the PC method versus method 1; n = 11, 12, 13 and 19 at speeds 1 – 4, respectively. 110

Figure 50 - Bland-Altman plot comparing methods of calculating lower limb stiffness at speed 3. The upper and lower dashed lines represent the 95% confidence interval, while the middle solid lines represent the mean difference between the values produce using the two methods being compared. 111

Figure 51 – Mean and standard deviation (n=11, 12, 13 and 19 at speeds 1 – 4, respectively) of lower limb stiffness and vertical stiffness as a function of speed. 112

Figure 52 – Lower limb stiffness vs. vertical stiffness at each speed. n=11, 12, 13 and 19 at speeds 1 – 4, respectively, and speeds 1 – 4 correspond to 3.3, 3.9, 4.8 and 5.6 m/s, respectively..... 113

Figure 53- Pictorial representation of the forces used to calculate stiffness. The solid line represents the experimental vertical GRF, while the dotted line represents the GRFs projected onto the limb axis. 117

Figure 54 - Pictorial representation of the displacements used to calculate stiffness. The solid line represents the experimental CoM being modelled by the spring mass model, while the dashed line represents the trajectory of an inverted pendulum of length l_0 , the resting length of the spring. 118

Figure 55 – Lower limb force from GRF, where θ_a represents the difference between the resultant angle, θ_{GRF} , of the GRFs, GRF_x & GRF_z , and the approach angle, θ_0 . The lower limb force, F_{limb} , is then determined by projecting the resultant GRF onto the lower limb axis..... 121

Figure 56 - Example experimental segment length changes during the stance phase of running..... 125

Figure 57 - Experimental joint angles. 125

Figure 58 - Spring mass model implemented in OpenSim; here x and y indicate the horizontal and vertical distances between the fixed contact point and the point mass, θ_0 the approach angle and v_l and v_θ the compression and rotational velocities. 130

Figure 59 - CoM movement from experiment (black) and spring mass model simulation (blue) from n = 11, 12, 13 and 19 forefoot strikers running at speed 1 – 4 (3.3, 3.9, 4.8, 5.6 m/s), respectively..... 134

Figure 60 - AP GRFs from experiment (black) and spring mass model simulation (blue) from n = 11, 12, 13 and 19 forefoot strikers running at speed 1 – 4 (3.3, 3.9, 4.8, 5.6 m/s), respectively..... 136

Figure 61 - Vertical GRFs from experiment (black) and spring mass model simulation (blue) from n = 11, 12, 13 and 19 forefoot strikers running at speed 1 – 4 (3.3, 3.9, 4.8, 5.6 m/s), respectively..... 136

Figure 62 - Comparison of CoM trajectories presented here (top: mean(SD) for running at 3.9 m/s, blue = simulation, black = experimental) and previous studies assessing the ability of the spring mass model (bottom: Lipfert et al. (2012) for running at 4 m/s, black = simulation, grey = experimental)..... 141

Figure 63 - Comparison of vertical GRFs presented here (top: mean(SD) for running at 3.9 m/s, blue = simulation, black = experimental) and previous studies assessing the ability of the spring mass model (middle: Bullimore et al. (2007) for running at 3 m/s and bottom: Lipfert et al. (2012) for running at 4 m/s; black = simulation, grey = experimental). 142

Figure 64 - Comparison of the simulated CoM trajectories, using the experimental value for stiffness ($k = \text{expVal}$) versus the optimised value ($k = \text{optimVal}$), of a single subject at a speed 2 (3.9 m/s)..... 144

Figure 65 – Knee joint angles during treadmill running at 2.5 m/s (solid blue), 3.5 m/s (dashed red), and 4.5 m/s (dot-dash black) (Fukuchi et al. 2017). Positive degree changes imply flexion, adduction and internal rotation. The dashed vertical line indicates the braking and propulsive phases of stance, while the solid vertical line indicates toe-off... 147

Figure 66 - Stance phase sagittal plane knee moment (Kulmala et al. 2013)..... 148

Figure 67 – Left: Spring mass model and the two-segment model developed by Rummel et al. (2008); Right: two-segment model developed by Phan et al. (2017). 150

Figure 68 - OpenSim SK models (left *SKlinear* and right: *SKtorsional*). Segment lengths, l , were determined from subject-specific anatomical data. The point mass account for the combined weight of the head, arms, trunk and swing leg ($m_{\text{pm}} = 0.845 \cdot \text{total body mass}$). The model segment masses, m , and moments of inertia, I , were approximated used data from Dempster (1955). The model “thigh” segment approximated the anatomical thigh ($m_{\text{thigh}} = 0.096 \cdot \text{total body mass}$; $I_{\text{thigh}} = m_{\text{thigh}} \cdot (0.323 \cdot l_{\text{thigh}})^2$). Finally, the model “shank” segment represented the combined anatomical shank and foot ($m_{\text{shank}} = 0.059 \cdot \text{total body}$

mass; $I_{\text{shank}} = m_{\text{shank}} * (0.303 * l_{\text{shank}})^2$), and its length was estimated as the mean distance from the knee joint to the average CoP.	153
Figure 69 - Example changes in the experimental segment lengths (red: thigh, green: shank, and blue: foot) versus model segment lengths (red: thigh and purple: shank and foot) during the stance phase of running.	154
Figure 70 - OpenSim SK model configuration.....	155
Figure 71 - Example of the spring force in the <i>SKlinear</i> model (top) spring torque in the <i>SKtorsional</i> model (bottom). The red circle denotes the minimum of the spring force/torque, while the blue circle denotes the point where the knee angle passes 0 °.	157
Figure 72 - Force diagram of the SK model.....	158
Figure 73 – Simulated CoM trajectories of the <i>SKlinear</i> (blue dashed) and <i>SKtorsional</i> (red dashed) compared to the experimental CoM trajectory (black solid) for the participant with the lowest RMSD at speed 1 [3.3 m/s] (left) and the participant with the highest RMSD speed 4 [5.6 m/s] (right).	161
Figure 74 - Experimental (black solid) and simulated (<i>SKlinear</i> : blue dashed; <i>SKtorsional</i> : red dashed) GRF profiles from the participant with the lowest RMSD at speed 1 [3.3 m/s] (top) and the participant with the highest RMSD at speed 4 [5.6 m/s] (bottom).	163
Figure 75 – Experimental (black solid) and simulated (<i>SKlinear</i> : blue dashed; <i>SKtorsional</i> : red dashed) hip joint angle profiles from the participant with the lowest RMSD at speed 1 [3.3 m/s].....	166
Figure 76 – Experimental (black solid) and simulated (<i>SKlinear</i> : blue dashed; <i>SKtorsional</i> : red dashed) knee trajectories from the participant with the lowest RMSD at speed 1 [3.3 m/s].	167
Figure 77 - Experimental (black solid) and simulated (<i>SKlinear</i> : blue dashed; <i>SKtorsional</i> : red dashed) knee joint angles from the participant with the lowest RMSD at speed 1 [3.3 m/s].	169
Figure 78 - Mean and standard deviations of the experimental vs. optimised hip angular velocities [deg/s] used when simulating the SK models. The dark grey bar represents the	

experimental data, the blue the *SKlinear* model and the red the *SKtorsional* model. * indicates value is significantly different ($p \leq 0.013$) from the experimental value..... 170

Figure 79 - Mean and standard deviations of the experimental vs. optimised knee angular velocities [deg/s] used when simulating the SK models. The dark grey bar represents the experimental data, the blue the *SKlinear* model and the red the *SKtorsional* model..... 170

Figure 80 - Mean and standard deviations of experimental and optimised lower limb stiffness values [kN/m]. The dark grey bar represents the experimental data and the blue represents the *SKlinear* model.* - indicates optimised and experimental values are significantly different ($p \leq 0.013$) at that speed..... 171

Figure 81 - Mean and standard deviations of experimental and optimised knee joint stiffness values [Nm/rad]. The dark grey bar represents the experimental data and the red represents the *SKtorsional* model..... 172

Figure 82 - Example of the difference in the simulated CoM trajectories from the spring mass model (red dashed line), the *SKlinear* SK model (dotted green line), the *SKtorsional* model (dashed green line) and the experimental data (solid black line) for one subject at speed 1 [3.3 m/s]..... 174

Figure 83 – Horizontal and vertical CoM movement and GRFs from the spring mass model (red dashed line), the *SKlinear* SK model (dotted green line), the *SKtorsional* model (dashed green line) and the experimental data (solid black line) for one subject at speed 1 [3.3 m/s]..... 175

Figure 84 - Sagittal plane angle kinematics for habitual forefoot and rearfoot strikers running at 4 m/s (Kulmala et al. 2013)..... 180

Figure 85 - Ankle kinematics during running (with a rearfoot strike pattern) (Preece et al. 2016). Positive degree changes imply dorsiflexion, inversion and external rotation. The gait cycle begins and ends with right foot initial contact and the vertical lines represent right foot toe off, left foot initial contact and left foot toe off, respectively..... 180

Figure 86 - Normalised sagittal plane ankle kinetics (internal joint moments) for habitual rearfoot and imposed forefoot strike patterns (Kuhman et al. 2016)..... 181

Figure 87 - Three-segment planar model used by Seyfarth et al. (2001). The configuration of the leg is defined by the ankle (ϕ_{12}) and knee (ϕ_{23}) angles and M_{01} , M_{12} and M_{23} represent the joint torques at the ball, ankle and knee joints, respectively..... 183

Figure 88 - Motor-damper-spring (MDS) model used by Qiao et al. (2017). The proximal mass incorporates the head, trunk, arms, and the lower limb in swing. The middle mass represents the thigh, and the lower mass the shank and foot. The segment resting lengths are $r_1 = l_{0,MDS}$, $r_2 = 67\%l_{0,MDS}$ ($67\% = \text{CoM}_{y,\text{upper leg}}/\text{CoM}_{y,\text{human body}}$), and $r_3 = 27\%l_{0,MDS}$ ($27\% = \text{CoM}_{y,\text{lower leg+foot}}/\text{CoM}_{y,\text{human body}}$). 184

Figure 89 - OpenSim SKA models (left *SKAconstraint*, middle: *SKAcontact* and right: *SKAactuator*). Segment lengths, l , were determined from subject-specific anatomical data, where the point mass account for the combined weight of the head, arms, trunk and swing leg ($m_{\text{point mass}} = 0.845 \cdot \text{total body mass}$). The model segment masses, m , and moments of inertia, I , were approximated used data from Dempster (1955). The model “thigh” and “shank” segments approximated the anatomical thigh and shank ($m_{\text{thigh}} = 0.096 \cdot \text{total body mass}$; $I_{\text{thigh}} = m_{\text{thigh}} \cdot (0.323 \cdot l_{\text{thigh}})^2$ and $m_{\text{shank}} = 0.045 \cdot \text{total body mass}$; $I_{\text{shank}} = m_{\text{shank}} \cdot (0.302 \cdot l_{\text{shank}})^2$, respectively). The model “foot” segment represented the anatomical foot ($m_{\text{foot}} = 0.014 \cdot \text{total body mass}$; $I_{\text{foot}} = m_{\text{foot}} \cdot (0.475 \cdot l_{\text{foot}})^2$), and its length was estimated as the mean distance from the ankle joint to the average CoP..... 187

Figure 90 - Example experimental segment length changes during the stance phase of running. The segments are defined as follows: red - thigh, green - shank, blue – modelled foot, purple – foot segment defined using the distal end of the Visual3D shank and the proximal end of the Visual3D foot, and orange – anatomical foot (defined as the distance between the proximal and distal ends of the Visual3D foot). The Visual3D foot segment was defined using the ankle malleoli and the first and fifth metatarsal markers (Mason et al.)..... 188

Figure 91 - OpenSim SKA model configuration..... 189

Figure 92 - Example of the control function used for the ankle actuator in the *SKAactuator* model for a single participant (who had the lowest RMSD between simulated and experimental CoM trajectories) at speed 1 [3.3 m/s]..... 192

Figure 93 - Force diagram of the SKA model..... 193

Figure 94 – Example of a failed simulation of the <i>SKAcontact</i> model	195
Figure 95 – Example of typical simulated CoM trajectories of the <i>SKAconstraint</i> (blue dashed), <i>SKAcontact</i> (red dashed) and <i>SKAactuator</i> (green dashed) compared to the experimental CoM trajectory (black solid) at speed 1 [3.3 m/s] (left) and speed 4 [5.6 m/s] (right).....	196
Figure 96 – Example of typical experimental (black solid) and simulated (<i>SKAconstraint</i> : blue dashed; <i>SKAcontact</i> : red dashed; <i>SKAactuator</i> : green dashed) GRF profiles at speed 1 [3.3 m/s] (top) and speed 4 [5.6 m/s] (bottom).....	199
Figure 97 – Example of typical experimental (black solid) and simulated (<i>SKAconstraint</i> : blue dashed; <i>SKAcontact</i> : red dashed; <i>SKAactuator</i> : green dashed) hip joint angle profiles at speed 1 [3.3 m/s].....	203
Figure 98 – Example of typical experimental (black solid) and simulated (<i>SKAconstraint</i> : blue dashed; <i>SKAcontact</i> : red dashed; <i>SKAactuator</i> : green dashed) knee trajectories at speed 1 [3.3 m/s].....	204
Figure 99 - Example of typical experimental (black solid) and simulated (<i>SKAconstraint</i> : blue dashed; <i>SKAcontact</i> : red dashed; <i>SKAactuator</i> : green dashed) knee joint angles at speed 1 [3.3 m/s].....	206
Figure 100 – Example of typical experimental (black solid) and simulated (<i>SKAconstraint</i> : blue dashed; <i>SKAcontact</i> : red dashed; <i>SKAactuator</i> : green dashed) ankle trajectories at speed 1 [3.3 m/s].....	207
Figure 101 - Example of typical experimental (black solid) and simulated (<i>SKAconstraint</i> : blue dashed; <i>SKAcontact</i> : red dashed; <i>SKAactuator</i> : green dashed) ankle joint angles at speed 1 [3.3 m/s].....	209
Figure 102 - Mean and standard deviations of the experimental vs. optimised hip angular velocities [deg/s] used when simulating the SKA models. The dark grey bar represents the experimental data, the blue the <i>SKAconstraint</i> model and the red the <i>SKAcontact</i> model.	210

Figure 103 - Mean and standard deviations of the experimental vs. optimised knee angular velocities [deg/s] used when simulating the SKA models. The dark grey bar represents the experimental data, the blue the *SKAconstraint* model and the red the *SKAcontact* model.
.....210

Figure 104 - Mean and standard deviations of the experimental vs. optimised ankle angular velocities [deg/s] used when simulating the SKA models. The dark grey bar represents the experimental data, the blue the *SKAconstraint* model and the red the *SKAcontact* model.
.....211

Figure 105 - Mean and standard deviations of experimental and optimised knee (top) and ankle (bottom) joint stiffness values [Nm/rad]. The dark grey bar represents the experimental data, the red the *SKAconstraint* model, and the red the *SKAcontact* model. All optimised stiffness values were significantly different from the experimental values.
.....212

Figure 106 - Example of the difference in the simulated CoM trajectories from the experiemntal data (solid black line), spring mass model (red dased line), *SKtorsional* model (dashed green line) *SKA constraint* model (dotted blue line), *SKAcontact* (dashed blue line) and *SKAactuator* model (dashed purple line) for one subject at speed 1 [3.3 m/s].
.....214

Figure 107 - Example of the difference in the simulated CoM trajectories from the experiemntal data (solid black line), spring mass model (red dased line), *SKtorsional* model (dashed green line) *SKA constraint* model (dotted blue line), *SKAcontact* (dashed blue line) and *SKAactuator* model (dashed purple line) for one subject at speed 1 [3.3 m/s].
.....216

Figure 108 - Failed simulation using the SKA models.224

Figure 109 – Comparison of ensemble averages (n = 11, 12, 13 and 19) of the OpenSim (red) and MATLAB (blue) CoM trajectories at speeds 1-4 [3.3, 3.9, 4.8, 5.6 m/s], respectively.....234

Figure 110 – Comparison of ensemble averages (n = 11, 12, 13 and 19) of the OpenSim (red) and MATLAB (blue) AP GRFs at speeds 1-4 [3.3, 3.9, 4.8, 5.6 m/s], respectively.	235
Figure 111 – Comparison of ensemble averages (n = 11, 12, 13 and 19) of the OpenSim (red) and MATLAB (blue) vertical GRFs at speeds 1-4 [3.3, 3.9, 4.8, 5.6 m/s], respectively.....	235
Figure 112 - Relationships between the PC method and the other methods of calculating lower limb stiffness at speed 1 (3.3 m/s).....	238
Figure 113 - Relationships between the PC method and the other methods of calculating lower limb stiffness at speed 2 (3.9 m/s).....	238
Figure 114 - Relationships between the PC method and the other methods of calculating lower limb stiffness at speed 3 (4.8 m/s).....	239
Figure 115 - Relationships between the PC method and the other methods of calculating lower limb stiffness at speed 4 (5.6 m/s).....	239
Figure 116 – Bland-Altman analysis comparing the PC method and the other methods of calculating lower limb stiffness at speed 1(3.3 m/s)	240
Figure 117 – Bland-Altman analysis comparing the PC method and the other methods of calculating lower limb stiffness at speed 2 (3.9 m/s)	240
Figure 118 – Bland-Altman analysis comparing the PC method and the other methods of calculating lower limb stiffness at speed 3 (4.8 m/s)	241
Figure 119 – Bland-Altman analysis comparing the PC method and the other methods of calculating lower limb stiffness at speed 4 (5.6 m/s)	241
Figure 120 - Ensemble averages of CoM position (top) and velocity (bottom) from the reduced model (dotted), reduced model including offset (dashed) and full-body model (solid) at speed 1. The grey outline represents the standard deviation of the full-body model, and therefore the variability in CoM motion across participants not the difference between the two models. Positive x represents forward movement, while positive y represents motion towards the contralateral side. Note, data is plotted from right initial	

contact (RIC) to the following RIC and for plotting purposes the CoM position data (AP and ML) were referenced to mean position of the full-body model.....246

Table of Tables

Table 1 – Level of agreement between model predictions and experimental data as found by Bullimore et al. (2007). Agreement was assessed using a percentage difference: $((\text{predicted value} - \text{measured value})/\text{measured value}) * 100$	25
Table 2 – List of the markers used for the experimental data collection, * indicates the marker was used for the static trial only.....	55
Table 3 - Definitions of terms (Parker 2003).	59
Table 4 - Proportion of forefoot and rearfoot strikers at each speed.	68
Table 5 – Mean (SD) RMSr [BW] values between experimental loading and unloading portions of the force-length curve and the “perfect elastic line”.....	77
Table 6 - Mean (SD) values of hysteresis [J/kg] from the experimental force-length curves.	80
Table 7 - Mean (SD) values of hysteresis [J/kg] from the experimental force-length curves (if 100 % of stance is considered).	85
Table 8 – “Running economy” in forefoot versus rearfoot strike patterns. Oxygen consumptions in represented by VO_2 and cost of transport by O_c	86
Table 9 - Estimated values for the energy cost of running at the four speeds considered here.	87
Table 10 - Estimates of the hysteresis per stride [J/kg/m].....	88
Table 11 - Contribution of hysteresis to the energy cost of running [%].	88
Table 12 – Different approaches to calculating lower limb stiffness. * Indicates most commonly used method.....	96
Table 13 – Different approaches for determining vertical stiffness. * Indicates most commonly used method.....	97

Table 14 – Mean (SD) RMSr [BW] values for the loading phase for the three different lower limb length definitions.....	105
Table 15 – Mean (SD) RMSr [BW] values for the unloading phase for the three different lower limb length definitions.....	105
Table 16 – Mean (SD) lower limb stiffness [kN/m] values for the three different lower limb length definitions.....	107
Table 17 - F-ratio and significance is the overall results from the repeated measure ANOVA, significance values for each method indicate the Bonferroni post-hoc significance values relating each method to the PC method.	108
Table 18 - Mean (SD) of lower limb stiffness values [kN/m], linear regression equation coefficients (m , b) and correlation coefficients (r) relating the PC method to methods 1-4. m refers to the slope and b to the offset (intercept).	109
Table 19 - Model properties.	121
Table 20 - Modelling terminology.....	122
Table 21 – Equations used for determining the experimental joint angles.	126
Table 22 – Mean (SD) of the initial conditions (position) from the experimental data versus when all the initial conditions and the stiffness were allowed to vary.....	133
Table 23 – Mean (SD) of the initial conditions (velocities) from the experimental data versus when all the initial conditions and the stiffness were allowed to vary.....	133
Table 24 - Mean (SD) of the RMSD [m] between the experimental and simulated CoM trajectories.	134
Table 25 - Maximum vertical CoM displacement [m]......	135
Table 26 – Mean (SD) RMSD [BW] between the experimental and simulated GRFs.	135
Table 27 – Mean (SD) AP GRF troughs [BW] and percentage differences (mean(SD)) from the experimental and simulated data.....	137

Table 28 – Mean (SD) AP GRF peaks [BW] and percentage differences (mean(SD)) from the experimental and simulated data	137
Table 29 – Mean (SD) Peak vertical GRF [BW] and percentage differences (mean(SD)) from the experimental and simulated data.....	137
Table 30 – Mean (SD) contact time [s] and percentage difference (mean(SD)) between experimental data (Exp.) and the best-fitting model simulations (Sim.).....	138
Table 31 – Mean (SD) Stiffness values [kN/m] and percentage difference (mean(SD)) between experimental data (Exp.) and the best-fitting model simulations (Sim.)	139
Table 32 - Equations for determining the SK model joint angles.	154
Table 33 - Equations for calculating the GRFs	159
Table 34 - Mean (SD) of the RMSD [m] between the simulated and experimental CoM trajectories.	161
Table 35 - Mean (SD) correlation coefficients between the simulated and experimental vertical CoM trajectories. * indicates correlations were significant for all participants ($p \leq 0.013$).....	161
Table 36 - Mean (SD) of the maximum vertical displacement [m] of the experimental data and simulations. No significant differences were found between the simulated and experimental values ($p \geq 0.121$).	162
Table 37 - Mean (SD) of the RMSD [BW] between the simulated and experimental anterior-posterior (AP) GRF profiles.	164
Table 38 - Mean (SD) of the RMSD [BW] between the simulated and experimental vertical GRF profile.....	164
Table 39 - Mean (SD) of the correlation coefficients between the simulated and experimental anterior-posterior (AP) GRF profile.	164
Table 40 - Mean (SD) of the correlation coefficients between the simulated and experimental vertical GRF profile. All correlations were significant ($p \leq 0.013$).	165

Table 41 - Mean (SD) of the trough/peak AP GRF values [BW] of the experimental data and simulations. * indicates the respective simulation value is significantly ($p \leq 0.013$) different from the experimental value.	165
Table 42 - Mean (SD) of the peak vertical GRF [BW] of the experimental data and simulations. * indicates the respective simulation value is significantly ($p \leq 0.013$) different from the experimental value.	166
Table 43 - Mean (SD) of the RMSD [deg] between the simulated and experimental hip joint angles.....	167
Table 44 – Mean (SD) RMSD [m] between the simulated and experimental knee trajectories.	168
Table 45 - Mean (SD) correlation coefficients between the simulated and experimental knee trajectories. All correlations were significant ($p \leq 0.013$).	168
Table 46 - Mean (SD) of the RMSD [deg] between the simulated and experimental knee joint angles.....	169
Table 47 - Equations for determining the SKA model joint angles.	189
Table 48 - Equations for calculating the GRFs	193
Table 49 - Number of failed solutions using the contact model.....	195
Table 50 - Mean (SD) of the RMSD [m] between the simulated and experimental CoM trajectories.	197
Table 51 - Mean (SD) correlation coefficients between the simulated and experimental vertical CoM trajectories. Correlations for all participants were significant ($p \leq 0.013$)..	197
Table 52 - Mean (SD) of the maximum vertical displacement [m] of the experimental data and simulations. * indicates a significant difference between the simulated and experimental values ($p \leq 0.013$).	198
Table 53 - Mean (SD) of the RMSD [BW] between the simulated and experimental anterior-posterior (AP) GRF profiles.	200

Table 54 - Mean (SD) of the RMSD [BW] between the simulated and experimental vertical GRF profile.....	200
Table 55 - Mean (SD) of the correlation coefficients between the simulated and experimental anterior-posterior (AP) GRF profile. * indicates the correlation was significant ($p \leq 0.013$).	201
Table 56 - Mean (SD) of the correlation coefficients between the simulated and experimental vertical GRF profile. * indicates the correlation was significant ($p \leq 0.013$).	201
Table 57 - Mean (SD) of the trough AP GRF force values [BW] of the experimental data and simulations.	202
Table 58 - Mean (SD) of the peak AP GRF force values [BW] of the experimental data and simulations. All simulated values were significantly different from the experimental value ($p \leq 0.013$).	202
Table 59 - Mean (SD) of the peak vertical GRF force values [BW] of the experimental data and simulations. * indicates simulated values were significantly different from the experimental value ($p \leq 0.013$).	202
Table 60 - Mean (SD) of the RMSD [deg] between the simulated and experimental hip joint angles.....	203
Table 61 - Mean (SD) of the RMSD [m] between the simulated and experimental knee trajectories.	205
Table 62 - Mean (SD) correlation coefficients between the simulated and experimental knee trajectories. * indicates correlation was significant ($p \leq 0.013$).	205
Table 63 - Mean (SD) of the RMSD [deg] between the simulated and experimental knee joint angles.....	206
Table 64 - Mean (SD) of the RMSD [m] between the simulated and experimental ankle trajectories.	207

Table 65 - Mean (SD) correlation coefficients between the simulated and experimental ankle trajectories. All correlations were significant ($p \leq 0.013$).	208
Table 66 - Mean (SD) of the RMSD [deg] between the simulated and experimental ankle joint angles.....	208
Table 67 - Equations for calculating the GRFs	233
Table 68 - Mean and standard deviation RMSD between simulated and experimental CoM trajectories [m] and GRF profiles [BW] for n=11, 12, 13 and 19 participants at speeds 1 to 4, respectively.....	234
Table 69 - Comparison of the mean (SD) GRF trough/peaks from the OpenSim and MATLAB solutions.....	236
Table 70 - Comparison of the mean (SD) maximum vertical CoM displacements and contact times from the OpenSim and MATLAB solutions.	237
Table 71 - Root mean square error (mean (SD)) between the full-body and reduced model for the CoM position, velocity and the RoM, as well as the correlation coefficient (mean (SD)) indicating waveform similarity between the full-body and reduced model. * indicates correlation was significant ($p < 0.005$) for all participants.	247

Acknowledgments

For their support and guidance throughout my PhD I would like to extend my sincere gratitude to my supervisors, Dr. Stephen Preece and Prof. Richard Baker. I would also like to acknowledge the University of Salford for providing the funding that made this project possible. I would also like to recognise and thank Duncan Mason and Chris Bramah for collecting the experimental data used, and Dr. Stephen Preece for giving me access to it. Finally, I would like to thank my family and friends for their support over the past three years.

Abbreviations

2D	Two dimensional	lin	Linear
3D	Three dimensional	MDS	Motor-damper-spring model
AP	Anterior-posterior	MFS	Midfoot strike
BW	Bodyweight	ML	Medio-lateral
CE	Contractile element	mod	Model
cFO	Contralateral foot-off	MS	Midstance
cFS	Contralateral foot strike	PC	Physically consistent
CNS	Central nervous system	PE	Potential energy
CoM	Centre of mass	PEE	Parallel elastic element
CoP	Centre of pressure	POFA	Point of force application
dof	Degrees of freedom	RF	Rectus femoris
EMG	Electromyography	RFS	Rearfoot strike
EP	End point	RoM	Range of motion
exp	Experimental	SEE	Series elastic element
FDA	Forward dynamics analysis	SI	Foot strike index
FFS	Forefoot strike	sim	Simulated
GAS	Combined medial and lateral compartments of gastrocnemius	SK	Sprung knee
GMAX	Superior middle and inferior gluteus maximus	SKA	Sprung knee and ankle
GPE	Gravitational potential energy	SLIP	Spring loaded inverted pendulum
GRF	Ground reaction force	SO	Static optimisation
HAMS	Combined biceps femoris long head, semimembranosus and semitendinosus	SOL	Soleus
IC	Initial contact	TE	Total mechanical energy
IDA	Inverse dynamics analysis	TIBANT	Tibialis anterior
iFO	Ipsilateral foot-off	TO	Toe off
iFS	Ipsilateral foot strike	tor	Torsional
ILPSO	Combined iliacus and psoas	VAS	Combined vastus medialis, vastus intermedius and vastus lateralis
KE	Kinetic energy	Vert	Vertical

Abstract

Mathematical models of human movement have the potential to provide information about how and why humans move the way they do. However, due to the existing gap between the current simple and complex models of running, it is unclear as to the level of complexity required to model normal distance running. Therefore, the aim of this PhD was to develop an “appropriately complex” biomechanical model of running.

The first investigation aimed to assess the validity of the fundamental assumption of the spring mass model, the simplest model of running. The model assumes that during running the human body acts similar to a point mass bouncing on a massless linear spring of constant stiffness. It was found that forefoot strikers exhibited a relatively linear force-length relationship, but rearfoot strikes did not. In addition, significant differences were found when a range of definitions for calculating lower limb stiffness were compared to the most physically consistent definition.

A series of models, each with increasing complexity, were developed using OpenSim. Simulations were compared to experimental data and agreement appeared to increase as model complexity increased. Due to problems with using a fixed length segment, introducing a knee joint alone prevented successful simulations across the entire stance phase. In contrast, a model with passive knee and ankle joints resulted in good agreement between the experimental and simulated center of mass (CoM) trajectories. However, joint kinematics and ground reaction forces (GRFs) did not show as good a match.

The next level of complexity was to add actuation at the ankle joint. Within OpenSim this required introducing a contact model at the foot-ground interface, and led to difficulties in ensuring sensible behaviour of the contact model as well as matching the CoM trajectories. Including actuation provided better agreement between the joint kinematics and GRFs. Therefore, it is predicted that if these difficulties can be overcome, a three-segment sagittal plane model with torsional springs at the knee and ankle, and a small amount of actuation, will be able to match experimental data to within the measurement error of the data.

1. General Introduction

1.1. Running

1.1.1. Running as a leisure activity

Running is a fundamental part of life for many people. Historically it would have been synonymous with survival, providing a means of transport and escape, as well as a method for hunting. In modern society, on the other hand, it shapes the foundation of a healthy lifestyle for many people, and is a fundamental part of many sporting activities.

In the year 2015-2016 it was estimated that approximately 15 % of the UK's population actively participated in running (Sport-England 2016), with Sport England reporting 896,700 adults (Sport-England 2015) participating in athletics events, and Sport Wales reporting 351,000 adults (Sport-Wales 2016) participating in running events, in the year 2014/15. Amongst runners more than half (55%) choose to run outdoors (Sports-Insight 2014, SMS-INC. 2014b), with road being the surface of choice (96% of runners chose roads in the last year (SMS-INC. 2016, Sports-Insight 2016b)). According to Sport England, more than 2 million people run every week (NPD-Group 2015, Sports-Insight 2015) with the average weekly mileage being approximately 34 km (SMS-INC. 2016, Sports-Insight 2016b).

The increase in participation, and interest, in running has had a comparable effect on both the product industry and the health sector. The average runner spent £130 on running apparel in 2015 (Sports-Insight 2016a), with approximately £80 of that being on a pair of running shoes (Sports-Insight 2016a). In total, British consumers spent £100 million more on running shoes in 2014 than they did in 2010 (NPD-Group 2015, Sports-Insight 2015), the result of a 13 % increase in the running market (NPD-Group 2015, Sports-Insight 2015).

The ease of accessibility, and the associated health benefits, has made running the sport of choice for many. However, running injuries are common with incidence rates reported ranging between 18.2 and 92.4 % (van Gent et al. 2007, Lopes et al. 2012). The large range in incidence rates can be attributed to the wide variety of injuries. The knee is

considered the most injury prone area for runners, with incidence rates ranging from 7.2 to 50 %. The next most affected area is the foot (and toes) with incidences between 5.7 and 39.3 %, then the upper leg (hamstrings, thigh and quadriceps) with incidence rates between 3.4 and 38.1 % and finally the lower limb (Achilles, shin, calf and heel) with incidence rates reported between 9 and 32.2 % (van Gent et al. 2007). It should be noted that the large variation in injury rates may be influenced by what is classified as an injury.

1.1.2. The biomechanics of running – what we know

The popularity of running has resulted in large amounts of interest in the sport; in research, media and non-fiction writing. However, the majority of the biomechanics research is made up of descriptive investigations into the kinematics and kinetics. A review of the literature pin-points a few key texts, including a review article by Novacheck (1998, 952 citations), a book of papers edited by Cavanagh (1990, 227 citations) as well as a few others; for example Williams (1985, 182 citations), Ounpuu (1994, 201 citations) and Dugan et al. (2005, 164 citations). Based on this literature, a brief outline of what is currently known about running biomechanics will now be discussed; this information is presented under the following headings: the gait cycle, CoM movement, kinematics and kinetics. However, it should be noted that the key texts mentioned above are somewhat dated; therefore, an effort will be made to include several more recent studies which have aimed to develop further insights into running, as well as highlight areas of running biomechanics that are still relatively unexplored.

The Gait Cycle

In gait analysis, the gait cycle is the basic unit of measurement. It describes the spatiotemporal parameters of one complete cycle of the movement, i.e. between successive ground contacts with the same foot. A gait is described as running when a period of double float and a period of single support occur twice during each cycle (Figure 1), i.e. when the stance phase accounts for less than 50 % of the cycle (Ounpuu 1994, Nicola et al. 2012). As speed increases the amount of time spent in stance (i.e. the contact time) decreases, and the maximum force going through the single support stance limb increases (Adelaar 1986). The gait cycle is often further sub-divided. However, there is less agreement about these

subdivisions than in walking, and many of these proposed subdivisions are unconvincing. For example, the gait cycle has been sub-divided into stance phase absorption, reversal, and generation, and swing-phase generation, reversal, and absorption (Dicharry 2010). Where these phases of absorption and generation are said to correspond to alternating periods of vertical acceleration and deceleration of the centre of mass (CoM), respectively (Novacheck 1998). However, absorption and generation must relate to some sort of energy or power consideration, not accelerations, and thus more likely correspond to the in-phase changes in kinetic energy and gravitational potential energy. Parameters such as stride time, step time, stride length, step length, gait velocity, and cadence all define the spatial-temporal characteristics of running gait.

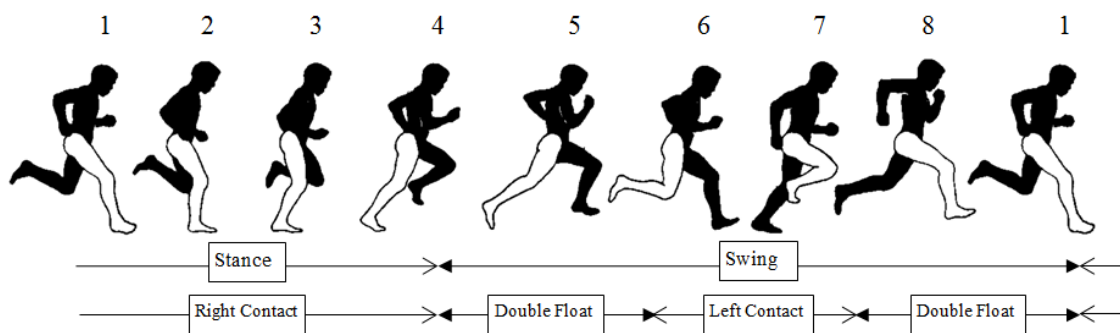


Figure 1 - Running gait cycle (Adelaar 1986) showing the alternating (right side) stance and swing phases.

Centre of Mass Movement

In running, the CoM of the body moves in an approximately sinusoidal pattern, with the lowest point at midstance and highest point at midswing. This sinusoidal pattern is synonymous with an in-phase relationship between the gravitational potential energy (GPE) and the kinetic energy (KE), which are both at a minimum when the CoM is at its lowest point, i.e. midstance (Farley et al. 1998, Kehler et al. 2014). Because of this in-phase relationship, the total mechanical energy (TE) is at a minimum at midstance (Figure 2), and thus, energy must either be conserved in some other way, or dissipated and then actively regenerated. One possible mechanism for how energy could be conserved is via

the storage and return of elastic energy (to be discussed in more detail in Chapter 4). It is hypothesised that in order for running to be both mechanically and metabolically economical the elastic properties of the tendons and muscles of the stance leg must be harnessed during each step (Kehler et al. 2014). This reasoning is the fundamental premise for the most common conceptual model of running, the spring mass model, which assumes that the KE and GPE of the CoM could be elastically stored during landing and returned during push off.

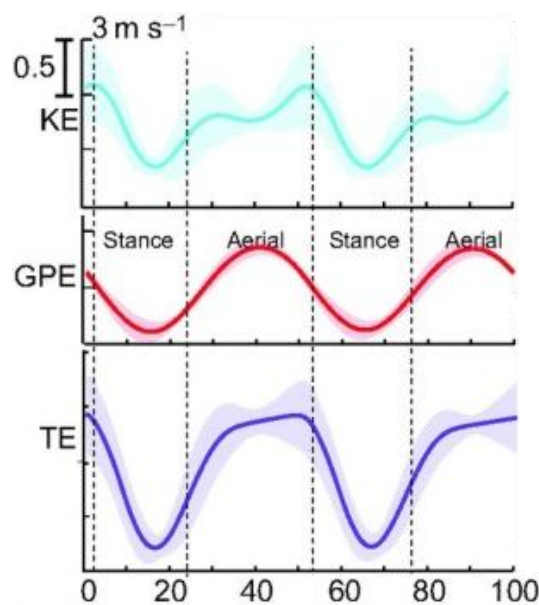


Figure 2 - CoM mechanical energy fluctuations (J/kg) as a function of the gait cycle (%) (Kehler et al. 2014). Kinetic energy (KE), gravitational potential energy (GPE) and the total mechanical energy (TE) are normalised to body mass. The dotted vertical lines represent the start of the different phases of the gait cycle, i.e. touch down and take off.

Kinematics

Motion analysis allows reconstruction of joint angles in all three planes of movement (Figure 3). During running, the majority of the segment rotations are in the sagittal plane, with smaller amplitude rotations in both the frontal and transverse planes (Figure 4 & Figure 5).

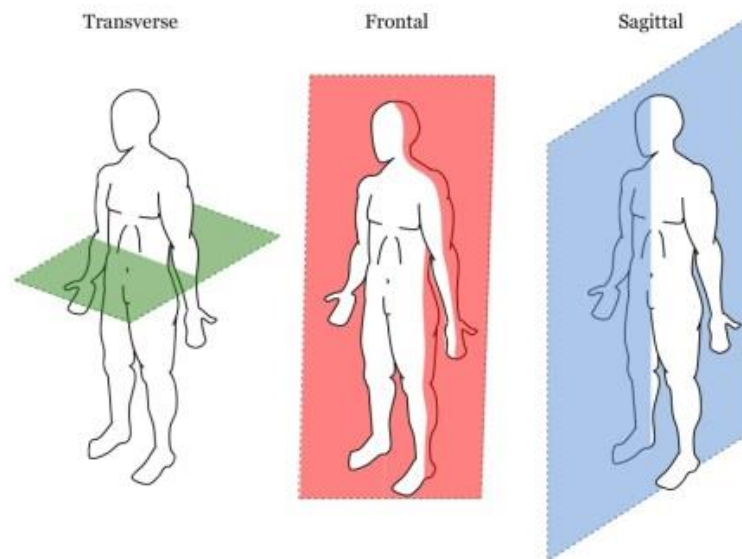


Figure 3 – The three planes of movement include the transverse, frontal and sagittal planes. The sagittal plane is perpendicular to the ground and divides the body into left and right. The frontal plane is also perpendicular to the ground, but divides the body into dorsal and ventral portions. Finally, the transverse plane is parallel to the ground and divides the body into superior and inferior portions.

In the sagittal plane, the hip extends during stance and flexes during swing (Ounpuu 1994) (Figure 4a). The knee flexes during the first half of stance, as a possible mechanism for controlling the movement of the CoM, and reaches peak flexion at midstance (Ounpuu 1994) (Figure 4d). During mid to late stance, the knee extends driving the CoM upwards (Figure 4d). It then slowly flexes during early swing, and rapidly extends during mid to late swing before beginning to flex again, seemingly in preparation for stance (Ounpuu 1994). The ankle kinematics somewhat depend on the foot strike pattern adopted. Heel-strikers plantar flex the ankle immediately after initial contact, whilst forefoot strikers immediately dorsiflex the ankle (Ahn et al. 2014). From early stance to midswing, both groups show similar ankle kinematics; dorsiflexion occurs until midstance, then rapid plantar flexion until toe off (Figure 4g). Heel-strikers then dorsiflex until the next initial contact, while forefoot strikers dorsiflex until midswing before beginning to plantar flex and presumably reposition for initial contact (Ahn et al. 2014).

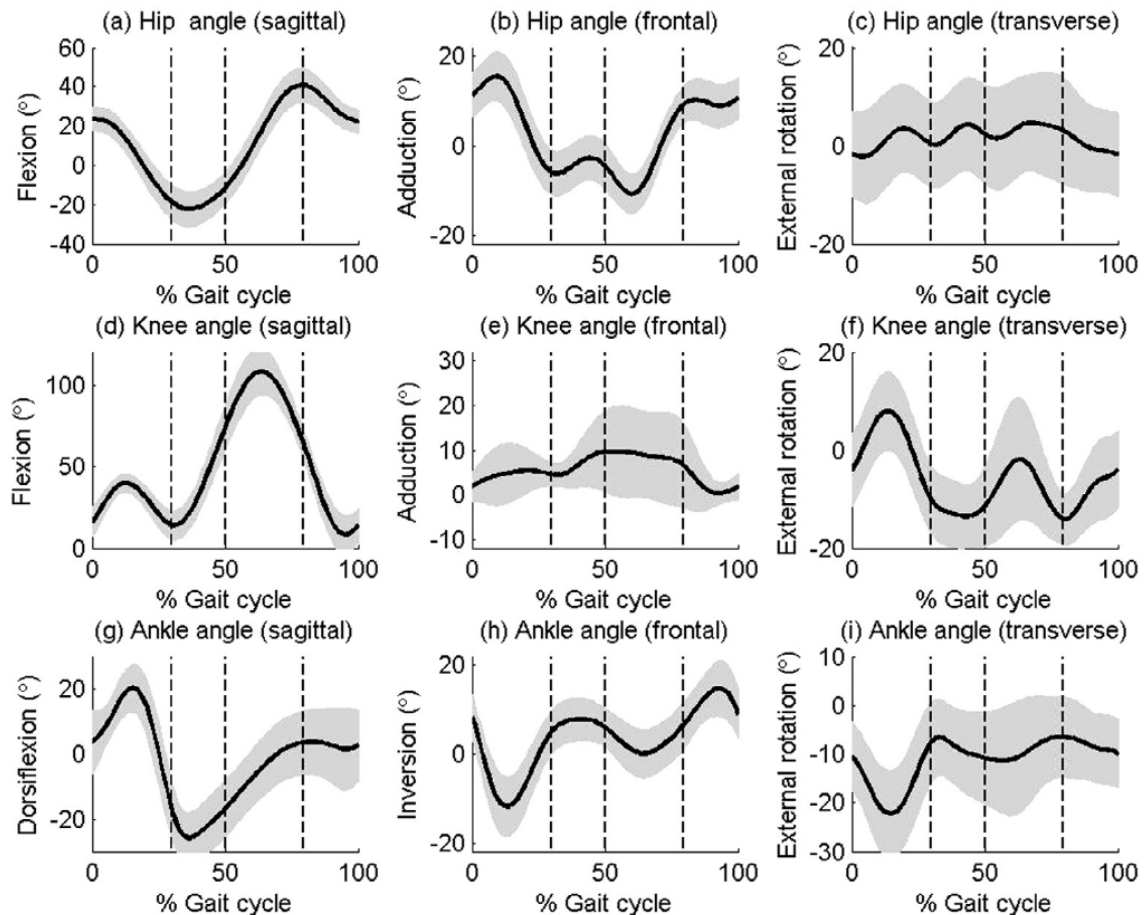


Figure 4 – Hip (a-c), knee (d-f), and ankle (g-i) kinematics during overground running at 3.9 m/s. Data is plotted from right initial contact, and the three vertical lines indicate right toe off, left initial contact and left toe off, respectively.

In the transverse and frontal planes rotations are more subtle than in the sagittal plane. However, there are a few key features to note in terms of movement of the hip, pelvis and foot. In the transverse plane, the pelvis is externally rotated (rotated towards the stance limb) at the point of initial contact, and reaches a maximum at midstance, possibly to maximise horizontal propulsion (Novacheck 1998). It is in a neutral position at take-off and reaches maximum internal rotation (rotated away from the stance limb) at midswing, which has been suggested to slightly reduce the stride length (Preece et al. 2016). During early stance and midstance the foot pronates, which has been suggested as means of dissipating impact loads and allowing for “*solid contact*” between the foot and the ground, before supinating during mid to late stance to provide a “*steady lever*” for push off

(Novacheck 1998, Dugan et al. 2005). However, it is unclear as to the mechanical meaning of the terms “*steady lever*”, “*solid contact*” and “*dissipation*”.

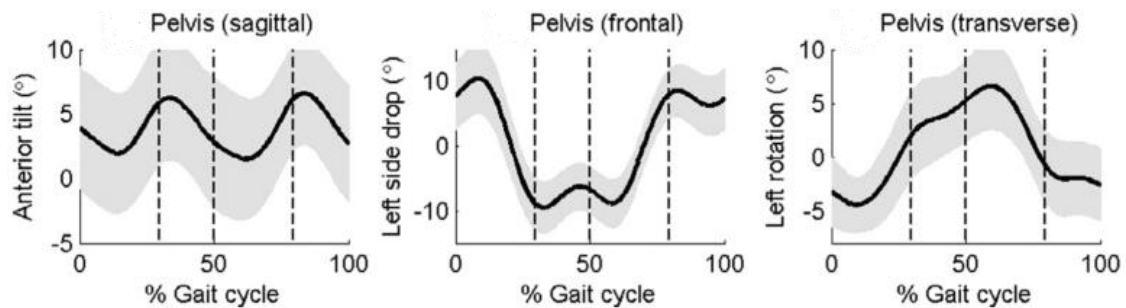


Figure 5 - Pelvis movement during running (Preece et al. 2016), where the dashed vertical lines represent right toe off, left initial contact and left toe off, respectively.

In the frontal plane, the hip adducts as the pelvis rises, both reaching a peak at midstance (Figure 4 & Figure 5). This movement pattern has been proposed as a way to “*dissipate loading forces*” and “*stabilise*” the lower extremity (Dugan et al. 2005). However, this explanation may be unsuitable since “*dissipation*” is a process by which useful energy is transformed, and is therefore not appropriate for describing how forces are distributed throughout the body. From midstance to midswing, the hip abducts and the pelvis lifts on the contralateral side, providing a mechanism to ensure foot clearance and extend the stride length (Preece et al. 2016). Then from midswing, the hip adducts and the pelvis rises to prepare for initial contact.

It should be noted that some of the mechanisms proposed as justification for these kinematic patterns, are fundamentally conjectures. The chosen descriptive terms can also be misleading and ambiguous. For example, a “*lever*” is a rigid body that pivots about one point, used to rotate an object about another point via a force being applied at a third point. While the assumption that the foot acts as a rigid body may seem reasonable, the movement of the CoP during the stance phase of running means the lever analogy may not be appropriate. In a similar way, the use of the term “*stabilise*” is vague. For example, it is unclear whether this “*stability*” of a joint under applied forces refers to a mechanism for resisting loads, or a way of regulating the amount of force that crosses the joint, or perhaps

it refers to a means of controlling the range of motion. This uncertainty in terms can lead to doubts in the current explanations proposed for how and why humans run the way they do.

Kinetics

Kinetics of gait can be subdivided into ground reactions forces (GRFs), centre of pressure (CoP) and joint moments and powers. Using Newtonian mechanics, and specifically Newton-Euler equations, the kinematics and GRFs can be combined to determine the joint moments based on a method known as ‘inverse dynamics’ (Ounpuu 1994). Inverse dynamics is a method by which the net turning effect (of all anatomical structures crossing a particular joint) required to produce a given movement is calculated (D. Gordon E. Robertson et al. 2013) (discussed in detail in Chapter 2.7.1).

Ground reaction forces (GRFs) are forces exerted by the ground on the body during ground contact. They can be measured using force plates imbedded into the running surface or a force instrumented treadmill. The data can then be resolved into the anterior-posterior (AP), mediolateral (ML) and vertical directions. It has been reported that the vertical GRF during running has one or two peaks (Figure 6) depending on whether the runner is a forefoot or a rearfoot striker, respectively (Lieberman et al. 2010, Kulmala et al. 2013, Almeida et al. 2015). The (first) impact peak is said to be a consequence of the landing, and is influenced by the foot strike pattern, cadence and velocity of the foot at initial contact, while the (second) active peak is influenced by the mass of the runner, velocity of the runner and the compliance (stiffness) of the lower limb (Dicharry 2010).

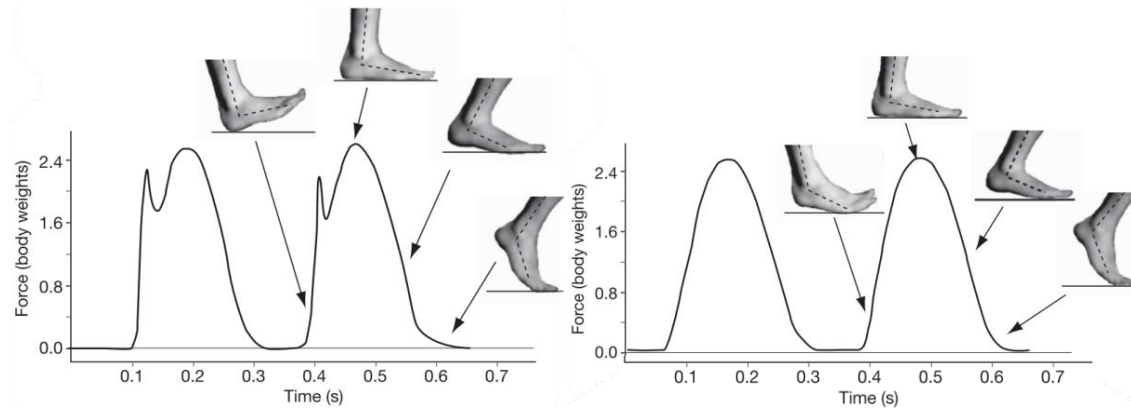


Figure 6 - Vertical GRFs for rearfoot and forefoot strikers, highlighting a key difference between the two strike patterns, where the impact peak characteristic of rearfoot strike patterns is generally not seen in forefoot strikers (Lieberman et al. 2010).

The vertical GRF is highest during midstance, suggesting that peak internal joint moments will generate the highest mechanical strain on tissues at this point (Dicharry 2010). This may be true for the knee and ankle, but since the hip is approximately in-line with the vertical GRF vector at midstance, the internal joint moment of the hip is likely to be small at this point. It is said that it is necessary for a runner to “*stabilise*” these forces in order to avoid injury (Dicharry 2010). However, whether this “*stabilising*” refers to limiting or resisting the loads is unclear. The AP GRF is influenced by the runner’s foot strike pattern, stride frequency and the gradient of the running surface (Dicharry 2010). ML GRFs are associated with the trajectory of the CoM in the frontal plane, where excessive deviation from the midline has been linked to hip and/or core “*instability*” (Dicharry 2010), which presumably refers to the inability of the structures (muscles, ligaments, tendons, etc.) surrounding/of the hip/core to resist the ML GRFs. It has also been suggested that minimised ML GRFs are energetically efficient and contribute to lateral balance during running (Arellano et al. 2011).

The CoP marks the origin of the GRF vector (Dicharry 2010) and is defined as the point of force application where a single force of equal magnitude to a distributed force causes the same effect on a rigid body (D. Gordon E. Robertson et al. 2013). The origin of the CoP, and therefore the progression through stance, is influenced by the foot strike pattern

adopted (Figure 7) (Dicharry 2010). Typically, rearfoot strikers tend to land on the posterior-lateral edge of the foot; therefore, the CoP originates at this point then travels distally towards the metatarsal heads. At approximately two-thirds of stance the CoP turns medially progressing across the metatarsal heads before terminating at the medial edge of the first toe (Dicharry 2010). Midfoot and forefoot strikers on the other hand, have an initial CoP progression in the proximal direction as the heel lowers to (near) heel contact. The CoP then rapidly travels distally toward the medial forefoot, and again terminates at the medial edge of the first toe. The origin of the CoP in midfoot strikers is more proximal than that of forefoot strikers (Dicharry 2010).



Figure 7 – Approximate CoP trajectories for rearfoot, midfoot and forefoot strikers (left to right respectively). Rearfoot strikers tend to land on the posterior-lateral edge of the foot and the CoP travels distally to the medial edge of the first metatarsal head. On the other hand, midfoot and forefoot strikers tend to land more distally, with the CoP initially travelling proximally as the heel lowers before moving distally towards the medial edge of the first metatarsal head.

Joint kinetics describe the forces, and moments of force, acting on a joint at any instance in time (Figure 8). The joint moments describe the net moments that must be generated at a joint in order for the body to move (accelerate), i.e. to move the CoM and support the body against gravity. They also describe the load that must be generated and/or resisted by the body structures acting across the joint, essentially indicating the dominant muscle group associated with each movement. Power, on the other hand, is the rate of doing work or the

energy consumed (or generated) per unit time. In biomechanics, joint powers are calculated as the product of the joint moment and the angular velocity. They indicate whether a uniarticular muscle is generating or absorbing energy, i.e. if a muscle contracts concentrically it does positive work and the muscle shortens, indicating power absorption is occurring; on the other hand, if a muscle contracts eccentrically it does negative work and the muscle is stretched, indicating power generation is occurring. However, if a muscle is biarticular there is a more complex interaction that needs to account for the effects on both joints. In running, magnitudes of moments and powers in the frontal and transverse planes are smaller than those in the sagittal plane, and have been suggested to act primarily to resist and limit joint motions (Novacheck 1998); therefore only sagittal plane joint moments and powers will be discussed below.

Prior to, and immediately after, initial contact the hip extends and the hip extensors generate power. Throughout the rest of stance, the hip flexes and the hip flexors absorb power, while during swing, the hip extends and again the hip extensors generate power. At the knee, flexion occurs during early stance and midstance, the quadriceps are the dominant muscle group and as they contract eccentrically (Novacheck 1998) they produce a knee extensor moment that corresponds with power absorption. From mid to late stance, the quadriceps begin to contract concentrically (Novacheck 1998) extending the knee and generating power. Then during mid and late swing, the hamstrings become dominant (Novacheck 1998), producing a knee flexor moment that limits the range of motion and prevents knee hyperextension. In heel-strike running, there is an initial plantar flexor moment that controls the forefoot lowering to the ground. This is not seen in forefoot running, where there is an immediate dorsiflexor moment after initial contact. Initial plantar flexion and dorsiflexion during early stance and midstance corresponds with a decreasing ankle moment and power absorption, while plantar flexion from midstance to take-off is associated with an increasing ankle moment and power generation, and the magnitude of the ankle power appears to be directly related to the speed (Novacheck 1998).

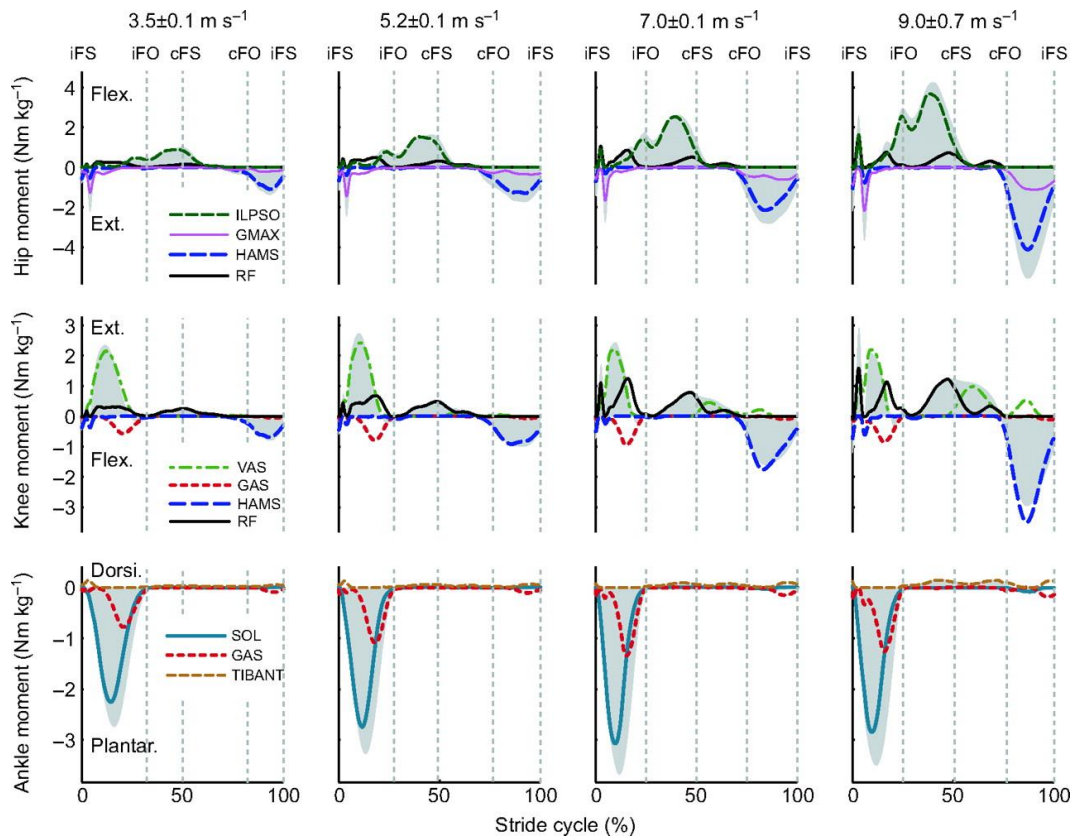


Figure 8 – Individual muscle contributions to the hip, knee and ankle moments during the stance phase of running (Dorn et al. 2012). Shaded region represents the net sagittal plane joint moment, normalised to body mass, with a positive moment indicating hip extension, knee flexion and ankle plantar flexion. cFO, contralateral foot-off; cFS, contralateral foot strike; iFO, ipsilateral foot-off; iFS, ipsilateral foot strike. ILPSO, combined iliacus and psoas; GMAX, superior, middle and inferior gluteus maximus; HAMS, combined biceps femoris long head, semimembranosus and semitendinosus; RF, rectus femoris; VAS, combined vastus medialis, vastus intermedius and vastus lateralis; GAS, combined medial and lateral compartments of gastrocnemius; SOL, soleus; TIBANT, tibialis anterior.

1.1.3. The biomechanics of running – what we don't know

Despite the detailed descriptions of the observed kinematics and kinetics, we still do not fully understand the key mechanisms behind how and why people run the way they do. Firstly, the choice of language and the ambiguity associated with definitions makes it

difficult to formulate robust biomechanical arguments, with different explanations for kinematic patterns often contradicting one another. From EMG data, it is possible to determine which muscles are contributing to each phase of the running gait cycle. However, this does not necessarily explain which muscles/tendons/ligaments/etc. are storing and returning elastic energy. It also remains unclear whether certain running styles are more/less efficient, or whether different strike patterns use different energy conservation mechanisms. A clearer explanation of the fundamental biomechanics of running would likely mean a better understanding of the differences between strike patterns and thus a better understanding why people run the way they do. Furthermore, understanding why people run the way they do would have an influence on both clinical practice and training protocols for increased performance. Essentially if the fundamental movement is not understood then there is limited scope for identifying biomechanical abnormalities that could lead to injury or restrict performance. Furthermore, since it is often unstated, it is unclear if certain modelling techniques are appropriate for different foot strike patterns. Therefore, a more comprehensive modelling approach has the potential to shed light on some of the fundamental principles that define the way in which people run.

1.2. Computer Modelling and Simulation

1.2.1. Modelling – what is it?

Modelling and computer simulation can provide a means of eradicating some of the constraints associated with experimental testing protocols (D. Gordon E. Robertson et al. 2013). Such constraints include variable coordination patterns, fatigue, and limitations in both strength and speed. Considering this, modelling has the potential to provide information about the fundamental mechanisms that contribute to human movement. Pritsker (1979) described computer modelling as the “*setting up of mathematical equations to describe the system of interest*”. Although modelling inherently requires a degree of simplification, these models can be both predictive and descriptive and have a range of uses within the field of biomechanics.

Mathematical models have the potential to provide information about how and why people move the way they do. They can aid in the understanding of fundamental principles that govern movement, identify risk factors for injury or characteristics of pathologies, and calculate internal joint and muscle forces. They also can be used in the design and implementation of rehabilitation, treatment and training protocols. However, it should be noted that the choice of model, and the required complexity of the model, depends on the research question and type of investigation being conducted (Yeadon et al. 2007). It is widely accepted that the simpler the model the better, and that using “... *the simplest possible model capable of capturing the essence of the task being studied*” (Sprigings et al. 2004) is most appropriate. As Alexander (2003a) states that “*the simpler the model, the clearer it is which of its features is essential to the calculated effect*”, a concept that can be related back to the principle of Ockham’s razor, which essentially states that the simplest adequate explanation, with the least number of assumptions possible, should always be used

Despite the need for simple models of running, there is a clear lack of progression in the complexity of models being used. With the development of more advanced technologies, more powerful computers and faster processors there has been a turn towards the more complex musculoskeletal models. These models are three-dimensional with multiple degrees-of-freedom (dof) and often incorporate bones, joints, and muscles; allowing more aspects of the kinematics and kinetics to be investigated with a single model. However, these models tend to require the use of more complicated solvers, with complex optimisation methods to determine the solution to an indeterminate problem (where there are more variables than equations). Although these models are unquestionably useful, the jump from the simple to the complex leads to a question of the natural progression of modelling methods. There is also the question of model validity; for example if the optimisation methods and solvers have not been tested using simpler models how can we be confident of their solutions?

1.2.2. The importance of validating models

It is essential that a model be validated against real life experimental data. This ensures that the results do not surpass the physiological constraints of the human body. However,

these validations are specific to the experimental data and participant groups used in the validation process. The results may not extrapolate to other populations or movements. Panjabi (1979) acknowledged this by stating, “*a mathematical analogue can be validated only in a given number of known situations, yet the main purpose of the analogue is to predict behaviour in unknown situations – thus, no perfect validation is possible*”.

The concept of an imperfect validation highlights one of the major limitations of computer modelling and simulation. These complex musculoskeletal models are often designed as a method for investigating parameters that are not easily measured experimentally (Hicks et al. 2015), therefore it begs the question of the validity of their results. To address this, efforts have been made to develop a series of guidelines and protocols for validating and verifying these models (Panjabi 1979, Anderson et al. 2007, Henninger et al. 2010, Lund et al. 2012, Hicks et al. 2015). However, fundamentally the question still remains, if the solutions cannot be compared to representative real-world experimental data - is it correct to accept the solutions? Furthermore, many computational models often use average input parameters as it is assumed they will produce average results representative of a certain population. Contradictory to this assumption, a recent study found consistent discrepancies between the results of average models (those using averages as inputs) and the average behaviour of population, suggesting a need for specific models with complete data sets (Cook et al. 2016).

1.3. Chapter Summary

This general introduction has introduced some areas of the biomechanics of running that are still relatively misunderstood. Despite the interest in running, and the amount of research into running, as well as advances in experimental technology and computer methods, relatively little is known about the fundamental mechanisms that define how and why people run the way they do. Computer modelling has provided a means of investigating some aspects of running, but a large gap remains between the current simple and complex models of running. Which leads to the question of what happens in between? In addition, whether there is justification for a more natural progression from the simple to the complex, i.e. a series of sequentially more complex models. By initially investigating the fundamental assumption of the spring mass model, and highlighting some of its major

limitations, this thesis aims to progressively develop the complexity of the model and subsequently investigate what mechanical characteristics contribute to how and why humans run the way they do.

The thesis will initially discuss the existing simple models of running (Chapter 2.1), highlighting the information these models have been able to provide, as well as their shortcomings and limitations. It will then discuss the complex models of running (Chapter 2.7), explaining how, although they provide a means of investigating aspects of running that are not easily measured experimentally, their inherent complexity and associated optimisation methods leads to questions about over-fitting and unrealistic solutions. The fundamental assumption of the spring mass model (that the body acts similar to a massless linear spring) will be investigated for a range of foot strike patterns and running speeds (Chapter 4). Additionally, since the spring mass model requires calculation of the spring stiffness, a review of current methods will be conducted and compared to the physics definition (Chapter 5). The thesis will then go on to investigate the accuracy of this model (Chapter 7) and the effects of sequentially adding complexity to this model, with the aim of identifying the biomechanical consequences of adding a knee (Chapter 8) and ankle (Chapter 9) joint.

Chapter Summary

<p>Chapter 2 – Literature Review Chapter will review the current literature of running models. It will describe the simplest models and how they have been modified, as well as highlight the limitations of these models and how they fail to explain key features of running. This chapter will then describe complex models of running, again highlighting the limitations and explaining how these models focus on musculoskeletal contributions to running, rather than a full conceptual understanding of running. The chapter will end by highlighting the key gaps in the current literature and a statement of the aims and research questions of this PhD.</p>	
<p>Chapter 3 – Experimental Data The chapter summarises the experimental data used for this PhD. It includes a description of the participants, the data collection protocol and the data processing methods.</p>	
<p>Chapter 4 – ...Force-Length Relationships Chapter focuses on the appropriateness of the spring mass model. It will discuss force-length curves and the elastic hysteresis of running, and the validity of using the spring mass model for different types of participant.</p>	<p>Chapter 5 – ... Calculating lower limb stiffness Chapter will discuss stiffness as a characteristic of the human body: how it has been calculated, and how these methods compare to the fundamental physics definition of stiffness.</p>
<p>Chapter 6 – Common Modelling Methods... This chapter will briefly describe the data collection and processing methods of the experimental data. It will also explain the modelling methods that are common between all the models.</p>	
<p>Chapter 7 – The Spring Mass Model... The chapter will begin by discussing how the spring mass model has been validated for modelling running, reviewing any papers that have investigated its ability at simulating running. The chapter will then outline how the spring mass can be implemented (using MATLAB and OpenSim) and discuss the characteristics of the corresponding simulations, highlighting any differences between foot strike patterns and speeds.</p>	
<p>Chapter 8 – ... adding a knee joint The chapter will begin with a discussion about the function of the knee during running. It will then review any models that have incorporated a “knee” joint highlighting their findings and limitations. The chapter will then outline the modelling methods used, analysis, results and implications of the findings.</p>	
<p>Chapter 9– ... adding an ankle joint The chapter will begin with a discussion about the function of the ankle during running. It will then review any models that have incorporated an “ankle” joint highlighting their findings and limitations. The chapter will then outline the modelling methods used, analysis, results and implications of the findings.</p>	
<p>Chapter 10 – General Discussion Chapter will summarise and discuss findings of the PhD. It will outline the implications of the findings, how they contribute to our knowledge of running biomechanics as well as outline potential avenues of further research.</p>	

2. Literature Review

2.1. The Simplest Model of Running

Simple running models can provide useful information about the fundamental relationships between key running variables. The simplest of these is the spring mass model, sometimes referred to as a SLIP (spring loaded inverted pendulum) model, a concept originally explored by Blickhan (1989) and McMahon et al. (1990). Based on the assumption that the musculoskeletal system acts similar to a single point mass bouncing on a passive, massless, linear spring, Blickhan (1989) and McMahon et al. (1990) used the model to investigate the interactions between the mechanical parameters that define running. The model consists of a mass, m , representing the total mass of the body, attached to a massless linear spring of stiffness, k , representing the lower limb, travelling at a velocity, v (Figure 9). The spring compression and extension represents the movement of the CoM of the body, where the period of oscillation of the bouncing spring can be divided into two phases: the contact phase and the aerial phase. As such, the sinusoidal displacement during the contact phase is followed by parabolic flight during the aerial phase, indicative of the stance and swing phases of a running gait cycle.

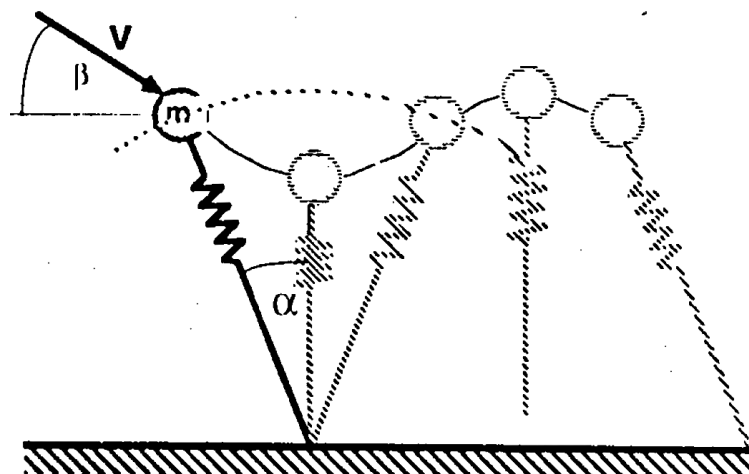


Figure 9 - Simple spring mass model, where m represents the entire mass of the system, β represents the angle of the landing velocity, v the absolute value of the landing velocity and α the angle of attack of the spring (Blickhan 1989).

This model was used to vary mechanical parameters (i.e. stiffness, approach angle and landing velocity) in order to determine their effect on various running parameters (i.e. CoM trajectory, step frequency, aerial & contact length and aerial & contact time) (Blickhan 1989, McMahon et al. 1990). Using a combination of Hooke's Law and Newton's Second Law the equations of motion were derived, where non-linear differential equations for the horizontal and vertical accelerations described the planar movement of the system during ground contact (Blickhan 1989). Simulations were compared to experimental data (Cavagna et al. 1976, Cavagna et al. 1977), in the form of relationships and general trends, and the authors concluded the model was "successful" if the parameters were constrained within physiological limits. Since the bouncing mechanism associated with a running gait places certain restrictions on the free parameter space where solutions can be found, parameters needed to be adjusted with respect to each other in order to allow for bouncing to occur (Blickhan 1989).

Original investigations using the spring mass model showed that running, or hopping forward, can be described by five independent variables (mass m , spring length l , spring stiffness k , absolute value of the landing velocity v , and angle of the landing velocity β) (Blickhan 1989). However due to the interdependence of some outcome parameters (i.e. contact time and step frequency both depend on landing velocity) the number of possible solutions is restricted by the physiological constraints of a human. These physiological limitations are largely defined by muscle properties and skeletal dimensions, hence, in the spring mass system the spring length and the spring stiffness are integral for determining the movement of the CoM. In the literature, there is always reference to leg length and leg stiffness, however in anatomy, the leg refers only to the body parts between the knee and the ankle (the crus), therefore it seems more appropriate to make reference to lower limb length and lower limb stiffness.

The spring mass was found to 'run' in a manner similar to human running. It was found that the spring mass model produced estimations of vertical CoM acceleration and displacement that were generally in good agreement with experiment (McMahon et al. 1990). Furthermore, when working under physiological constraints, the model was able to predict the pattern of energy changes of the CoM correctly (Blickhan 1989), and account for the increase in both stride length and step length with increasing speed for a lower limb with constant stiffness (McMahon et al. 1990). From this it was determined that, for

running at a particular speed, there is a preferred stride frequency for which the energy expenditure is minimised, and hence there is an optimum landing angle, lower limb stiffness and contact length for which this preferred stride frequency is possible (Blickhan 1989). Therefore, not only does this model seem to predict useful relationships between various running parameters, but it is also capable of correctly calculating the mechanical energetics of the CoM (Blickhan 1989).

Despite the spring mass model's apparent success, the simplicity should not be overlooked. The model assumes symmetric take-off and landing angles and velocities, which is generally not the case during human running (McMahon et al. 1990). It also assumes symmetry in the rates of loading and unloading during the contact phase. However, in reality the intrinsic properties of muscles and tendons are what control the compliance of the lower limb, and these properties will generally result in more non-linear force-length characteristics (McMahon et al. 1990). The human body is much more complex than a single mass and a single spring, therefore the fact that the spring mass model is even capable of describing the most general characteristics of running is remarkable. The model does not imply that running is solely an elastic movement, but it does suggest that a bouncing movement, like running, can be investigated using the concepts of a spring mass system.

2.2. Using the Spring Mass Model to Study Running

At the time of writing, there were over 2276 citations for the original spring mass model papers (Blickhan 1989, 1323 citations, McMahon et al. 1990, 953 citations). Since these original articles were published the simple spring mass model, as applied to running, has been used as a framework for studying various aspects of running. For example, the model has been used to determine the effects of changes in stride frequency (Farley et al. 1996, Morin et al. 2007), speed (He et al. 1991, Farley et al. 1993), and gravity level (He et al. 1991, Donelan et al. 2000). Therefore, these models are not only useful for investigating general principles of locomotion, but they can be used to identify the key characteristics of a moving human, or animal, that significantly influences a specific aspect of its locomotion (Bullimore et al. 2007).

2.2.1. Stiffness as a parameter to describe running

As a consequence of the spring mass model, stiffness has become considered as one of the fundamental characteristics that describe running. It is considered as a consequence of the cumulative interaction of anatomical structures in which the compliance of the individual musculoskeletal components, such as tendons, muscles, cartilage and bones are combined to give a single value that represents the system; which is assumed to behave like a single linear spring (Butler et al. 2003, Brughelli et al. 2008b). However, this linear spring analogy assumes the lower limb anatomy acts as a passive element. In reality, skeletal muscle and tendons combine to produce passive and active force; where the passive force is produced via the parallel and series elastic components, while the active force is produced by the contractile component (Nordin et al. 2001). The total force produced by a musculotendon unit is then the combination of these. Therefore, at some point, this concept of springs and stiffness becomes invalid and the active properties of muscle must be considered.

Generally, the literature refers to two forms of stiffness, lower limb stiffness and vertical stiffness. However, the relationship between these two parameters and their individual relationships with running parameters and performance is often misinterpreted. For example, many studies use the terms ‘lower limb stiffness’ and ‘vertical stiffness’ synonymously, or in fact just use the term ‘stiffness’ without clarification. A more detailed discussion of stiffness as a descriptor of running will be undertaken in Chapter 4; however, it will be briefly outlined here in the context of the spring mass model.

In physics, stiffness is a mechanical characteristic of an object. It defines how an object passively deforms under an applied load, where the relationship between the applied load and subsequent deformation is based on Hooke’s Law. This physical law states that the force, F , required to deform, or extend, an object is proportional to the distance, s , that object is deformed multiplied by a proportionality constant, k (Young et al. 2008). This proportionality constant is referred to as the stiffness of the object. In terms of the spring mass model, this law implies that the deformation of the spring from its resting length is proportional the force being applied to the spring (Brughelli et al. 2008a). When this occurs, the spring is said to be exhibiting ideal linear force-length behaviour.

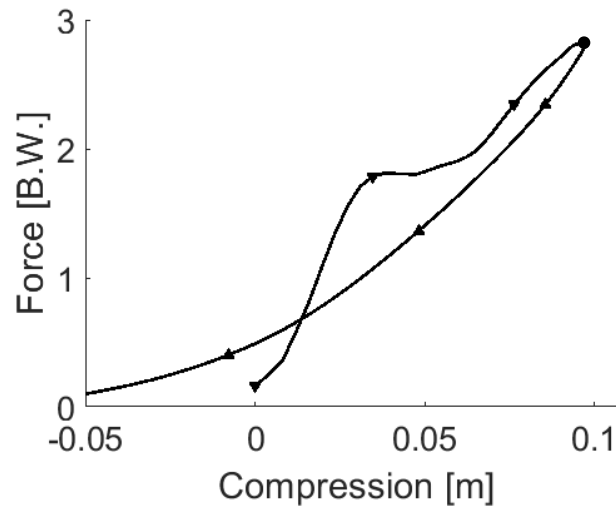


Figure 10 - Example force-length curve for the stance phase of running. Initial contact is indicated by the triangle at 0 m compression, and arrows indicate the direction of loading. Maximum compression is at approximately midstance (black circle), and the spring extension towards the end of stance occurs as the CoM prepares for flight.

In the context of running, stiffness is more often used as a method for defining the relationship between force and “lower limb length” changes. It is worth noting, biological systems are likely to exhibit non-linear force-length relationships, and thus cannot be explained by a single passive stiffness (Figure 10). Therefore, although the relationship results in the same units as stiffness, stiffness might not be the most appropriate term. Instead, some authors have posed the idea of “variable stiffness” where the force-length curve can be explained by a series of phases, each with its own individual stiffness (Hunter 2003), or, as a single higher order equation (Peter et al. 2009). However, it is difficult to conceive how a biological structure could have “variable stiffness” and, instead, it is more likely that the non-linearity of the force-length curve is the result of active force generation. It would therefore be more suitable that actuators be used, instead of springs, as a more appropriate representation of the structures within the musculoskeletal system. This idea will be explored later in this thesis (Chapter 9).

Vertical stiffness refers to a measure of the resistance of the body to changes in the vertical position of the CoM due to the application of a vertical GRF (Brughelli et al. 2008b). This

parameter is often used when describing linear movements that occur in the vertical direction only, for example hopping or jumping in place. When considered independently, it would not appear to be appropriate for running, as running is a three-dimensional movement (Brughelli et al. 2008b). Lower limb stiffness, on the other hand, describes the changes in “lower limb length”, the distance between the most distal and most proximal points, after application of both internal and external forces (Butler et al. 2003). This parameter is not clearly defined in the literature, with the choice of definition of lower limb length and determination of the lower limb force being different in most studies. Multiple studies also claim to investigate lower limb stiffness, but use the definition of vertical stiffness when describing their calculation methods (Ferris et al. 1997, Farley et al. 1999), however these studies tend to refer more generally to “bouncing gaits” and focus on hopping.

2.2.2. Stiffness and its relationship to other running parameters

Stiffness has been associated with many task-specific parameters. These include the rate of force development (Butler et al. 2003, Brughelli et al. 2008b), the storage and return of elastic energy (Kubo et al. 2010) as well as performance (Butler et al. 2003, Pearson et al. 2012). Therefore, numerous studies have looked at the link between both vertical and lower limb stiffness and running velocity. The general consensus within the literature is that the overall lower limb stiffness remains relatively constant (McMahon et al. 1990, He et al. 1991, Farley et al. 1993, Farley et al. 1996, Morin et al. 2005, Brughelli et al. 2008a), while vertical stiffness increases with increasing running velocity (He et al. 1991, Kuitunen et al. 2002, Morin et al. 2005, Brughelli et al. 2008a).

During running, lower limb stiffness is modulated by the combinations of individual joint stiffness values, where the knee joint stiffness increases (Arampatzis et al. 1999, Kuitunen et al. 2002, Brughelli et al. 2008a), but ankle joint stiffness remains relatively constant with increasing running velocity (Arampatzis et al. 1999, Kuitunen et al. 2002, Brughelli et al. 2008a). Therefore, it has been suggested that the knee joint stiffness plays a pivotal role in regulating the overall lower limb stiffness during running (Arampatzis et al. 1999, Günther et al. 2002, Kuitunen et al. 2002, Brughelli et al. 2008a). However, others have argued that ankle stiffness is more important, for bouncing gaits, due to the influences of

the Achilles tendon (Farley et al. 1999), therefore as it stands there is contradictory evidence associated with these theories. These different conclusions are likely due to the different definitions of lower limb length and stiffness calculation methods used, further emphasising the need for clear and distinct definitions of stiffness.

It has been stated that humans have the ability to adjust their lower limb stiffness to accommodate different stride frequencies (Farley et al. 1996) as well as, as a method for adapting to different surfaces (Ferris et al. 1997, Ferris et al. 1998, Kerdok et al. 2002) and gravity levels (He et al. 1991, Donelan et al. 2000). This ability to adapt has been linked to mechanisms for minimizing the energy cost, and thus implies that it is possible to use the elastic components of the musculoskeletal system to run economically and support body weight (Shen et al. 2015a, Shen et al. 2015b). The spring mass model has also been used to investigate these characteristics of locomotion, yet, due to the different methods for calculating stiffness, it is difficult to compare results from different investigations. For example, by exploring relationships between stiffness and running parameters it has been shown that higher lower limb stiffness is associated with a lower energy cost of running (Dalleau et al. 1998). However it was later argued that the increase in stiffness was actually a result of the changes in contact time (Morin et al. 2007), a result that was possibly only apparent because of the stiffness calculation method being used. This reiterates the need to understand how elastic structures are used during running, and therefore requires a clear definition of stiffness.

2.3. Accuracy of the Spring Mass Model

The spring mass model has often been used to investigate relationships between parameters, for example how stiffness effects stride frequency (Farley et al. 1996), or the effect of running velocity on stiffness (McMahon et al. 1990, Brughelli et al. 2008a). The results of these investigations are often only qualitatively compared to previously published values or experimental data. Therefore, there is a question concerning the validity and ability of the spring mass model at replicating human running. A few studies have been conducted to address this question, and their results and limitations will be discussed now.

An effort was made to determine the accuracy of the spring mass model at predicting running parameters. By comparing model predications to previously published experimental data (Donelan et al. 2000), at both normal and reduced gravity (Bullimore et al. 2007), the ability of the model ‘to predict’ ten running parameters was investigated. To do this, the experimental data was used as input parameters for the spring mass model; lower limb length was defined as the height of the greater trochanter above the ground when standing in shoes and contact time, aerial time, velocities and displacements were determined from GRFs. In summary, vertical acceleration was determined by first subtracting body weight from the vertical GRF and then dividing the result by body mass. The trapezoidal method was then used to determine vertical velocity by numerically integrating acceleration with respect to time, and assuming the mean vertical velocity was zero to get the integration constant. Displacement was then calculated by integrating the velocity data. Then the approach angle was varied to give a “symmetrical bounce” (Bullimore et al. 2007). Good agreement ($<\pm 20\%$ of measured value) was found for six parameters, whilst four were overestimated ($>\pm 20\%$) (Table 1). In this investigation, the percentage error was used as the agreement measure.

Table 1 – Level of agreement between model predictions and experimental data as found by Bullimore et al. (2007). Agreement was assessed using a percentage difference: $((\text{predicted value} - \text{measured value})/\text{measured value}) * 100$.

Good Agreement ($< \pm 20\%$)	Overestimated ($> \pm 20\%$)
Stance time	Aerial time
Vertical impulse	Peak CoM displacement (vertical)
Contact length	Change in mechanical energy of CoM
Duty factor	Horizontal impulse (contact)
Stride length (relative)	
Peak force (relative)	

It should be noted that in this study the resting lower limb length, l_0 , was defined as the height of the subject's greater trochanter while standing, an assumption that would underestimate the height of the CoM. This definition has been suggested as a reasonable approximation of the distance between the point of force application (POFA) and the CoM at landing as runners tend to land with a bent knee (McMahon et al. 1987). However, this assumption implies that the POFA is at the heel, and may not be appropriate in the case of forefoot strikers where the POFA would be closer to the ball of the foot and thus longer than if the POFA were at the heel (Figure 11). This suggests that it would be appropriate to state the foot strike pattern exhibited during these kinds of investigations.

The CoM trajectories associated with the predicted GRF curves were not shown. Therefore, it is not possible to infer if they matched well with the experimental data. However, since the peak vertical CoM displacement during stance was systematically overestimated it would imply that the CoM trajectories did not match closely with the experimental data, and that the systematic offset may have been a consequence of the inaccuracy of the definition of lower limb length. As stated previously, during this investigation the approach angle was varied in order to find the solution that gave a symmetrical bounce, a method that would essentially force a smooth CoM trajectory with a minimum at midstance. This in turn would result in the symmetrical force curves described in the paper, given the relationship between GRF and CoM trajectory.

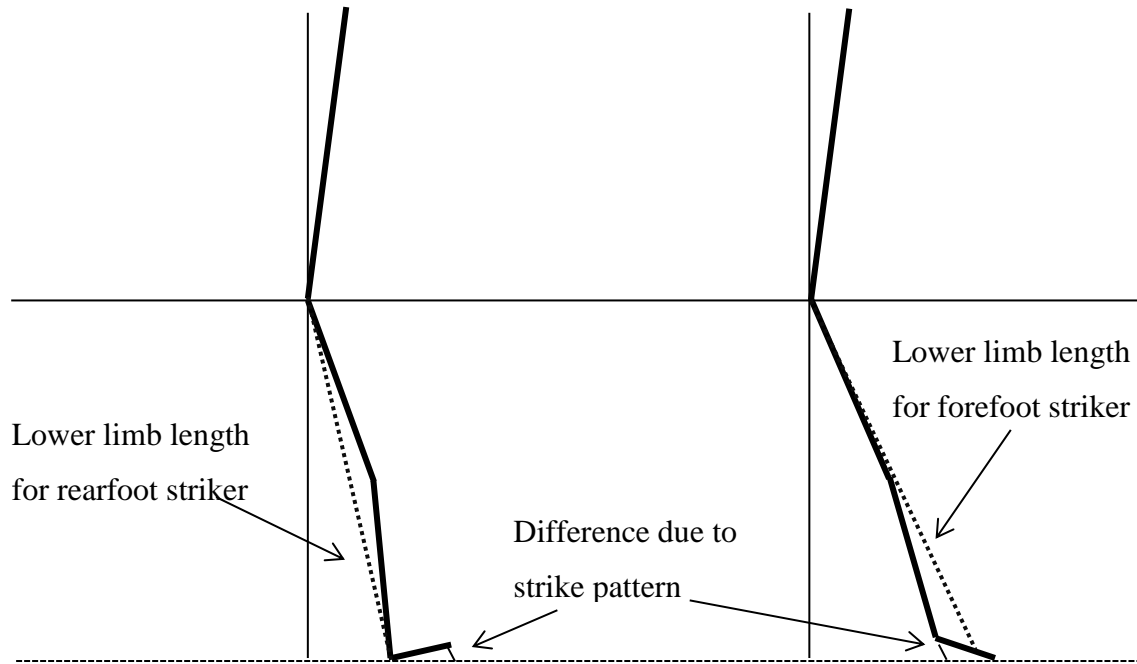


Figure 11 – Example of the influence of the lower limb length definition when considering different foot strike patterns.

More recently, a study sought to determine the ability of the spring mass model at predicting CoM movement over a range of speeds (Lipfert et al. 2012). Experimental sagittal CoM trajectories were compared to model simulations; where the model parameters (resting lower limb length, l_0 and the lower limb stiffness, k_{limb}) were determined via a linear least squares method, fit to the lower limbs force–length curve. The lower limb force, F_{limb} , was defined as a linear function of lower limb length (Eq. 1) and the approach angle, θ_0 , was varied to find the best fitting solution, obtained via the coefficient of determination, R^2 (Eq. 2) (Lipfert et al. 2012):

$$F_{limb}(t) = k_{limb}(l_0 - l_{limb}(t)) \quad 1$$

$$R^2 = \left(1 - \frac{\text{sum of least squares due to error}}{\text{total sum of squares}}\right) \quad 2$$

$$* \left(1 - \frac{|t_{c,exp} - t_{c,mod}|}{|t_{c,exp}|}\right)$$

where $t_{c,exp}$ and $t_{c,mod}$ are the model and experimental contact times, respectively. In cases where the resting length of the lower limb was below the apex height (the highest

point) of the CoM, a characteristic that would imply the system was in flight, the apex height was also varied to find the best fitting solution for each approach angle considered. For running speeds greater than 3 m/s, “*good qualitative agreement*” of the CoM trajectories and GRF curves were found. However, the amplitudes of these curves were consistently overestimated, whilst contact time was consistently underestimated (Lipfert et al. 2012). The sensitivity and inaccuracy of the system to the way in which the initial lower limb length was defined was emphasised by the fact that for the slower speeds the resting length of the lower limb was consistently below the apex height – implying that the system was in fact airborne at the point that should have represented initial contact.

The simple spring mass model and its ability to predict GRF patterns during sprint running was investigated by Clark et al. (2014). Their primary aim was to determine if the fastest human running speeds could be reached using simple, linear spring-like mechanics. Their results showed that the runners that could achieve the fastest speeds applied the greatest mass-specific vertical forces, with patterns that deviated most from the symmetric GRF predicted by the spring mass model. Therefore it was suggested that in order to attain higher speeds, sprinters deviate from simple-spring stance mechanics and adopt an asymmetrical GRF pattern with greater mass-specific GRFs applied earlier in stance (Clark et al. 2014). However, the mechanism by which this is done has not yet been identified. This mechanical solution, common among sprinters, implies that a single most effective mechanism for attaining higher speeds exists.

This result emphasises the risk of using such a simple model, and the derived stiffness variables, to describe stance mechanics at higher speeds. Again, the inaccuracies in the model predictions compared to experimental data are essentially due to the inherent simplicity of the model. For example, the use of the CoP in the definition of the lower limb length can be argued as inappropriate in this case, as its translation during the contact phase is not incorporated into the simple spring mass model; which assumes a fixed point of force application. Furthermore, the linearity of the spring mass model means it is inherently incapable of replicating asymmetrical GRF patterns.

2.4. Limitations of the Spring Mass Model

These previous studies suggest that the spring mass model is able to replicate certain running parameters well, while others are consistently under or overestimated. For example, the model is able to replicate the trajectory of the CoM during the stance phase of running, although the amplitude is often overestimated (Bullimore et al. 2007, Lipfert et al. 2012). Furthermore, the model correctly predicts that shorter contact times follow increases in stride frequency and the peak vertical GRF increase as speed increases (Blickhan 1989). However, the model cannot explain which anatomical structures are used to store and return elastic energy. This implies that the model may contain some of the main contributing characteristics that influence certain running parameters, but lacks the detail, or complexity, to describe others. Therefore, care should be taken when interpreting results. This further suggests that additional complexity is needed for accurately replicating the dynamics of human locomotion. The accuracy of the spring mass model has been shown to depend on the way in which the input parameters are defined (Morin et al. 2005), and requires that parameters be properly adjusted to each other (Seyfarth et al. 2002). For example, the model fails if the lower limb length is shorter at initial contact than during any other point in stance (Lipfert et al. 2012).

2.5. Modifications to the Spring Mass Model

In a further effort to understand running, many studies have adapted the spring mass model by adding complexity. For example, the effects of variable stiffness, multiple rigid and wobbling masses, and a moving point of force application have all been individually examined, and will be explained briefly below.

2.5.1. Variable stiffness

The effect of including variable stiffness during heel strike was investigated using a high-low method, where the vertical stiffness was altered during the stance phase of running (Hunter 2003). The spring mass model in its simplest form predicts a smooth GRF, where

the rate of loading and unloading are essentially symmetrical. However, experimental GRF curves of runners, especially heel-strikers, often exhibit an initial impact peak as well as the main active peak (Figure 12). Therefore, this study aimed to incorporate variable stiffness into the spring mass model and thus better represent the typical GRF profile of heel-strike runners. Vertical stiffness values were determined using the original spring mass model and experimental GRFs. A half cosine wave was then used to model the smooth transition from high (initial) stiffness, through two transition points to low (final) stiffness at the end of stance (Hunter 2003), which was argued to be more representative of the way anatomical structures respond to loading. The authors suggested that this “*variable stiffness*” method matched experimental GRFs more closely than the constant stiffness method, however only vertical displacement and GRFs were considered. These results also suggest that runners that produce an impact peak must have more stiff lower limbs at landing than at take-off. However, the “stiffness” of a passive system cannot be changed, thus “variable stiffness” implies active mechanisms are taking place at initial contact and that an actuator might be more appropriate than a spring for modelling running.

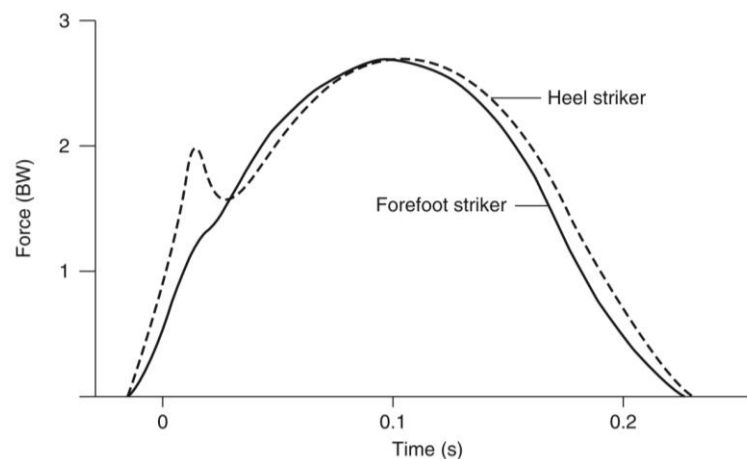


Figure 12 - Example of different GRF profiles depending on running strike pattern (Watkins 2014). Note the existence of the characteristic impact peak in the heel-striker that is not evident in the forefoot striker.

2.5.2. Spring-Mass-Damper models

Spring-mass-damper models were developed with the intention of more accurately representing the human body than the simple spring-mass system. These models made it possible to model the skeleton and soft tissues by using springs and dampers to represent the mechanical properties of the different musculoskeletal components, i.e. muscles, tendons, ligaments and bones. Due to their ability of better representing the mass distribution (a combination of rigid and wobbling masses to represent the bones and soft tissue) of the segments, including the influence of soft tissue movement, these models have primarily been used to investigate the loading and unloading properties of the human body during impact related activities (Nikooyan et al. 2011). However, they tend to investigate the effects in the vertical direction only.

A series of models have been developed with the aim of capturing the characteristic impact peak seen in the vertical GRF of running. A spring-mass-damper system was added to the simple spring mass model (Figure 13) to simulate the components of the body that influence the impact peak of the vertical GRF (Derrick et al. 2000). The upper mass and spring were used to simulate the active peak of the GRF, whilst the lower mass, spring, and damper were used to simulate the behaviour of the components that contribute to the impact peak of the GRF. Similarly, a three degree-of-freedom mass-spring-damper system (Figure 14) was developed to investigate and explain the dissipation and attenuation of the dynamic loading initiated at the point of ground contact (Kim et al. 1994). By using such a model the authors found that varying the damping coefficients of the foot-ground interaction had the largest effect on the dissipation and attenuation of the landing loads (Kim et al. 1994).

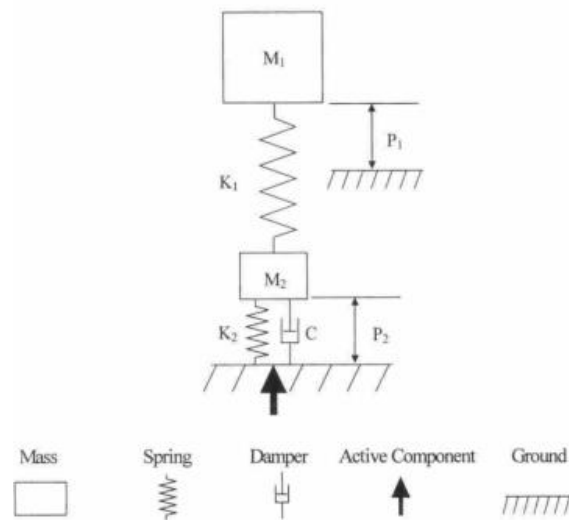


Figure 13 - Modified two-body spring mass model used by Derrick et al. (2000) to simulate the vertical ground reaction forces during human running. M_1 and M_2 are the point masses, P_1 and P_2 the vertical positions, and K_1 and K_2 the spring stiffness of the upper and lower elements, respectively, while C is the damping constant.

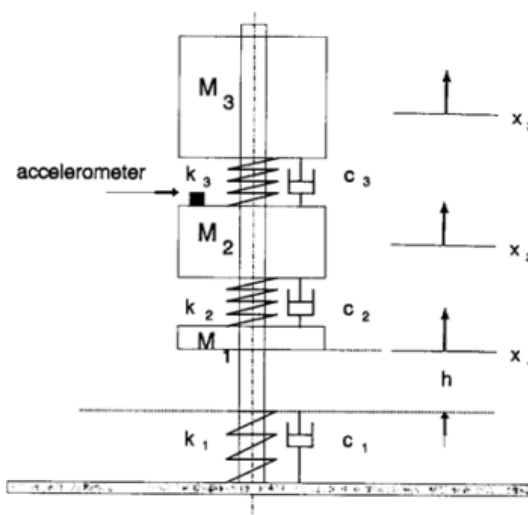


Figure 14 -Three body model used by Kim et al. (1994) to investigate the vertical impact vibrations during running. M represents the mass, k the spring stiffness, c the damping constant and x the vertical positions of the different elements.

This approach of using mass-spring-damper systems has also been used as a way to understand the effects of mass and mass distribution on the GRF during running. The cornerstone of these investigations is the LN (Liu & Nigg) model (Nigg et al. 1999, Liu et al. 2000) consisting of four masses, five springs and four dampers (Figure 15). The original model was used to study both the effects of stiffness and damping coefficients of muscles (Nigg et al. 1999), and of the mass and mass distributions of the body (Liu et al. 2000) on the impact peaks of the GRF during running. Since then, the model has been developed (Ly et al. 2010, Zadpoor et al. 2010) and corrected (Zadpoor et al. 2006). Zadpoor et al. (2006) showed that the simulations produced by the original LN model were incorrect and therefore modified the model parameters to better match experimental data, thus came the LNZN model (Zadpoor et al. 2006, Zadpoor et al. 2007). This model showed how parameters affect the impact peak of the vertical GRF during running, i.e. that the impact peak increases as the touchdown velocities increase, and that the distribution of mass between the upper and lower bodies affects both the impact (lower) and active (upper) peaks in the vertical GRF.

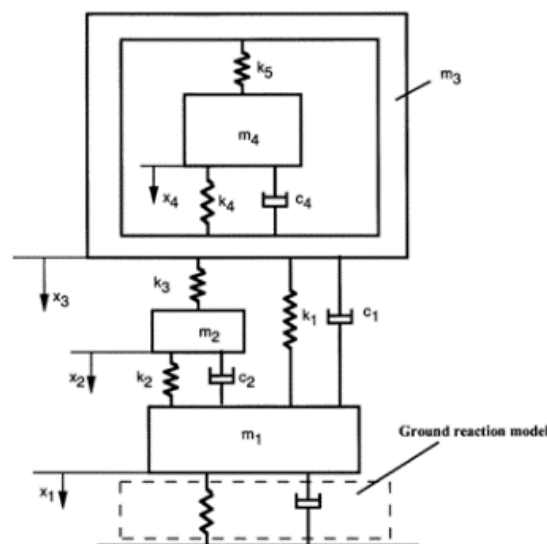


Figure 15 - LN model used by Nigg et al. (1999) to simulate the impact dynamics of heel-toe running. This model consisted of four masses, m_{1-4} , five springs, k_{1-5} , and four dampers, c_{1-4} , with x_{1-4} representing the vertical positions of each of the masses, as well as a separate spring-damper ground reaction model.

Ly *et al.* 2010 replaced the non-linear foot-ground interaction in the LNZN model with a bi-layered spring-damper-mass model (Figure 16) to “better represent” the interaction between the shoe and the ground. However, because results were only compared to previously published data, without clear knowledge of the participants or shoe characteristics, it is difficult to determine the true ability of the model. It should also be reiterated that these spring-mass-damper models are restricted to one dimension, and that running is a multi-dimensional movement.

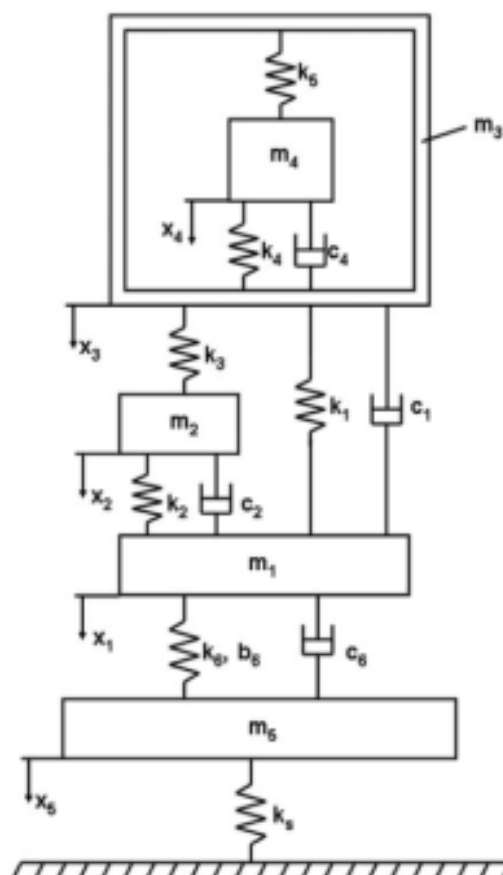


Figure 16 - Five-body modified spring mass model used by Ly et al. (2010). Springs ($k_{3,5}$), spring-damper units ($k_{2,4,6}$, $c_{2,4,6}$) connected rigid masses ($m_{1,3}$) and wobbling mass ($m_{2,4}$). Spring-damper unit (k_6 , b_6 , c_6) connected the lowest rigid mass (m_1) to the shoe rigid mass (m_5) and finally spring (k_5) represents the ground stiffness.

2.5.3. *Moving centre of pressure*

The simple spring mass model assumes a fixed point of contact between the spring and the ground. However, during the stance phase of running, the CoP translates in a proximal-to-distal pattern for rearfoot strikers or a distal-to-proximal-to-distal pattern for forefoot and midfoot strikers (Figure 17). Bullimore et al. (2006) aimed to determine the mechanical consequences of this translating CoP movement using a modified version of the spring mass model (Figure 18). This was done by incorporating a shift, equal to the distance of the force translation, into the equation for the approach angle and subsequent stiffness calculation. In both the simple model and the modified model the approach angle was then varied to get a solution with a symmetric bounce. If lower limb stiffness was adjusted appropriately, by accounting for foot translation, the modified model and the simple model give very similar outcomes for peak vertical GRF, stance time, contact length and vertical CoM displacement, but the peak horizontal GRF and mechanical work per step were lower (and closer to experimental values) in the modified model (Bullimore et al. 2006). However, this method varies the approach angle to determine a symmetrical stance phase, which effectively alters that lower limb orientation at touch down.



Figure 17 - Example of CoP movement in rearfoot (left), midfoot (middle) and forefoot (right) strikers.

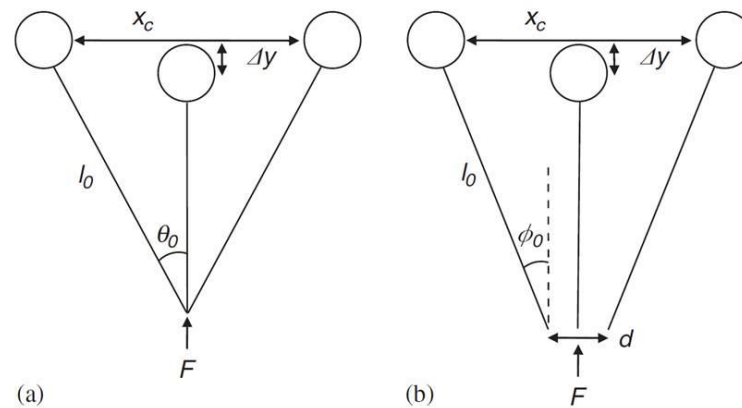


Figure 18 - Spring mass model with and without foot translation (Bullimore et al. 2006). Circles represent the point mass and lines the spring. Peak vertical ground reaction force, F , initial spring length, l_0 , contact length, x_c , peak vertical CoM displacement during stance phase, Δy , magnitude of landing and take-off angles, θ_0/ϕ_0 , and the distance of point of force translation, d .

Maykranz *et al.* (2009) later argued that the CoP in human running moves at a variable rate. Therefore suggesting that the method used by Bullimore *et al.* (2006) was unrealistic for human running. Instead they developed a foot-spring-model consisting of a telescopic spring, representing the thigh and shank, and rigid foot segment which is coupled to the telescopic spring by an elastic ankle joint (rotational spring). This model produced steeper angles of attack, which supposedly counteracted the additional breaking forces induced by the ankle torque at the beginning of stance. The telescopic stiffness associated with loading and unloading of the lower limb also replicated that seen in human running, and since in this model the CoP is a result of lower limb mechanics the authors argued that it replicated human running more closely than that of a translating point of force application (Maykranz *et al.* 2009). However, due to the uncoordinated nature of the ankle (rotational) and leg (telescopic) springs in this model, there is unsynchronised extension of the springs during unloading (Maykranz *et al.* 2009). This is uncharacteristic of human running where the knee and ankle release elastic energy almost in sync, and thus suggests a need for a model where unloading of the knee influences unloading of the ankle joint, and vice versa.

2.5.4. Bipedal models

The symmetry of the running gait cycle means that most theoretical models tend to consider only one of the lower limbs. However, when it comes to practical running machines both sides must be considered. These models primarily offer a framework for the design of robotics, and thus can provide useful information about fundamental mechanics used in running. Using a model comprised of massless semi-circular feet, straight limbs of arbitrary mass (representing the thigh and shank) and a point mass at the hip (Figure 19), McGeer (1990) investigated the mechanisms behind passive bipedal running. Each limb included a massless translational spring parallel to its axis, allowing for compression during stance and rebound during swing. While the hip included a torsional spring which allows the limbs to move back and forward in a ‘scissor’ like action (McGeer 1990). When on a decline, no force is required for such a model to run and with careful tuning it is possible for the energy consumption to approach zero. In cases of alternative terrains, the model can be ‘pumped’ to maintain its running pattern, and if necessary by using simple control laws a stable pattern can be enforced (McGeer 1990).

Despite its simplicity, this model shows it is possible to simulate a full running gait cycle using purely passive elastic structures, implying that the storage and return of elastic energy is a fundamental characteristic of running. However, we know that running is not a passive movement and that energy cannot simply be pumped into the system; therefore, an effort has been made to investigate which muscles, tendons, ligaments, etc. are storing and returning elastic energy as well as the influence of the bi-articular configuration of springs, as muscles, during running.

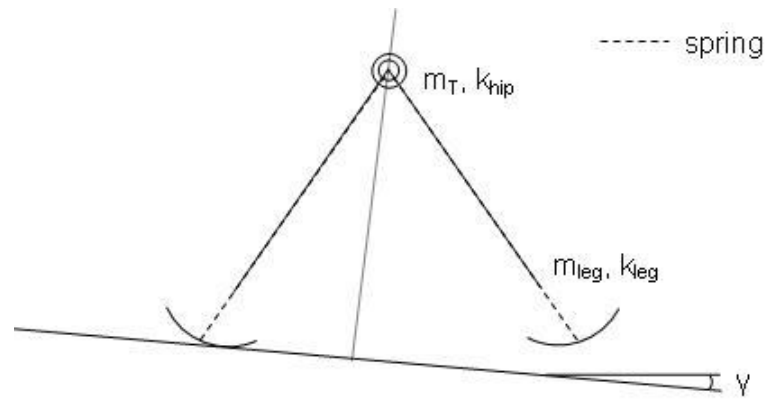


Figure 19 - Passive bipedal running model designed by McGeer (1990). The limbs have arbitrary mass, m_{leg} , and compress telescopically via linear springs, k_{leg} . The point mass at the hip, m_T , approximates the torso, and the torsional spring at the hip, k_{hip} , allows the limbs to swing back and forth. The feet are modelled using massless rigid semicircles, and γ indicates the incline of the surface.

The spring mass model combines the effects of musculoskeletal components and assumes linear elasticity in a single spring. Although such an assumption may allow for human like trajectories of the CoM, it fails to provide information about how the individual components of a segmented limb behave. Iida et al. (2008) developed a minimalistic model to investigate the behaviour of compliant elements of muscle-tendon systems during human walking and running. The model consists of an actuated hip joint, as well as four linear tension spring connected across passive knee and ankle joints to represent the biarticular nature of the musculoskeletal system. This biarticular arrangement allowed for energy efficient self-stabilisation of the model (Iida et al. 2008).

This model was able to reproduce the rudimentary patterns of human locomotion, including both joint kinematics and GRFs. However, it should be noted that the velocities investigated for “running” were very slow and the pattern produced by the model was more akin to hopping or skipping than human running (Figure 20). Furthermore, although this model appears to predict running well, the simulations are only qualitatively compared to experimental data of human running. For example, the magnitudes of the vertical GRF and CoM trajectory appear to be under- and over- estimated, respectively. It could also be argued that this model verges on the complex, and that a more comprehensive understanding of the individual contributions of each joint is required before introducing

bi-articular muscles; reinforcing the importance of sequentially adding complexity to models.

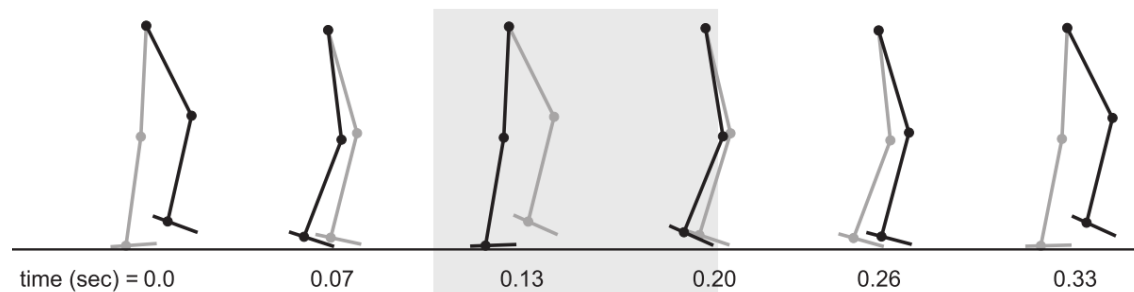


Figure 20 - Bi-pedal model with compliant limbs used by (Iida et al. 2008) to study the influence of bi-articular muscles during walking and running. The model is comprised of three limb segments connected via hinge joints, and an actuator at the hip. Tension springs are attached across the joints and two ground contact points are located on the foot segment.

2.5.5. Limitations of the modified models

Each modification to the simple spring mass model brought with it an additional level of complexity and thus allowed for investigations into new aspects of running. These models have shown that, to an extent, it is possible to better represent various aspects of running with relatively simple adjustments to the spring mass model. However, it should be noted this also meant a new set of limitations. Be it a restricted speed range, CoP transformations, or the way in which the foot interacts with the ground. Therefore, in order to overcome these limitations and understand how and why people run the way they do, these models need to be further adapted and modified. Previous studies have not sequentially added complexity; however this approach offers a means of identifying the influence of each layer of complexity and thus may provide better insight into how and why people run the way they do. It should then be possible to determine the point at which a simple model is sufficiently complex to describe the fundamental mechanisms of normal distance running.

2.6. Questions Still Unanswered by the Modified Models

The simple spring mass model and the various modified spring mass models have been used to investigate some of the basic principles of human locomotion. However, there are still many questions about how and why individuals run the way they do. For example, although efforts have been made to improve the understanding of the role of bi-articular muscles during running (Iida et al. 2008), it is still unclear which muscle directly contribute to the storage and return of elastic potential energy. There have also been a larger number of investigations into the impact peak of the vertical GRF (Zadpoor et al. 2007, Ly et al. 2010, Addison et al. 2015), but these have often focused on the relationship between, and influence of, vertical and shoe/ground stiffness. Furthermore, few comments have been made about the influence of the foot strike pattern on the accuracy of these running models, and what adjustments should be made to account for the differing biomechanical characteristics associated with the different foot strike patterns.

Fundamentally, these models still cannot explain the differences in the running biomechanics between humans. This may partly be due to the inherent complexity of the musculoskeletal system. This, with the advent of newer technologies and increased computing power, has led to a jump towards complex musculoskeletal models. These models are generally developed with the aim of identifying the individual contributions of anatomical structures to a certain movement. However, by sequentially adding complexity to the spring mass model, an approach that will be used for this PhD, there is the potential to address some of these unanswered questions. This sequential approach could aid in identifying the mechanical features that contribute to specific biomechanical characteristics of running.

2.7. Complex Models of Running

Unlike simple models, which are either one- or two-dimensional, complex models generally consider all three planes of movement. These multi-segment, multi-degree-of-freedom models aim to incorporate all the major anatomical components contributing to movement. Fundamentally, what to include in the model will depend on the intended use of the model (Yeadon et al. 2007). Therefore, brief overview of the components of

musculoskeletal models will be discussed prior to a discussion of complex running models.

2.7.1. Components of complex models

As a general rule, models designed to investigate human movement consist of a series of rigid segments. These rigid segments represent the basic structure of the human body, incorporating geometric data and inertial properties characteristic of the limb being modelled. Rigid segments are connected by joints. Joints are typically assumed to be frictionless, with adjacent segments sharing a common axis or point (Yeadon et al. 2007). The choice of which joint to use is again dependent on the model and the movement being modelled. For example, pin joints allow rotation about a single axis, and may be appropriate for modelling a knee, while a ball-and-socket joint allows rotation in all three planes of movement and is likely more appropriate for modelling a shoulder.

Muscles in musculoskeletal models are often modelled as musculotendon actuators using a Hill-type muscle model (Hill 1938). This model consists of three components, the contractile element (CE), the series elastic element (SEE), and the parallel elastic element (PEE) (Figure 21). The CE is the “active” component that converts signals from the central nervous system (CNS) into force. The amount of force produced by the CE depends on its mechanical characteristics, such as the muscle length, muscle velocity and muscle activation dynamics (Yeadon et al. 2007, D. Gordon E. Robertson et al. 2013). The SEE consists of elastic elements in series with the CE, and so any force that the CE produces acts across the SEE. Whereas, the PEE consists of elastic elements in parallel with the CE, and accounts for the inactive elastic response (lengthening) of a passive muscle to an applied external force (D. Gordon E. Robertson et al. 2013).

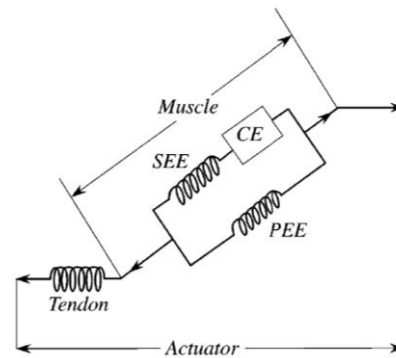


Figure 21 - Schematic diagram of a musculotendon actuator (Pandy 2001). *CE* represents the contractile element, *SEE* the series elastic element and *PEE* the parallel elastic element.

It is also necessary to consider the interaction between the body and the environment. One option is to use the rigid constraint approach, where the motions of one or more points of the body are constrained so that movement only occurs about one point (Pandy et al. 1990, Neptune et al. 2000). However, this approach may not be appropriate for modelling the ground-foot interaction in locomotion, as the number of independent degrees-of-freedom would change as the foot transitioned during stance. An alternative approach would be to use a compliant constraint. This consists of using a series of viscoelastic elements placed at one or more points on the plantar aspect of the model's foot segment. The force at each contact point is proportional to the amount the element is compressed and the velocity at which it is compressed (Gerritsen et al. 1995, Cole et al. 1996).

2.7.2. Complex model analysis and simulation

At this point one must consider how the skeletal and musculotendon dynamics can be combined to produce a model of movement. There are two fundamental methods by which this can be achieved, inverse dynamics analysis (IDA) (Figure 22) and forward dynamics analysis (FDA) (Figure 23). The intended use of the model determines which type of method is most appropriate.

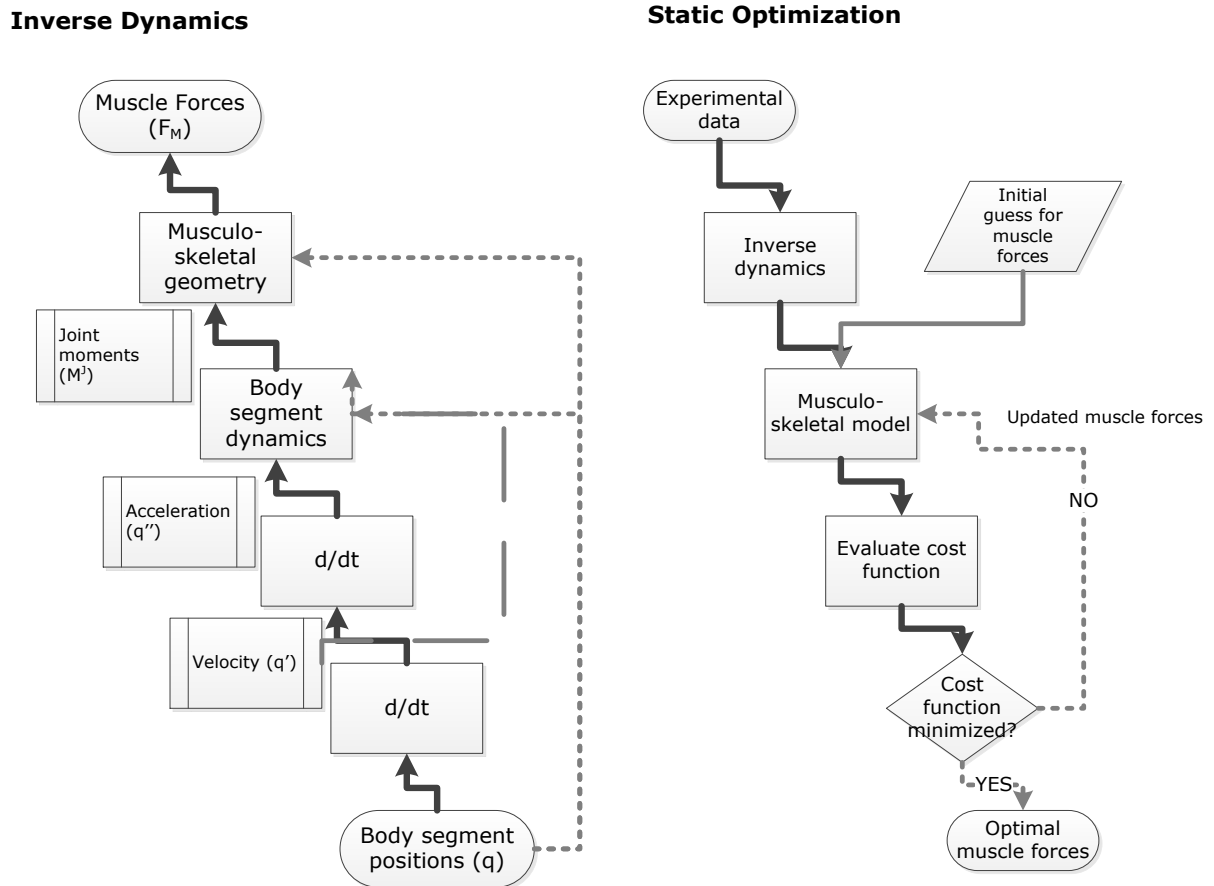


Figure 22 - Overview of IDA and static optimisation (D. Gordon E. Robertson et al. 2013).

Inverse dynamics uses body segment positions, velocities, accelerations and external forces to determine internal joint moments. IDA is derived from Newton's second law ($F=ma$) and is often used in conjunction with static optimisation (SO). SO solves a unique optimisation problem (cost function), at each instant in time, in order to calculate forces in individual muscles which are compatible with the joint moments. The validity of the result is explicitly dependent on the accuracy of the input data (D. Gordon E. Robertson et al. 2013). There are inherent errors associated with motion capture systems used for collection of experimental data, and these errors can be amplified during processing, which can result in significant errors in the calculated values of the net joint torques and subsequent estimates of the muscle forces. Another limitation associated with static optimisation is that due to the independent nature of the solutions, non-physiological switching on and off

of muscle forces can occur for sequential time increments. Finally, if physiological constraints are not included in the model, it can also result in unrealistic solutions for the muscle forces (D. Gordon E. Robertson et al. 2013).

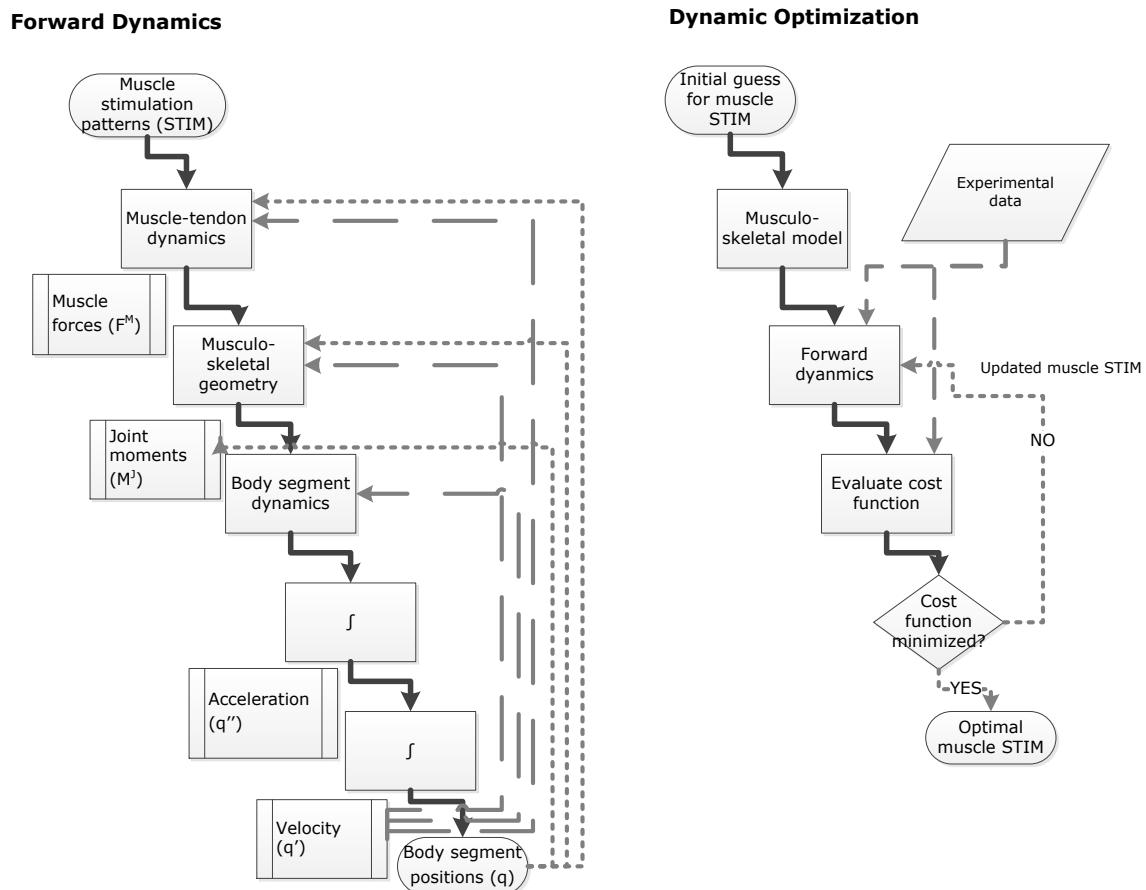


Figure 23 - Overview of FDA and dynamic optimisation (D. Gordon E. Robertson et al. 2013).

Forward dynamic analysis uses muscle excitations (activation potentials) to determine the motion of the body. FDA is often used in conjunction with dynamic optimisation, which solves one optimisation problem for the whole movement - so the cost function can only be determined after one complete cycle (D. Gordon E. Robertson et al. 2013). An advantage of dynamic optimisation is that it allows predictions of movements for which no experimental data exists, since experimental data is not required to obtain a solution. However, given that solutions to dynamic optimisation involve the simulation of the whole

movement, it is generally more computationally demanding than static optimisation. Dynamic optimisation can also be used to solve a tracking problem, where experimental data (kinematics, kinetics, EMG) is tracked by the model and hence the resulting motion should closely match the way in which humans actually move (D. Gordon E. Robertson et al. 2013). The main limitation of this tracking method is that it compromises the predictive power of dynamic optimisation; however, this method also improves convergence (Pandy 2001) – a benefit that may outweigh the limitation depending on the investigation.

2.7.3. Complex models of running

In recent years there have been a few complex models designed to investigate running. These models have been developed using OpenSim, freely available open-source musculoskeletal modelling software (Delp et al. 2007) that allows users to develop and analyse dynamic simulations of human movement. For example, Hamner et al. (2010) aimed to investigate how individual muscles contribute to both propulsion and support, and thus the motion of the CoM, during running. The model developed was a three-dimensional, subject-specific, full-body representation; consisting of 29 degrees-of-freedom (dof), 12 segments and incorporating 92 musculotendon actuators to represent 76 muscles of the lower limb and torso (Figure 24) (Hamner et al. 2010).

In this model, the hip and lumbar spine were modelled as a ball-and-socket joints (3 dof), the knee as a custom joint (1 dof) and the ankle and elbow joints, and forearm rotation, as revolute (pin) joints (1 dof). The lower extremity and back joints were actuated by 92 musculotendon actuators, while the arms were driven by torque actuators. The foot-ground interaction was modelled using a rolling constraint and a non-penetrating unilateral constraint. These restricted slipping and twisting, and stopped the foot passing through the floor but allowed it to lift off the floor (Hamner et al. 2010).

Inverse kinematics was used to solve for joint angles, minimizing the difference between a virtual marker set, attached to the scaled model based on anatomical landmarks, and the experimental marker set (Hamner et al. 2010). The joint moments required to replicate the motion were then determined using a residual reduction algorithm (Hamner et al. 2010). This involves using the inverse dynamics solution and tuning the joint kinematics and

model mass properties to reduce the magnitude of the residuals (Delp et al. 2007). The corresponding muscle excitations were then calculated using a computed muscle control algorithm; this incorporates static optimisation as a means of resolving the muscle redundancy problem (Delp et al. 2007). Computed muscle control also estimated the initial conditions for each muscle, by solving a static optimisation that used experimental kinematics and kinetics to find a solution where muscle fibre and tendon force equalled the musculotendon force (Hamner et al. 2010). Constraint conditions, consisting of one position and three velocity constraints, were applied to allow simultaneously solving of constraint forces and system accelerations. Finally, an ‘induced acceleration analysis’ determined the contributions of individual muscles to the overall CoM acceleration, and the sum of the accelerations due to muscles, gravity and velocity effects were checked to ensure it was equal to the total CoM acceleration (Hamner et al. 2010).

The muscle-actuated simulation was compared to averaged data from previous studies. The simulation was seen to track the experimental joint angles well, and the sum of the joint moments generated by all muscles closely matched the joint moments determined using IDA - after residuals were reduced (Hamner et al. 2010). Simulated activations were compared to the subject’s experimental EMG data, and speed-matched averaged EMG data from a previous study, and showed similar features but failed to account for the anticipatory activations. From this investigation, the quadriceps were found to be the main contributors to both deceleration and support during the braking phase of stance. On the other hand, the soleus and gastrocnemius were determined to be the main contributors to acceleration and support during the propulsive phase of stance (Hamner et al. 2010). Using a model that included the head, arms and torso enabled the quantification of the contributions to mass centre accelerations due to both muscles and arm dynamics. It was shown that by including the arms the dynamic consistency of the model was increased even though the arms did not contribute substantially to either propulsion or braking (Hamner et al. 2010).

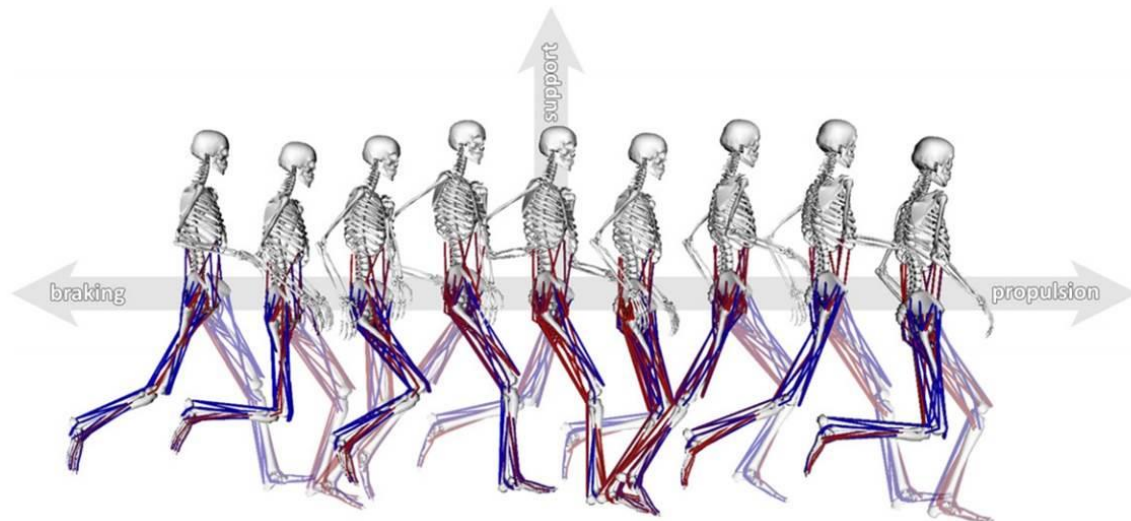


Figure 24 - Full body musculoskeletal model of running developed by Hamner et al. (2010) to study the muscle contributions to propulsion and support. Muscles coloured in red indicate they are fully activated, while those in blue indicate they are fully deactivated. Forward acceleration of the CoM signifies propulsion, backward acceleration braking, and upward acceleration support.

This model appears to provide a lot of information about muscle action during running. However, it should be noted that only a single subject was investigated, meaning that the results may not be generalisable to an entire running population. The same can be said for speed; since only a single speed was investigated, it is not possible to assume that the same movement strategies would be adopted over the large range of running speeds. Furthermore, there is still the question of over-fitting. For example, in order to achieve this simulation, the joint kinematics are tracked, joint moments optimised, joint kinematics adjusted, muscle excitations optimised, and initial conditions revised. This introduces a lot of possibilities for error and leads to the question of how far the model must deviate from the real system for the simulations to work. For instance, due to the large number of variables being incorporated into the optimisation problem, over-fitting might result in certain combinations of variables that portray “successful solutions”, but that are in fact not possible in reality.

More recently, this model by Hamner et al. (2010), was combined with two other OpenSim models to create a full-body lumbar spine (FBLS) model (Raabe et al. 2016). The aim of

this 21 segment, 30 degree-of-freedom, and 324 musculotendon actuator model was to investigate the contribution of trunk muscles to dynamic tasks, such as running. A similar method to Hamner et al., and described in detail by Delp et al. (2007), was used to determine muscle function and joint moments, and it was assumed that the validation of the individual muscle still applied in the combined model (Raabe et al. 2016). To check model parameters, a single experimentally measured moment arm for each muscle group was compared to all corresponding fascicles in the model. However, it should be noted it was unclear which fascicles were represented by the experimental data if multiple fascicles, in a single muscle group, crossed a given joint level (Raabe et al. 2016). Finally, it was assumed that all muscles that could contribute to a joint moment were doing so at full capacity (Raabe et al. 2016), which is likely not to be the case in reality.

Joint angles and moments simulated using this model matched relatively well with experimentally measured values previously published in literature (Raabe et al. 2016). However, it was not possible to validate all muscles included in the upper body, and as simulated data from two subjects were compared, conclusions were based on general trends only. Again, although experimental EMG data and simulated muscle activations showed similar characteristics, the nature of static optimisation meant that anticipatory activations were not accounted for (Raabe et al. 2016). To date, this is the most complex biomechanical model of running, and as such, it highlights some of the key limitations associated with using this type of modelling. These limitations include difficulty in determining muscle parameters, for example, maximum isometric force properties for several muscles had to be adjusted as the experimental (cadaveric) values were found to be too weak for jogging (Raabe et al. 2016). There is also the consideration of computational cost, and accuracy of making the model subject-specific, for example a generic ribcage geometry and spinal curvature was used in this model (Raabe et al. 2016). These, and other, limitations of complex musculoskeletal modelling will be discussed in more detail in the next paragraph.

2.7.4. Limitations of complex models

The inherent complexity of these musculoskeletal models means there are a series of limitations that must be considered. For example, with all musculoskeletal models, muscle

parameters are often based on older studies and data collected from cadaveric studies, so are not necessarily representative of the subjects being investigated. There is also a time cost associated with both model development, making a model subject specific, and with running the simulation, i.e. the optimisation method being used. Generally, the more complex the model, the more complex the optimisation, and the larger the number of parameters that need to be solved for, which can lead to problems of over-fitting, where solutions determined are improbable and may not be representative of the system under investigation.

In many cases, these models are only applicable to the specific conditions under investigation, so the results and conclusions may not extrapolate or apply to a greater population or parameter range. Moreover, constraints are often required for the system to provide reasonable results; and due to the nature of certain optimisation methods non-physiological switching ‘on and off’ of muscle forces can occur for successive time increments. If physiological constraints are not included in the model, it can also result in solutions of muscle forces beyond those capable of actual muscles. Finally, since these models are being used to determine parameters that cannot be directly measured it is innately difficult to validate their results.

2.8. Questions Still Unanswered By Complex Models

Despite the large amount of information that complex models can provide they are more focused on the functioning of specific anatomical components than developing a novel insight into why humans move the way they do. Similar to the existing simple models of running, these complex models fail to explain the why behind the kinematic and kinetic patterns (described in Chapter 1.1.2) observed during running. It is apparent that the simple and complex models both aid in the understanding of human running, but the natural progression in complexity is lacking. These complex models of running have so many components it is difficult to determine which component is contributing to a specific biomechanical effect. On the other hand, most of the simple models do not have enough complexity to identify the musculoskeletal components that contribute to certain biomechanical characteristics. Therefore, there is a reasonable argument to explore the gap between the current simple and complex models. By sequentially adding complex to a

simple model, the individual contribution of each component can be identified, and an argument made as to how these components contribute to how and why people run the way they do.

2.9.Aims and Research Questions

The spring mass model was designed to investigate the fundamental relationships between running parameters and the mechanical variables. By adjusting these mechanical variables (i.e. stiffness, velocity, approach angle), the effects on running parameters (i.e. contact and aerial times and lengths, CoM displacement) could be investigated. However, when compared to experimental data the limitations of the model became obvious (e.g., the spring mass model consistently overestimated the CoM displacement). Furthermore, the sheer simplicity and the associated assumptions of this model mean that certain elements of running cannot be investigated. Therefore, this PhD aims to answer: **is the spring mass model appropriate for modelling running?**

The assumption of a massless linear spring also introduces the concept of lower limb stiffness. In physics, linear stiffness is defined by Hooke's law, where the amount the spring is deformed is directly proportional to the applied force. However, in the literature surrounding running biomechanics various methods are used to calculate this spring (lower limb) stiffness. Therefore, this PhD aims to answer: **do the commonly used methods for determining stiffness, during running, have a clear mechanical (physics) basis?**

On the other hand, the complex nature of musculoskeletal modelling theoretically allows for a variety of running patterns to be adopted. However, the time consuming nature of making these models subject specific means they are often only developed based on one participant, and therefore cannot be taken as representative of an entire population. Additionally, the muscle parameters used within these models are often based on previously published cadaveric data, so the fundamental characteristics of the model may not be representative of the one participant being modelled. Furthermore, the complex nature of the optimisation methods means there is a possibility of misleading results, with successful solutions being determined due to over-fitting of the large number of variables. Therefore, by returning to the idea of the "simpler the better" this PhD aims to sequentially

add complexity to the spring mass model, and hence identify: **the minimum level of model complexity required to accurately describe the kinematics and kinetics of distance running?** By sequentially adding complexity to models there is the potential to identify the key mechanisms that contribute to how humans produce certain kinematic and kinetic patterns. By starting simple and carefully adding complexity, it will be clear as to the contribution of each component, and provide a means of testing optimisation techniques, so we can be confident in their solutions.

Research questions:

- 1) Is the spring mass model appropriate for modelling running?
- 2) Do the commonly used methods for determining stiffness, during running, have a clear mechanical (physics) basis?
- 3) What level of model complexity is required to accurately describe the kinematics and kinetics of distance running?

3. Experimental Data

Data used throughout this PhD had been previously collected at, and made available through, the University of Salford database. This data was used as it comprised of an equal number of elite and recreational runners (classification described below), running overground at a range of speeds⁺. A detailed description of the methods and protocol are explained in Preece et al. (2016) and Mason et al. (2014). An outline of the participants, collection protocol and processing methods will be described below.

3.1. Participants

Kinematic and kinetic data were collected for 28 participants (12 female). Subject demographics are as follows mean (SD): age: 28 (4) yrs., height: 1.75 (0.93) m, weight: 62.9 (9.1) kg. Fourteen participants were classified as elite (10 km personal best of 35 min or less). The mean (SD) 10 km race time of the elites was 32 (2) min (range 30 – 35 min) while that of the recreational runners was 43(3) min (range 40 – 47 min). Signed informed consent was obtained from each participant prior to testing, and the research was approved by the Local Ethics Committee.

3.2. Data Collection

Data were collected while participants ran overground (32 m indoor track) at four different speeds (3.3, 3.9, 4.8 and 5.6 m/s). Three-dimensional kinematic data were collected at 240 Hz using a twelve-camera motion capture system (ProReflex, Qualisys AB, Gothenburg, Sweden). Synchronised kinetic data were collected at 1200 Hz using three AMTI force plates (Advanced Medical Technologies Inc., Newton, MA, USA), 600 mm x 900 mm in dimension and embedded into the track (laboratory floor). In total fifty-eight 15 mm retro-

⁺ Through the University of Salford Running Performance Clinic, a clinical service geared towards recreational runners who want to improve their running biomechanics, I have collected data using a similar protocol, though on a treadmill as opposed to overground. Furthermore, through the Running Performance Clinic I collected and processed a dataset for a study investigating centre of mass movement during running (Gill et al. 2017) - see Appendix AI; and therefore I am familiar with the study design and data collection methods.

reflective markers were placed on anatomical landmarks of the torso and lower extremity (thorax, lumbar spine, pelvis, and lower limbs), this included four rigid cluster plates (of four markers each) placed bilaterally on the participant's shank and thigh (Table 2 and Figure 25). This marker set was used as it allowed for recording and quantifying of the lower limb and pelvic motion as well as the coordinated pelvic-spinal movement during running (Preece et al. 2016, Preece et al. 2016).

A static calibration trial was recorded, during which the participant was requested to stand as still as possible in an anatomically neutral position (Figure 25). Static markers were then removed and participants were given time to warm up and familiarise themselves to running with markers. Dynamic data was then collected, the participant was requested to run along a 32 m track at each of the four speeds (3.3, 3.9, 4.8 and 5.6 m/s). The length of the track ensured that participants had adequate space to accelerate to the required speeds. Running speed was controlled using optical timing gates and 7 – 10 trials were collected for each subject at each speed, where speeds within 2.5 % of the required speed were deemed acceptable. Participants wore their own running shoes during the testing period.

3.3.Data Processing

The data were labelled using Qualisys Track Manager (Qualisys AB, Gothenburg, Sweden) and exported to Visual 3D (Visual 3D Inc., Rockville, MD, USA). Data processing as described in Preece et al. (2016) was used, in which the raw marker data were first low pass filtered (10Hz). Data from Dempster (1955) was then used to approximate CoM positions and velocities of each of the nine segments in the model. Model segments were then approximated as simple geometrical shapes, with diameters and depths determined from marker positions. The pelvis, lumbar and thorax segments were approximated as elliptical cylinders, whilst each of the lower limb segments were assumed to be frusta of cones.

Kinetic data were down-sampled (from 1200 Hz to 240 Hz) and the CoP data was checked as resampling tends to introduce errors in the first and last points. The stance phase was then identified using GRF data, with a cut-off threshold of 20 N. Kinematic and kinetic data were then interpolated to 101 data points, which corresponded to 0-100 % of the

stance phase, and averaged over the participant's number of trials. Data was then exported to MATLAB (R2016a, The MathWorks, Inc., MA, USA) for further analysis. The specific biomechanical data used for each model will be detailed in the following chapters. However, the CoM trajectory, CoP path and GRFs were used for all of the models.

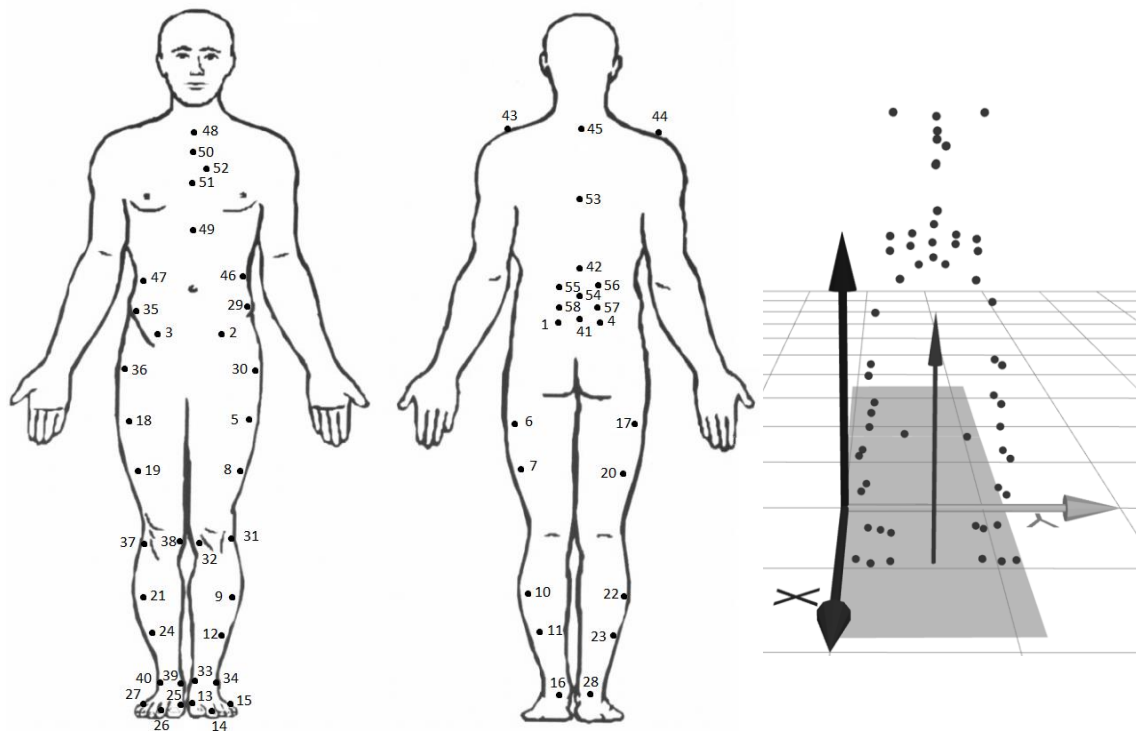


Figure 25 – Anatomical marker positions and QTM static trail showing the marker positions.

Table 2 – List of the markers used for the experimental data collection, * indicates the marker was used for the static trial only.

Marker No.	Marker name	Marker No.	Marker name	Marker No.	Marker name
1	L – Posterior Superior Iliac Spine (PSIS)	21	R – Leg 1	41	L5
2	L – Anterior Superior Iliac Spine (ASIS)	22	R – Leg 2	42	T12
3	R – Anterior Superior Iliac Spine (ASIS)	23	R – Leg 3	43	L – Acromion process*
4	R – Posterior Superior Iliac Spine (PSIS)	24	R – Leg 4	44	R - Acromion process*
5	L – Thigh 1	25	R – First Metatarsal Head	45	C7
6	L – Thigh 2	26	R – Second Metatarsal Head	46	L Rib
7	L – Thigh 3	27	R – Fifth Metatarsal Head	47	R Rib
8	L – Thigh 4	28	R - Calcaneus	48	Jug notch
9	L – Leg 1	29	L - Iliac Crest*	49	X Sternum
10	L – Leg 2	30	L – Greater Trochanter*	50	Sternum 1
11	L – Leg 3	31	L – Lateral Femoral Condyles*	51	Sternum 2
12	L – Leg 4	32	L – Medial Femoral Condyles*	52	Sternum 3
13	L – First Metatarsal Head	33	L – Medial Malleoli*	53	T6
14	L – Second Metatarsal Head	34	L – Lateral Malleoli*	54	L Centre
15	L – Fifth Metatarsal Head	35	R - Iliac Crest*	55	Lumbar 1
16	L - Calcaneus	36	R – Greater Trochanter*	56	Lumbar 2
17	R – Thigh 1	37	R – Lateral Femoral Condyles*	57	Lumbar 3
18	R – Thigh 2	38	R - Medial Femoral Condyles*	58	Lumbar 4
19	R – Thigh 3	39	R – Medial Malleoli*		
20	R – Thigh 4	40	R – Lateral Malleoli*		

4. A Simple Model of Running: Force-Length Relationships and Foot Strike Patterns

4.1. Introduction

4.1.1. The spring mass model

The spring mass model (Figure 26) is the simplest mathematical model that can be applied to bouncing gaits, i.e. running (Blickhan 1989, McMahon et al. 1990, Bullimore et al. 2007). The model is comprised of a single point mass bouncing on a massless linear spring. The mass should be equal to the entire mass of the body and thus characterises the movement of the CoM. The spring, on the other hand, represents the lower limb in contact with the ground, combining the effect of all the relevant joints. Although the model is very simple, it has had success in modelling certain characteristics of running. For example, the model follows an approximately sinusoidal CoM trajectory and, due to the inverse relationship with GRFs, approximately sinusoidal vertical and horizontal GRF profiles are produced (Figure 27) (Blickhan 1989, McMahon et al. 1990, Bullimore et al. 2007, Lipfert et al. 2012). It also exhibits in-phase fluctuations of potential and kinetic energy, a distinct characteristic of bouncing gaits.

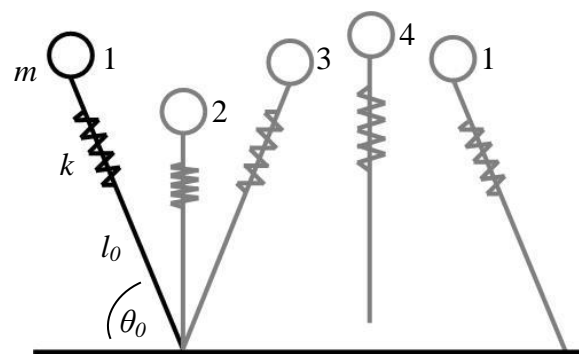


Figure 26 - Simple spring mass model at four phases of the gait cycle: 1) initial contact, 2) midstance, 3) take-off and 4) aerial phase (since a ballistic trajectory is assumed the spring will have no influence during this phase). The initial spring length is denoted by l_0 , approach angle by θ_0 , spring stiffness by k , mass by m .

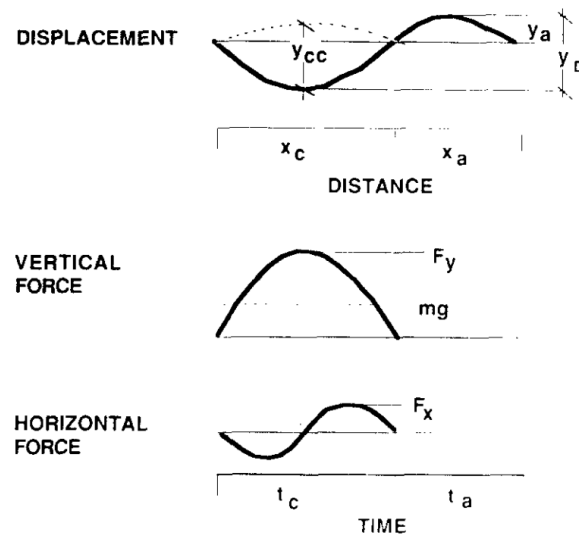


Figure 27 - Simulations using the spring mass model (Blickhan 1989); x_c and x_a indicate the contact length and hopping distance, t_c and t_a the contact and hopping times, y_{cc} the spring compression at midstance (not equivalent to the total vertical displacement, y_D , which is the sum of the stance phase vertical displacement, y_c , and the hopping phase vertical displacement, y_a) and F_y and F_x the peak vertical and horizontal forces, respectively.

Even though the model seems to exhibit some of the main characteristics of running, it consistently overestimates others. For example, in a study comparing published experimental data to spring mass model simulations, aerial time and horizontal impulse, as well as peak vertical CoM displacement and the change in mechanical energy during stance, were consistently overestimated (Bullimore et al. 2007). Therefore, the results of the spring mass model simulations must be interpreted with caution, since, as with all models, it brings with it a series of assumptions and limitations. The system is generally set-up to alternate between the contact phase, where the mass rotates about a fixed point on the ground, and the aerial phase, where the mass travels ballistically. This assumption of a fixed point of rotation obviously cannot model any translation of the centre of pressure under foot during the contact phase. Furthermore, another common assumption, that the contact phase is symmetrical (i.e. the pattern of elongation of the spring in the second half of stance is the mirror image of that of compression in the first half), is uncharacteristic of

running, as depending on the foot strike pattern adopted the lower limb may be more, or less, extended at contact than at take-off (Blickhan 1989).

The most fundamental assumption of this model is that it assumes a human runner acts similar to a single mass bouncing on a massless linear spring. The oscillation of the mass on the spring is said to reflect the movement of the CoM of humans, and other animals, as they run (McMahon et al. 1990, Shen et al. 2015a, Müller et al. 2016). The degree to which the mass oscillates is determined by the characteristics of the spring, the most fundamental of which is its stiffness. This relationship introduces the concept of lower limb stiffness, a parameter that describes the integration of all the individual musculoskeletal components' stiffness values (Brughelli et al. 2008a). It is said to be related to the way in which muscles, tendons, ligaments and other soft-tissue structures control against lower limb collapse during landing (Blickhan 1989).

The concept of lower limb stiffness relies on the key assumption of the model, that the lower limb can be approximated by a passive linear system. This assumption will inevitably be violated due to the complexity of the musculoskeletal system. For example, multiple levers (bones) articulated by joints introduce non-linearities due to their geometric configuration, and lower limb movement is controlled by muscles (active elements) capable of generating energy. Whilst the spring mass model is widely accepted and predicts some of the high-level characteristics of running, it must still be regarded as a hypothesis that needs to be tested against experimental data and this has not been previously attempted. This chapter will aim to test two hypotheses that are based on the physical characteristics of a linear spring. Firstly, that there will be a linear force-length relationship, and second, that there will be no energy loss to hysteresis over the stance phase of running.

4.1.2. Force-length relationships

Stiffness

Stiffness, in linear cases, is described by Hooke's Law. Hooke's law states that the amount an object is stretched or compressed is proportional to the force being applied, and is described by:

$$F = ks$$

3

where F is the applied force, k is a spring dependent constant that denotes its stiffness, and s is the compression or elongation of the spring element (Young et al. 2008). Graphically, the stiffness of an elastic object can be determined from the slope of the force-displacement curve (often referred to as a force-length relationship when discussing a biological system, such as muscles). Applying this to the spring mass model of running, the displacement would be the change in length of the spring, defined as the distance from the point of contact with the floor to the CoM, and the force would be the component of the GRF acting in that direction.

Another way of looking at this is that stiffness refers to the rigidity of an object and the extent to which it resists deformation in response to an applied force. Descriptors such as *rigidity*, *flexibility*, and *compliance* are all complementary concepts that are used describe the stiffness of an object. However, each of these terms have strict definitions in mechanics (Table 3), and their somewhat complacent use can lead to misleading conclusions about how a system works; for example, only the definition of *compliance* refers to linear behaviour.

Table 3 - Definitions of terms (Parker 2003).

Compliance	The displacement of a linear mechanical system under a unit of force
Elasticity	The property whereby a solid material changes its shape and size under action of opposing forces, but recovers its original configuration when the forces are removed The existence of forces which tend to restore to its original position any part of a medium (solid or fluid) which has been displaced
Flexibility	The quality or state of being able to be flexed or bent repeatedly
Rigidity	The quality or state of resisting change in form
Stiffness	The ratio of a steady force acting on a deformable elastic medium to the resulting displacement

The shape of a force-length curve can provide information about the type of system being investigated (Figure 28), i.e. spring (linear and mechanical) vs. muscle (non-linear and

biological). A linear force-length curve indicates a ‘mechanically ideal’ system. Therefore, in terms of the spring mass system, the more linear the force-length relationship, the more appropriate the assumption that the body acts similar to a massless linear spring during the stance phase of running. The strength and direction of a relationship can be measured using a correlation coefficient, r , where a value of 1.0 indicates a perfectly linear relationship. This characteristic will provide one means of testing the first hypothesis, that there will be a linear force-length relationship between GRFs and CoM displacement during the stance phase of running.

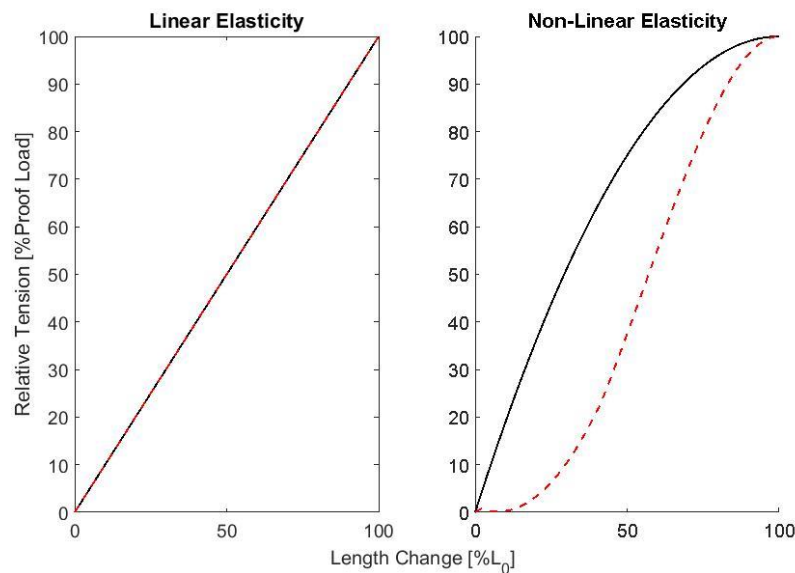


Figure 28 - Example force-length relationships. Here the length change is in relative to the resting length of the system, l_0 , and the relative tension is related to the proof load of the system. The proof load of the system represents the greatest load that can be applied before stretching the system beyond its elastic limit.

Work and energy relationship

Work and energy are interlinked properties. Work is said to be done when the result of a force causing an object to move is a change in the overall energy of the object. It is dependent on the distance that the point of application of the force moves (Young et al. 2008). Physics defines this concept as:

$$W = F \cdot s \cdot \cos\varphi \quad 4$$

where φ is the angle between the applied force vector, F , and the direction of displacement, s . If the displacement has a component in the same direction as the applied force, positive work is done (the energy of the system increases), whereas if the displacement has a component in the opposite direction of the applied force, negative work is done (the energy of the system decreases) (Young et al. 2008).

Energy refers to the capacity for doing work, and can exist in many forms. In terms of mechanical energy, it is the sum of two components; kinetic energy – that which is associated with a moving an object with mass, and gravitational potential energy – that which is associated with an objects potential to do work due to its location in space (Young et al. 2008). However, when describing springs, the elastic potential energy – that which is associated with the storage of elastic energy due to the deformation of an elastic object – must also be considered.

This elastic potential energy refers to the amount of energy that can be stored in a stretched or compressed spring, and is related back to Hooke's law and force-length relationships (Young et al. 2008). According to Newton's third law, if an object applies a force to a spring, an equal and opposite force is applied by the spring on the object, where, k is the spring constant and s is the displacement, i.e. the amount the spring is stretched or compressed.

$$\text{Force applied by the object: } F = ks \quad 5$$

$$\text{Force applied by the spring: } F = -ks \quad 6$$

Work done, W , is the product of the force and the distance over which the force is applied. Therefore, since the change in potential energy is the work done in moving an object a distance, the change in elastic potential energy, ΔE , in the spring can be derived as follows (and can be visualised as, or determined from, the area under the force-length curve) (Young et al. 2008):

$$W = \int F ds \quad 7$$

$$W = \int k \cdot s \, ds \quad 8$$

$$W = \frac{1}{2} \cdot k \cdot s^2 \quad 9$$

$$\Delta E = W = \frac{1}{2} \cdot k \cdot s^2 \quad 10$$

In perfectly elastic springs, the net elastic potential energy change during loading and unloading would be zero. If, however, a spring is not perfectly elastic, there is an energy loss associated with the deformation, known as the elastic hysteresis (Figure 29). It should be noted that positive work is done (work is being done by gravity) if the force has a component in the same direction as the displacement, i.e. the loading path in Figure 29. While, negative work is done (work is being done against gravity) if the force has a component in the opposite direction to the displacement, i.e. the unloading path in Figure 29. If considering the assumption that the body acts like a single linear spring, then the size of the hysteresis loop determines the amount of elastic potential energy lost, ΔE , during each stance phase of running. Therefore, since the average runner strikes the ground approximately 600 times per kilometre (Lieberman et al. 2010), the total loss in elastic potential energy will presumably contribute to the overall energy cost of running. Thus, the size of the hysteresis loop has the potential to allude to the differences in energy losses between specific groups of runners, e.g. those with different foot strike patterns.

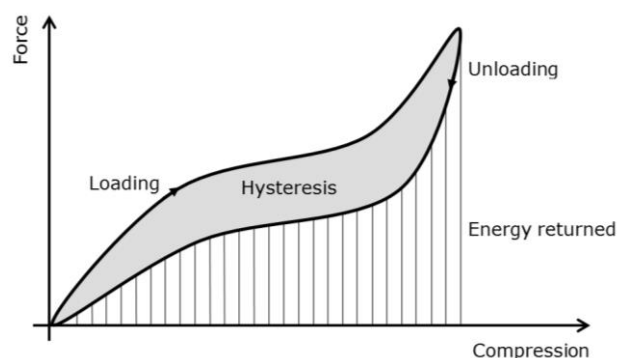


Figure 29 - Example hysteresis loop. Hysteresis determines the amount of elastic potential energy lost during each step, assuming no losses during the aerial phase.

4.1.3. Definition of foot strike pattern

Another assumption of the spring mass model is that of a fixed point of contact with the ground throughout stance. This is clearly an approximation, as during the stance phase of running there is a net proximal-to-distal translation of the CoP. However, it remains unclear how the foot-ground interaction, i.e. foot strike pattern and CoP path, influences the appropriateness of this assumption. Previous authors have argued that incorporating the CoP translation into the spring mass model, either by introducing an ankle spring and rigid foot segment (Maykranz et al. 2009) or including a horizontal shift in the equations of motion (Bullimore et al. 2006), provides a better representation of experimental data. However, neither of these studies considered the results in terms of a specific foot strike pattern.

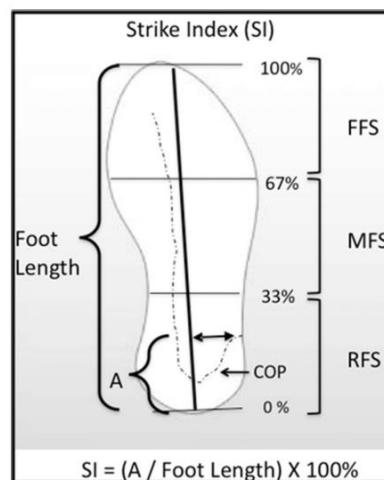


Figure 30 - Foot strike index (SI) calculation (Altman et al. 2012). The SI represents the location of the CoP, at initial contact, as a percentage of the foot length, along the longitudinal axis of the foot coordinate system (A).

In running literature, three primary foot strike patterns (forefoot, midfoot and rearfoot) have been used to describe the way in which the foot contacts the ground. These categories were chosen to quantify the location of the CoP at initial contact (Cavanagh et al. 1980).

The foot strike index (so termed by Cavanagh et al. (1980)) is then an indication of the CoP at initial contact, along the longitudinal axis of the foot's coordinate system, normalised to the foot length (and multiplied by 100 to get a percentage) (Altman et al. 2012). A strike index between 0 and 33 % is said to indicate rearfoot strikers, greater than 33 % and less than 67 % midfoot strikers, and equal to or greater than 67% forefoot strikers (Figure 30). However, to ensure sufficient statistical power foot strike patterns are sometimes grouped by combining two of the three groups into one (i.e. midfoot and forefoot (Gruber et al. 2013, Ogueta-Alday et al. 2014)).

Different runners have different foot strike patterns. Approximately 89 % of distance runners are thought to be rearfoot strikers, which may be partly attributed to the large amount of heel cushioning in conventional running shoes (Lieberman et al. 2010, Almeida et al. 2015). On the other hand, the forefoot strike pattern is generally associated with faster running and sprinting (Almeida et al. 2015). Between runners, there is large variability in biomechanical parameters, which may be attributed to the different strike patterns being adopted. For example, stride length, ankle angle at initial contact, knee flexion range of motion, and knee internal rotation at initial contact have all been shown to be significantly different between rearfoot and forefoot strikers (Williams et al. 2012, Almeida et al. 2015, Thompson et al. 2015, Kuhman et al. 2016). Furthermore, forefoot strikers tend to exhibit significantly shorter contact times and lower peak internal knee abduction moments than rearfoot strikers (Kulmala et al. 2013). In addition, a significant foot strike main effect was found for ankle dorsiflexion, ankle plantar flexion, and knee extensor moments (Kuhman et al. 2016).

The different foot strike patterns lead to different CoP paths during stance. Rearfoot strikers tend to land on the posterior-lateral side of their heel. The CoP then travels distally along the lateral edge of the foot during the first two-thirds of stance before it begins to move more medially towards the metatarsal heads and terminates on the medial side of the first toe (Figure 31)(Dicharry 2010). On the other hand, forefoot and midfoot strikers follow a more distal-to-proximal-to-distal pattern (Figure 31). The initial distal movement during landing is followed by the proximal CoP movement as the heel lowers to (near) heel contact just prior to midstance. Finally, from midstance to push off there is a rapid distal movement of the CoP as it travels towards the medial forefoot and terminates on the medial side of the first toe (Dicharry 2010).



Figure 31 - Example of CoP movement in rearfoot (left), midfoot (middle) and forefoot (right) strikers.

There are distinct differences in the vertical GRF profiles between forefoot and rearfoot strikers (Figure 32). Generally, rearfoot strikers exhibit impact peaks in their vertical GRF profiles (Figure 32 - top). These impact peaks are a consequence of high magnitude forces (1.5-3 times body weight) and a high loading rate (the peaks occur within the first 50 ms of stance) (Lieberman et al. 2010). Furthermore, considering these high loading rates, there is an accepted association between rearfoot striking and increased risk of injury (Lieberman et al. 2010). However, recently it has been shown that non-rearfoot strikers also exhibit impact frequencies characteristic of the impact transients associated with rearfoot strikers (Gruber et al. 2017). The authors suggested that the time-domain GRF signal hides the presence of these frequencies because the maximum lower extremity segment deceleration occurs later in stance for non-rearfoot strikers than it does for rearfoot strikers. Forefoot strikers tend not to show these high impact peaks (Figure 32 - bottom), and have a lower loading rate than rearfoot strikers; Lieberman et al. (2010) found that forefoot strikers, who habitually run barefoot, had loading rates seven times lower than rearfoot strikers running barefoot, but who habitually run shod, and half that of rearfoot strikers running shod. This resulted in “impact peaks” of the forefoot strikers (habitually barefoot) being three times lower than rearfoot strikers (habitually shod).

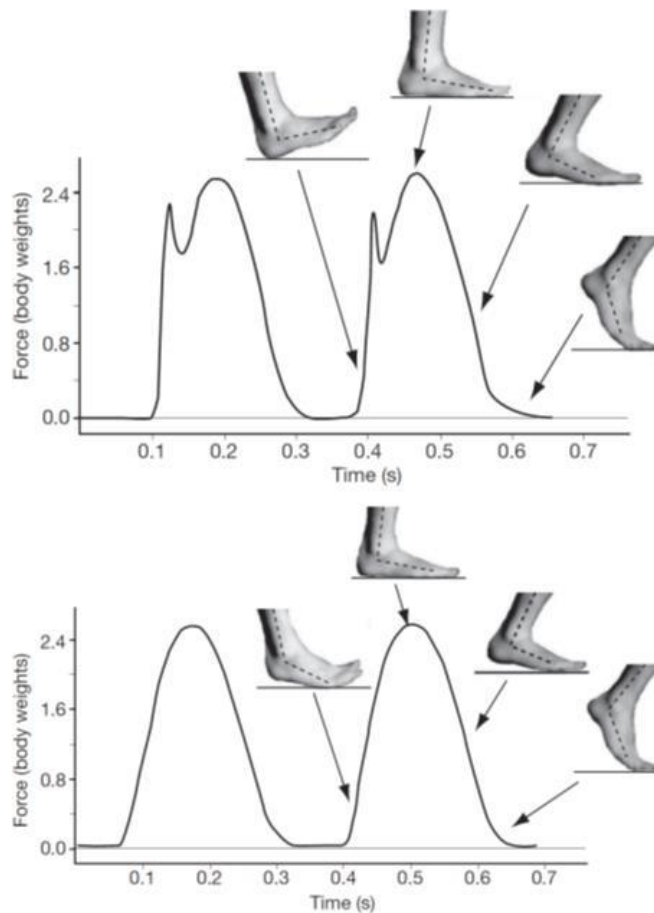


Figure 32 - Typical vertical GRF profiles from rearfoot (top) and forefoot (bottom) strikers running at 3.5 m/s. Characteristic impact peak and high loading rate associated with rearfoot striking are evident in the rearfoot strike profile, but not in the forefoot strike profile. (Lieberman et al. 2010).

4.1.4. Aims

The spring mass model is the simplest model of running and is often used to investigate the relationship between different running parameters. However, the model relies on the assumption that during running, the CoM moves similar to a point mass bouncing on a passive linear spring, and thus that humans exhibit linear force-length relationships. This assumption of linearity has not been previously investigated. Therefore, this chapter aims to identify if the assumption of linear elasticity is appropriate for a range of runners and speeds. To do this, runners will be categorised based on their natural foot strike pattern at four speeds. The degree of force-length linearity will then be quantified and the amount of

hysteresis, the loss of elastic potential energy associated with each step, measured. The variability in the force-length relationships across a cohort of runners will be investigated, and the differences between foot strike groups explored. Fundamentally, this investigation aims to answer the question: Is the spring mass model appropriate for modelling all foot strike patterns associated with running?

4.2. Methods

4.2.1. Experimental data

The full set of previously collected kinematic and kinetic data from 28 participants (12 female, age: 28 ± 4 , height: 1.75 ± 0.93 m, weight: 62.9 ± 9.1) was used for this investigation (see Chapter 3). GRF data, CoP data, and positional data of the hip joint centre (which was taken as a surrogate for CoM position), were extracted from Visual3D to MATLAB for the duration of the contact phase. A detailed explanation of the data collection and processing methods was discussed in Chapter 3.

4.2.2. Foot strike patterns

A preliminary investigation into the distribution of foot strike patterns was carried out for all 28 participants. A scatter plot of the strike index (Figure 33) indicates a clear bimodal distribution in the foot strike index, which is consistent across speeds. For this reason, any participant exhibiting a foot strike index up to and including 33 % was defined as a rearfoot striker, while anyone exhibiting a foot strike index equal to or greater than 50 % was defined as a forefoot striker. Those participants, at a particular speed, exhibiting a foot strike index between these values (34 to 49 %) were excluded from further analysis. Figure 33 shows that only three participants fall into this “middle” group of foot strike indexes, and all these are at speed 3. Furthermore, one of these participants is very much on the border of being classified as a forefoot striker.

An interesting relationship between foot strike pattern and speed also becomes apparent from Figure 33. It appears that some athletes transitioned from rearfoot patterns at the

slower speeds to forefoot strike patterns at the faster speeds (Figure 33 and Table 4). In general, participants had only a small variability in their foot strike index as speed increased; this is evident from the clusters in Figure 33. However, eight participant's transitions from a rearfoot pattern at speed 1, 2 or 3 to a forefoot pattern at speed 4; these are indicated by the dotted vertical lines in Figure 33. Furthermore, three of these eight were those participants who had a strike index between these 34 to 49 % at speed 3.

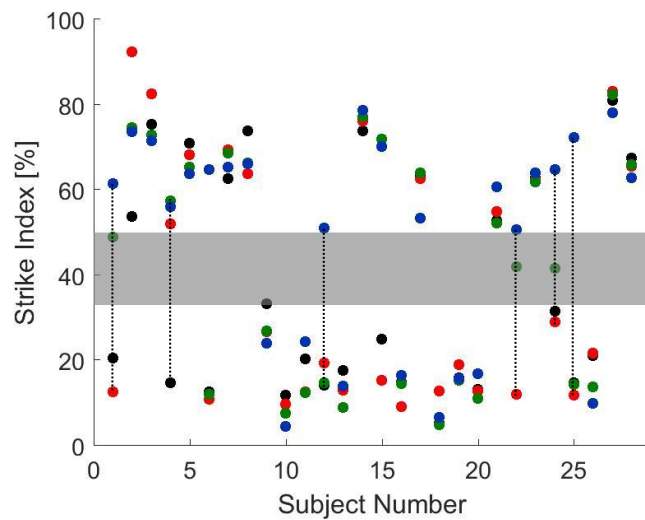


Figure 33 – Scatter plot showing the distribution of the foot strike index among (n=28) participants. The black, red, green, and blue markers represent speeds 1 – 4, respectively. The dotted vertical lines show the participants who transitioned from a rearfoot strike pattern at the slower speeds to a forefoot strike pattern at faster speeds.

Table 4 - Proportion of forefoot and rearfoot strikers at each speed.

	Speed 1	Speed 2	Speed 3	Speed 4
Forefoot	11	12	13	19
Rearfoot	17	16	12	9

4.2.3. Force-length relationships

In this investigation, the lower limb length was defined as the distance from the instantaneous hip joint centre (used as a surrogate for the CoM) to average CoP of the foot (over the stance phase) (Figure 34). In the literature there are a variety of ways in which the lower limb length is defined, including estimating the distance from the CoM to CoP throughout stance (Lipfert et al. 2012) and using the height of the greater trochanter during standing as the resting length and estimating the change in length using the velocity, contact time and the change in vertical CoM position (McMahon et al. 1990, Farley et al. 1996, Morin et al. 2007). There appears to be no clear rationale for choosing one over the other. However, using the CoP as the distal end of the spring violates the assumption of a fixed contact point and essentially changes the spring throughout stance. On the other hand, estimating the length change with the vertical CoM displacement assumes appropriate integration of the vertical acceleration and that maximum spring compression occurs at exactly the point of the maximum vertical GRF, which is not necessarily the case. In contrast, the definition chosen in this investigation satisfies the assumption of the spring mass model, a fixed ground contact point, and provides an in-plane estimate of the CoM. Furthermore, since the Visual3D model used here does not include the arms and head, the estimated CoM will be offset from the anatomical CoM in both the AP and vertical directions (Gill et al. 2017), suggesting using the hip joint centre as an approximation of the CoM movement is appropriate. If and how the definition of lower limb length affects the force-length relationship will be discussed in more detail later (chapter 5.2.2 and 5.3.1).

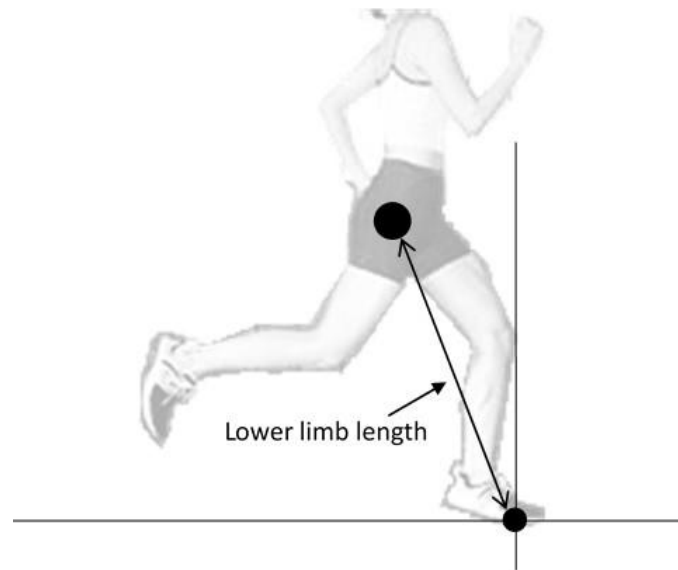


Figure 34 - Definition of the lower limb length.

To address the fundamental assumption of the spring mass model (that the spring exhibits linear elastic properties) force-length relationships for individuals were determined. The lower limb force was calculated as the component of the GRF acting along the line of the lower limb (defined above) from the GRFs, the approach angle of the lower limb and the angle of the resultant GRF (Figure 35, Eq. 11). In this case, x and z are the horizontal and vertical distances between the proximal and distal endpoints of the lower limb, respectively. Therefore, the lower limb force, F_{limb} , was calculated by first determining the resultant GRF, and projecting this vector onto the lower limb axis. It is worth noting that the force perpendicular (F_{perp} in Figure 35) to the lower limb force is neglected in this scenario; a simplification inherent to the spring mass model. Although this perpendicular component would have an influence on the moment acting at the contact point and the rotational velocity of the spring, the contact point is assumed to be a fixed frictionless pin joint and only the relationship between the spring compression and the force acting along the lower limb are considered to be important here.

$$F_{limb} = GRF * \cos \theta_d$$

$$\theta_d = \theta_{GRF} - \theta_0$$

11

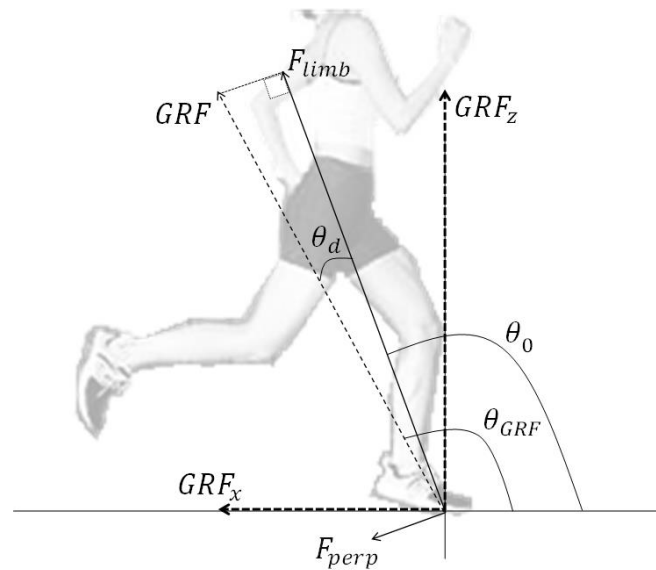


Figure 35 – Lower limb force, F_{limb} , determined by projecting the resultant GRF onto the lower limb axis, where θ_d represents the difference between the resultant angle, θ_{GRF} , and the approach angle, θ_0 .

4.2.4. *Quantifying the linearity of the force-length curve*

Physics defines the stiffness of a linear spring as the ratio between the forces applied along the spring to the spring's deformation. In other words, the stiffness of a spring can be determined from the slope of the line of the force-length curve (Figure 36). Therefore, to assess how much the experimental force-length curves deviated from this assumed linear behaviour, i.e. the linearity, a root mean square residual (RMSr) was calculated. An RMSr between the data for each half of stance and the line of perfect elasticity was determined for each participant at each speed (Figure 37). The “perfectly elastic line” was defined as the straight line between the force-length values at initial contact and midstance (point of maximum compression). When using the spring mass model authors often assume a symmetric stance phase (Blickhan 1989, Morin et al. 2005, Bullimore et al. 2006, Bullimore et al. 2007), and thus ignore the period where the spring extends beyond its resting length. Therefore, to investigate the assumption of an ideal linear system associated with the spring mass model only the period of stance where compression of the “spring” was occurring was considered when calculating the stiffness; the period that was neglected from the calculation worked out as approximately the final 10 % of stance; this was

consistent across participants and speeds. Furthermore, since this last 10 % of stance appears to be similar across subjects and speeds, regardless of foot strike pattern, it is unlikely to significantly influence the ability to detect differences between forefoot and rearfoot strikers.

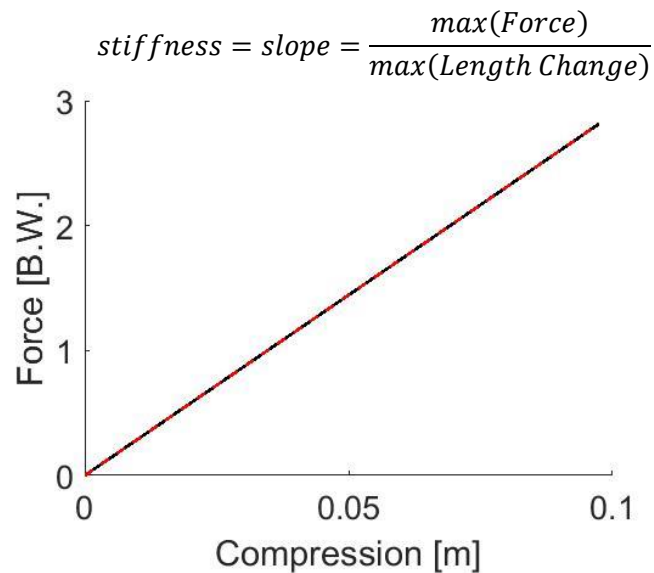


Figure 36 - Typical force-length curve of a linear spring. The slope of the line can then be used to determine the stiffness of the spring.

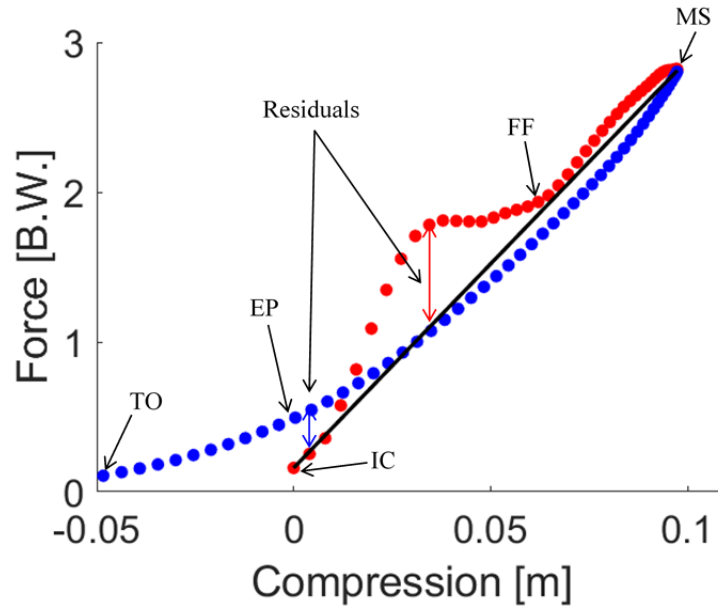


Figure 37 – Example loading (red dots) and unloading (blue dots) force-length data, and the “perfectly elastic line” (solid black line). The “perfectly elastic line” was defined as the straight line between the force-length values at initial contact (IC) and midstance (MS – the point of maximum compression). FF indicates foot flat, EP the endpoint for calculating the RMSr, and toe off is indicated by TO.

4.2.5. *Hysteresis*

Hysteresis was defined as the change in elastic potential energy, ΔE , associated with each force-length curve, normalised to body mass. It was estimated as the difference between the area under the loading and unloading curves (Figure 38). A positive change in elastic potential energy implies absorption, or storage of elastic energy, is taking place with work being done on the runner by gravity. On the other hand, a negative change in elastic potential energy implies generation, or return of elastic energy, with work being done by the runner against gravity. The net change in elastic potential energy, or the elastic potential energy cost, was then defined as the sum of the changes throughout the contact phase (Figure 39).

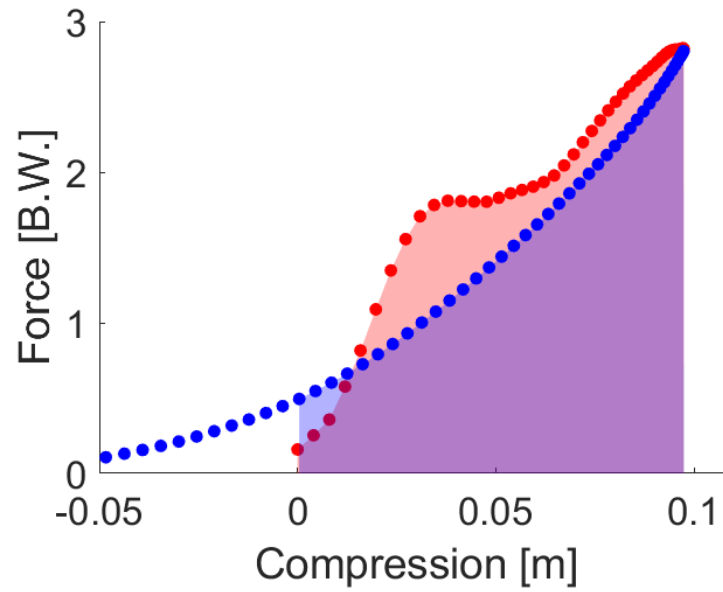


Figure 38 - Example of the area under the loading and unloading portions of the force length curve.

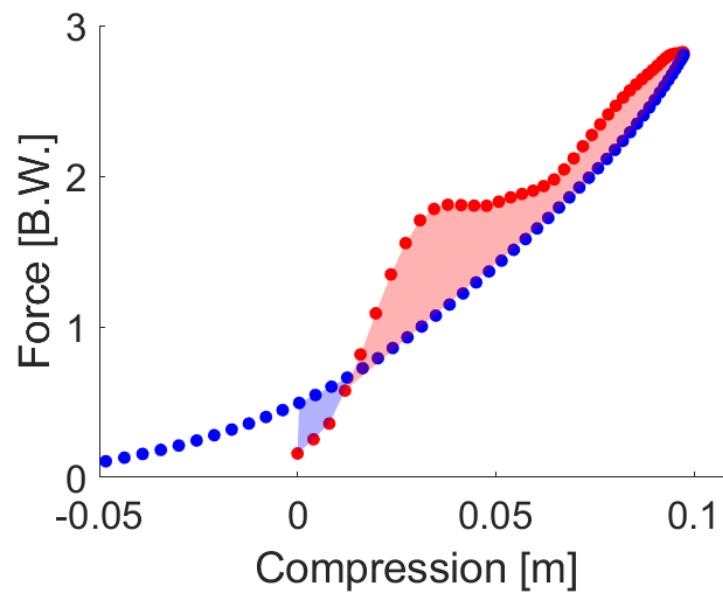


Figure 39 - Example of the hysteresis loop calculated for each participant's force-length curve.

4.2.6. Statistics

Participants were grouped based on their foot strike index. This was done to establish whether obvious trends in the linearity or hysteresis could be solely attributed to the foot strike pattern. As mentioned previously, a foot strike index between 0 and 33 % indicates rearfoot strikers, while a foot strike index equal to or greater than 50 % indicates forefoot strikers.

Statistical analysis was conducted using MATLAB. To compare between foot strike patterns an independent t-test was used for both the linearity and hysteresis measures. The effect sizes (where small, medium and large effects were indicated by values of 0.01, 0.09 and 0.25, respectively) were also calculated as follows:

$$Effect\ size = \sqrt{\frac{t^2}{t^2 + df}} \quad (\text{Field 2009}) \quad 12$$

To address the problem of multiple comparisons, the significance level ($p \leq 0.05$) was corrected for the four speeds, resulting in a new significance level of $p \leq 0.013$. A two-way ANOVA with group vs. speed would have been a better statistical test to use here, however due to the changing number of participants in each group at the different speeds using a two-way ANOVA was not possible. In addition to the t-tests, a correlation analysis was performed to check for the existence of a relationship between linearity and hysteresis and foot strike index. In this case foot strike index was considered a continuous variable, and again considering the four speeds individually, the significance level was adjusted ($p \leq 0.013$). A correlation was considered strong if r great than 0.7, moderate if r was greater than 0.5 and weak if r was greater than 0.3.

As a final method of comparison, MATLAB was used to perform a linear mixed effect analysis of the relationship between both linearity and hysteresis, and foot strike pattern. Foot strike index and speed were entered as fixed effects and subject was added as a random effect, with speed as a grouping variable, with independent intercepts. This random intercept model would account for baseline differences in either linearity or hysteresis, but assume that the effect due to foot strike index would be the same at all speeds. An ANOVA was then used to determine the R-squared, F-ratio and p-value. For

these models a visual inspection of the residual plots did not reveal any obvious deviations from homoscedasticity and normality.

4.3. Results

4.3.1. Force-length relationships

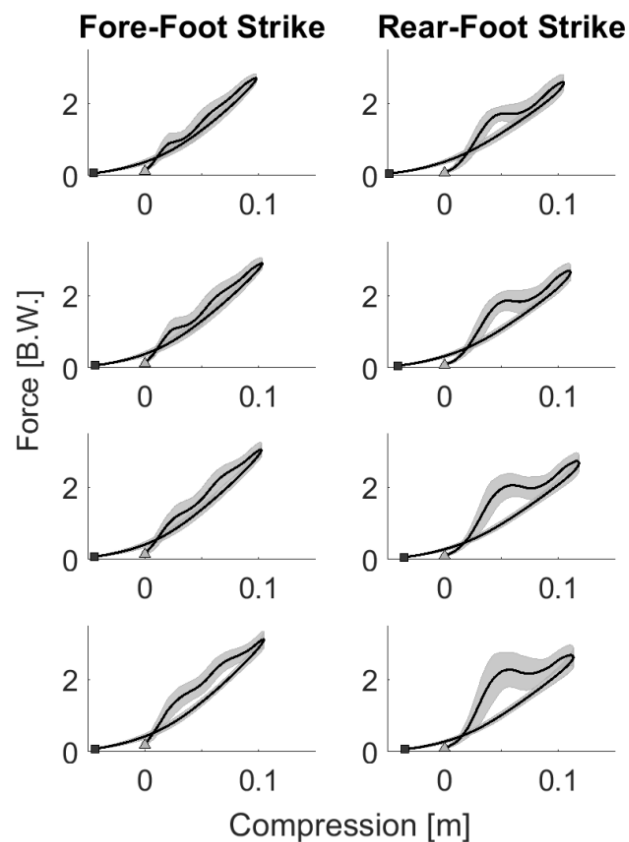


Figure 40 – Mean (solid black line) and standard deviation (grey shaded area) force-length relationships from all participants, separated into the different foot strike groups. Initial contact is indicated by the triangle, while toe off is indicated by the square. Rows (top to bottom) correspond to speeds 1 – 4, respectively.

The ensemble force-length curves shown in Figure 40 indicate a more linear relationship in the forefoot strikers than the rearfoot strikers. This result appears to be consistent across

speeds, however, it should be reiterated that as the speed increased some participants transition from a rearfoot to a forefoot strike pattern. Therefore, the number of participants in each foot strike group changed as the speed increased (17 rearfoot and 11 forefoot at speed 1 compared to 9 rearfoot and 19 forefoot at speed 4).

4.3.2. *Quantifying the linearity of the force-length curve*

The RMSr for the loading phase of stance was consistently higher than that for the unloading phase of stance (Table 5). Furthermore, the RMSr for both loading and unloading was consistently higher for rearfoot strikers than forefoot strikers. This trend was seen at all four speeds. In addition, t-tests revealed significant differences ($p \leq 0.013$) between forefoot and rearfoot strikers for the loading portion of the force-length curve at speeds 1, 3 and 4, and near significance ($p = 0.017$) at speed 2, and no significant differences for the unloading portion at any speed (Table 5). Finally, comparing the effect sizes (Table 5) shows there is a large effect between forefoot and rearfoot strikers for the loading phase (effect sizes > 0.48), while the effect sizes for the unloading phase are all below 0.26.

Table 5 – Mean (SD) RMSr [BW] values between experimental loading and unloading portions of the force-length curve and the “perfect elastic line”.

	Speed 1		Speed 2		Speed 3		Speed 4	
	load	unload	load	unload	load	unload	load	unload
Fore	0.162 (0.082)	0.155 (0.042)	0.170 (0.074)	0.154 (0.057)	0.199 (0.092)	0.158 (0.080)	0.279 (0.122)	0.181 (0.078)
Rear	0.251 (0.082)	0.163 (0.046)	0.280 (0.134)	0.186 (0.065)	0.376 (0.186)	0.183 (0.065)	0.502 (0.249)	0.157 (0.065)
(sig.)	(0.010)	(0.646)	(0.017)	(0.180)	(0.006)	(0.417)	(0.004)	(0.439)
Effect size	0.48	0.09	0.48	0.26	0.54	0.17	0.53	0.15

A scatter plot of the RMSr against the foot strike index for the loading phase of stance (Figure 41) indicates a negative weak-to-moderate relationship. The correlation coefficients were -0.381, -0.396, -0.446 and -0.446 at speeds 1 to 4, respectively. On the other hand, a scatter plot of the RMSr against the foot strike index for the unloading phase of stance (Figure 42) indicates a very weak, and nearly non-existent, relationship at all four speeds. Furthermore, the direction of the relationship was different at the different speeds. The correlation coefficients were -0.012, -0.254, -0.123 and 0.066 at speeds 1 to 4, respectively.

The results of the linear mixed effect model are in agreement with the statistics already presented; where the R^2 value shows that 29 % of the variance is explained by the model. Since this model includes subject as random effects, grouped by speed, it accounts for the changing number of participants. The results of the ANOVA again showed that there were significant effects on RMSr due to both foot strike index ($F_{(1,106)} = 24.62$, $p < 0.001$) and speed ($F_{(1,106)} = 22.67$, $p < 0.001$), for the loading phase of stance. On the other hand, for the unloading phase of stance, less than 1 % of the variance was explained by the model, and the ANOVA was insignificant for both foot strike index ($F_{(1,106)} = 0.81$, $p \leq 0.369$) and speed ($F_{(1,106)} = 0.66$, $p \leq 0.420$).

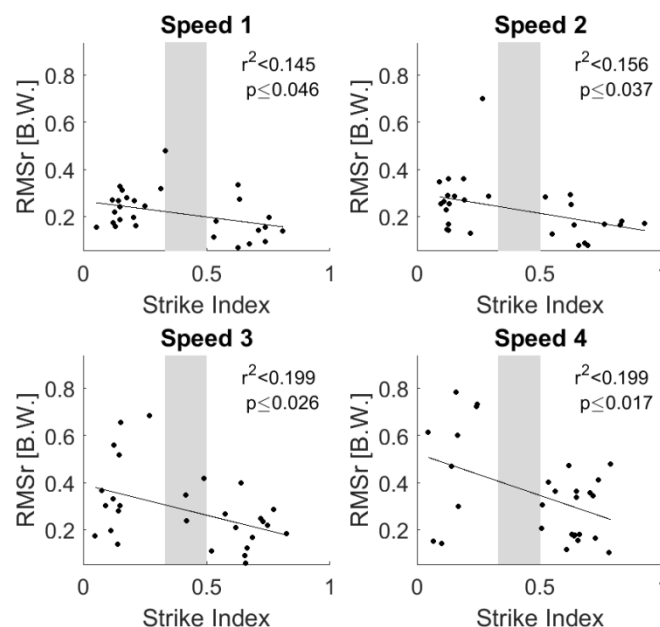


Figure 41 – RMSr [BW] against foot strike index for the loading phase of stance. Grey area indicates the foot strike indexes that were excluded from the analysis.

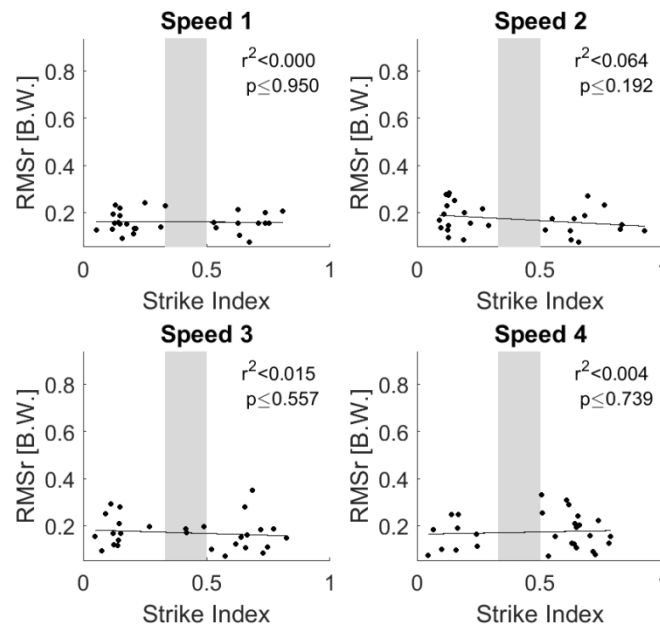


Figure 42 – RMSr [BW] against foot strike index for the unloading phase of stance. Grey area indicates the foot strike indexes that were excluded from the analysis.

4.3.3. Hysteresis

The mean hysteresis values of rearfoot strikers were consistently higher than those of the forefoot strikers across the speeds considered (Table 6). However, there were no significant differences found; although speed 3 appears to be approaching significance ($p \leq 0.029$). This is probably a consequence of the large amount of variability between participants, with the standard deviations ranging between 50 and 86 % of the mean values. Finally, the effect sizes appear to show a moderate effect of foot strike pattern on the hysteresis, therefore with a larger sample size it may be possible that the differences in hysteresis values be significant.

Table 6 - Mean (SD) values of hysteresis [J/kg] from the experimental force-length curves.

	Speed 1	Speed 2	Speed 3	Speed 4
Fore	0.161 (0.095)	0.205 (0.121)	0.259 (0.222)	0.412 (0.208)
Rear	0.201 (0.139)	0.320 (0.202)	0.477 (0.248)	0.567 (0.293)
(sig.)	(0.408)	(0.094)	(0.029)	(0.119)
Effect size	0.16	0.32	0.44	0.30

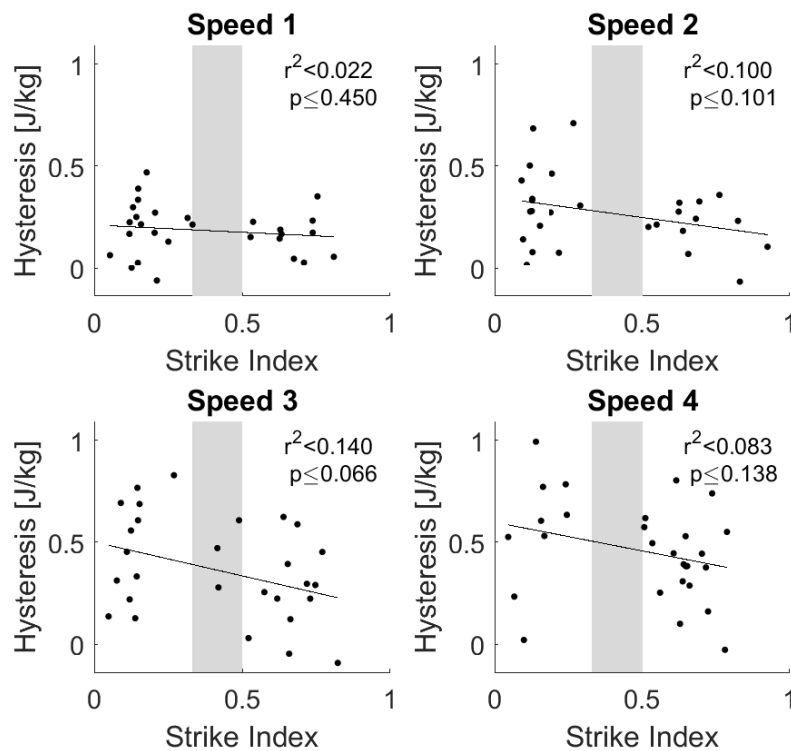


Figure 43 – Hysteresis against foot strike index. Grey area indicates the foot strike indexes that were excluded from the analysis.

A scatter plot of the hysteresis and the foot strike index (Figure 43) implies a negative relationship exists between foot strike index and hysteresis. The overall correlation coefficients (-0.149, -0.317, -0.374 and -0.287 at speed 1 to 4, respectively) indicate a weak relationship at each speed, and none of the correlations are significant. Although the

negative relationship would tend to suggest that the more forefoot strikers exhibit lower hysteresis values, elastic potential energy losses, than rearfoot strikers. Again, since a number of participants transitioned from rearfoot to forefoot strike patterns, as the speed increased, the distribution of the relationship is shifted across the different speeds.

The results of the linear mixed effect model contrast the statistics already presented; where the R^2 value shows that 33 % of the variance is explained by the model. The ANOVA showed there was a significant effect on hysteresis due to both foot strike pattern ($F_{(1,106)} = 13.03, p < 0.001$) and speed ($F_{(1,106)} = 41.94, p < 0.001$). This model considers subject as a random effect with speed as a grouping variable, and thus accounts for the changing number of participants with speed.

4.4. Discussion

A fundamental assumption of the spring mass model is that the human body acts similar to a single, massless, linear spring during the stance phase of running. To investigate this assumption, the relationship between the GRFs (projected onto the lower limb axis) and change in lower limb length was investigated for a range of foot strike patterns and running speeds.

Foot strike patterns

Runners are often classified into three distinct groups: forefoot, midfoot and rearfoot strikers, based on the location of the CoP at initial contact. The analysis presented here of the distribution of foot strike indexes within the participant groups, demonstrated a clear bimodal distribution (Figure 33). Therefore, participants were classified as either forefoot strikers, with a strike index less than or equal to 33 %, or rearfoot strikers, with a strike index equal to or greater than 50 %. Participants with foot strike indexes outside this range, at each particular speed, were excluded from comparisons ($n = 3$ at speed 3). This is a similar approach to other studies, where to ensure sufficient statistical power foot strike patterns have been grouped. It is common for researchers to combine forefoot and midfoot strikers (defined using the conventional thirds-division of the foot) into one forefoot group (Gruber et al. 2013, Ogueta-Alday et al. 2014)).

Interpretation of results

The force-length curves from forefoot strikers appear to be more linear than those from rearfoot strikers. However, there is a large amount of variability in both groups. A visual inspection of the force-length curves suggests that forefoot strikers tend to exhibit nearly symmetrical linear force-length behaviour during loading and unloading of stance (Figure 44). On the other hand, rearfoot strikers appear to show three distinct phases of stance (Figure 44), suggesting non-linear force-length behaviour. The three-phases include a rapid loading phase from initial-contact to 10 % of stance (the impact peak), a phase of relatively constant loading from 10 % to midstance, and a phase of unloading from midstance to take-off.

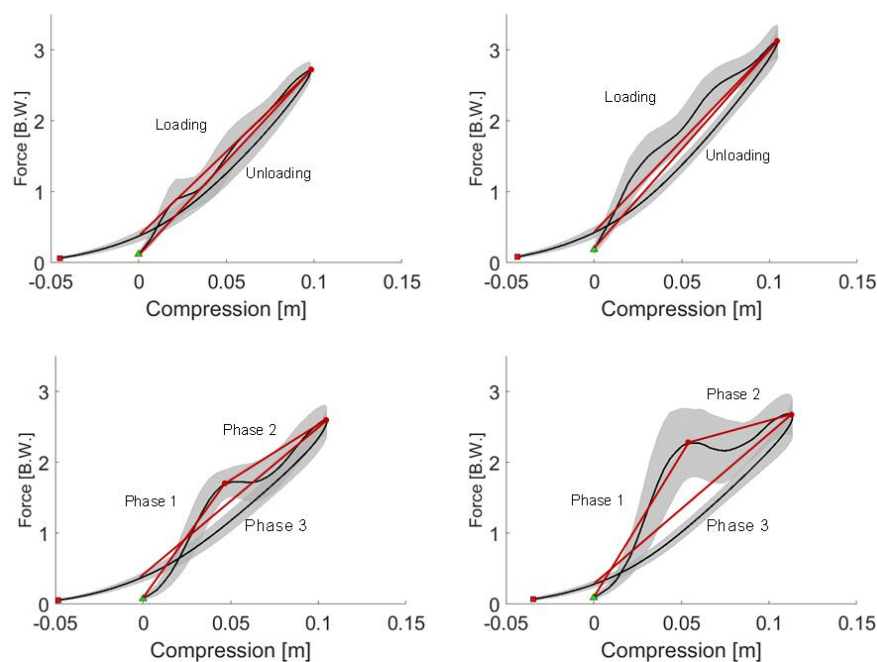


Figure 44 – Mean (solid black line) and standard deviation (grey shaded region) force-length curves of forefoot (top) rearfoot (bottom) strikers at the slowest (left: 3.3 m/s) and fastest (right: 5.6 m/s) speeds. The loading and unloading phases of forefoot running are shown in the top plots, whereas three phases of stance apparent during rearfoot running are indicated on the bottom plots.

Rearfoot strikers consistently had higher RMSr values during loading than forefoot strikers, at each of the speeds considered. Furthermore, although only a weak relationship was found between foot strike index and RMSr, at each of the speeds, significant differences were found between the groups. This finding was reiterated by the results of the linear mixed effects model which showed a significant relationship between both foot strike index and speed and RMSr for the loading phase of stance, but not the unloading phase. This would tend to suggest that the deviation from symmetrical force-length curves occurs as a result of the loading phase of stance. It is likely that since impact transients are often evident in the vertical GRF of rearfoot runners but not forefoot strikers, that this impact transient is the characteristic that causes non-linear force-length behaviour. This result implies that the assumption of a linear force-length curve, and therefore linear stiffness, is generally inappropriate for rearfoot strikers.

The non-linear force-length behaviour found for rearfoot strikers suggests that accurately modelling rearfoot running using a spring mass model is not appropriate. This has likely led some researchers to explore the idea of a “variable” stiffness (Hunter 2003). However, materials do not inherently possess “variable” stiffness. A more physically rigorous approach would be to recognise that non-linear force-length behaviour is a common property of many materials, especially complex structures like the musculoskeletal system. In an ideal system, hysteresis would suggest either dissipation (positive hysteresis) or generation (negative hysteresis) of energy, however the human body is not an ideal system, and thus although the non-linearity of the force-length curve suggests energy is being dissipated and actively generated, it is possible that the hysteresis found here may not be solely due to energy dissipation; as in reality the force is not being applied directly along the limb axis. Therefore, even though still not ideal, the classical spring mass model of running should only be used when investigating runners who exhibit linear force-length characteristics, which this investigation revealed are generally forefoot strikers. This result emphasises the need for classification of participants when investigating running. Unfortunately, many studies do not report the foot strike pattern adopted.

Two published studies have incorporated the use of force-length curves to calculate lower limb stiffness during running (Coleman et al. 2012, Lipfert et al. 2012). One study aimed to compare lower limb stiffness calculated using directly measure kinematic and kinetic methods to other published models (Coleman et al. 2012). However, this study defined the

lower limb from the CoP to the CoM, which inherently changes the “spring” throughout stance, and they only considered the loading phase of stance. On the other hand, the only study to use force-length curves to determine stiffness, and then use this stiffness in a spring mass model of running was Lipfert et al. (2012). However, for this study the CoM movement, and thus the changes in lower limb length, were derived from the GRFs which would again result in the lower limb being defined from the CoP to the CoM. Furthermore, neither of these studies commented on the foot strike adopted by participants, which, considering the results presented here, suggests use of a linear spring may not have been appropriate for their participant population.

Hysteresis

An initial comparison of the hysteresis showed that forefoot and rearfoot strikers had statistically similar elastic potential energy losses per step (Table 6). However, this calculation considered only the first 90 % (approximately) of stance, and concentric work is occurring during the final 10 % of stance. If this final 10 % of stance is included the hysteresis values become smaller (Table 7), however interestingly now a significant difference is found at speed 3, and speeds 2 and 4 appear to approach significance. Furthermore, the linear mixed effects model, where defining subject as a random effect with speed as a grouping variable accounts for the participants changing group, showed a significant effect on hysteresis due to both foot strike pattern and speed. This difference in significance values is likely due to the small number of participants considered. The effect sizes from the t-tests suggest moderate effects across all four speeds; however it is possible the sample size used here was too small for reliable statistical analysis. The linear mixed model overcomes this by considering speed as a random effect, this also accounts for the participants who change foot strike pattern with speed.

Table 7 - Mean (SD) values of hysteresis [J/kg] from the experimental force-length curves (if 100 % of stance is considered).

	Speed 1	Speed 2	Speed 3	Speed 4
Fore	0.071 (0.104)	0.120 (0.130)	0.165 (0.249)	0.321 (0.241)
Rear	0.110 (0.164)	0.268 (0.242)	0.460 (0.283)	0.571 (0.328)
(sig.)	(0.494)	(0.066)	(0.011)	(0.031)
Effect size	0.13	0.35	0.50	0.41

For both forefoot and rearfoot strikers the hysteresis values are positive. This suggests that there is greater net energy absorption over the stance phase for rearfoot runners than forefoot runners. These results imply that forefoot strikers are more efficient at storing and returning elastic energy, and thus over-time this may contribute to a lower energy cost of running for forefoot strikers. There are conflicting results relating energy cost and foot strike pattern in the literature, but the findings here may suggest one aspect of running where there is a distinct difference in energy cost between foot strike patterns.

Comparison with other work

It is interesting then to compare the findings of hysteresis presented here with other research that focused on energy expenditure during running. It has been shown that the range between the most and the least economical runners averaged $20\pm 2\%$ (Lacour et al. 2015). Body composition, testing protocols, and physiological factors account for some of this variability (Saunders et al. 2004a). Furthermore, biomechanical factors, such as foot strike pattern, height, and stride length have also been associated with affecting running economy (Scholz et al. 2008, Perl et al. 2012, Lacour et al. 2015). However, despite this, there is still inconsistency in the general conclusions drawn in terms of running economy and foot strike patterns (Table 8). Some studies state that there are no differences in the energy cost of running between rearfoot and forefoot strikers (Perl et al. 2012, Gruber et al. 2013, Ogueta-Alday et al. 2014, Lacour et al. 2015), while others state that rearfoot strike patterns are more efficient (Williams et al. 1987, Gruber et al. 2013, Ogueta-Alday et al. 2014, Miller et al. 2015).

Table 8 – “Running economy” in forefoot versus rearfoot strike patterns. Oxygen consumptions in represented by VO_2 and cost of transport by O_c .

Author(s)	Variable	Speed(s)	Athletes	Test	Outcome
Williams et al. (1987)	$VO_{2submax}$	3.6 [m/s]	Actively trained runners	Running mechanics vs. running economy	Increases as SI increases
Perl et al. (2012)	O_c [mL·O ₂ /kg/m]	3 [m/s]	Experienced runners (FFS)	Minimal vs. shod FFS & RRS	FFS ≈ RFS
Gruber et al. (2013)	VO_2 [mL/kg/min]	3, 3.5, 4 [m/s]	Experienced runners (FFS & RRS)	FFS & RRS	FFS ≈ RFS FFS > RFS
Ogueta-Alday et al. (2014)	VO_{2max} [mL/kg/min]	3.1, 3.6, 4.2 [m/s]	Sub-elite distance runners (MFS & FFS)	MFS vs. RFS	MFS ≈ RFS MFS > RFS
Miller et al. (2015)	44 cost functions	3.17 [m/s]	Simulations	Cost function minimised by strike patterns	RFS minimised cost (57 %)

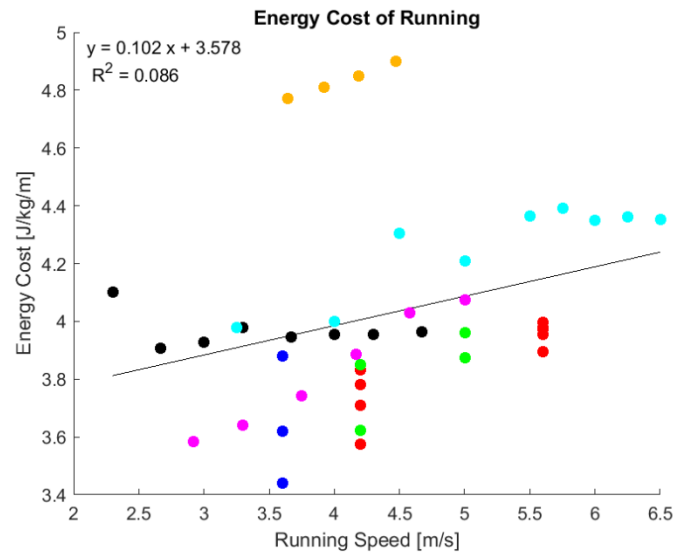


Figure 45 – Values for the energy cost of running collected from previous literature. Black (Mayhew 1977), blue (Williams et al. 1987), red (Svedenhag et al. 1984), green (Svedenhag et al. 1994), magenta (Jones et al. 1996), cyan (Kyrolainen et al. 2001) and yellow (Shaw et al. 2014) dots represent values determine from previously published papers.

Using the values for the energy cost of running published in literature it was possible to determine an approximate relationship between energy cost and speed (Figure 45):

$$\text{energy cost} = 0.102 * \text{speed} + 3.578$$

13

From this, it was possible to estimate the energy cost of running at the four speeds considered here (Table 9).

Table 9 - Esimated values for the energy cost of running at the four speeds considered here.

Speed [m/s]	3.3	3.9	4.8	5.6
Energy cost [J/kg/m]	3.91	3.98	4.07	4.15

Since no elastic potential energy is lost during the aerial phase of running, the amount of hysteresis per stride can then be determined using:

$$\text{Hysteresis per stride} = \frac{2 * (\text{Hysteresis per step})}{\text{stride length}} \quad 14$$

Table 10 - Estimates of the hysteresis per stride [J/kg/m].

	Speed 1	Speed 2	Speed 3	Speed 4
Fore	0.13 (0.08)	0.15 (0.09)	0.16 (0.14)	0.22 (0.12)
Rear	0.16 (0.11)	0.22 (0.14)	0.29 (0.15)	0.33 (0.17)

Therefore, using the estimated energy cost of running at each of the four speeds (Table 9), and the calculated hysteresis per stride (Table 10) it is possible to estimate the contribution of the hysteresis, the elastic potential energy loss, to the total energy cost of running:

$$\left(\frac{\text{Hysteresis per stride}}{\text{energy cost of running}} \right) * 100 \quad 15$$

Table 11 - Contribution of hysteresis to the energy cost of running [%].

	Speed 1	Speed 2	Speed 3	Speed 4
Fore	3.4 (2.0)	3.7 (2.2)	3.9 (3.3)	5.3 (3.0)
Rear	4.1 (2.9)	5.4 (3.6)	7.2 (3.7)	7.9 (4.1)

The estimated contribution of hysteresis to the total cost of running is lower for forefoot strikers than rearfoot strikers, at all four speeds (Table 11). Furthermore, although this is very much an approximation, it appears that as speed increases hysteresis has a greater

contribution to the total energy cost of running. Furthermore, the increase for rearfoot runners is larger than that for forefoot runners. This might suggest that at higher speeds a runner's ability to elastically store and return energy may contribute substantially to their running economy. However, it should be reiterated that this is a simple estimate based on previously published energy costs. Furthermore, this estimate assumes that forefoot strikers and rearfoot strikers have the same over-all energy cost of running, which is arguably untrue (Table 8). Another consideration is that total cost of running is usually the metabolic energy, calculated from oxygen consumption. This requires a conversion factor to account for the inefficiency in converting metabolic to mechanical energy in the muscles (estimated as ~25 % during running (Cavagna et al. 1977, Arellano et al. 2014)). Therefore, these figures for percentage of total work to the hysteresis may be considerably underestimated.

Published studies have argued that rearfoot strikers are more efficient than forefoot strikers (Gruber et al. 2013, Ogueta-Alday et al. 2014, Miller et al. 2015). It is possible that this argument has stemmed from analysis of the muscle activity, with the assumption that more muscle activity must mean more energy is being used, and since forefoot strikers tend to land with a more bent knee and therefore have increased electromyographic (EMG) activity in their muscles (Divert et al. 2005, Jenkins et al. 2011). This pre-activation possibly uses more energy in order to prepare for impact and support the body during the braking phase of stance, thus making them "less economical". On the other hand, rearfoot strikers tend to land with a more extended knee (Almeida et al. 2015), implying muscles are in a relatively passive state, and hence use less energy by relying on footwear and skeletal structures to attenuate the forces associated with loading.

Limitations

Due to the changing number of participants with speed, comparisons between linearity and hysteresis and foot strike pattern were done using t-tests instead of a two-way ANOVA. To account for multiple comparisons the p-value of the t-test was adjusted, using a Bonferroni correction, and therefore it is possible that the sample size was insufficient for detecting effects between linearity and hysteresis and foot strike pattern. For example, in order to detect a large effect with a (two-tail) significance value of 0.013, a sample size of 74 participants is recommended (Faul et al. 2007, Field 2009). However, it is worth noting

that using a Bonferroni correction is a conservative approach, and it is possible that because of this genuine differences may not have been detected (Field 2009).

Another limitation associated with this study is the possible influence of athlete ability on the linearity of the force-length relationship. The data used in this study consisted of biomechanical measurements from a cohort of elite runners (10 km personal best of 35 min or less) and a cohort of recreational runners (10 km personal best of 40 min or more). However, for this study all participants were grouped together and then divided based on their foot strike pattern. Interestingly, a forefoot strike pattern was found to be more common in elite runners (57, 64, 83 and 100 % of elites had a forefoot strike pattern at speeds 1-4, respectively, while only 21, 21, 29 and 31 % of recreational runners had a forefoot strike pattern at speeds 1-4, respectively), and this group also appeared to adjust their foot strike pattern at different speeds. Therefore, it is possible that the observation of more linear force-length behaviour in the forefoot group is a consequence of this group containing more elite runners. However, previous research has consistently observed differences in the vertical GRF profiles of forefoot and rearfoot runners, most notably the presence of an impact transient during early stance in rearfoot strike running, which is consistent with the idea of more non-linear force-length behaviour in rearfoot strikers.

Conclusions

The fundamental aim of this investigation was to answer the question: Is the spring mass model appropriate for modelling all foot strike patterns associated with running? Therefore, this chapter aimed to quantify and compare the linearity and hysteresis of the force-length relationships produced by forefoot and rearfoot strikers, and identify if the assumption of linear elasticity, associated with the spring mass model of running, is appropriate for a range of runners and speeds.

The findings presented here suggest that the assumption of linearity is not appropriate for rearfoot strikers. On the other hand, the trends indicate that forefoot strikers tend to exhibit reasonably linear force-length characteristics. Therefore, considering that the fundamental assumption of the spring mass model is that the body acts similar to a point mass bouncing on a massless linear spring; it would suggest that the use of the spring mass model should be restricted to forefoot strikers. Furthermore, comparing the amount of hysteresis in the force-length curve of forefoot and rearfoot strikers suggest that the linearity of the force-

length curve may play a part in the overall energy cost of running. However, it should be noted that there was a considerable amount of variability within each group and further research where energy consumption as well as kinematic and kinetic data is collected and compared across a larger population is needed before definitive conclusions can be made. This investigation highlights the need for clarity when reporting participant demographics otherwise conclusions drawn based on the assumption of linear force-length behaviour may be erroneous.

5. A Critical Analysis of Methods for Calculating Lower Limb Stiffness

5.1. Introduction

5.1.1. Stiffness of the human body

Stiffness as a descriptor of the human body has been the focus of considerable amounts of research over the past few decades (Brughelli et al. 2008a, Brughelli et al. 2008b, Pearson et al. 2012, Serpell et al. 2012); especially when considering the modelling of bouncing gaits, e.g. running (McMahon et al. 1987, McMahon et al. 1990, Derrick et al. 2000, Hunter 2003, Silder et al. 2015). This “*stiffness*” concept has been associated with multiple task-specific parameters, such as sprint kinematics, rate of force development, and storage and return of elastic energy (Brughelli et al. 2008b). There is also an assumption that stiffness is directly related to performance, but the effects have only been investigated over a relatively restricted range of speeds, and it should be noted that there are contradictory findings (Brughelli et al. 2008a). Despite the interest in the stiffness concept, the conflicting results in the literature imply a somewhat limited understanding about what this parameter actually means. As a result, how truly important this parameter is for describing and understanding running is yet to be established.

The approach developed in the previous chapter is the most physically consistent definition for calculating stiffness; and it was shown to be appropriate for forefoot strikers only. However, this approach is not commonly used in running literature; instead elastic linearity is generally assumed and either kinematic and/or kinetic data are estimated rather than measured. To the authors knowledge only one previous study has incorporated force-length relationships into their calculations and estimated CoM movement using the double integration of the GRFs (Lipfert et al. 2012), which would incorporate a moving CoP. Other studies have used a variety of approaches including estimating CoM movement from vertical GRFs (McMahon et al. 1990), which would only account for vertical displacement, and using a sinewave (Morin et al. 2005, Morin et al. 2007) which assumes symmetry between the acceleration and deceleration phases. The range of approaches adopted highlights the number of definitions currently being used to calculate stiffness

during running. This emphasises the need to determine if these different approaches are measuring the same parameter, otherwise it would seem unreasonable to compare between different studies using different methods.

In addition to limb stiffness, authors of running research often refer to vertical stiffness (Farley et al. 1996, Morin et al. 2005, Morin et al. 2007). Vertical stiffness relates to force and deformation in the vertical direction only, whereas limb stiffness relates to force and deformation along the lower limb axis (Figure 46). However, inconsistencies in definitions have resulted in vertical stiffness sometimes being wrongly referred to as limb stiffness (McMahon et al. 1990, Serpell et al. 2012). This interchangeability in terms highlights the need to determine distinct individual definitions when discussing stiffness of the human body.

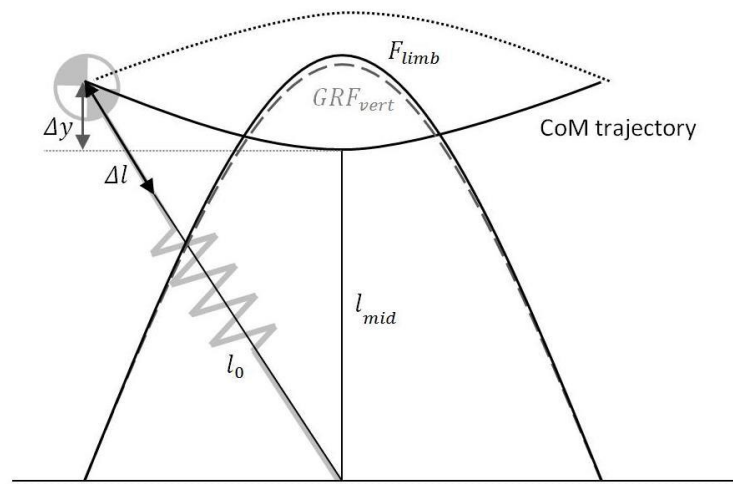


Figure 46 - Pictorial representation of force and displacement used to calculate stiffness.

5.1.2. Lower limb stiffness

Lower limb stiffness describes the combined effect of the individual musculoskeletal components, and their individual stiffness properties, of the lower limb (Farley et al. 1993). It is said to be modulated by the stiffness at the joints; where the relative

contribution of individual joint stiffness to the overall lower limb stiffness is both task and velocity dependent (Günther et al. 2002, Serpell et al. 2012). Furthermore, lower limb stiffness has been associated with optimal locomotion stability (Shen et al. 2015b). It has also been proposed that lower limb stiffness is an key factor for force distribution (Serpell et al. 2012) and performance (Bret et al. 2002, Butler et al. 2003, Pearson et al. 2012).

Four different methods for determining lower limb stiffness have been described in the literature (Table 12), with three methods using force plates (McMahon et al. 1990, Arampatzis et al. 1999, Lipfert et al. 2012) and one method using pressure sensors (Morin et al. 2005). All four methods assume linear elasticity and will be described below.

Force plates

In the method used by McMahon et al. (1990), the vertical GRF was measured directly from a force plate. The vertical CoM displacement was then calculated from the vertical GRF, and the landing angle from the velocity, contact time and initial lower limb length. The change in lower limb length was calculated from the vertical displacement, landing angle, and initial leg length (method 1 - Table 12). Finally, the lower limb stiffness was calculated as the ratio of the maximum vertical GRF to the maximum change in lower limb length, which assumes the vertical GRF and the lower limb force are equivalent at the point of maximum lower limb length change.

Arampatzis et al. (1999) used high speed video to determine the changes in lower limb length by capturing the positions of markers placed on the lateral side of the lower limb joints. Again, vertical force was measured directly using a force plate, and lower limb stiffness was calculated as the ratio of the maximum vertical GRF to the maximum change in lower limb length (method 2 - Table 12). In this model, the change in lower limb length was measured from the CoM to the point of force application, thus changing the “spring” throughout the stance phase.

The only method to use actual force-length curves in determining the lower limb stiffness was that presented by Lipfert et al. (2012). First, the GRFs were projected onto the lower limb axis, and then a linear function was fit to the lower limbs force-length curve. The values for lower limb stiffness and initial lower limb length were then estimated via a linear least squares method (Lipfert et al. 2012). It should be noted however, that for this

method, the CoM movement, and hence changes in lower limb length, were estimated by twice integrating the GRF, which incorporates a moving CoP thus essentially changing the “spring” with each iteration.

Pressure sensors

Finally, a method that does not require the use of force plates was presented by Morin et al. (2005). They used pressure sensors to determine contact time, measured the velocity using a radar gun, and the initial leg length was defined as 0.53 times the participant’s height (Morin et al. 2005, Brughelli et al. 2008b). The maximum vertical GRF and the changes in vertical CoM displacement were then estimated using a sine-wave (defined by the velocity, contact time and initial lower limb length) and the lower limb stiffness calculated from the ratio of maximum force to maximum length change (Morin et al. 2005). By estimating the vertical GRF and the CoM trajectory using a sine-wave, a perfectly symmetrical stance phase is assumed, which is uncharacteristic of normal running.

Table 12 – Different approaches to calculating lower limb stiffness. * Indicates most commonly used method.

Method	Stiffness equation	Force	Displacement	Initial lower limb length	Comments	Ref
1	$k_{limb} = F_{max}/\Delta l$ $\Delta l = \Delta y + l_0(1 - \cos\theta)$	Measured GRF_{vert}	Estimated $\Delta y (\iint GRF_{vert}), v, l, \theta$	CoM to CoP	Symmetric trajectories assumed	(McMahon et al. 1990)*
2	$k_{limb} = F_{max}/\Delta l$ $\Delta l = CoM \text{ to } CoP$	Measured GRF_{vert}	Measured $l = \sqrt{((x_{CoM} - x_{POFT})^2 + (y_{CoM} - y_{POFT})^2)}$	CoM to CoP	Δl digitised from video - no mention of how CoM was determined	(Arampatzis et al. 1999)
3	$F_{limb}(t) = k_{limb}(l_0 - l(t))$	Measured F_{limb}	Estimated $\sqrt{(\iint F_x)^2 + (\iint F_z)^2}$	CoM to CoP	Solved system of equations to get k_{limb} and l_0	(Lipfert et al. 2012)
4	$k_{limb} = F_{max}/\Delta l$ $\Delta l = l_0 - \left(l_0^2 - \left(\frac{vt_c}{2}\right)^2\right)^{\frac{1}{2}} + \Delta y$	Estimated Sine-wave $F_{max} = \frac{mg\pi}{2} \left(\frac{t_f}{t_c} + 1\right)$	Estimated $\iint Sine \text{ wave}$ $\Delta y = \frac{F_{max}t_c^2}{m[\pi^2]} + \frac{gt_c^2}{8}$	0.53*participant height	Leg compression estimated assuming a sinusoidal vertical GRF	(Morin et al. 2005)

where F_{max} the peak vertical GRF, Δy the maximum vertical displacement of the CoM, l_0 the initial lower limb length, Δl the maximum change in lower limb length, θ the approach angle, v the running velocity, t_c the contact time and t_f the flight time.

5.1.3. Vertical stiffness

Vertical stiffness is described as the resistance of the body to changes in vertical displacement. There are a variety of different approaches used within the literature to calculate vertical stiffness; however there appears to be two main definitions. One based on the periodicity of movement (McMahon et al. 1987, Cavagna et al. 1988) and one based on the ratio of a force to a displacement (McMahon et al. 1990, Morin et al. 2005, Serpell et al. 2012). The key difference between the different approaches is the way in which the parameters are derived. For example, where force plates were used, GRFs were collected and either: double integrated to determine the CoM movement during the stance phase (McMahon et al. 1990); or single integrated to determine the vertical velocity of the CoM (which was then combined with the contact time) to calculate the natural frequency of oscillation (McMahon et al. 1987). Alternatively, GRFs were used to determine the effective contact time (defined by the amount of time that the vertical GRF exceeded body weight) and hence the period of oscillation (Cavagna et al. 1988). When pressure sensors or accelerometers were used the contact and flight times were measured, but the vertical GRF was modelled as a sine wave (Morin et al. 2005, Serpell et al. 2012). From this, the maximum vertical GRF (Eq. 16, page 102) and maximum vertical displacement (Eq. 17, page 102) were then estimated (Morin et al. 2005).

Table 13 – Different approaches for determining vertical stiffness. * Indicates most commonly used method.

Equipment	Stiffness equation	Ref
Force plate	$k_{vert} = m\omega^2 = m\left(\frac{2\pi}{P}\right)^2$	(McMahon et al. 1987, Cavagna et al. 1988)
Force plate, Accelerometers, Pressure Sensors	$k_{vert} = \frac{F_{max}}{\Delta y}$	(McMahon et al. 1990, Morin et al. 2005, Serpell et al. 2012)*

where m is the mass of the body, ω the natural frequency of oscillation, $P = 2\pi/\omega$ the period of oscillation, F_{max} the peak vertical GRF and Δy the maximum vertical displacement of the CoM.

5.1.4. Aims

A large variety of definitions are used to describe stiffness in the running literature. It is possible that these methods have been suggested in order to calculate stiffness in the absence of a full dataset (both kinetic and full body kinematic data). However, using the slope of the experimental force-length curve is the most physically consistent (PC) definition, and therefore it is important to understand how it differs to the other methods presented in literature.

Lower-limb length definitions

One reason given for differences in the magnitudes of lower limb stiffness values presented in the literature is the way in which the lower limb length is defined. Therefore, an initial aim of this investigation is to determine if the choice of definition has an effect on the force-length relationship. However, it is hypothesised that the choice of definitions will not influence the force-length relationship.

Lower limb stiffness calculation

In an attempt to understand the differences between the methods for calculating lower limb stiffness, two studies compared a range of methods of calculating lower limb stiffness (Blum et al. 2009, Coleman et al. 2012). One focused on the definition of lower limb compression during contact and compared stiffness values to stable solutions of the spring mass model (Blum et al. 2009). The other, compared a “gold standard” definition of stiffness (ratio of peak lower limb force to maximum lower limb compression) to other published definitions (Coleman et al. 2012), however they considered only the braking phase of stance. Therefore, the primary aim of this investigation is to determine whether the alternative methods used to calculate lower limb stiffness, as described in running literature, are comparable to the physically consistent definition (discussed in detail in Chapter 4). It is hypothesised that there will be a relationship between some, but not all, of the other methods.

Vertical stiffness calculation and comparison

As well as lower limb stiffness, vertical stiffness is often reported in running literature. However, inconsistencies in the terms and definitions results in vertical stiffness

sometimes being wrongly referred to as lower limb stiffness. Therefore, the final aim of this investigation is to establish if a relationship exists between vertical stiffness and lower limb stiffness (defined using the physically consistent definition). It is hypothesised that there will be no relationship between lower limb and vertical stiffness.

5.2.Methods

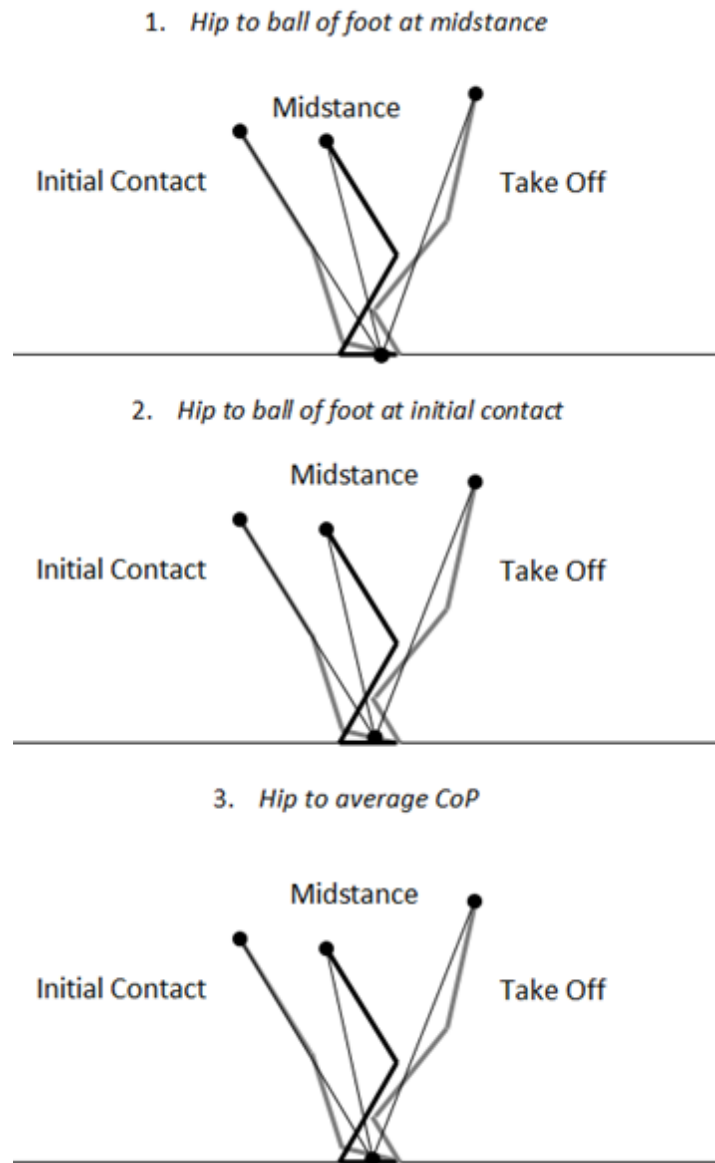
5.2.1. Experimental data

The findings of the Chapter 4, suggest that forefoot strikers are more likely to exhibit linear elastic behaviour, and therefore the assumption of linear stiffness is only applicable to these runners. Consequently, a subset of the previously collected kinematic and kinetic data (see Chapter 3) was used for this investigation; where those who adopted a rearfoot strike pattern were excluded. The subset of data was from 19 forefoot strikers, however as some participants transitioned from a rearfoot to a forefoot pattern with increasing speed, some data had to be excluded from the study at the slower speeds. After these data had been removed, there were datasets from n=11, 12, 13 and 19 athletes at speeds 1 – 4, respectively.

GRF data, CoP data, and positional data of the foot and hip joint centre were all extracted for the duration of the contact phase. The lower limb length definitions varied in the way the distal end was defined. Two definitions used the position of the ball of the foot (midpoint between the 1st and 5th metatarsal markers), one at midstance and one at initial-contact. The third definition used the average position of the CoP. For the various stiffness calculations, contact times and flight times were determined using Visual3D gait event detection, for the whole running gait cycle; these values were also averaged over the number of trials. In the Visual3D gait event detection algorithm left and right ON/OFF indicate kinetic cycles, whereas HS/TO (heel strike / toe off) indicate kinematic cycles. Contact time was then defined as the difference between the right ON and OFF events, and flight time as the difference between right OFF and left ON.

5.2.2. Lower-limb length definitions

The individual force-length relationships were determined for each of the participants and for each of the definitions of lower limb length being investigated. The method used in the previous chapter (Chapter 4) was also adopted for this investigation, where the lower limb force was determined by projecting the GRFs onto the limb axis (Chapter 4). The spring mass model assumes a fixed contact point, however during running there is a net proximal-to-distal translation of the CoP. Furthermore, how to choose the most appropriate “fixed contact point” remains unclear. Therefore, the lower limb length was defined using the following three definitions, where the fixed contact point differed between each definition.



Linearity was then quantified for each of the force-length curves. Again, the same approach as the previous chapter was used, where linearity was calculated using a root mean square residual (RMSr) between the experimental force-length curves and the assumed “perfectly” elastic line (Chapter 4.2.4). In addition, the lower limb stiffness was estimated as the ratio of the peak lower limb force to the maximum change in lower limb length, for each curve.

5.2.3. Lower limb stiffness calculation

Five different methods for calculating lower limb stiffness were examined; the physically consistent method (PC method) described in this investigation (using experimentally measured kinematic and kinetic data) as well as four methods that were previously published in the literature (Table 12). These methods are described in detail below:

PC Method. In this investigation, for calculating stiffness, the lower limb length was defined as the length from the hip joint centre to the average CoP of the foot during the contact phase (this definition was chosen based on the findings of the lower limb length investigation – see section 5.3.1). The change in lower limb length was then determined as the difference between the initial lower limb length and the length at each successive time point. The lower limb stiffness value was then determined by calculating the slope of a linear least squares fit to the point where the lower limb length returned to its initial length, approximately the first 90 % of the force-length curve, corresponding to the approximately first 90 % of the contact phase. Once the lower limb length exceeded the initial length, the force-length behaviour changed and resulted in a much gentler gradient. This is likely due to the “spring” extending as the foot planar flexes in preparation for flight.

Method 1 (McMahon & Cheng, 1990). For this method, GRFs were double integrated to give the changes in horizontal and vertical CoM positions during the contact phase. The approach angle was then determined using the horizontal velocity at initial contact, the contact time and the initial lower limb length. The change in the vertical CoM position was then calculated as the difference in this “initial” value and the values determined from the integration of the vertical GRF. The maximum change in lower limb length was then estimated by combining the maximum vertical change with the approach angle. Finally,

the lower limb stiffness was calculated as the quotient of the maximum vertical GRF and the maximum change in lower limb length.

Method 2 (Arampatzis et al. 1999). This method again defined lower limb stiffness as the quotient of the peak vertical GRF to the maximum change in lower limb length. However, in this case lower limb length was now defined as the distance from the CoM to the CoP. To determine the CoM the authors used a two-dimensional 15 segment model, however reproducing their model with our data would be difficult and time consuming, and therefore the CoM was approximated using the hip joint centre. This seemed reasonable as it has been shown that the hip position is a close approximation of the CoM when considering only two-dimensions. The change in lower limb length was then calculated as the difference between the instantaneous length and the length at initial contact.

Method 3 (Lipfert et al. 2012). Vertical and horizontal GRFs were double integrated to give the CoM positions. The lower limb length was then calculated as the distance from the CoM to the CoP during the contact phase. The lower limb force was also estimated by projecting the GRFs onto the lower limb axis. A linear least squares method was then used to determine the best fitting linear approximation of the force-length curve. A linear system of equations was solved (using matrix left division, MATLAB) to determine the corresponding initial lower limb length and lower limb stiffness values.

Method 4 (Morin et al. 2005). In this method, lower limb stiffness was again the quotient of the peak vertical GRF to the maximum change in lower limb length. However, both the vertical GRF and the changes in vertical CoM displacement were estimated using a sine wave. For this, the contact and flight times were determined using gait events, and the maximum vertical GRF and maximum change in the lower limb length were calculated using the following equations:

$$F_{max} = \frac{mg\pi}{2} \left(\frac{t_f}{t_c} + 1 \right) \quad 16$$

$$\Delta y = \frac{F_{max}t_c^2}{m[\pi^2]} + \frac{gt_c^2}{8} \quad 17$$

$$\Delta l = l_0 - \sqrt{l_0^2 - \left(\frac{vt_c}{2} \right)^2} + \Delta y \quad 18$$

Here m is the mass of the participant, g is the acceleration due to gravity, t_c and t_f are the contact and flight times, respectively, l_0 is the initial lower limb length defined as 0.53 times the height of the participant, and v is the running velocity.

5.2.4. Vertical stiffness calculation and comparison

Vertical stiffness is defined as the quotient of the peak vertical GRF to the maximum vertical change in the vertical CoM position during the contact phase (Brughelli et al. 2008a, Serpell et al. 2012). Here the CoM position was estimated by the hip joint centre (the proximal end of the thigh segment).

5.2.5. Statistics

Lower-limb length definitions

A repeated measures ANOVA was used to compare the lower limb stiffness and RMSr values for each of the definitions of lower limb length. Due to the changing number of participants at each speed, a separate ANOVA had to be run for each speed. Therefore, the standard p-value ($p \leq 0.05$) was adjusted for multiple tests (4 speeds), resulting in a new p-value of 0.013. In this case effect size was estimated using the partial eta squared, with small, medium and large effects indicated by values of 0.01, 0.06 and 0.14, respectively.

Lower limb stiffness calculation

A repeated measures ANOVA was also used to compare the values from each of the five methods of calculating lower limb stiffness (the physically consistent method and the four other methods). In addition, a linear regression analysis was completed to determine if a relationship existed, and the type of relationship, between the different methods of calculating lower limb stiffness. A Bland-Altman analysis was then completed to determine the level of agreement (95% confidence interval) between the methods (Altman et al. 1983, Bland et al. 1986).

Vertical stiffness calculation and comparison

Vertical stiffness was compared to the lower limb stiffness (calculated using the PC definition) using a bivariate (Pearson's) correlation. Correlation coefficients were determined to establish if a relationship existed between lower limb and vertical stiffness values. A correlation was considered strong if r greater than 0.7, moderate if r was greater than 0.5 and weak if r was greater than 0.3.

Repeated measures ANOVA were run using SPSS v23 (IBM Corp., Armonk, NY, USA). All other statistical analysis was conducted using MATLAB.

5.3. Results

5.3.1. Lower limb length definitions

Force-length relationships were investigated for three different lower limb length definitions at four different speeds. Figure 47 shows that the loading phase of stance is similar between all three definitions, at all four speeds. On the other hand, there are some differences in the unloading phase; however, the gradient appears to be similar between the definitions.

The RMSr for the loading phase of the force-length curves were significantly different at speed 4 only (Table 14). Mauchly's test for sphericity was significant ($p \leq 0.05$) for all four speeds and thus a Greenhouse-Geisser correction was applied to the degrees of freedom. Post-hoc Bonferroni analyses revealed that the RMSr was significantly larger for definition 1 compared to definition 2 ($p \leq 0.001$; 0.270 vs. 0.258). However the RMSr for definition 3 was not significantly different to that of definition 1 or definition 2.

Table 14 – Mean (SD) RMSr [BW] values for the loading phase for the three different lower limb length definitions.

Def.	Speed 1	Speed 2	Speed 3	Speed 4
	LOAD	LOAD	LOAD	LOAD
1	0.168 (0.087)	0.171 (0.078)	0.200 (0.089)	0.270 (0.111)
2	0.163 (0.082)	0.164 (0.073)	0.191 (0.087)	0.258 (0.111)
3	0.162 (0.082)	0.170 (0.074)	0.199 (0.092)	0.279 (0.122)
F _{df} (sig.)	0.43 _(1.3, 13.4) (0.583)	0.80 _(1.3, 14.0) (0.415)	0.72 _(1.1, 13.4) (0.426)	7.15 _(1.2, 20.7) (0.012)
Effect Size	0.04	0.07	0.06	0.28

The RMSr for the unloading phase of the force-length curves were not significantly different at any speed (Table 15). Mauchly’s test for sphericity was significant ($p \leq 0.05$) for speeds 1, 3 and 4, but not for speed 2. Therefore sphericity was assumed for speed 2 but a Greenhouse-Geisser correction was applied to the degrees of freedom for speeds 1, 3 and 4.

Table 15 – Mean (SD) RMSr [BW] values for the unloading phase for the three different lower limb length definitions.

Def.	Speed 1	Speed 2	Speed 3	Speed 4
	UNLOAD	UNLOAD	UNLOAD	UNLOAD
1	0.131 (0.071)	0.136 (0.072)	0.169 (0.092)	0.187 (0.091)
2	0.138 (0.046)	0.152 (0.046)	0.187 (0.075)	0.199 (0.100)
3	0.155 (0.042)	0.154 (0.057)	0.158 (0.080)	0.181 (0.078)
F _{df} (sig.)	1.26 _(1.3, 13.2) (0.296)	0.58 _(2, 22) (0.570)	0.51 _(1.3, 15.7) (0.536)	0.28 _(1.5, 27.1) (0.694)
Effect size	0.11	0.05	0.04	0.02

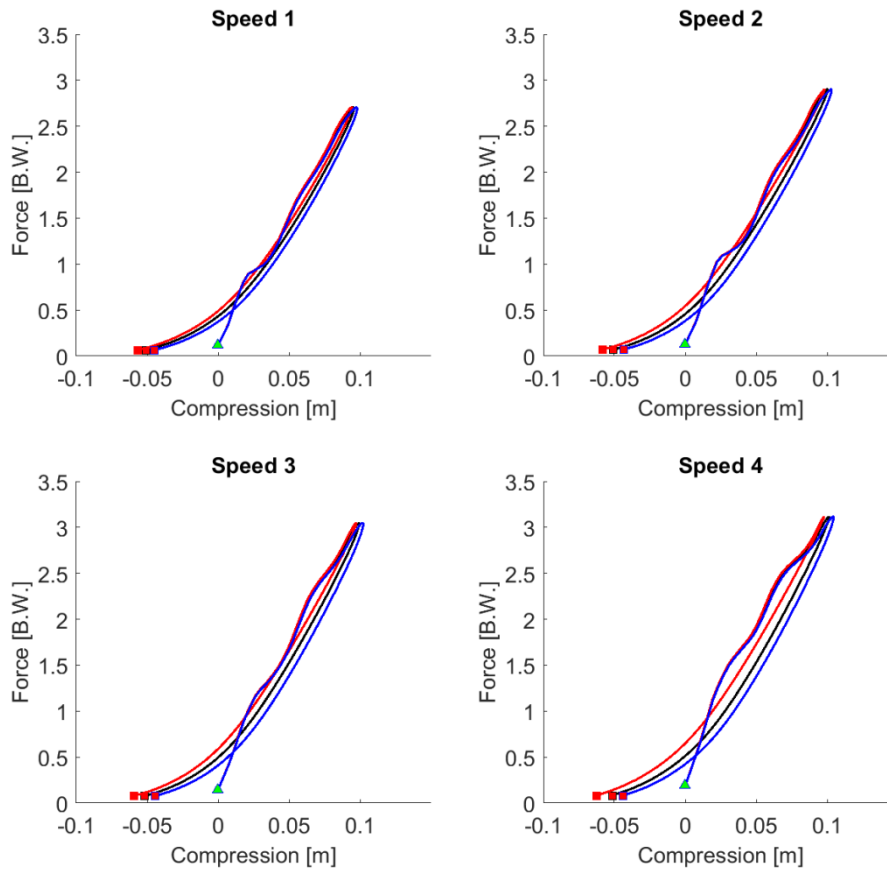


Figure 47 – Mean force-length curves produced from the different definitions of lower limb length. The definitions are as follows: black - hip to ball of foot at midstance; red - hip to ball of foot at initial contact; blue - hip to average CoP.

The lower limb stiffness values were statistically similar between the three definitions at speeds 1 – 3, but significantly different at speed 4 (Table 16). Mauchly’s test for sphericity was significant ($p \leq 0.05$) at all four speeds. Therefore a Greenhouse-Geisser correction was applied to the degrees of freedom for all speeds. Post-hoc Bonferroni analyses revealed that the lower limb stiffness value from definition 1 was significantly smaller than that from definition 2, and that from definition 2 was significantly larger than that from definition 3 ($p \leq 0.001$; 18.7 vs. 19.4 vs. 18.1 kN/m, respectively).

It seems appropriate to have chosen the third definition (hip to average CoP) as the lower limb length definition the previous investigation (Chapter 4). Furthermore, this definition will be used for the remainder of this chapter.

Table 16 – Mean (SD) lower limb stiffness [kN/m] values for the three different lower limb length definitions.

Def.	Speed 1	Speed 2	Speed 3	Speed 4
1	17.1 (4.1)	17.5 (3.8)	18.6 (3.9)	18.7 (3.2)
2	17.5 (4.3)	17.9 (4.0)	19.0 (4.0)	19.4 (3.3)
3	16.9 (4.5)	17.1 (4.1)	18.2 (4.3)	18.1 (2.9)
F _{df} (sig.)	2.59 _(1,1, 11,2) (0.134)	6.45 _(1,1, 12,0) (0.024)	2.80 _(1,0, 12,4) (0.119)	15.48 _(1,2, 21,2) (<0.001)
Effect size	0.21	0.37	0.19	0.46

5.3.2. Lower limb stiffness calculations

The repeated measures ANOVA analysis indicated significant differences between the lower limb stiffness values produced using the different calculation methods (Table 17). Mauchly’s test for sphericity was significant ($p \leq 0.013$) at all four speeds. Therefore, a Greenhouse-Geisser correction was applied to the degrees of freedom for all speeds. Post-hoc Bonferroni analyses revealed that the lower limb stiffness value from the PC method was significantly different from those from the other four methods at all four speeds. The other four methods were also consistently significantly different to each other (Table 17), except for methods 3 and 5 which were statistically similar at speeds 1 -3 ($p > 0.2$).

The correlation coefficients (Table 18) showed a moderate to strong, and significant, relationship between the PC method and the other four methods ($r = 0.84 - 0.98$). Method 1 (speed 1 and 2) and 2 (speed 3 and 4) showed the highest correlations to the PC method (Figure 48); method 4 consistently had the lowest correlation coefficient. However, the regression equation coefficients showed inconsistent relationships between the PC method and the other four methods, with differing values for both gradient and offset across the speeds (Figure 49 and Table 18). See Appendix AII, Figure 112 - Figure 115, for correlation plots between the PC method and each of the other methods at each speed.

Table 17 - F-ratio and significance is the overall results from the repeated measure ANOVA, significance values for each method indicate the Bonferroni post-hoc significance values relating each method to the PC method.

Speed	PC Method	Method 1	Method 2	Method 3	Method 4
F _{df}	52.14 _(1.4, 14.4)				
1 sig.	<0.001	0.008	0.002	0.006	<0.001
Effect size	0.84				
F _{df}	83.60 _(1.6, 18.0)				
2 sig.	<0.001	<0.001	0.001	0.005	<0.001
Effect size	0.88				
F _{df}	113.75 _(1.6, 18.9)				
3 sig.	<0.001	<0.001	<0.001	0.002	<0.001
Effect size	0.91				
F _{df}	268.8 _(2.3, 40.7)				
4 sig.	<0.001	<0.001	<0.001	<0.001	<0.001
Effect size	0.94				

Table 18 - Mean (SD) of lower limb stiffness values [kN/m], linear regression equation coefficients (m , b) and correlation coefficients (r) relating the PC method to methods 1-4. m refers to the slope and b to the offset (intercept).

Speed	PC Method	Method 1	Method 2	Method 3	Method 4	
1	mean	15.5	14.0 ^{bd}	18.5 ^{acd}	12.1 ^{bd}	8.2 ^{abc}
	(SD)	(4.2)	(4.2)	(5.3)	(2.3)	(1.9)
	m		0.972	1.201	0.503	0.392
	b		-1.042	-0.107	4.313	2.125
	r		0.970	0.955	0.920	0.860
2	mean	15.7	13.1 ^{bd}	18.7 ^{acd}	13.1 ^{bd}	8.6 ^{abc}
	(SD)	(3.9)	(3.4)	(4.8)	(2.8)	(1.8)
	m		0.859	1.177	0.645	0.413
	b		-0.308	0.268	3.015	2.176
	r		0.980	0.950	0.906	0.903
3	mean	16.5	12.9 ^{bd}	19.5 ^{acd}	13.4 ^{bd}	9.3 ^{abc}
	(SD)	(4.2)	(3.1)	(4.3)	(2.9)	(1.9)
	m		0.693	0.983	0.617	0.392
	b		1.416	3.327	3.206	2.835
	r		0.942	0.961	0.889	0.854
4	mean	15.9	11.8 ^{bd}	19.8 ^{acd}	13.1 ^{bd}	9.4 ^{abc}
	(SD)	(3.2)	(2.5)	(3.2)	(2.6)	(1.9)
	m		0.675	0.904	0.690	0.502
	b		1.041	5.432	2.165	1.403
	r		0.865	0.905	0.859	0.838

^a – significantly different to method 1; ^b – significantly different to method 2; ^c – significantly different to method 3; ^d – significantly different to method 4

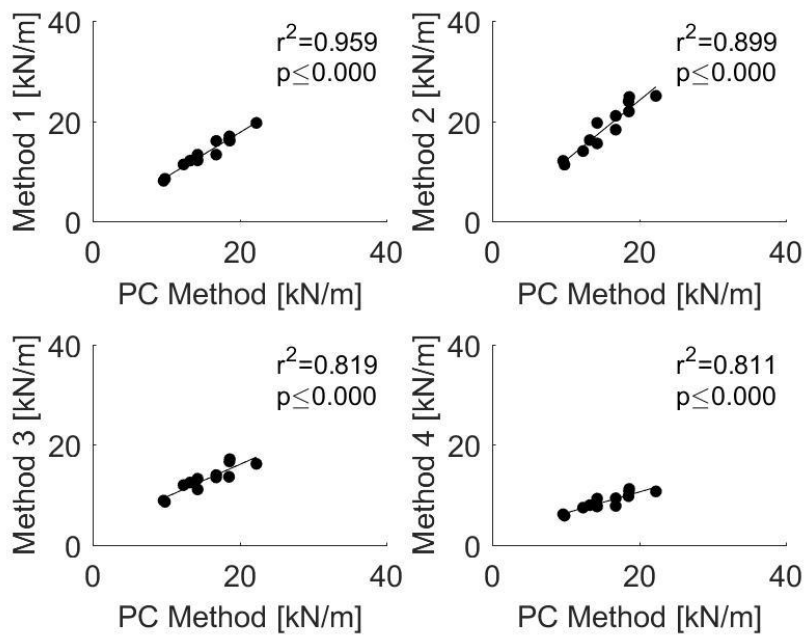


Figure 48 - Example of the relationships between the PC method and the other methods of calculating lower limb stiffness at speed 2 (3.9 m/s), n = 12.

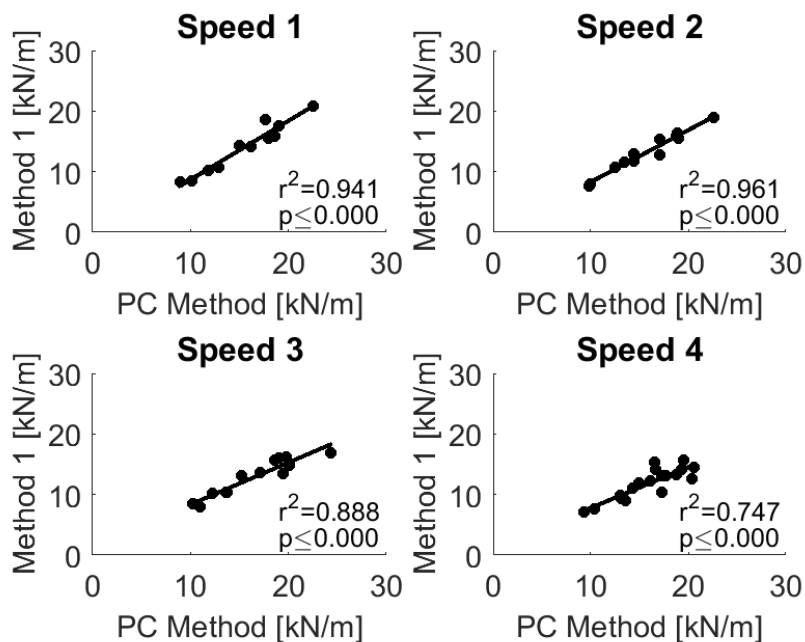


Figure 49 - Comparison of lower limb stiffness values calculated using the PC method versus method 1; n = 11, 12, 13 and 19 at speeds 1 – 4, respectively.

Regardless of the method used to calculate lower limb stiffness, the values appear to be relatively constant with running velocity (Table 18). However, the magnitudes of lower limb stiffness varied depending on the method used to calculate it. Bland-Altman analysis revealed a clear relationship between the mean of the values and the difference values. For example, at speed 3, for methods 1, 3 and 4 there appears to be a proportional error, i.e. the difference between the means was larger for larger lower limb stiffness values (Figure 50). On the other hand, the difference was relatively constant, i.e. there was a consistent error, between method 2 and the PC method. However, as stated previously, it should be noted that the relationship between the other four methods and the PC method appears to be different at the different speeds (Table 18). Furthermore, the Bland-Altman analysis showed that the 95 % limits of agreement ranged from -6.7 to 12.7 kN/m (-40 to 240 % of the mean difference value). See Appendix AII, Figure 116 - Figure 119 for Bland-Altman plots for each speed.

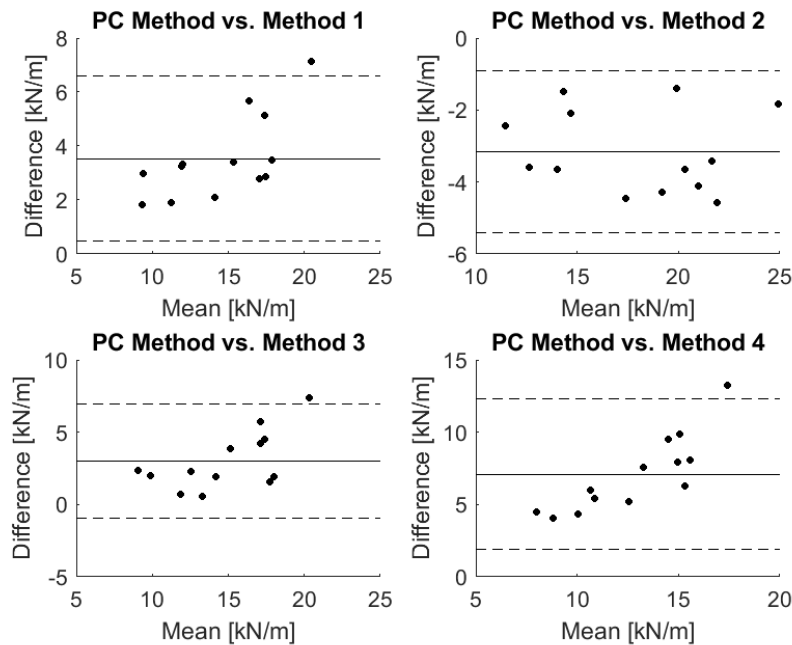


Figure 50 - Bland-Altman plot comparing methods of calculating lower limb stiffness at speed 3. The upper and lower dashed lines represent the 95% confidence interval, while the middle solid lines represent the mean difference between the values produce using the two methods being compared.

5.3.3. Lower limb stiffness vs. Vertical stiffness

Vertical stiffness was found to be consistently larger than lower limb stiffness at all speeds considered (Figure 51). Furthermore, vertical stiffness appears to increase with increasing speed, while lower limb stiffness appears to be approximately equal across all four speeds (Figure 51). Furthermore, a strong to moderate relationship was identified for speeds 1 and 2 ($r = 0.90$ and 0.72 , respectively), whilst weak relationships were identified for speeds 3 and 4 ($r = 0.21$ and 0.22 , respectively). However, the fact that the strength of the relationship changes considerably with each speed implies that it is an inconsistent relationship. However since the number of participants changed with speed it is not possible to conclude whether these relationships are due to speed or the new participants.

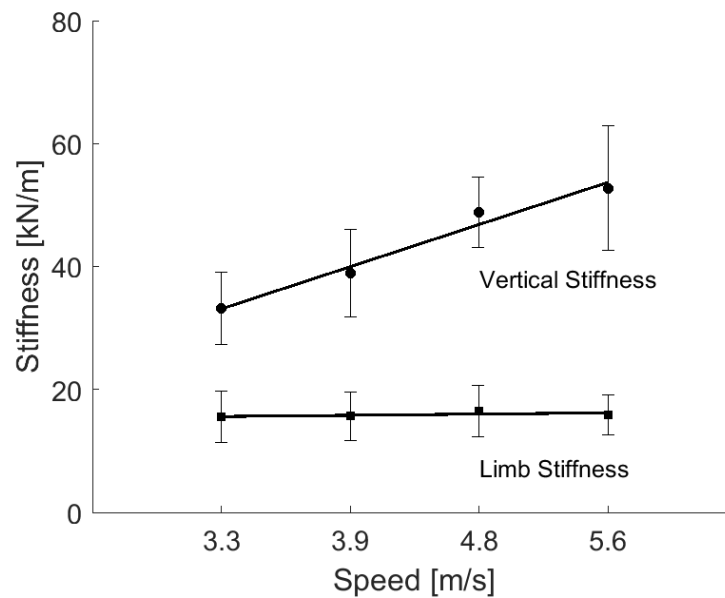


Figure 51 – Mean and standard deviation (n=11, 12, 13 and 19 at speeds 1 – 4, respectively) of lower limb stiffness and vertical stiffness as a function of speed.

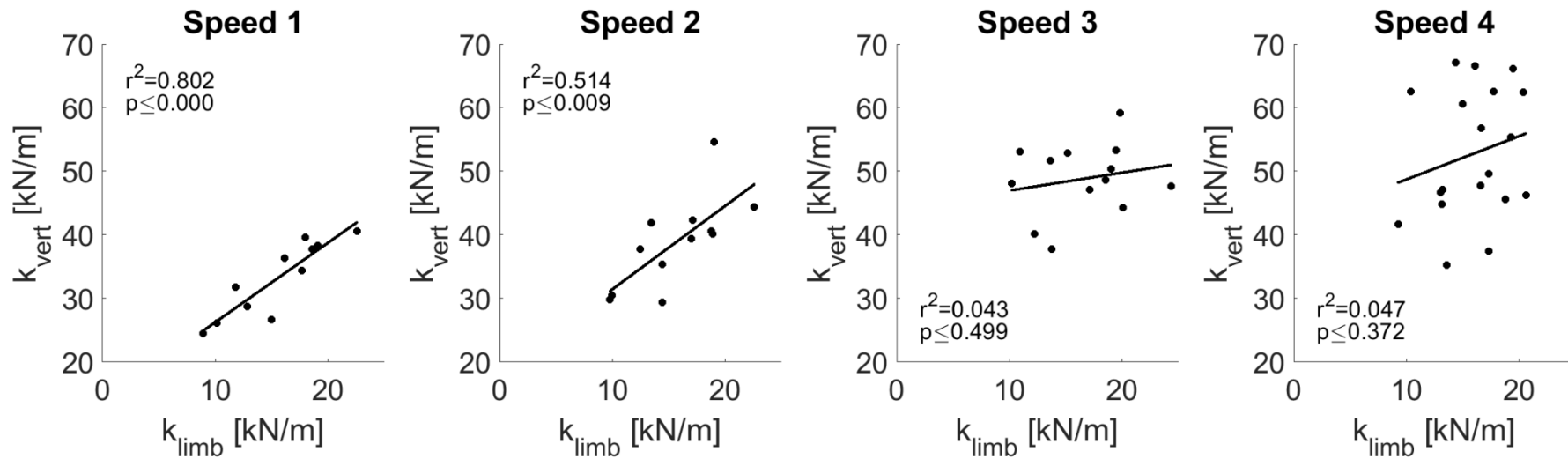


Figure 52 – Lower limb stiffness vs. vertical stiffness at each speed. $n=11, 12, 13$ and 19 at speeds 1 – 4, respectively, and speeds 1 – 4 correspond to 3.3, 3.9, 4.8 and 5.6 m/s, respectively.

5.4. Discussion

The fundamental aim of this investigation was to determine the relationship between the currently used methods, and the physically consistent definition, for calculating lower limb stiffness. Physics defines stiffness as the ratio of the force applied along the spring to its deformation, i.e. the slope of the force-length curve. Despite this, only one previous investigation has incorporated the use of force-length curves into their calculations of lower limb stiffness (Lipfert et al. 2012). However, this study also defined the lower limb length as the distance from the CoP to the CoM which fundamentally changes the spring as CoP translates along the foot axis.

Lower-limb length definitions

A common difference between the methods used in the literature is the way in which the lower limb length is defined. To determine if this would influence the linearity of the force length relationship, force-length curves were produced for three different lower limb length definitions. The results showed that the choice of lower limb length definition had only a marginal effect on the linearity and stiffness (slope) of the force-length curves, and therefore a choice was made to continue with the third lower limb length definition, hip to average CoP. This definition was chosen as it seemed reasonable when considering the assumption of a fixed point of contact that is inherent to the spring mass model of running. Furthermore, since we are considering only two-dimensional movement, the hip joint centre movement will be similar to the true CoM movement, calculated from weighted segments, in the AP and vertical directions. The hip joint centre is offset from the Visual3D estimate of the CoM by a fixed amount during running, therefore because we are considering a change in length this fixed offset will not make a difference to the force-length relationship.

Lower limb stiffness calculations

A range of different methods have been used in the literature to calculate lower limb stiffness during running. Key differences between these methods and the physically consistent definition were identified using linear regression and Bland-Altman analysis. For instance, the relationship between the mean and the difference of the values varies considerably between method and speed (Figure 50 and Figure 116 - Figure 119 in

Appendix AII). This is important as it shows that, at some speeds, as stiffness increases there is an increasing discrepancy between the physically consistent method and the other four methods. On the other hand, at other speeds, there appears to be a consistent bias between the physically consistent method and the four other methods, suggesting that if the mean difference was subtracted from the “other” method then it would be nearly equivalent to the physically consistent method. However, none of the four other methods should have the same bias at all four speeds, which would imply that the relationships are inconsistent and the “other” methods cannot reliably be corrected. Furthermore, lower limb stiffness values published in the literature, are known to vary substantially (<20 kN/m (McMahon et al. 1990, Morin et al. 2005, Lipfert et al. 2012) compared to >35 kN/m (Arampatzis et al. 1999)). However, it should be noted that in most cases, the ability level of the participants was not identified, and there was no comment on the type of foot strike patterns adopted. Additionally, the range of speeds considered varied considerably (2 – 7+ m/s). These results highlight the need for clarity and consistency when reporting participant demographics and calculating lower limb stiffness, otherwise appropriate comparisons cannot be made between studies. For example, the r^2 values from Figure 48 and Table 18 suggests that methods 1, 2 and 3 have a linear relationship with the PC method. This suggests that whilst not interchangeable they could be used to predict the true PC lower limb stiffness value. However, the value for method 4 suggests that this may not be the case.

Two previous studies have attempted to compare methods of calculating lower limb stiffness (Blum et al. 2009, Coleman et al. 2012). One focused on the definition of lower limb compression during contact (Blum et al. 2009) while the other considered only the braking phase (Coleman et al. 2012). Although the previous chapter revealed that differences in the linear characteristics are mainly in the braking phase, the spring mass model assumes a single value of stiffness for the whole contact phase, therefore it seems reasonable that the stiffness value should be calculated by considering the whole contact phase.

Blum et al. (2009) did not directly compare values determined from the different methods, but instead compared the different methods to the stable solutions of the spring mass model (Seyfarth et al. 2002). They concluded that using a method consisting of only temporal parameters, lower limb length, touch down angle and body mass was sufficiently

accurate to derive lower limb stiffness values that correspond to the spring mass model. Coleman et al. (2012), on the other hand, determined that the values predicted using alternative methods of calculating lower limb stiffness were significantly different to a “gold standard” definition. The authors suggested the reason for the discrepancies may be due to errors in estimating the changes in lower limb length during the braking phase. However, the results of this study suggest that the choice of lower limb length definition does not have a significant effect on the force-length relationship or subsequently the lower limb stiffness value; at least for forefoot strikers. However, considering that the foot strike pattern adopted was not reported by Coleman et al. (2012), it is possible that the choice of lower limb length definition is more important when considering rearfoot strikers (see appendix AIII).

The findings of these previous studies are consistent with those of this investigation, where values predicted using different methods follow similar trends, but the magnitudes are significantly different. This further emphasises the need for a standardised method for calculating lower limb stiffness during running. Since different methods are currently being used in the running literature, caution must be used when comparing results from different studies as it might result in misleading conclusions.

Lower limb stiffness vs. Vertical stiffness

Lower limb stiffness remains relatively constant with increasing speed, and generally has a lower value than vertical stiffness (He et al. 1991, Morin et al. 2005, Brughelli et al. 2008a). The peak lower limb force and the peak vertical GRF are similar in magnitude (Figure 53), and in general both increase as speed increases (Brughelli et al. 2011). Therefore, the consistency of lower limb stiffness with velocity can be attributed to the corresponding increase in the change in lower limb length as the velocity is increased. As velocity increases, the arc swept by out the lower limb also increases, thus offsetting the increase in peak force associated with increasing velocity (Brughelli et al. 2008a). However, it should be noted that lower limb stiffness values change with terrain and running surface. This adjustment of lower limb stiffness has been suggested as a method for lowering the energy cost of transport (Ferris et al. 1998, Voloshina et al. 2015, Shen et al. 2015a).

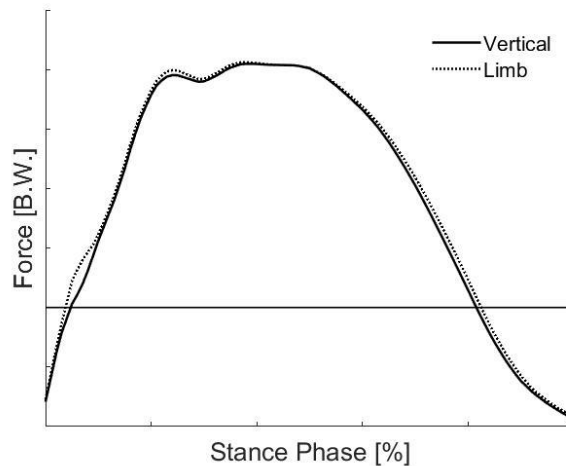


Figure 53- Pictorial representation of the forces used to calculate stiffness. The solid line represents the experimental vertical GRF, while the dotted line represents the GRFs projected onto the limb axis.

The results presented here show no consistent relationship between lower limb stiffness and vertical stiffness. Therefore, vertical stiffness cannot reliably be used as a proxy for lower limb stiffness, or vice versa. Vertical stiffness is described as the resistance of the body to changes in vertical displacement. From this definition it is assumed that a greater vertical stiffness implies a greater resistance to vertical collapse during the absorption (landing) phase, and an increased rate of force production during the propulsive (push off) phase (Brughelli et al. 2008a). This has presumably lead some authors to suggest that athletes should strive to increase their vertical stiffness in order to increase their performance (Hobara et al. 2010). A similar argument was made by Robilliard et al. (2005) who stated “*high stiffness limbs are beneficial since they result in small changes in mechanical energy and hence low hysteresis losses, since biological springs do not return all energy stored in them*”. On the other hand, it has been argued that greater compliance (decreased stiffness) improves the efficiency of elastic energy storage and return during the stretch-shortening cycle (Kubo et al. 2005, Brughelli et al. 2008b). Suggesting the opposite, that decreasing stiffness will increase energy efficiency, and hence performance. However, in physics there is no basis for assuming that stiffness is related to energy efficiency, as a ‘perfect’ linear spring does not absorb or generate energy. Therefore, the

direct association between lower limb or vertical stiffness and performance does not make sense.

Vertical stiffness does not correspond to any physical “spring”, therefore it doesn’t seem like an appropriate parameter to describe running. As a concept, vertical stiffness was initially used to describe hopping (Blickhan 1989, McMahon et al. 1990, Brughelli et al. 2008a, Serpell et al. 2012), a one-dimensional movement, and so considering the force and displacement in only the vertical direction was appropriate. However, running is usually studied as at least a two-dimensional movement, and so considering vertical stiffness seems illogical as it does not relate to any physiological “spring”, but only describes the vertical oscillation of the CoM (Morin et al. 2005). If, instead, lower limb stiffness is considered, it not only incorporates the vertical component (Figure 54), but also fundamentally describes the compliance of the lower limb during the stance phase of running. It is essentially a mechanical representation of the physiology, and describes the relationship between applied forces and changes in lower limb length during running, an inherent consequence of loading and unloading of the lower limb.

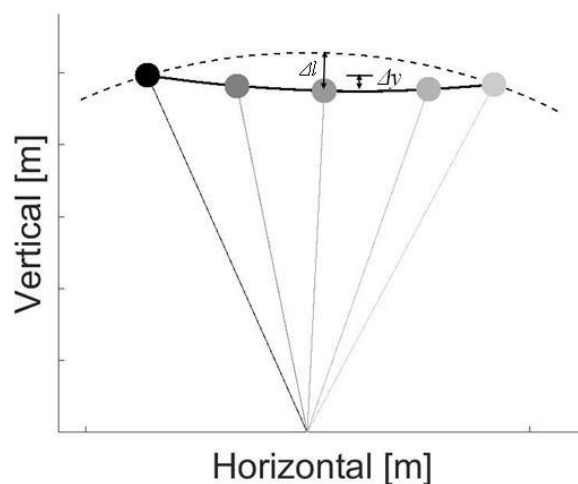


Figure 54 - Pictorial representation of the displacements used to calculate stiffness. The solid line represents the experimental CoM being modelled by the spring mass model, while the dashed line represents the trajectory of an inverted pendulum of length l_0 , the resting length of the spring.

The strength of the relationship between vertical and lower limb stiffness changed with speed. It was found that lower limb stiffness was approximately equal across the four speeds considered while vertical stiffness was approximately 1.5 times larger at the fastest speed than at the slowest speed. Therefore, this finding highlights the differences between vertical and lower limb stiffness, and emphasises the need for clarity when describing the two parameters. The lack of a consistent relationship between lower limb and vertical stiffness implies that one cannot be used as a proxy for the other. Therefore, although vertical stiffness might be easier to calculate, it does not provide information about how the lower limb works during running. Furthermore, since vertical stiffness does not correspond to any physical spring, it could be argued that it does not provide much information about running at all.

Conclusions

The aims of this chapter were three-fold. First the results of this chapter showed that the choice of definition for lower limb length does not have a significant influence on the force-length curve of the lower limb stiffness value. Secondly, this chapter showed that the choice of method for calculating lower limb stiffness does significantly influence the lower limb stiffness value. Furthermore, inconsistent relationships were found between the alternative methods and the physically consistent method, suggesting a need for one distinct definition of lower limb stiffness if results across studies are to be compared. Finally, no relationship was found between lower limb stiffness and vertical stiffness, suggesting these are distinct and individual parameters that require unique definitions. However, it should be noted that the used of lower limb stiffness for describing running is somewhat ambiguous and rudimentary. It describes a net response of the lower limb joints, muscles, ligaments etc. to loading of the CoM, but it does not explain what is happening at the joint level. Therefore, in my opinion, understanding and measuring joint stiffness would provide more useful information than the “all-encompassing” lower limb stiffness.

6. Common modelling methods

Having discussed and explored the theory behind the simplest model of running, the remainder of this thesis will focus on modelling. This chapter will describe the common modelling methods used throughout the remaining chapters. Chapter 7 will go on to explore the ability of the spring mass model. Chapter 8 and chapter 9 will then discuss the effects of sequentially adding complexity to this model. Finally chapter 10 will consolidate the findings of this PhD, discuss limitations, and outline potential areas for future research.

6.1. Experimental data

The findings of the Chapter 4 suggest the assumption of linear elasticity is valid for forefoot strikers only. Therefore, those who adopted a rearfoot strike pattern were excluded from the remaining chapters. Considering this, a subset of the previously collected kinematic and kinetic data was used for this investigation (see Chapter 3). The subset of data was from 19 forefoot strikers, however as some participants adopted a rearfoot strike pattern at the slower speed, some data had to be excluded from the study. Therefore, the final dataset consisted of $n=11, 12, 13$ and 19 participants at speeds $1 - 4$, respectively.

6.2. Model parameters

The CoM movement was estimated using the hip joint centre, which is common to other studies using the spring mass model, and will be close to the Visual3D estimate of the CoM in the AP and vertical directions. This is because the arms and head are not included in the Visual3D model, therefore the Visual3D estimate of the CoM will be offset compared to the anatomical CoM in both the AP and vertical directions (Gill et al. 2017). Model parameters/variables were then calculated based on the following definitions and equations (Table 19). The horizontal and vertical positions are denoted by subscripts x and z , respectively. The subscript 0 indicates the starting value, taken as the value at initial contact.

Table 19 - Model properties.

Parameter/Variable	Symbol	Equation
Approach angle	θ_0	$\theta_0 = \tan\left(\frac{hip_z}{hip_x}\right)$
Lower limb length	l	$l = \sqrt{((hip_x - CoP_x)^2 + (hip_z - CoP_z)^2)}$
Change in lower limb length	Δl	$\Delta l = l_0 - l$
Vertical displacement	Δz	$\Delta z = z_0 - z$
GRF angle	θ_{GRF}	$\theta_{GRF} = \tan^{-1}\left(\frac{GRF_z}{GRF_x}\right)$
Resultant GRF	GRF_{res}	$GRF_{res} = \sqrt{GRF_x^2 + GRF_z^2}$
Lower limb force (Figure 35)	F_{limb}	$F_{limb} = GRF_{res} * \cos(\theta_d)$ $(\theta_d = \theta_{GRF} - \theta_0)$
Lower limb stiffness	k_{limb}	$k_{limb} = \frac{\max(F_{limb})}{\max(\Delta l)}$

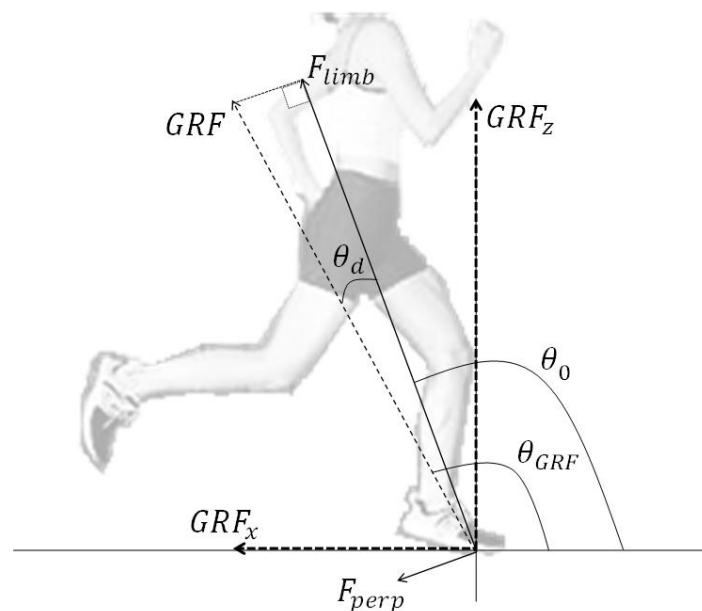


Figure 55 – Lower limb force from GRF, where θ_d represents the difference between the resultant angle, θ_{GRF} , of the GRFs, GRF_x & GRF_z , and the approach angle, θ_0 . The lower limb force, F_{limb} , is then determined by projecting the resultant GRF onto the lower limb axis.

6.3. OpenSim

OpenSim is an open-source software system, developed at Stanford University, which provides a means for developing models and running dynamic simulations (Delp et al. 2007). The software aims to provide a freely available library of models and simulations (see Table 20 for definitions of terms) that can be “*exchanged, tested, analysed and improved*” (Delp et al. 2007) by the biomechanics community. Such collaboration has the potential to extend the understanding of the fundamental principles that control movement, and thus advance the methods used when treating individuals with movement pathologies.

Table 20 - Modelling terminology

Modelling	Methods associated with deriving mathematical models, including simplifications and assumptions, and running dynamic simulations. (D. Gordon E. Robertson et al. 2013)
Model	A simplified description of a physical system intended to capture the essential aspects of the system in a sufficiently simple form to enable the mathematics to be solved. (Daintith et al. 2010)
Simulation	The iterative process of solving the equations of motion of a predefined model to determine time-based kinematics (and possibly kinetics). (D. Gordon E. Robertson et al. 2013)

Newton’s laws of motion are used to derive equations of motion based on the inertia properties of the model. Bones (rigid bodies), joints (mobilisers, constraints and forces), contact elements (rigid constraints and compliant forces) as well as ligaments and muscle actuators (forces) are combined to represent the body being modelled. OpenSim works in a parent-child topology where joints provide the possible number of degrees of freedom, whilst constraints determine the number of allowed degrees of freedom. Therefore, each child body in the system introduces a single joint or constraint that determines its degrees of freedom relative to its parent body. Constraints also mean it is possible to close the loop in the multibody “tree” (Seth et al. 2011, Sherman et al. 2011). OpenSim includes a range of options for joints, however only three will be used in this thesis. The free joint which

has six degrees of freedom, the pin joint which has one degree of freedom about the medio-lateral (z) axis, and the weld joint which essentially fuses the bodies together.

In order to understand and interpret the results of an OpenSim simulation, OpenSim provides a series of analysis and reporting tools (Seth et al. 2011). These tools enable the determination of the model kinematics (internal or spatial) and kinetics (body forces, generalised forces, or muscle and ligament tensions). Analysis consists of three phases; the modeller, solver, and reporter. The modeller creates or alters models according to prescribed criteria. The solver evaluates a series of equations indicated by the type of model. This may include the equations of motion to determine the model kinematics (i.e. trajectories), and/or solving the inverse dynamics problem in order to calculate the joint moments. Finally, the reporter processes (i.e. filters), stores and displays the results. The way in which results are reported is important for comparisons with experimental data. How well models replicate these experimental measures provides a level of confidence for using the model, especially in terms of interpretation of simulations of predictive movements (Seth et al. 2011, Hicks et al. 2015).

6.4. Model set up and simulation

There are some methods common to all the models. These will be discussed below, and only referred to in the description of the individual models.

All of the models were set up and controlled using MATLAB. The OpenSim MATLAB API (Application Programming Interface) was used to access OpenSim libraries and functions. This allows users to create or edit OpenSim models and run OpenSim tools through MATLAB rather than programming in C++ or using the OpenSim GUI (Graphical User Interface). Throughout this PhD OpenSim 3.3 was used.

To perform the optimisation the MATLAB built-in *fminsearch* function was used; *fminsearch* finds the minimum of an unconstrained multivariable function. The cost-function used with these optimisations was defined as the root mean square difference (RMSD) between the experimental and simulated CoM trajectories (Eq. 19). Thus, the optimisation would adjust certain variables, the number of variables in the optimisation

depended on the model being used, to determine the solution that would result in the smallest RMSD between model and experiment.

$$RMSD = \sqrt{\frac{\sum_1^n ((x_{exp} - x_{sim})^2 + (y_{exp} - y_{sim})^2)}{n}} \quad 19$$

The simulations were generally performed using a built-in OpenSim function called the *ForwardTool*. The *ForwardTool* uses a 5th-order Runge-Kutta-Feldberg integrator to solve the equations of motion (OpenSim 2007). It is an open-loop system that applies controls without feedback or correction, thus solutions are not required to “track” a certain trajectory. The integrator settings allow the user to define the minimum and maximum time-step the integrator can take over a pre-defined time interval. For the simulations performed here, the minimum and maximum time-steps were set to 1e-6 and 1e-3 s, respectively, and the time interval as 0 to 2 s.

6.5. Joint angles

Experimental segments were defined using Visual3D. However, the Visual3D segment lengths tend to change slightly during the gait cycle (Figure 56), most likely due to soft tissue marker movement and joint translation during the data collection. Therefore the mean value over the stance phase was used. Furthermore, to avoid including discontinuities at the joints the distal end of the upper segment was used as the proximal end of the lower segment; i.e. the thigh segment was defined using proximal and distal ends of the Visual3D thigh segment, the shank using the distal end of the Visual3D thigh segment and the distal end of the Visual3D shank segment, and the foot using the distal end of the Visual3D shank segment and the distal end of the Visual3D foot segment (Figure 57). Experimental joint angles were then calculated using the means of the Visual3D segment lengths (Table 21). Zero degrees (0 °) of flexion was defined as vertical for the hip, fully extended for the knee and perpendicular to the shank for the foot. These joint angles would then be compared to the joint angles from the different model simulations.

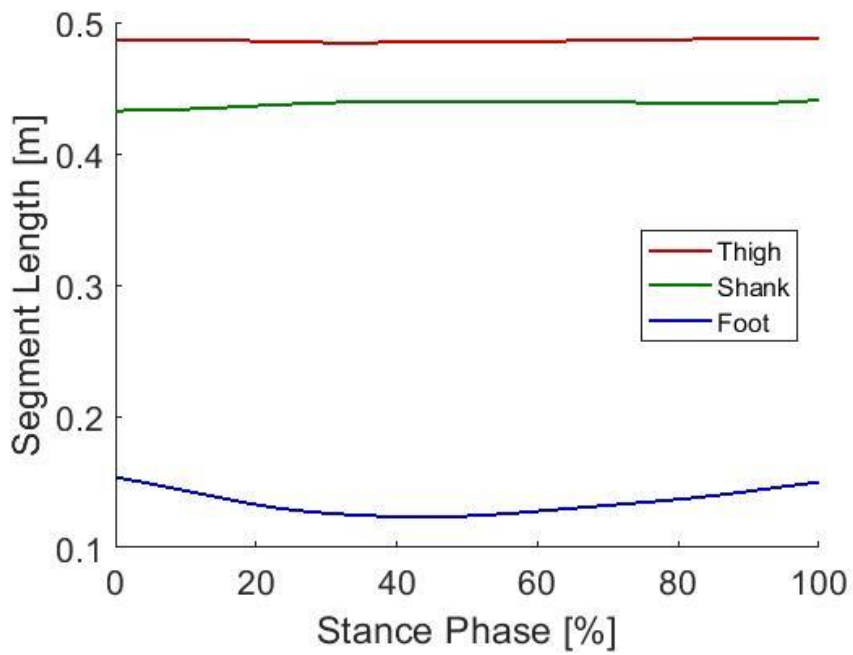


Figure 56 - Example experimental segment length changes during the stance phase of running.

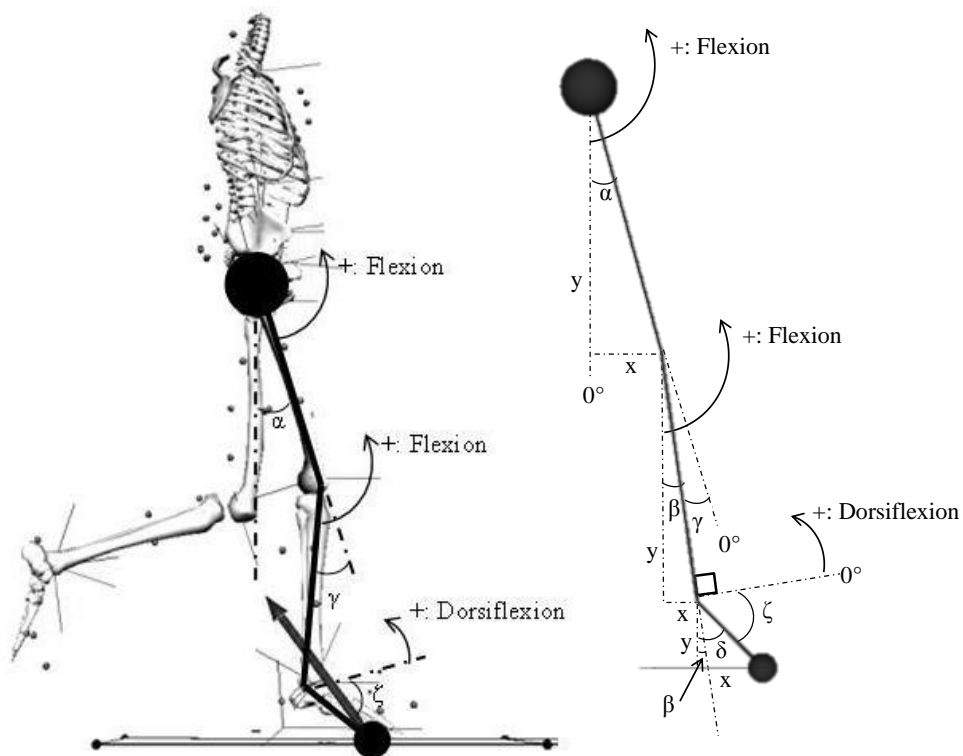


Figure 57 - Experimental joint angles.

Table 21 – Equations used for determining the experimental joint angles.

Hip Angle: $\alpha = -\operatorname{atan}\left(\frac{\text{thigh}_x}{\text{thigh}_y}\right)$	20
$\beta = -\operatorname{atan}\left(\frac{\text{shank}_x}{\text{shank}_y}\right)$	21
Knee Angle: $\gamma = \alpha - \beta$	22
$\delta = -\operatorname{atan}\left(\frac{\text{foot}_x}{\text{foot}_y}\right)$	23
$\varepsilon = \delta - \beta$	24
Ankle Angle: $\zeta = -\left(\frac{\pi}{2} - \varepsilon\right)$	25

This chapter has briefly described the experimental data and the modelling methods that are common to the next few chapters. More detailed methods individual to each of the models/chapters will be described in detail in the relevant methods sections. The next chapter will discuss the simplest model of running, the spring mass model, before complexity is added in chapters 8 and 9.

7. The Simple Spring Mass Model

7.1. Introduction

The spring mass model is the simplest model of running. It is based on the assumption that the CoM movement of a human running can be approximated by a single point mass bouncing on a massless linear spring (Blickhan 1989, McMahon et al. 1990). The model was originally developed by Blickhan (1989) and McMahon et al. (1990) as a means of investigate the fundamental relationships between the mechanical parameters used to describe running. It consists of a single point mass, equivalent to the entire mass of the body, connected to a fixed point on the ground via a massless linear spring of constant stiffness. The compression and extension of the spring is then said to be equivalent to the absorption and propulsive phases of stance, respectively. The swing phase is then approximated by a parabolic flight trajectory of the point mass.

The spring mass model has been used to investigate various aspects of running. For example, the effects of changes in stride frequency (Farley et al. 1996, Morin et al. 2007), speed (He et al. 1991, Farley et al. 1993), and gravity level (He et al. 1991, Donelan et al. 2000) have been determined. However, results from these studies are often only qualitatively compared to previously published values or experimental data, and although the model seems capable of predicting relationships that correspond to those seen experimentally, its ability of actually replicating the kinematics and kinetics of running has yet to be thoroughly established. A few studies have made an effort to quantify the ability of the spring mass model at replicating running (Bullimore et al. 2007, Lipfert et al. 2012). However, these studies were limited by the way they compared the results to experimental data.

Bullimore et al. (2007) aimed to determine the accuracy of the spring mass model at predicting ten running parameters. They used experimental data to determine the input parameters for the spring mass model, and quantitatively compared the model simulations to the experimental parameters, using the percentage error as a measure of agreement. Although they reported “good” agreement (percentage difference $\leq 20\%$) between six of the ten parameters, the CoM trajectories and GRF curves were not directly compared to

experimental data. Instead they reported that the peak CoM displacement and the peak vertical GRF were overestimated and the location of the peaks occurred later in stance than in the experimental data. Furthermore, in this investigation they adjusted the approach angle in order to achieve a symmetrical trajectory, something that is uncharacteristic of human running.

In a more recent study, Lipfert et al. (2012) aimed to determine the ability of the spring mass model at replicating the CoM movement over a range of running speeds. Initial conditions for the simulation were determined using a linear least squares fit to the experimental force-length curve, and simulation trajectories were optimised to find the best fit to the experimental data using a coefficient of determination. The coefficient of determination incorporated the sum of least squares error, total sum of square and the difference between the simulation and experimental contact times. Although a quantitative measure was used to determine the best-fitting solution, the experimental and simulated CoM trajectories were only qualitatively compared. The authors stated “*good qualitative agreement*” was found between the CoM trajectories and the GRF curves. Visual inspection of the graphs presented show similar results to previous studies, where the peak CoM displacement and peak horizontal and vertical GRFs were consistently overestimated. However, in contrast with previous results, the location of these peaks occurred earlier in stance, and the contact times were thus consistently underestimated.

These previous studies suggest that the spring mass model is reasonably good at replicating certain running parameters; however other parameters are consistently under or overestimated. Furthermore, although the model has been used to investigate and further the understanding of the relationships between mechanical characteristics and running parameters, the model is inherently unrealistic. Fundamentally, anatomical limbs are not massless linear elastic springs, but complex musculoskeletal systems. Hysteresis occurs as energy is dissipated by the loading and unloading of tendons, and muscle activation is then required to generate energy to compensate for this loss. In addition, the CoP translates forward during stance, thus the assumption of a fixed contact point will ignore forward translations of the CoM due to the forward movement of the CoP. Despite this, the spring mass model has been a fundamental part of movement research, with the original articles being cited over 2270 times (at the time of writing).

Due to the popularity of the spring mass model, it is essential that the accuracy and validity of the results are properly understood. Considering this, the aim of this chapter was to determine the ability of the spring mass model to replicate running. An imperfect match between model and experiment is both expected and acceptable. Fundamentally, the model is imperfect, as are the systems used to collect the experimental data, therefore marginal differences may be reasonable but large differences would suggest that the model is not simulating the same event. Furthermore, a perfect match between the spring mass model and the experimental data would suggest this very simple model is fully capable of replicating running and there would be no need to add complexity.

Aims

The results of Chapter 4 revealed that the assumption of linear stiffness (force-length behaviour) is not applicable for all runners. This would suggest that the spring mass model is most likely to successfully simulate those runners who exhibit linear force-length behaviour. Therefore, this chapter aims to investigate the performance of the spring mass model when the assumption of linear force-length behaviour is most valid. Based on the findings of the previous chapter, this is generally the case for forefoot strikers. Therefore, to investigate the ability of the spring mass model, the solutions from the model will be compared to experimental data for forefoot strikers at a range of speeds.

7.2. Methods

7.2.1. The model

The spring mass model (Figure 58) consists of a point mass, equivalent to the body's entire mass, connected to a fixed contact point on the ground via a massless linear spring. In this investigation the model is two-dimensional, therefore the contact point was assumed to be the average centre of pressure (CoP) during contact, and the point mass was assumed to be equivalent to the centre of mass (CoM), estimated as the hip joint centre (JC). The initial conditions of the model were determined based on participants' experimental data at initial

contact, based on previously collected kinematic and kinetic data (Chapter 3). The spring mass model was then implemented in OpenSim.

7.2.2. *OpenSim implementation*

The CoM was modelled as a sphere, with finite mass, connected to ground via a free joint (see chapter 6.3). The massless linear spring was modelled as a *PointToPointSpring* where one end was attached to the centre of the CoM sphere and the other to the average CoP. For visual clarity the average CoP was modelled as a massless sphere fixed to the ground via a weld joint (see chapter 6.3, Figure 58). Since OpenSim works in Cartesian coordinates, the initial conditions were taken directly from the experimental data and the *ForwardTool* was used to run the forward simulation.

OpenSim is most commonly used in the development of complex musculoskeletal modelling. Therefore, to validate the use of OpenSim for developing simple mechanical models, solutions for the spring mass model were compared to manually derived equations of motion, implement in MATLAB, and solutions were found to be the same (see Appendix AI).

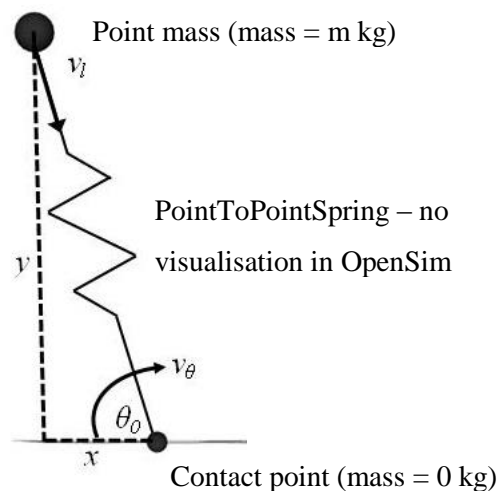


Figure 58 - Spring mass model implemented in OpenSim; here x and y indicate the horizontal and vertical distances between the fixed contact point and the point mass, θ_0 the approach angle and v_l and v_θ the compression and rotational velocities.

7.2.3. *Model simulation*

Two different approaches were used to determine the best fit between the simulation and the experimental data. In the first approach, only the stiffness was varied in the optimiser, whereas in the second approach all initial conditions, as well as the stiffness were allowed to vary in the optimiser. Simulations were run for 2 s, and the results cut to the point where the spring force reached or went below 0 N. If this condition was not reached, the cut-off was defined as the minimum point between the force peaks. Kinematic and kinetic solutions were then interpolated to 101 points to represent 0 to 100 % of the stance phase.

OpenSim has a built-in function called *ForceReporter* that internally calculates the forces involved in the system. Therefore, with this model the *ForceReporter* outputs the forces associated with the *PointToPointSpring*. Because no other forces are acting on this system the spring force is equivalent to the GRFs.

7.2.4. *Compare solutions and statistics*

To assess the predictive ability of the model the simulations were compared to experimental data. The primary indicator of accuracy was the RMSD between the experimental and simulated CoM trajectories, calculated over 101 points, equivalent to 0 to 100 % of the stance phase. This was determined from the minimised cost function described above. The RMSD between the GRFs was also calculated. Additionally, the difference in the contact time, peak CoM displacement, and the peak amplitude of the GRFs were also computed and compared. Finally, when the initial conditions were allowed to vary the optimised values were compared to the experimental initial conditions. Since fixing the initial conditions forces a match between the experimental data and the simulation at initial contact, this method provides another outcome measure of model fit.

The optimised initial conditions were then compared to the experimental values using a paired t-test and the percentage difference was calculated as the follows:

$$\left(\frac{\text{experimental value} - \text{optimised value}}{\text{experimental value}} \right) * 100 \quad 26$$

Statistically the experimental and simulated CoM and GRF waveforms were compared using a correlation coefficient (Gutierrez-Farewik et al. 2006). A correlation was considered strong if r greater than 0.7, moderate if r was greater than 0.5 and weak if r was greater than 0.3. The stiffness values, contact time, peak amplitudes and maximum displacements were statistically compared using multiple paired t-tests. Multiple t-test had to be used instead of an ANOVA because of the changing number of participants as the speeds increased (n=11, 12, 13 and 19 at speeds 1 – 4, respectively). Due to multiple tests, the significance level of the t-test had to be adjusted to avoid the increased probability of type 1 errors. Therefore, the new significance level was set to 0.013.

7.3. Results

7.3.1. Initial conditions vs. Experimental data

When all initial conditions, as well as the stiffness, were allowed to vary, the optimised values for the initial conditions were all significantly different ($p \leq 0.013$) to the experimental data (Table 22 and Table 23). The percentage difference in the horizontal and vertical positions of the CoM varied between 0.03 % smaller and 9.42 % larger than the experimental values. The percentage difference in the velocities, were consistently larger than the corresponding positions, with values ranging between 33.40 % smaller and 157.43 % larger than the experimental values. Since the optimised initial conditions were significantly different to the experimental data further comparisons were isolated to the cases where only the stiffness was allowed to vary.

Table 22 – Mean (SD) of the initial conditions (position) from the experimental data versus when all the initial conditions and the stiffness were allowed to vary.

	Speed 1		Speed 2		Speed 3		Speed 4	
	x	y	x	y	x	y	x	y
Experimental	-0.307 (0.031)	0.935 (0.068)	-0.334 (0.024)	0.929 (0.066)	-0.355 (0.027)	0.925 (0.068)	-0.370 (0.023)	0.907 (0.066)
All varied	-0.319 (0.029)	0.953 (0.069)	-0.349 (0.025)	0.945 (0.068)	-0.371 (0.028)	0.940 (0.071)	-0.388 (0.027)	0.921 (0.067)
Percentage difference	4.1 (2.0)	1.8 (0.5)	4.5 (2.0)	1.7 (0.4)	4.6 (2.1)	1.6 (0.7)	4.9 (2.0)	1.5 (0.6)
sig.	<0.001	<0.001	<0.001	<0.001	<0.001	<0.001	<0.001	<0.001

Table 23 – Mean (SD) of the initial conditions (velocities) from the experimental data versus when all the initial conditions and the stiffness were allowed to vary.

	Speed 1		Speed 2		Speed 3		Speed 4	
	x	y	x	y	x	y	x	y
Experimental	3.117 (0.197)	-0.675 (0.134)	3.706 (0.246)	-0.707 (0.159)	4.512 (0.280)	-0.661 (0.168)	5.247 (0.283)	-0.618 (0.184)
All varied	3.755 (0.385)	-0.713 (0.138)	4.370 (0.252)	-0.742 (0.144)	5.262 (0.456)	-0.704 (0.182)	6.285 (0.614)	-0.709 (0.199)
Percentage difference	-20.7 (13.1)	-5.9 (4.9)	-18.1 (5.8)	-5.6 (5.6)	-16.6 (6.7)	-7.6 (14.0)	-19.7 (8.7)	-18.8 (36.0)
sig.	<0.001	0.004	<0.001	0.014	<0.001	0.115	<0.001	0.010

7.3.2. CoM trajectories

The experimental and simulated CoM trajectories were similar during early stance, but deviated considerably from mid to late stance (Figure 59 and Table 24). Furthermore, the experimental and simulated CoM trajectories were significantly correlated at each speed. In the horizontal direction the mean correlation coefficient was greater than 0.999, the standard deviation less than 0.001, and the p-value less than 0.0005, at all speeds. In the

vertical direction, the correlation coefficients were lower, but still significant, with the means greater than 0.820, the standard deviations less than 0.132, and the p-values less than 0.0005. In addition, the maximum vertical displacements of the CoM were significantly different between experiment and simulation at all speeds (Table 25).

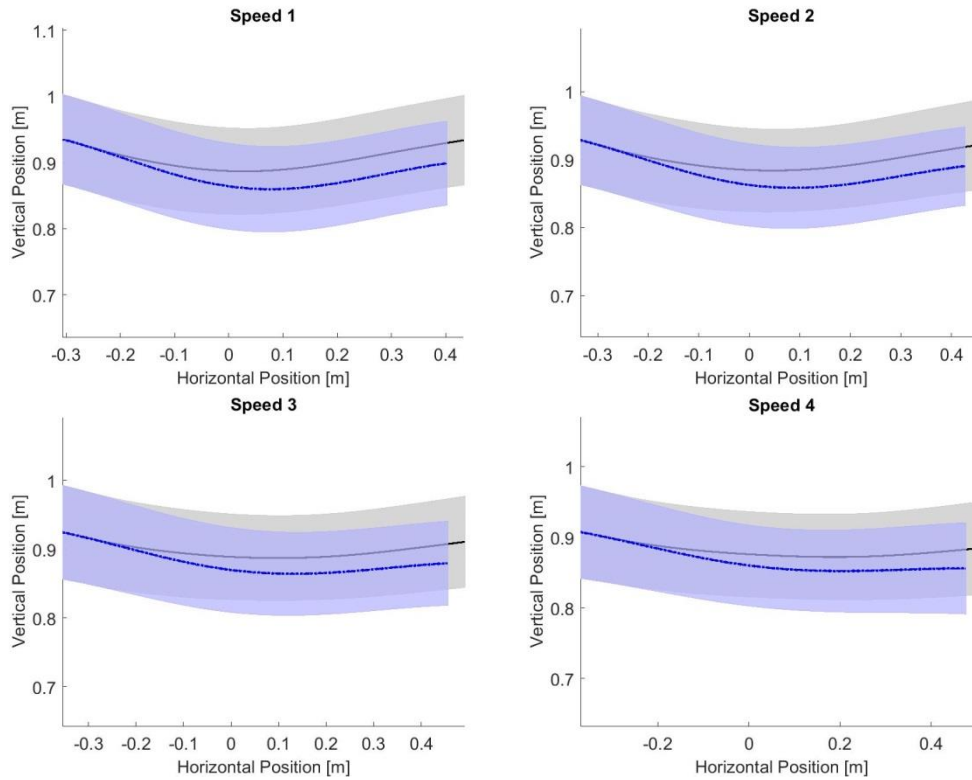


Figure 59 - CoM movement from experiment (black) and spring mass model simulation (blue) from n = 11, 12, 13 and 19 forefoot strikers running at speed 1 – 4 (3.3, 3.9, 4.8, 5.6 m/s), respectively.

Table 24 - Mean (SD) of the RMSD [m] between the experimental and simulated CoM trajectories.

	Speed 1	Speed 2	Speed 3	Speed 4
RMSD _x	0.013 (0.003)	0.014 (0.003)	0.015 (0.004)	0.015 (0.004)
RMSD _y	0.025 (0.008)	0.023 (0.006)	0.020 (0.006)	0.018 (0.006)

Table 25 - Maximum vertical CoM displacement [m].

	Speed 1		Speed 2		Speed 3		Speed 4	
	Exp.	Sim.	Exp.	Sim.	Exp.	Sim.	Exp.	Sim.
Mean (SD)	0.052 (0.005)	0.076 (0.012)	0.047 (0.007)	0.070 (0.013)	0.039 (0.008)	0.062 (0.012)	0.037 (0.009)	0.059 (0.012)
Percentage difference	-44.7 (21.6)		-49.5 (19.3)		-63.2 (27.7)		-62.1 (24.7)	
sig.	<0.001		<0.001		<0.001		<0.001	

7.3.3. GRFs

The experimental and simulated GRF profiles were similar in shape at each speed (Table 26, Figure 60 and Figure 61). In the horizontal direction the mean correlation coefficient was greater than 0.954 (the standard deviation less than 0.020) and the p-value less than 0.0005, at all speeds. Similar to the CoM trajectories, in the vertical direction, the correlation coefficients were again lower than in the horizontal, with the means greater than 0.913, the standard deviations less than 0.046, and the p-values less than 0.0005.

Table 26 – Mean (SD) RMSD [BW] between the experimental and simulated GRFs.

	Speed 1	Speed 2	Speed 3	Speed 4
RMSD _x	0.119 (0.029)	0.119 (0.031)	0.117 (0.032)	0.113 (0.040)
RMSD _y	0.423 (0.063)	0.468 (0.094)	0.618 (0.155)	0.812 (0.188)

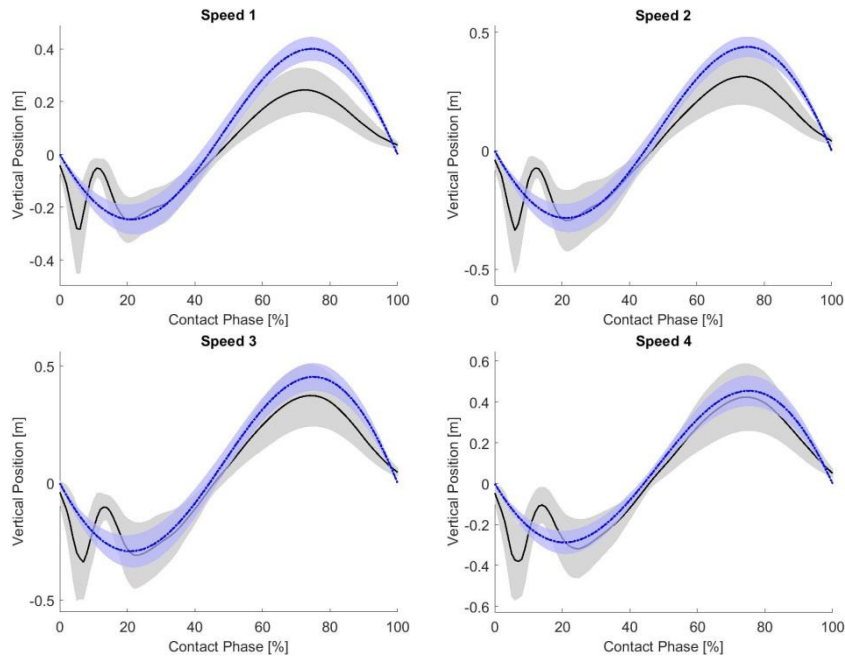


Figure 60 - AP GRFs from experiment (black) and spring mass model simulation (blue) from n = 11, 12, 13 and 19 forefoot strikers running at speed 1 – 4 (3.3, 3.9, 4.8, 5.6 m/s), respectively.

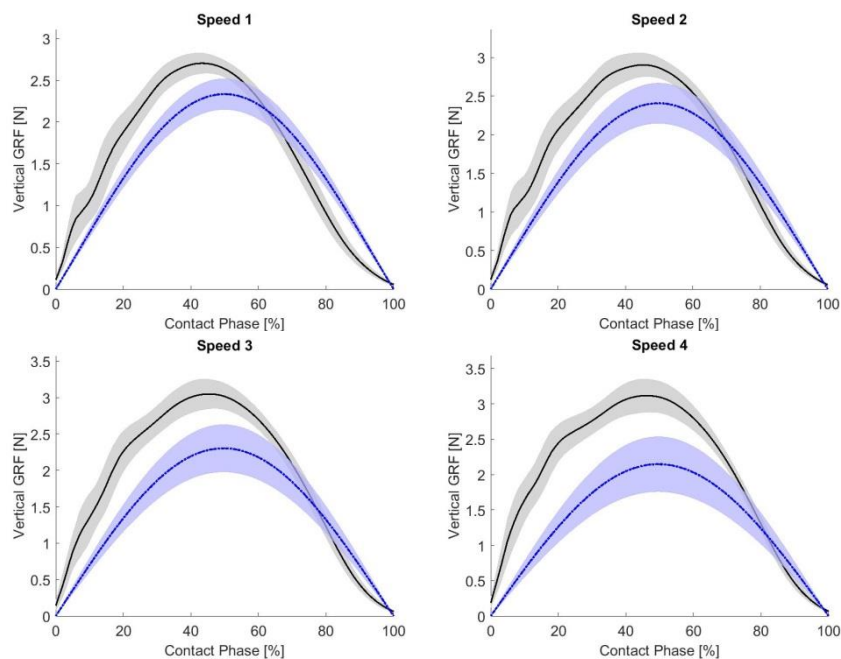


Figure 61 - Vertical GRFs from experiment (black) and spring mass model simulation (blue) from n = 11, 12, 13 and 19 forefoot strikers running at speed 1 – 4 (3.3, 3.9, 4.8, 5.6 m/s), respectively.

Table 27 – Mean (SD) AP GRF troughs [BW] and percentage differences (mean(SD)) from the experimental and simulated data

	Speed 1		Speed 2		Speed 3		Speed 4	
Mean (SD)	-0.324 (0.165)	-0.247 (0.057)	-0.364 (0.170)	-0.285 (0.058)	-0.389 (0.189)	-0.292 (0.068)	-0.429 (0.208)	-0.286 (0.055)
Percentage difference	10.4 (31.9)		9.1 (31.7)		11.9 (32.3)		19.5 (36.1)	
sig.	0.078		0.075		0.046		0.006*	

Table 28 – Mean (SD) AP GRF peaks [BW] and percentage differences (mean(SD)) from the experimental and simulated data

	Speed 1		Speed 2		Speed 3		Speed 4	
Mean (SD)	0.249 (0.085)	0.400 (0.045)	0.317 (0.119)	0.439 (0.042)	0.381 (0.131)	0.454 (0.058)	0.428 (0.164)	0.454 (0.073)
Percentage difference	-79.8 (62.5)		-55.9 (53.9)		-31.8 (44.1)		-20.6 (46.9)	
sig.	<0.001		0.003		0.078		0.530	

Table 29 – Mean (SD) Peak vertical GRF [BW] and percentage differences (mean(SD)) from the experimental and simulated data

	Speed 1		Speed 2		Speed 3		Speed 4	
	Exp.	Sim.	Exp.	Sim.	Exp.	Sim.	Exp.	Sim.
Mean (SD)	2.717 (0.123)	2.339 (0.178)	2.913 (0.151)	2.407 (0.258)	3.062 (0.196)	2.304 (0.323)	3.123 (0.232)	2.137 (0.381)
Percentage difference	13.7 (8.4)		17.3 (8.3)		24.8 (9.8)		31.7 (10.5)	
sig.	<0.001		<0.001		<0.001		<0.001	

The magnitudes of the peaks were different between the experimental and simulated GRFs (Table 27, Table 28 and Table 29). The AP (anterior-posterior) GRF trough was similar between the experimental data and the simulation, with a significant difference ($p \leq 0.013$) at speed 4 only (Table 27). Interestingly, the peak AP GRFs were significantly different at speeds 1 and 2, but not at speed 3 and 4 (Table 28). On the other hand, the peak vertical GRFs were significantly different at all four speeds (Table 29). Furthermore, the location of the peaks appears to occur later in the simulated stance phase than in the experimental stance phase (Figure 60 and Figure 61).

7.3.4. Contact time difference

Simulated contact times were consistently higher than the experimental contact times (Table 30). These differences were significant at speeds 2 – 4, but not at speed 1. Although, it should be noted the means and standard deviations appear similar between the experimental data and simulation results. Furthermore, the mean (SD) percentage difference suggest that the simulation contact times were relatively similar to the experimental values.

Table 30 – Mean (SD) contact time [s] and percentage difference (mean(SD) between experimental data (Exp.) and the best-fitting model simulations (Sim.)

	Speed 1		Speed 2		Speed 3		Speed 4	
	Exp.	Sim.	Exp.	Sim.	Exp.	Sim.	Exp.	Sim.
Mean	0.223	0.230	0.199	0.209	0.173	0.182	0.157	0.163
(SD)	(0.010)	(0.014)	(0.010)	(0.015)	(0.009)	(0.013)	(0.009)	(0.013)
Percentage difference	-3.5		-4.9		-4.8		-4.0	
	(5.0)		(4.9)		(5.1)		(4.8)	
sig.	0.047		0.005		0.005		0.002	

7.3.5. Stiffness values

Stiffness values calculated from the experimental data (see Chapter 5) were consistently higher than those determined from the model optimisation (Table 30). Paired t-tests showed that the values were significantly different ($p \leq 0.013$) at all speeds. Furthermore, the percentage difference shows there was a considerable difference between the experimental and optimised stiffness values.

Table 31 – Mean (SD) Stiffness values [kN/m] and percentage difference (mean(SD) between experimental data (Exp.) and the best-fitting model simulations (Sim.)

	Speed 1		Speed 2		Speed 3		Speed 4	
	Exp.	Sim.	Exp.	Sim.	Exp.	Sim.	Exp.	Sim.
Mean	15.338	11.402	15.470	11.368	16.292	11.312	15.703	10.623
(SD)	(4.130)	(2.540)	(3.845)	(2.380)	(4.135)	(2.524)	(3.198)	(2.233)
Percentage difference	24.4 (6.9)		25.5 (7.3)		29.7 (7.5)		31.9 (8.6)	
sig.	<0.001		<0.001		<0.001		<0.001	

7.4. Discussion

The simplest model of running is that of the spring mass model. This model relies on the assumption that the CoM movement of a human running is approximately similar to that of a single point mass bouncing on a massless linear spring (Blickhan 1989, McMahon et al. 1990). This chapter aimed to investigate the performance of the spring mass model for forefoot strikers. The solutions from the spring mass model were compared to experimental data at a range of speeds in order to assess the ability of this model at replicating the biomechanics of normal distance running.

In the cases where the initial conditions and stiffness were allowed to vary, significant differences were found between the experimental and optimised initial conditions (Table 22). These optimised variables were between 0.03 % smaller and 9.42 % larger than the

experimental values. This suggests that optimising these variables could inherently change the system being modelling. Thus, the validity of this solution comes into question, i.e. if the initial conditions are altered from the experimental values, then how much of the real system is actually being modelled? Therefore, only the case where the stiffness alone was allowed to vary will be discussed further.

The question of validity could also be asked of the previous studies which have looked at the ability of the spring mass model for replicating running. Bullimore et al. (2007) allowed the approach angle to vary, and argued that they chose to do this “*because animals tend to keep [stiffness] constant and to vary [approach angle] when they change speed*”. However, the assumption of the lower limb as a spring is only an approximation, and the exact value cannot be directly known. Therefore, it seems more reasonable to allow the stiffness of the system to be adjusted, and keep the geometry the same as the experimental data. Furthermore, in this investigation a symmetrical bounce was not enforced as a condition of the simulation, as human running is generally not symmetrical.

When only the stiffness was allowed to vary, the inability of this simple spring mass model is highlighted. Simulations resulted in the overall CoM trajectory and the vertical GRF being underestimated, with the peaks/troughs occurring later in the simulated stance phase than in the experimental stance phase. This finding for the CoM trajectories is similar to previous studies (Bullimore et al. 2007, Lipfert et al. 2012) that have attempted to assess the ability of the spring mass model (Figure 62). However, our results show the peak horizontal GRF is overestimated while the peak vertical GRF is underestimated by the model, a finding that contradicts these previous studies (Figure 63). This difference is likely due to the differences in how the model was optimised and the choice of the cut-off point of the simulation. Furthermore, although the peak values differ, the simulated CoM trajectories and GRF profiles follow similar trends to the experimental data. This would explain why this model is so often used to investigate running parameters. If the relationships between running parameters are of more interest than the values, then this model can provide insight into how these parameters might affect each other and be affected by speed. However, care must be taken if the magnitudes of these parameters are being assessed.

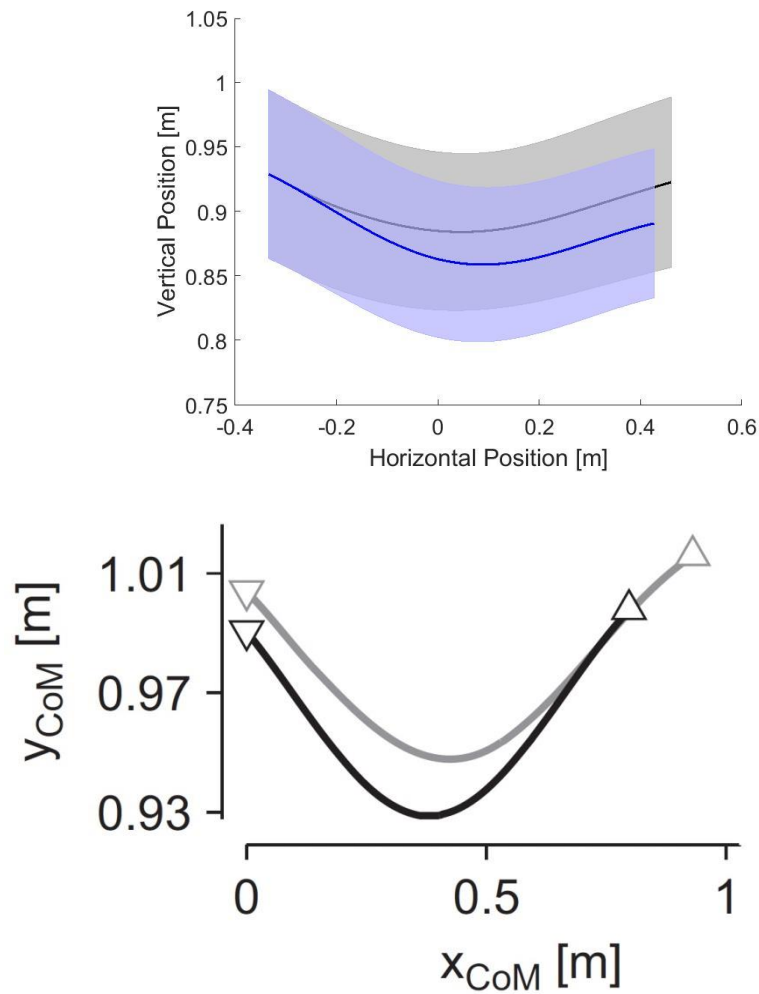


Figure 62 - Comparison of CoM trajectories presented here (top: mean(SD) for running at 3.9 m/s, blue = simulation, black = experimental) and previous studies assessing the ability of the spring mass model (bottom: Lipfert et al. (2012) for running at 4 m/s, black = simulation, grey = experimental).

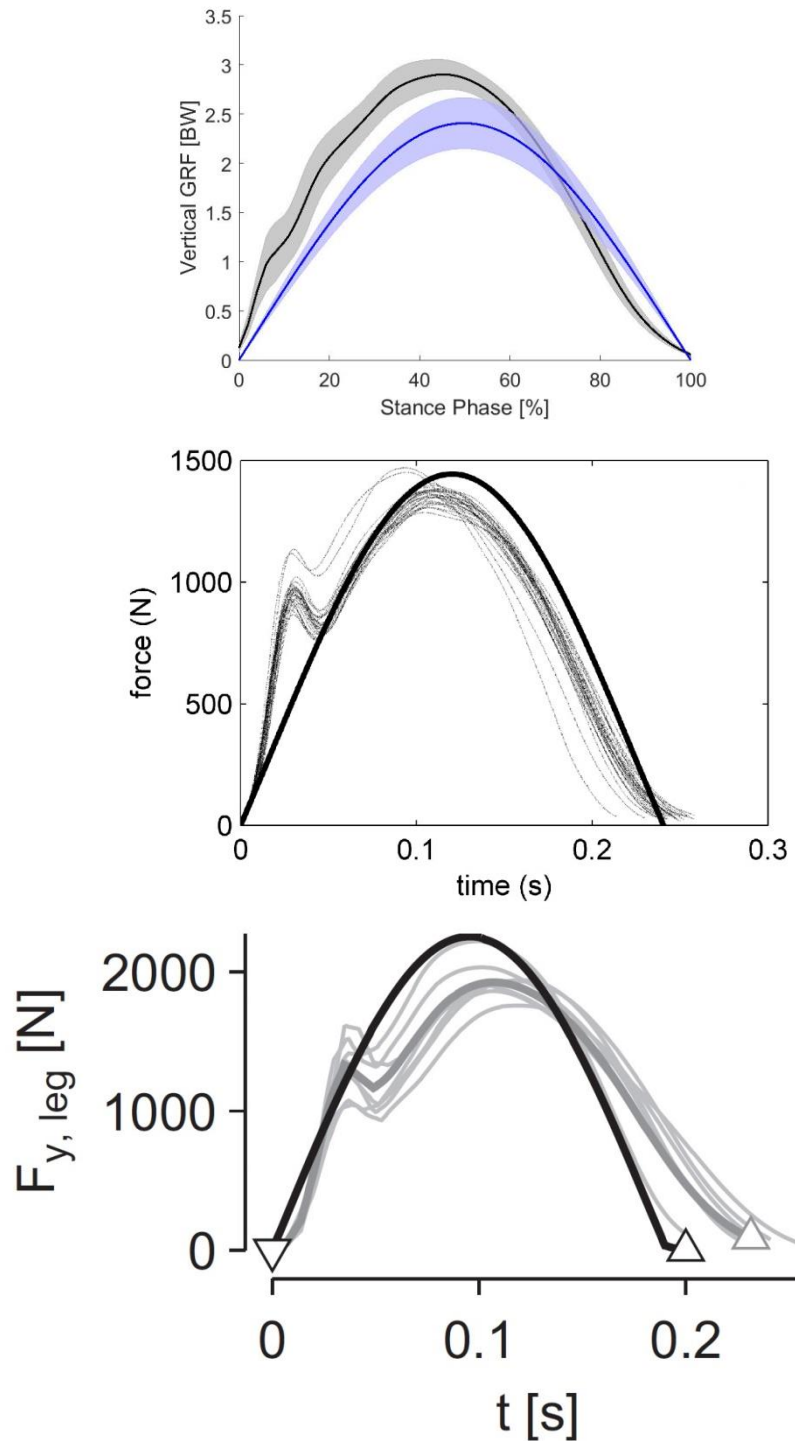


Figure 63 - Comparison of vertical GRFs presented here (top: mean(SD) for running at 3.9 m/s, blue = simulation, black = experimental) and previous studies assessing the ability of the spring mass model (middle: Bullimore et al. (2007) for running at 3 m/s and bottom: Lipfert et al. (2012) for running at 4 m/s; black = simulation, grey = experimental).

The simulated contact times were consistently larger and significantly different from the experimental values (for three of the four speeds). These differences could explain the discrepancies in the GRFs. Since the contact times are larger, but the trajectories similar, the simulated CoM accelerations must differ from the experimental values. If the vertical component of the CoM decelerates more slowly than the experimental CoM, the resulting vertical GRFs would be lower than the experimental values. Furthermore, since the simulated CoM fails to rebound sufficiently from mid to late stance it suggests the model has insufficient mechanical energy to accelerate the CoM upwards during this phase. On the other hand, the horizontal component of the GRF match closely between model and experiment during early stance and midstance, but the model overestimates the GRF during late stance. Since the horizontal component of the CoM is nearly identical to the experimental CoM until late stance when it underestimates the displacement, it would again suggest the model has insufficient mechanical energy to accelerate the mass forward.

Another important difference to note is that the optimised lower limb stiffness values from the model are consistently and significantly smaller than those determined from the experimental values. A previous chapter on calculating lower limb stiffness showed that large differences in magnitude exist depending on the method being used (see Chapter 5). Here the stiffness was optimised to minimise the difference between the simulated and experimental CoM trajectories, thus determining the “best-fitting” solution. If the experimental stiffness values were used the vertical displacement of the simulated CoM becomes more similar to the experimental displacement, however the horizontal distance covered becomes much smaller than the experimental data (Figure 64). Thus there is a trade-off in accuracy, and the optimised solution is the one that best fits both the horizontal and vertical components of the CoM trajectory.

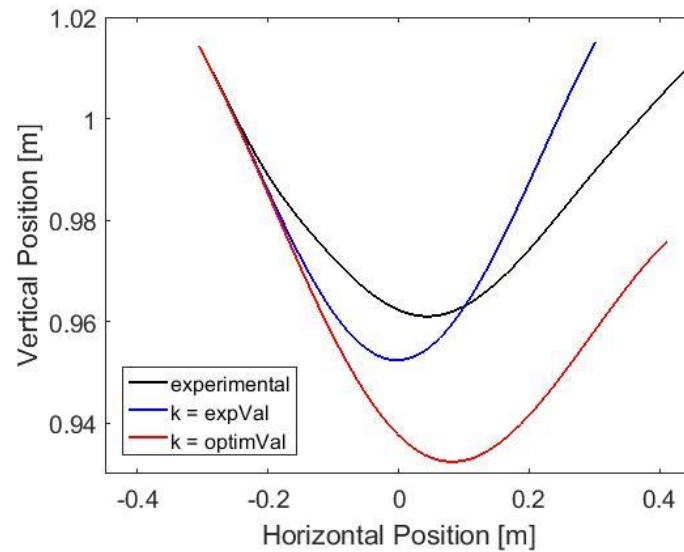


Figure 64 - Comparison of the simulated CoM trajectories, using the experimental value for stiffness ($k = \text{expVal}$) versus the optimised value ($k = \text{optimVal}$), of a single subject at a speed 2 (3.9 m/s).

Considering these differences between the model simulations and the experimental data it would appear to suggest the spring mass model is not appropriate for modelling running. Furthermore, this investigation was restricted to those participants who exhibited the more linear force-length relationships, thus theoretically should have been the most appropriate runners to be modelled. Although, previous studies have identified some of the pitfalls of this model, suggesting it be “*used only to investigate parameters which it can predict accurately*” (Bullimore et al. 2007). However, these authors argued that the spring mass model predicted stance time and relative peak force (among others) well (within 20 % of the measured values), whereas our results showed these to be significantly different to the experimental data despite appearing to have a similar percentage difference between simulated and experimental values (Table 29 and Table 30). Therefore, since significant differences were found between the contact times, stiffness values, maximum vertical CoM displacement, and peak GRFs it suggests care must be taken when using this model to investigate and describe normal distance running.

The spring mass model is said to be capable of predicting the relative relationships between certain running parameters (Blickhan 1989, McMahon et al. 1990, Farley et al.

1996, Bullimore et al. 2007). For example, shorter contact times follow increases in stride frequency and the peak vertical GRF increase as speed increases (Blickhan 1989), however the model lacks the complexity required to accurately replicate the biomechanics of normal distance running. This was highlighted by Lipfert et al. (2012) who argued that, at slow running speeds successful model locomotion was not possible within the allowed parameter range, and suggested that “*the existing limitations [of the spring mass model] may be improved by adding complexity to the model*” (Lipfert et al. 2012). The inaccuracy of this model is expected due to its inherent simplicity. The human body is a very complex musculoskeletal system which cannot be accurately described by such a simple mechanical system. However, the fact the model can replicate certain relationships suggests that it may be possible to model running using a simple, but slightly more complex, mechanical system. This model, with a single linear spring, indicates the possible importance of storing and returning elastic energy during running. However, without joints it is impossible to determine which muscles and/or tendons are required and used to harness this conservation of elastic energy.

The following chapter will discuss adding the first layer of complexity to the model. The choice of the first layer of complexity is somewhat arbitrary; however it seemed logical to first introduce a knee joint due to its suggested importance during the stance phase of running. The knee joint has the largest range of motion of all the lower limb joints during running, with approximately 25 degrees of flexion occurring during the stance phase (Nicola et al. 2012, Gross et al. 2013). It has been suggested that the knee joint, and the muscles crossing the knee joint, act mainly to control the collapse of the lower limb during the loading phase of stance (Novacheck 1998). Considering this, introducing the knee as the first added layer of complexity to the spring mass model could provide a discrete way of testing this rationale.

8. ... adding a knee joint

8.1. Introduction

The results of the previous chapter highlight the limitations of the spring mass model. Although the general characteristics of running appear to be reproduced by such a simple model, the amplitudes of the CoM trajectories and the vertical GRFs are consistently over and underestimated, respectively; suggesting the model needs to be adapted. Therefore, the next phase of this PhD was to add the first layer of complexity to the spring mass model. It seemed reasonable that the first layer of complexity take the form of a knee joint. This layer of complexity would potentially determine the phases of stance during which the knee is most important.

It is generally accepted that primary function of the knee joint in running is to act as a “*shock absorber*” (Novacheck 1998, Nicola et al. 2012) and that the muscles crossing the knee joint provide “*dynamic control and stabilisation*” (Ferber et al. 2014). However, as mentioned previously, in the discussion of the kinematics of running (Chapter 1.1.2), the use of words like *stabilise*, *control* and *shock absorber* are ambiguous and can be misleading. For example, it is unclear whether the “*control and stabilisation*” of the knee joint refers to a mechanism for resisting applied loads, or controlling the range of motion, or whether it refers to a method of controlling the amount of force that crosses the knee joint. Furthermore, it is likely that here “*shock absorption*” actually refers to the observed dissipation of the kinetic energy as the CoM decelerates from initial contact to midstance, and thus has resulted in some authors describing the primary function of the knee as a “*damper*” (Farris et al. 2017). However, Farris et al. (2017) showed that the secondary function of the knee was as a spring, and the more energy that can be stored rather than dissipated the lower the energy cost; therefore, describing the knee as a “*spring-damper*” might be more appropriate.

The dominant muscle groups acting about the knee are the hamstrings and quadriceps (Ferber et al. 2014). During the braking phase, the first half of stance, the knee flexes and there is a corresponding increase in the knee extensor moment (Figure 65). It has been suggested that during this phase the vasti and gluteus muscles act to control the amount of

knee flexion which arises as a consequence of the external knee flexor moment (Hamner et al. 2010, Farris et al. 2017). Conversely, during propulsion, the second half of stance, these movements are reversed, and the soleus and gastrocnemius become dominant (Hamner et al. 2010). However, the gastrocnemius is a knee flexor and the soleus doesn't cross the knee joint. This suggests some other mechanism contributes to knee extension during the second half of stance, possibly return of stored elastic energy, and active control of the ankle joint movement is taking place during this mid to late phase of stance.

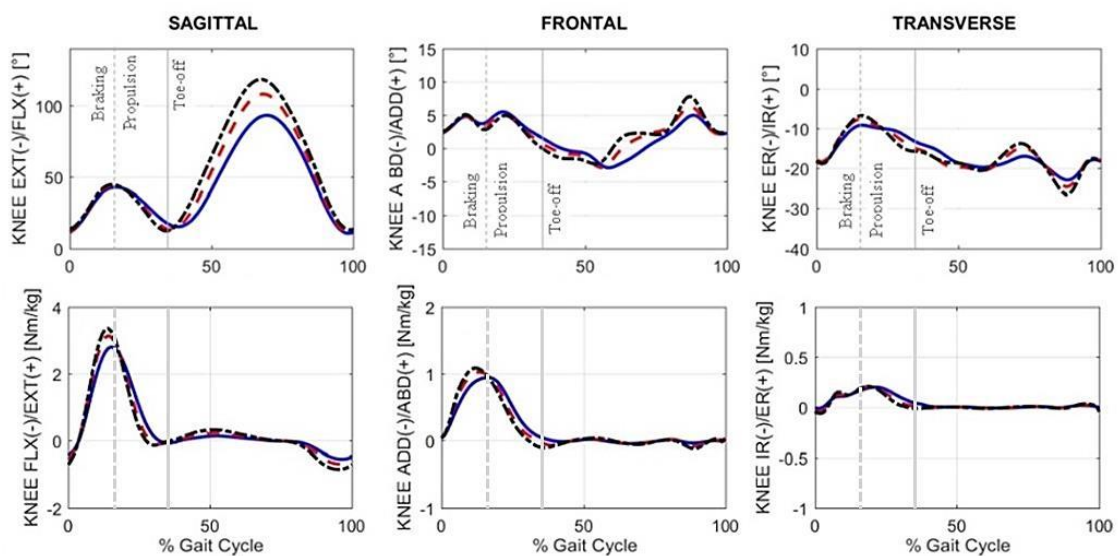


Figure 65 – Knee joint angles during treadmill running at 2.5 m/s (solid blue), 3.5 m/s (dashed red), and 4.5 m/s (dot-dash black) (Fukuchi et al. 2017). Positive degree changes imply flexion, adduction and internal rotation. The dashed vertical line indicates the braking and propulsive phases of stance, while the solid vertical line indicates toe-off.

Depending on the foot strike pattern adopted, differences exist in the knee joint kinetics and kinematics associated with running (Almeida et al. 2015, Thompson et al. 2015, Kuhman et al. 2016) (Kulmala et al. 2013). For example, in a group of habitual rearfoot strikers, the sagittal plane knee range of motion (Figure 66; left), peak knee extensor moment (Figure 66; right) and peak knee eccentric extensor power were all greater during their normal running trial as compared to trials where they were asked to run with a

forefoot strike pattern (Kuhman et al. 2016). In this example, most kinetic and kinematic variables had a significant main effect with both foot strike pattern and speed; where values increased with speed. Therefore, it appears that forefoot strikers generally have a lower peak knee flexion angle (Kulmala et al. 2013, Almeida et al. 2015), a lower knee flexion range of motion (Almeida et al. 2015) and a higher knee internal rotation at initial contact (Thompson et al. 2015), than rearfoot strikers. However, although these differences have been reported as significant, there appears to be a large amount of variability between participants, with the standard deviations overlapping between forefoot and rearfoot strikers (Figure 66).

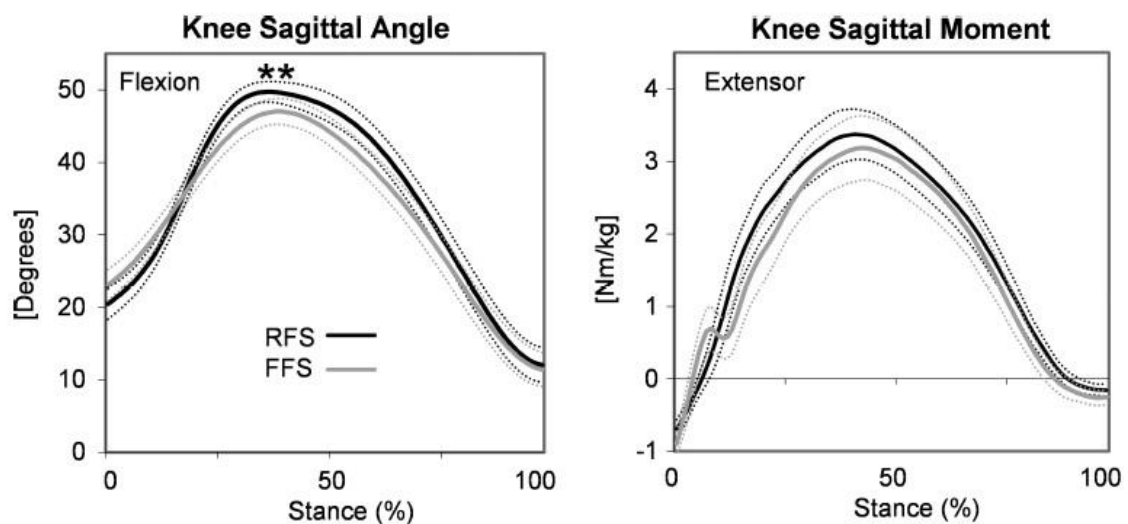


Figure 66 - Stance phase sagittal plane knee moment (Kulmala et al. 2013)

In running literature, references are often made to limb, vertical and joint stiffness. Limb stiffness refers to the changes in the lower limb length as a response to the force applied along the limb, while vertical stiffness describes the resistance of the body to changes in vertical CoM displacement (discussed in detail in Chapter 5). Joint stiffness, on the other hand, is often calculated from the ratio of its moment to angular displacement (Farley et al. 1998, Günther et al. 2002). Although it has been argued that this method does not account for the instantaneous mechanical properties of the joint (Pfeifer et al. 2012), alternative model-based methods have nevertheless determined similar estimates for knee stiffness (Pfeifer et al. 2012). This suggests this perturbation method (the ratio of the joint moment

to angular displacement) is an appropriate non-invasive approach for estimating joint stiffness during locomotion. Knee joint stiffness is instinctively adjusted during natural locomotion in order to adapt to specific obstacles and terrains (Pfeifer et al. 2012). This regulation of joint stiffness has been proposed as a method for minimising the energy required for locomotion (Shen et al. 2015a), as well as being related to optimal locomotion stability (Shen et al. 2015b). However, “*regulating joint stiffness*” seems to suggest a system with “*variable stiffness*”, and as mentioned previously (Chapter 2.5.1) stiffness is a characteristic of a passive system, and a passive system cannot be changed. Therefore, non-linearity in moment-angular displacement (force-displacement) curves more likely indicate active mechanisms, and this “*regulation of joint stiffness*” relates to differing amounts of muscle activation when running on different surfaces.

Both knee joint stiffness and the change in knee angle have been shown to increase as running velocity increases (Arampatzis et al. 1999, Günther et al. 2002, Kuitunen et al. 2002). The ankle stiffness is significantly lower than knee stiffness; and shows less change with increasing speed, which has led authors to suggest that the knee predominantly contributes to the overall lower limb stiffness during running (Farley et al. 1998, Günther et al. 2002). However, in physics the overall stiffness of multiple springs (that adhere to Hooke’s law) in series, is a combination of the individual stiffness values and is predominantly dependent on the least stiff element. Therefore, it likely makes more sense to consider the ranges of motion and the length of the lever arms of the joints. The knee has a greater range of motion than the ankle, and thus functioning over a longer lever arm has the potential to modify the CoM movement more than the ankle. This gives support to the decision for the first added layer of complexity to take the form of a knee joint. Therefore, the aim of this chapter is to develop a model incorporating a knee joint in order to investigate the biomechanical properties of the knee joint, and how the knee joint stiffness contributes to how and why people run the way they do.

Few running models incorporating a knee joint currently exist in the literature. A limited number of two-segment lower limb models (Figure 67) have been developed to investigate the effects of lower limb compliance, focusing on the joint level, on running stability (Rummel et al. 2008, Phan et al. 2017). These models aimed to build on previous work by investigating the stability region of the simple-spring mass model, and address the fact that biological limbs are not springs but instead exhibit spring-like behaviour at the joint level

(Seyfarth et al. 2001, Günther et al. 2002, Kuitunen et al. 2002, Rummel et al. 2008). It has been argued that symmetrical joint flexion during dynamic loading can be achieved if the joint stiffnesses in a segmented lower limb are appropriately adjusted (Seyfarth et al. 2001). To investigate the potential impact of lower limb segmentation on the stability of running, two-segment models were developed (Figure 67). These incorporated either a rotational spring at the intersegmental joint (Rummel et al. 2008) or two linear springs representing the major muscle groups of the upper leg (Phan et al. 2017).

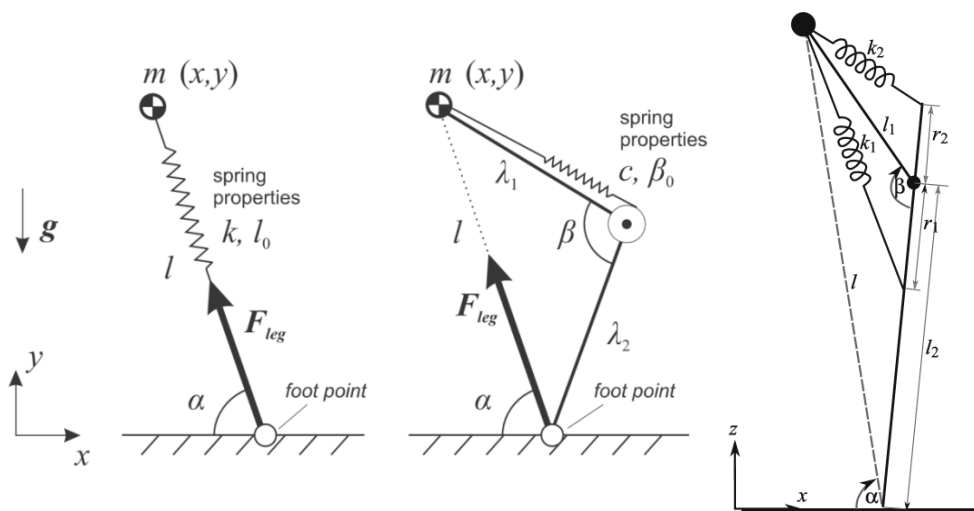


Figure 67 – Left: Spring mass model and the two-segment model developed by Rummel et al. (2008); Right: two-segment model developed by Phan et al. (2017).

In the model by Rummel et al. (2008) the two-segments were massless and had equal lengths, $\lambda_1 = \lambda_2$. The model parameters were fixed to those of a generic human (mass $m = 80$ kg and lower limb length $l_0 = 1$ m), and the joint stiffness, c , was determined using the joint torque and the change in joint flexion, i.e. the perturbation method. Similarly, in the model by Phan et al. (2017), again the two segments were massless but in this case the segment lengths, l_1 and l_2 , were optimised. The hamstrings and quadriceps femoris muscle groups were modelled using two linear springs of equal stiffness, $k_1 = k_2$. For both springs the proximal end was attached to the point mass, m . However, the distal end was attached to either an arbitrary point on the lower limb segment (between the knee joint and the foot)

for k_1 (representing the hamstrings), or to the upper tip of the lower limb, for k_2 (representing the quadriceps femoris) (Figure 67).

The results of the two-segment models presented by Rummel et al. (2008) and Phan et al. (2017), were compared to the spring mass model, instead of experimental data. The comparisons focused on the stable regions of the model simulations, i.e. the parameter combinations where multiple “steps” could be achieved. Although, in the case of a torsional spring the joint stiffness, c , was compared to experimental knee joint stiffness and found to be similar (Rummel et al. 2008). Both versions of the two-segment model showed that lower limb segmentation provides a larger range of self-stable running speeds and that the lower limb force is reduced compared to the spring mass model (Rummel et al. 2008, Phan et al. 2017). Furthermore, these models revealed that a maximum running speed existed for a given joint stiffness, suggesting that joint stiffness must be increased to attain higher running speeds, a finding that is supported by experimental data. When the segment lengths differed, successful simulations occurred when the ratio of the upper segment to the lower segment were in a range similar to that of an anatomical distribution of a humans lower limb (Phan et al. 2017). However, it should be reiterated that the “*running pattern*” produced by these models were not quantitatively compared to experimental data, thus it is not possible to ascertain how well they replicated normal human running.

Aims

The aim of this chapter is to develop a two-segment model in OpenSim and compare it to experimental data. The chapter aims to determine the contributions of adding segments, with finite mass, and a knee joint to the movement characteristics of the model. How these layers of complexity affect the models ability at replicating normal distance running biomechanics will be established, and thus suggestions will be made as to how these features influence the way in which people run.

8.2. Methods

8.2.1. The Model

The sprung knee (SK) model added a layer of complexity to the spring mass model. It consisted of four parts (point mass, thigh, shank and contact point). The point mass and contact point were equivalent to that in the spring mass model, but in this new model they were connected via two segments with fixed inertial properties (calculated using $I = mr_g^2$, where I is the segment moment of inertia, m is the segment mass and r_g is the radius of gyration (Dempster 1955, D. Gordon E. Robertson et al. 2013)), representing the ‘thigh’ and the ‘shank and foot’ (Figure 68). In this model, the mass of each of the segments was defined based on an approximated anatomical distribution; with the mass of the swing lower limb, torso, head and arms collated at the point mass. The thigh segment was connected to the point mass via a weld joint (see chapter 6.3), the shank to the thigh via a pin joint (see chapter 6.3) and the contact point, modelled as a massless sphere for visual clarity, to the shank via a weld joint. The contact point was then connected to ground via a point constraint.

Two versions of this model were developed (Figure 68); these will be referred to as the *SKlinear* and *SKtorsional* models, respectively. The *SKlinear* model incorporated a linear *PointToPointSpring*, identical to that in the spring mass model of the previous chapter, and thus provided a means of determining the sole effect of adding the rigid segments (with finite mass). The linear spring was connected between the point mass and the contact point. The resting length was defined as the distance between the point mass and the contact point, at initial contact, and the stiffness was determined from optimisation. On the other hand, the *SKtorsional* model incorporated a *SpringGeneralizedForce* which acted about the intersegmental “knee” joint. This spring operated as a torsional spring with the resting length defined as the “knee” angle at initial contact, and again the spring stiffness was determined from optimisation. This model design provided a means of modelling the net effect of the muscles and tendons crossing the knee joint, and thus represents a more anatomically correct configuration.

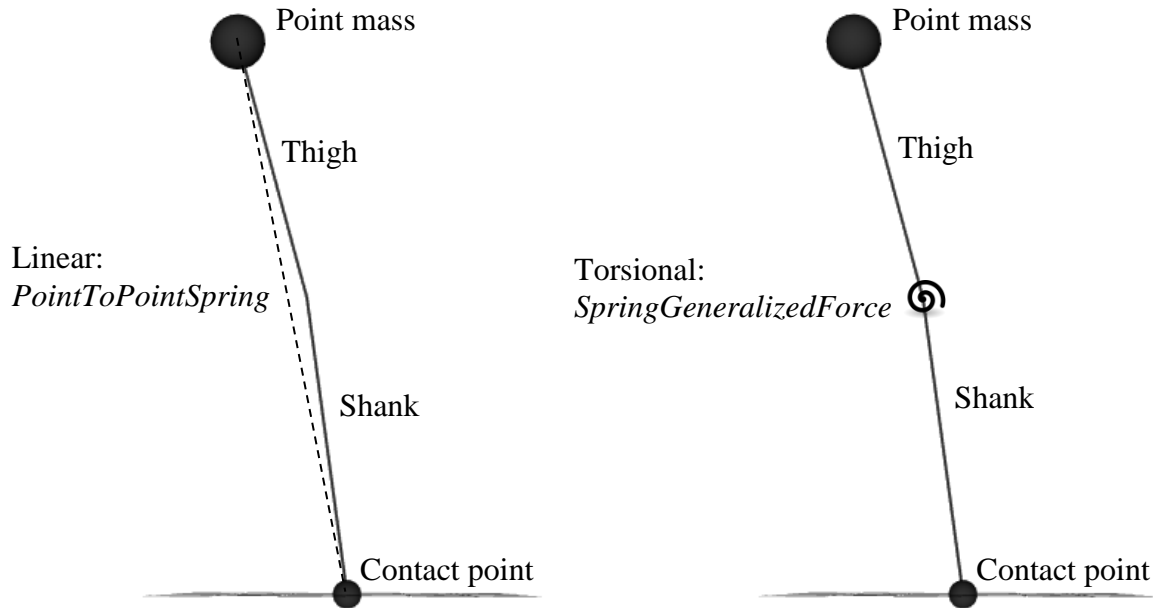


Figure 68 - OpenSim SK models (left *SKlinear* and right: *SKtorsional*). Segment lengths, l , were determined from subject-specific anatomical data. The point mass account for the combined weight of the head, arms, trunk and swing leg ($m_{pm} = 0.845 \cdot \text{total body mass}$). The model segment masses, m , and moments of inertia, I , were approximated used data from Dempster (1955). The model “thigh” segment approximated the anatomical thigh ($m_{thigh} = 0.096 \cdot \text{total body mass}$; $I_{thigh} = m_{thigh} \cdot (0.323 \cdot l_{thigh})^2$). Finally, the model “shank” segment represented the combined anatomical shank and foot ($m_{shank} = 0.059 \cdot \text{total body mass}$; $I_{shank} = m_{shank} \cdot (0.303 \cdot l_{shank})^2$), and its length was estimated as the mean distance from the knee joint to the average CoP.

The thigh segment was defined in the same way as the experimental segment (Chapter 6.5), i.e. as the average distance between the hip and knee joint centres. On the other hand, the “shank” was defined as the average distance between the knee joint centre and the average CoP during stance. There was considerable variation in the length of the model “shank” segment because this “shank” segment combined the anatomical shank and foot, and thus there is a large difference in the combined segment length as the ankle dorsiflexes (Figure 69). Due to this discrepancy, the segment was too short and it was not possible to model early and late stance using this segment length. However, if a different segment length was used it is likely that it would be possible to model these periods separately.

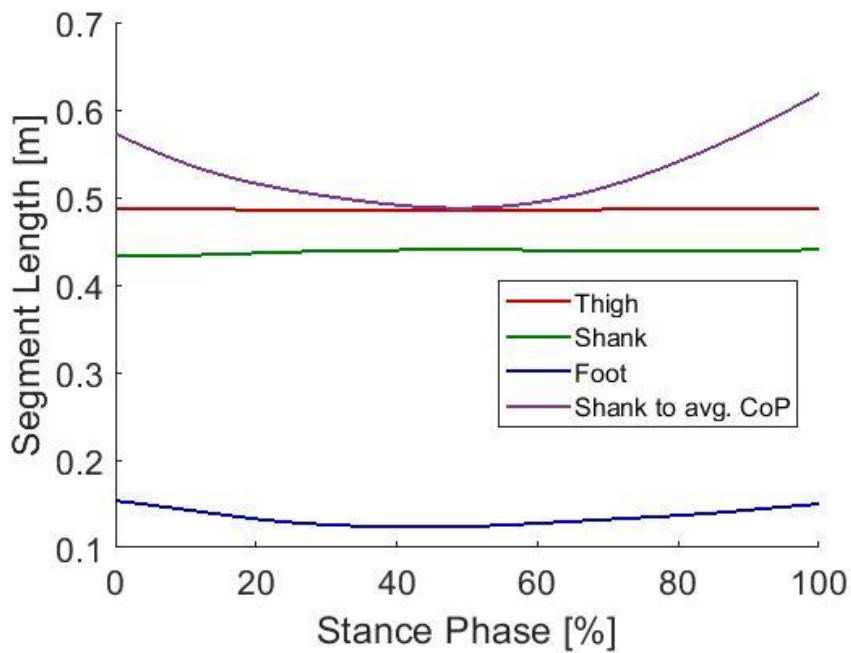


Figure 69 - Example changes in the experimental segment lengths (red: thigh, green: shank, and blue: foot) versus model segment lengths (red: thigh and purple: shank and foot) during the stance phase of running.

8.2.2. Joint angle calculations

In the SK model the anatomical shank and foot are combined into a single “shank” segment. Therefore, the model joint angle calculations (Table 32) are slightly different to those used to calculate the experimental joint angles (Table 21 – Chapter 6.5). Again, zero degrees (0 °) of flexion was defined as vertical for the hip and fully extended for the knee, however in this case no ankle joint exists (Figure 70).

Table 32 - Equations for determining the SK model joint angles.

$$\alpha = -\sin\left(\frac{hip_x}{hip_l}\right)$$

$$\beta = \cos^{-1} \left(\frac{hip_l + thigh_l^2 - shank_l^2}{2 * hip_l * thigh_l} \right)$$

$$\gamma = \cos^{-1} \left(\frac{shank_l + thigh_l^2 - hip_l^2}{2 * shank_l * thigh_l} \right)$$

Hip Angle: $\alpha\beta = \alpha + \beta$

Knee Angle: $\delta = \gamma - \pi$

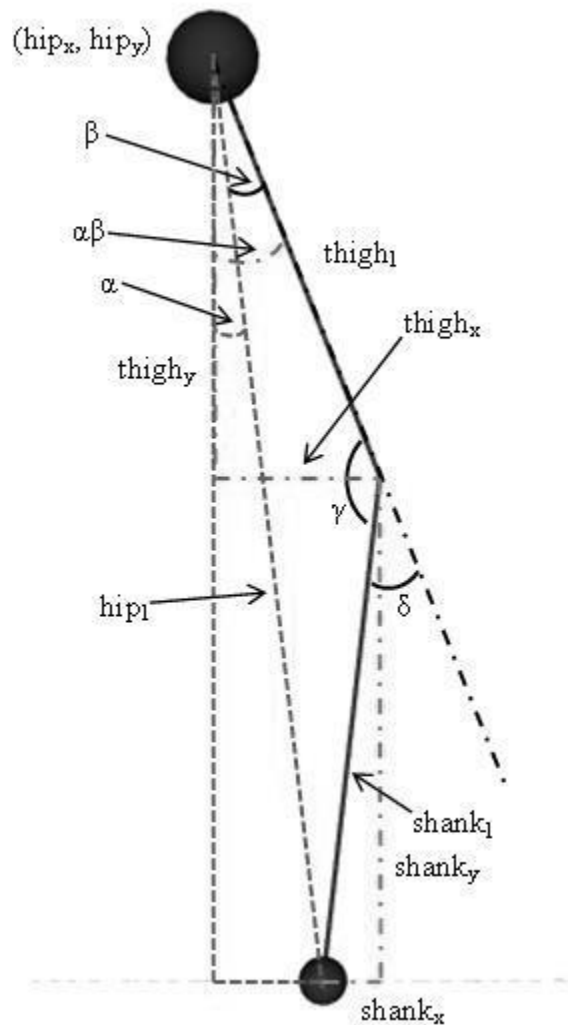


Figure 70 - OpenSim SK model configuration.

8.2.3. *Initial conditions, optimisation and simulation*

Both *SKlinear* and *SKtorsional* models adopted the same model parameters and initial conditions; the only difference was in the way the spring was defined. The initial position of the CoM and the corresponding linear velocities were taken from the experimental data. The initial joint angles (hip and knee) were taken from the calculated model joint angles (Table 32) and the initial angular velocities were determined from the optimisation. This was because the joints did not directly correspond to the anatomical joints, and therefore the corresponding velocities might have been erroneous. The spring stiffness was also determined from the optimisation.

The start and endpoints of the simulation had to be determined prior to optimisation. Based on the segment lengths, the start point, i , was defined as the first point in the stance phase where the following inequality was true (Eq. 27). Similarly, the end point was then defined as the last point, i , in the stance phase where the following inequality was true (Eq. 27). The inequality meant the knee must be flexed and the joint angle must be a real number. Based on an initial inspection of the results, a further condition that the knee angle must be greater than 10° of flexion was added for determining the start point. If this condition was not included the simulations tended to follow a trajectory similar to the inverted pendulum rather than the spring mass model. The choice of 10° of flexion was selected as most runners land with the knee flexed between 10 and 20° (Nicola et al. 2012). This changed the start point by $1.3 \pm 0.5\%$.

$$\begin{aligned} & (hip_l(i) - shank_l) < thigh_l \\ & \& \hspace{15em} 27 \\ & thigh_l < (hip_l(i) + shank_l) \end{aligned}$$

As with the spring mass model (Chapter 7), the equations of motion for each of the models were determined within OpenSim. The equations were automatically generated based on the mass and inertia properties of the model segments, and the *ForwardTool* was used to integrate these forward in time. The spring stiffness and the hip and knee angular velocities were allowed to vary in the *fminsearch* optimisation, and the simulation cut-off was defined using the spring force. In the case of the *SKlinear* model, the simulation cut-off

was defined as the first minimum in the vertical component of the spring force (Figure 71). On the other hand, in the case of the *SKtorsional* model, the simulation cut-off was defined as the first minimum of the spring torque or the point where the knee angle passes 0° , whichever came first (Figure 71). The values for the angular velocities were determined during the optimisation; however initial estimates were taken from the experimental values in the model configuration (combined shank and foot). The optimisation was also run using two other initial estimates to reduce the possibility of the optimiser getting stuck in a local minimum. Finally, the cost function associated with the optimisation was the same as before, the RMSD between the experimental and simulated CoM trajectories (Chapter 6.4).

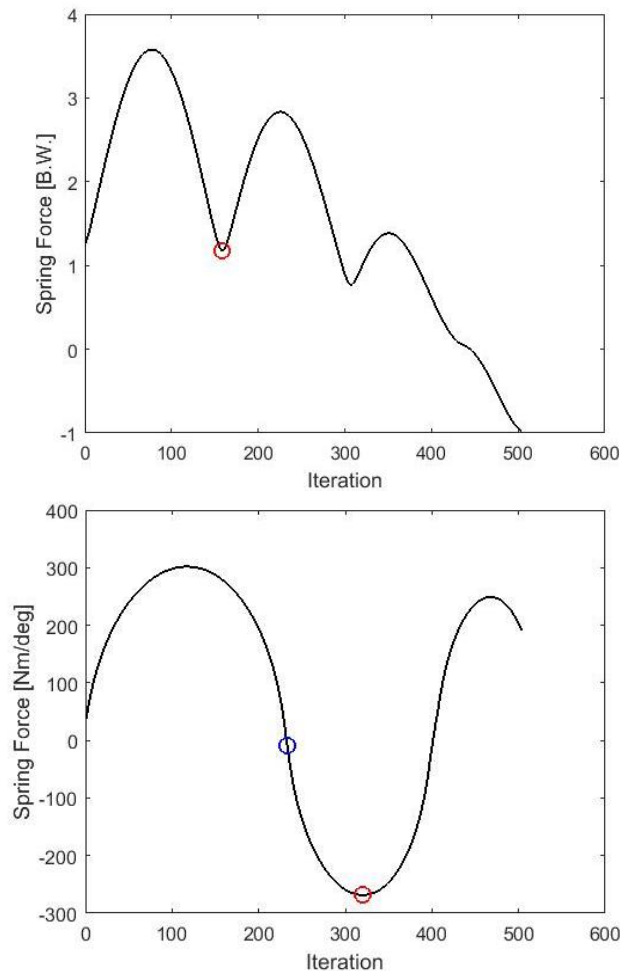


Figure 71 - Example of the spring force in the *SKlinear* model (top) spring torque in the *SKtorsional* model (bottom). The red circle denotes the minimum of the spring force/torque, while the blue circle denotes the point where the knee angle passes 0° .

8.2.4. Ground reaction force calculations

The built-in OpenSim *ForceReporter* was used to determine the torque in the torsional spring. Meanwhile, the GRFs were manually determined based on the mass and accelerations of the segments, using MATLAB. The segment CoM positions were calculated using the segment ratios specified in Dempster (1955), and the accelerations were determined by the double differentiation of the segment CoM positions. The total anterior-posterior and vertical forces were then the sum of the forces, due to each component, in each direction (Table and Figure 72).

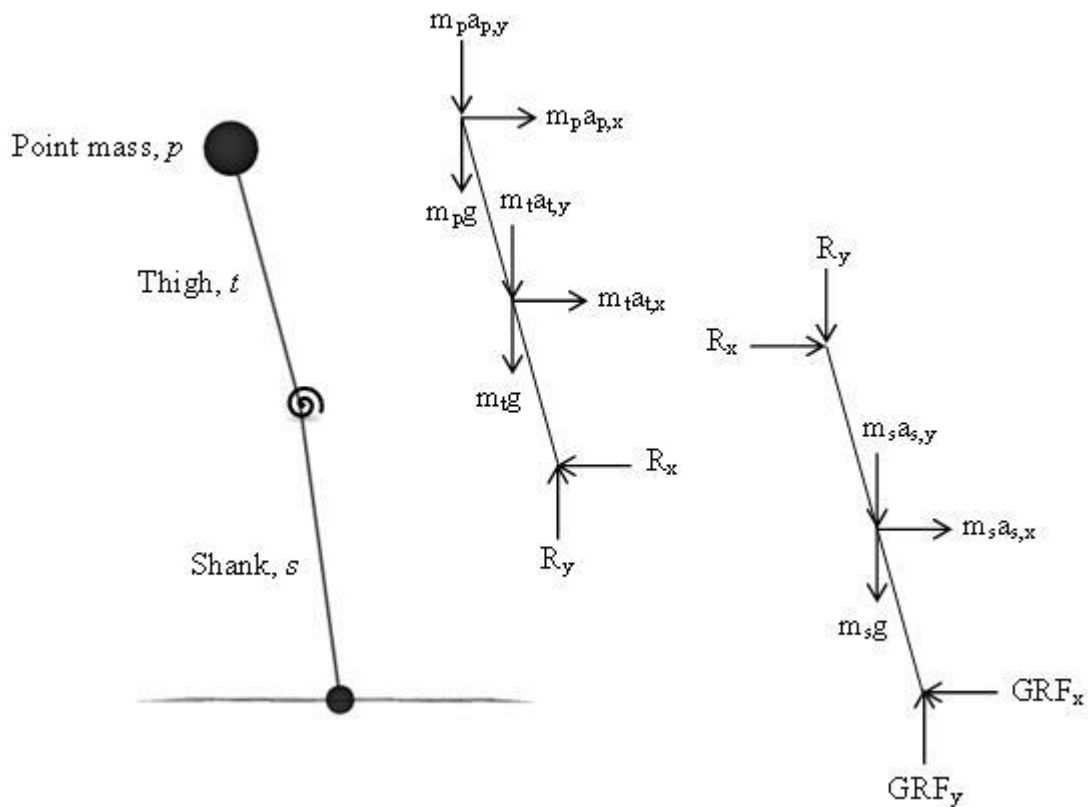


Figure 72 - Force diagram of the SK model.

Table 33 - Equations for calculating the GRFs

$$\begin{aligned} \sum F_x &= ma_x \\ R_x &= m_p a_{p,x} + m_t a_{t,x} \\ GRF_x &= m_s a_{s,x} + R_x \\ \\ \sum F_y &= ma_y \\ R_y &= m_p a_{p,y} + m_p g + m_t a_{t,y} + m_t g \\ GRF_y &= m_s a_{s,y} + m_s g + R_y \end{aligned}$$

8.2.5. Comparing solutions & Statistics

Solutions from the *SKlinear* and *SKtorsional* models were compared to the experimental data. Similar to the spring mass model, the cost function was again defined as the root mean square difference (RMSD) between the simulated and experimental CoM trajectories (see Chapter 6.4 for details), and this RMSD was the primary indicator of accuracy between the experimental and simulated CoM trajectories. The maximum vertical CoM displacement for each model was calculated, as the difference between the maximum and minimum vertical CoM positions during the simulation, and compared to the experimental data. These simulated maximum vertical displacements were compared to the experimental values using a paired t-test and the percentage difference was calculated as follows:

$$\left(\frac{\text{experimental value} - \text{optimised value}}{\text{experimental value}} \right) * 100 \quad 28$$

The RMSD between the GRFs were also determined, and the difference in the peak amplitudes of the GRFs calculated and compared. Finally, since these SK models included an intersegmental joint, the simulated “knee” trajectory was also compared to the experimental knee trajectory using a RMSD. In addition to determining the RMSD, the CoM and knee trajectories and the GRF profiles were also correlated to assess the relationship between the model simulations and the experimental data (Gutierrez-Farewik

et al. 2006). A correlation was considered strong if r great than 0.7, moderate if r was greater than 0.5 and weak if r was greater than 0.3.

For each of the SK models the optimised initial conditions were compared to the experimental values using a paired t-test and the percentage difference (Eq. 28). Finally, the lower limb stiffness for the *SKlinear* model and the knee joint stiffness for the *SKtorsional* model were compared to the experimental values using a paired t-test. The experimental knee joint stiffness was calculated using the peak joint moment and the maximum change in joint angle, during the stance phase, where the knee joint angle and the net joint moment were determined using Visual3D.

It should be noted that because of the changing number of participants as the speeds increased ($n=11, 12, 13$ and 19 at speeds 1 – 4, respectively), individual t-tests were determined for each speed, resulting in a new significance level of 0.013.

8.3. Results

8.3.1. CoM trajectory curves

The root mean square differences (RMSD) between the experimental and simulated CoM trajectories were similar between models (Table 34). The simulated and experimental CoM trajectories were significantly and highly correlated ($r \geq 0.999$; $p \leq 0.013$) in the horizontal direction at all speeds. The strength of the correlation in the vertical direction was more variable and smaller than in the horizontal direction (Table 35). These correlations were significant at speeds 1 to 3, but not at speed 4. Figure 73 shows an example of the lowest RMSD at the slowest speed compare to the highest RMSD at the fastest speed.

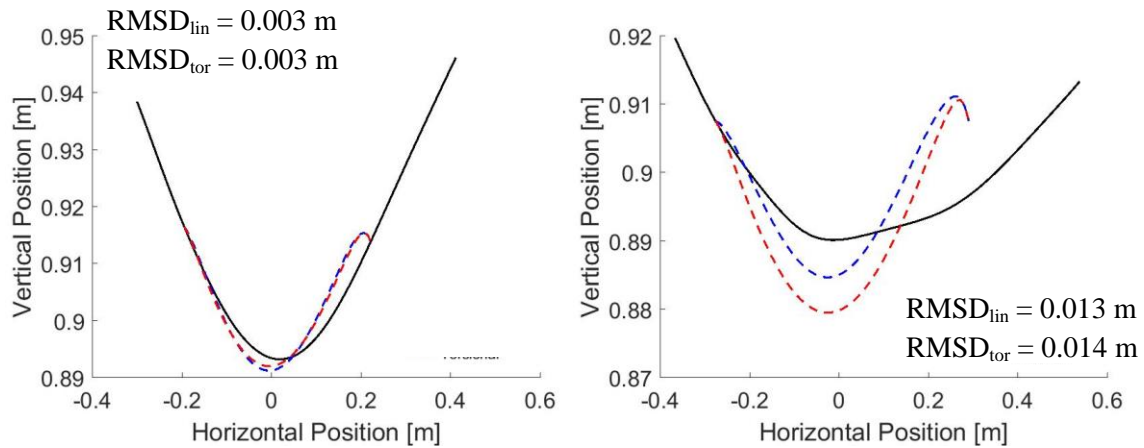


Figure 73 – Simulated CoM trajectories of the *SKlinear* (blue dashed) and *SKtorsional* (red dashed) compared to the experimental CoM trajectory (black solid) for the participant with the lowest RMSD at speed 1 [3.3 m/s] (left) and the participant with the highest RMSD speed 4 [5.6 m/s] (right).

Table 34 - Mean (SD) of the RMSD [m] between the simulated and experimental CoM trajectories.

	Speed 1	Speed 2	Speed 3	Speed 4
SKlinear	0.005 (0.001)	0.006 (0.001)	0.007 (0.002)	0.008 (0.002)
SKtorsional	0.005 (0.001)	0.006 (0.002)	0.007 (0.002)	0.008 (0.003)

Table 35 - Mean (SD) correlation coefficients between the simulated and experimental vertical CoM trajectories. * indicates correlations were significant for all participants ($p \leq 0.013$).

	Speed 1	Speed 2	Speed 3	Speed 4
SKlinear	0.910 (0.050)*	0.849 (0.066)*	0.714 (0.158)*	0.603 (0.204)
SKtorsional	0.919 (0.048)*	0.862 (0.072)*	0.738 (0.146)*	0.633 (0.228)

8.3.2. Maximum vertical displacement

The maximum vertical displacements relate only to the period being simulated (middle 60 % approximately) as opposed to the whole stance phase. However, this is the period during which the maximum vertical displacement generally occurs during running. Similar to the experimental data, the values for the maximum vertical CoM displacements of the simulated trajectories (both *SKlinear* and *SKtorsional* models) were larger at the slower speeds than at the faster speeds (Table 36). However, the largest percentage difference between the models and the experimental displacements occurs at speeds 2 and 3, with speeds 1 and 4 having relatively low percentage differences (*SKlinear*: -11.3 (8.5), -17.0 (17.5), -25.1 (38.5) and -1.1 (20.8) and *SKtorsional*: -4.2 (11.7), -15.2 (16.8), 15.4 (30.0) and 6.3 (11.7), for speed 1-4 respectively).

Table 36 - Mean (SD) of the maximum vertical displacement [m] of the experimental data and simulations. No significant differences were found between the simulated and experimental values ($p \geq 0.121$).

	Speed 1	Speed 2	Speed 3	Speed 4
Experimental	0.026 (0.003)	0.023 (0.004)	0.020 (0.006)	0.021 (0.005)
SKlinear	0.029 (0.005)	0.027 (0.005)	0.024 (0.005)	0.021 (0.005)
SKtorsional	0.028 (0.005)	0.027 (0.005)	0.022 (0.005)	0.019 (0.005)

8.3.3. GRF curves

The simulated AP and vertical GRFs profiles have a similar shape to the experimental profiles (Figure 74). The RMSD between the AP and vertical GRF profiles suggest large errors between the experimental and simulated profiles (Table 37 and Table 38). However, it should be noted that the differences in the forces were considerably larger during the first and last 5 % (approximately) of the simulation, and it is likely these large initial and final differences considerably affect the overall RMSD.

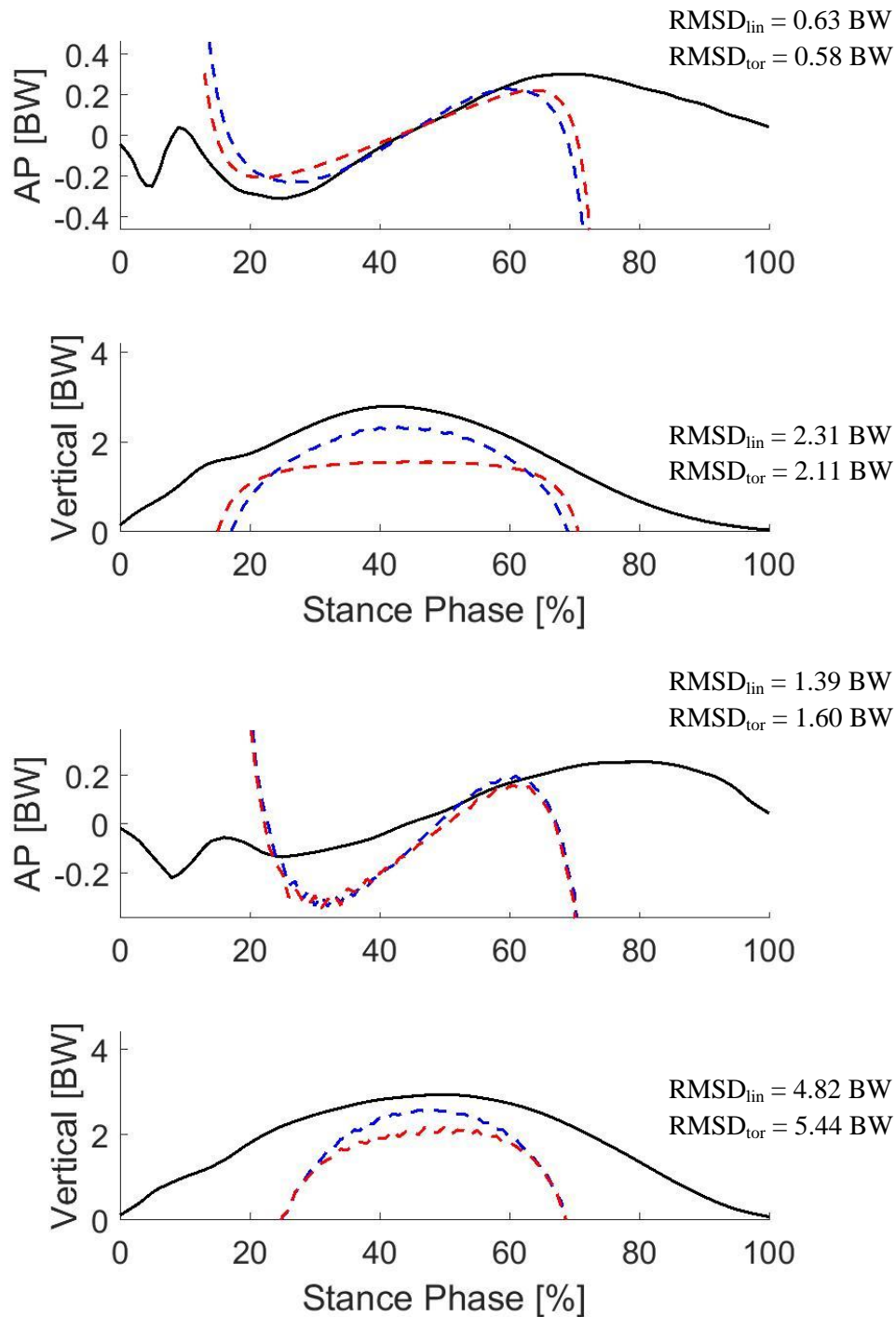


Figure 74 - Experimental (black solid) and simulated (*SKlinear*: blue dashed; *SKtorsional*: red dashed) GRF profiles from the participant with the lowest RMSD at speed 1 [3.3 m/s] (top) and the participant with the highest RMSD at speed 4 [5.6 m/s] (bottom).

Table 37 - Mean (SD) of the RMSD [BW] between the simulated and experimental anterior-posterior (AP) GRF profiles.

	Speed 1	Speed 2	Speed 3	Speed 4
SKlinear	0.726 (0.138)	0.860 (0.162)	1.065 (0.303)	0.974 (0.204)
SKtorsional	0.731 (0.336)	0.789 (0.354)	1.094 (0.472)	1.131 (0.295)

Table 38 - Mean (SD) of the RMSD [BW] between the simulated and experimental vertical GRF profile.

	Speed 1	Speed 2	Speed 3	Speed 4
SKlinear	2.927 (0.531)	3.231 (0.622)	3.655 (0.892)	3.282 (0.565)
SKtorsional	2.924 (1.026)	3.007 (1.055)	3.728 (1.325)	3.605 (0.729)

The correlation analysis revealed insignificant relationships in the AP GRFs and significant relationship in the vertical GRFs (Table 39 and Table 40). Weak negative relationships were consistently found in the AP direction, with both the *SKlinear* and *SKtorsional* models, at all four speeds (Table 39). On the other hand, moderate-to-strong relationships were consistently found in the vertical direction (Table 40), with both the *SKlinear* and *SKtorsional* models, at all four speeds. Again, it is likely that the large differences at the beginning and end of the simulation affected these correlation coefficients.

Table 39 - Mean (SD) of the correlation coefficients between the simulated and experimental anterior-posterior (AP) GRF profile.

	Speed 1	Speed 2	Speed 3	Speed 4
SKlinear	-0.185 (0.066)	-0.204 (0.090)	-0.248 (0.098)	-0.239 (0.076)
SKtorsional	-0.064 (0.201)	-0.071 (0.189)	-0.199 (0.097)	-0.211 (0.082)

Table 40 - Mean (SD) of the correlation coefficients between the simulated and experimental vertical GRF profile. All correlations were significant ($p \leq 0.013$).

	Speed 1	Speed 2	Speed 3	Speed 4
SKlinear	0.804 (0.038)	0.800 (0.034)	0.799 (0.037)	0.809 (0.026)
SKtorsional	0.716 (0.045)	0.720 (0.037)	0.731 (0.042)	0.743 (0.028)

Unlike the RMSDs, comparison of the peak GRF values indicates reasonably good agreement between model simulations and the experimental data (Table 41 and Table 42). The peak and trough of the AP GRFs and the peak vertical GRF were generally all underestimated by both the *SKlinear* and *SKtorsional* models at all speeds (Figure 74, Table 41). Significant differences were found between the simulated values and the experimental values at the faster speeds, and the peak vertical GRF from the *SKtorsional* model was significantly different the experimental value at speed 2 as well (Table 42).

Table 41 - Mean (SD) of the trough/peak AP GRF values [BW] of the experimental data and simulations. * indicates the respective simulation value is significantly ($p \leq 0.013$) different from the experimental value.

	Speed	Experimental	SKlinear	SKtorsional
AP trough	1	-0.324 (0.165)	-0.280 (0.060)	-0.290 (0.096)
	2	-0.364 (0.170)	-0.290 (0.045)	-0.291 (0.081)
	3	-0.388 (0.189)	-0.293 (0.041)	-0.307 (0.075)
	4	-0.429 (0.208)	-0.256 (0.033)*	-0.297 (0.047)
AP peak	1	0.248 (0.085)	0.243 (0.030)	0.248 (0.085)
	2	0.317 (0.119)	0.249 (0.028)	0.317 (0.119)
	3	0.381 (0.131)	0.254 (0.050)	0.381 (0.131)
	4	0.428 (0.164)	0.228 (0.034)*	0.428 (0.164)*

Table 42 - Mean (SD) of the peak vertical GRF [BW] of the experimental data and simulations. * indicates the respective simulation value is significantly ($p \leq 0.013$) different from the experimental value.

	Speed 1	Speed 2	Speed 3	Speed 4
Experimental	2.717 (0.123)	2.913 (0.151)	3.062 (0.196)	3.123 (0.232)
SKlinear	2.678 (0.367)	2.533 (0.415)	2.400 (0.497)*	1.975 (0.282)*
SKtorsional	2.717 (0.123)	2.913 (0.151)*	3.062 (0.196)*	3.123 (0.232)*

8.3.4. Hip joint angles

The simulated hip joints angles overestimated the experimental values (Figure 75 and Table 43). Although the initial joint angle was similar to the experimental joint angle, the simulated peak hip joint angle was much higher than the experimental peak hip joint angle. Interestingly, the RMSD between the simulated and experimental hip joint angles were smaller at the faster speeds than at the slower speeds.

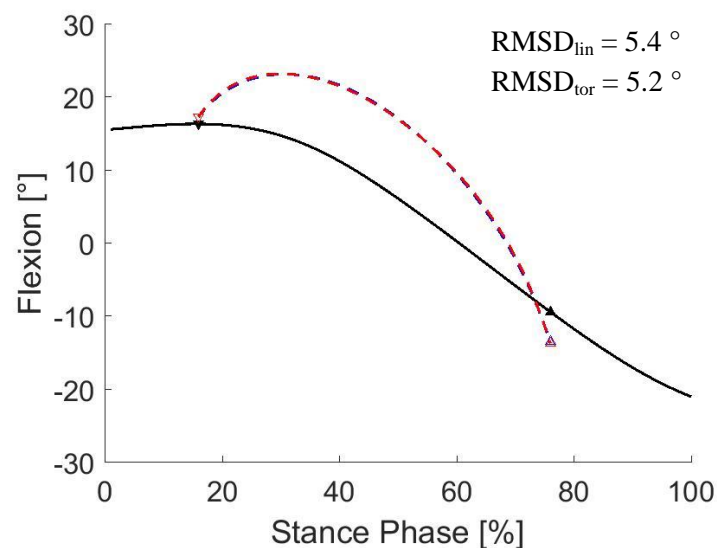


Figure 75 – Experimental (black solid) and simulated (*SKlinear*: blue dashed; *SKtorsional*: red dashed) hip joint angle profiles from the participant with the lowest RMSD at speed 1 [3.3 m/s].

Table 43 - Mean (SD) of the RMSD [deg] between the simulated and experimental hip joint angles.

	Speed 1	Speed 2	Speed 3	Speed 4
SKlinear	7.35 (1.52)	7.0 (1.27)	6.77 (1.0)	6.44 (0.99)
SKtorsional	7.35 (1.58)	7.05 (1.33)	6.70 (0.95)	6.52 (0.82)

8.3.5. Knee kinematics

The simulated knee joint trajectories were very different to the experimental knee joint trajectory (Figure 76). The difference between the simulations and the experimental data was larger at the slower speeds than at the faster speeds (Table 44). In addition, the correlation analysis comparing the simulated and experimental trajectories revealed significant and strong relationships in both the horizontal and vertical directions, with both models, at all speeds (Table 45).

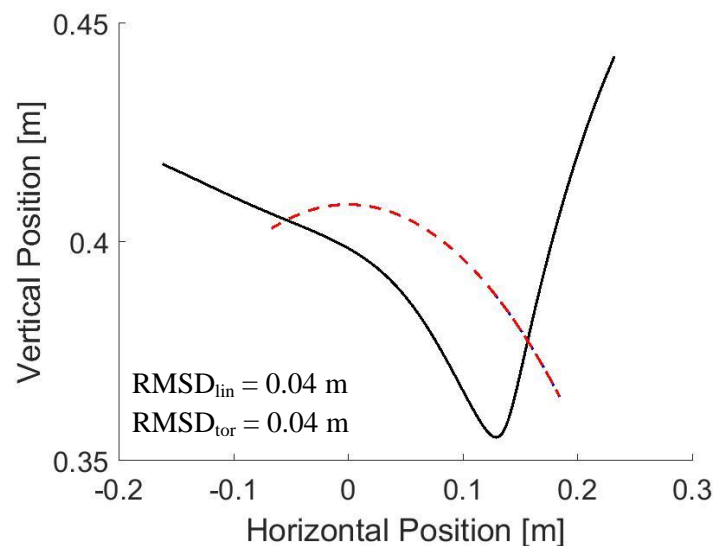


Figure 76 – Experimental (black solid) and simulated (*SKlinear*: blue dashed; *SKtorsional*: red dashed) knee trajectories from the participant with the lowest RMSD at speed 1 [3.3 m/s].

Table 44 – Mean (SD) RMSD [m] between the simulated and experimental knee trajectories.

	Speed 1	Speed 2	Speed 3	Speed 4
SKlinear	0.060 (0.013)	0.058 (0.010)	0.057 (0.008)	0.056 (0.009)
SKtorsional	0.060 (0.013)	0.058 (0.011)	0.057 (0.008)	0.056 (0.008)

Table 45 - Mean (SD) correlation coefficients between the simulated and experimental knee trajectories. All correlations were significant ($p \leq 0.013$).

Speed	SKlinear		SKtorsional	
	x	y	x	y
1	0.908 (0.023)	0.937 (0.032)	0.910(0.024)	0.931 (0.033)
2	0.915 (0.019)	0.954 (0.021)	0.917 (0.019)	0.950(0.021)
3	0.921 (0.015)	0.962 (0.016)	0.923 (0.014)	0.959 (0.018)
4	0.928 (0.014)	0.967 (0.014)	0.930 (0.012)	0.964 (0.015)

The discrepancies in the knee trajectories are highlighted in the difference between the knee joint angle profiles (Figure 77). In contrast to the RMSD in the trajectories, the difference between the experimental joint angles and the simulated joint angles were larger at the faster speeds than at the slower speeds (Table 46). Furthermore, the differences between the *SKtorsional* model and the experimental values were statistically the same as those between the *SKlinear* model and the experimental values.

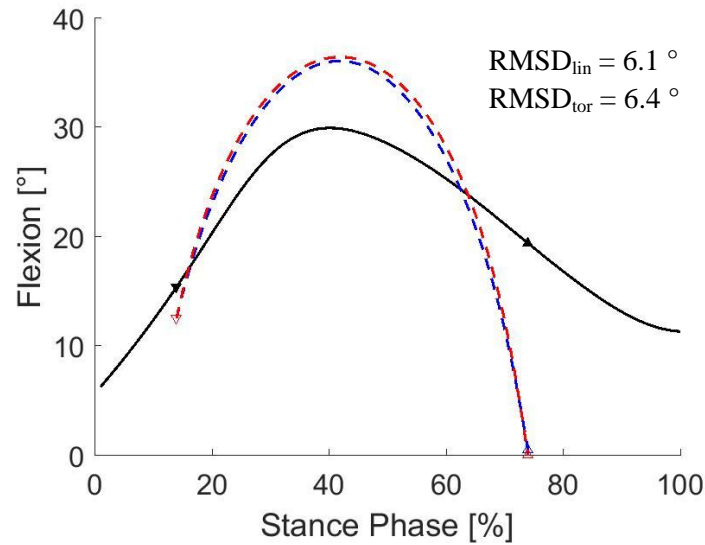


Figure 77 - Experimental (black solid) and simulated (*SKlinear*: blue dashed; *SKtorsional*: red dashed) knee joint angles from the participant with the lowest RMSD at speed 1 [3.3 m/s].

Table 46 - Mean (SD) of the RMSD [deg] between the simulated and experimental knee joint angles.

	Speed 1	Speed 2	Speed 3	Speed 4
<i>SKlinear</i>	7.85 (1.38)	8.42 (1.61)	8.51 (1.60)	8.96 (1.71)
<i>SKtorsional</i>	7.80 (1.28)	8.31 (1.38)	8.44 (1.51)	8.76 (1.62)

8.3.6. Initial conditions vs. Experimental data

Paired t-test showed that the optimised values for the hip angular velocities, for both the *SKlinear* and the *SKtorsional* models, were significantly different ($p \leq 0.013$) from the experimental values at all speeds (Figure 78). The optimised knee angular velocities were not significantly different from the experimental values at any speed, for either the *SKlinear* or the *SKtorsional* models (Figure 79).

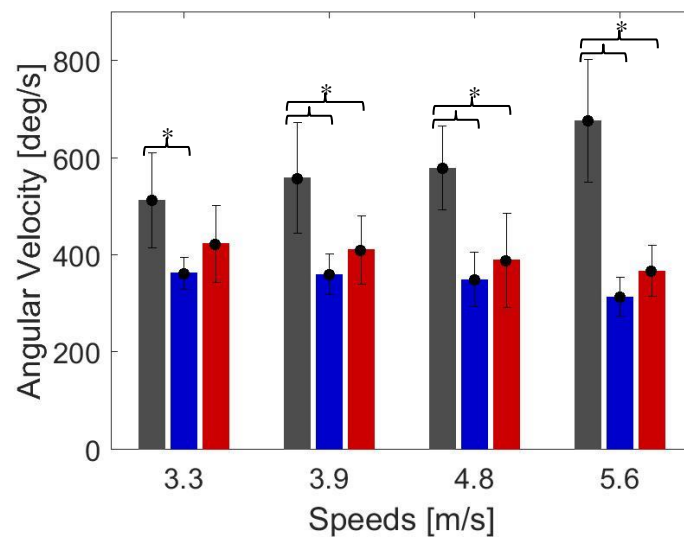


Figure 78 - Mean and standard deviations of the experimental vs. optimised hip angular velocities [deg/s] used when simulating the SK models. The dark grey bar represents the experimental data, the blue the *SKlinear* model and the red the *SKtorsional* model. * indicates value is significantly different ($p \leq 0.013$) from the experimental value.

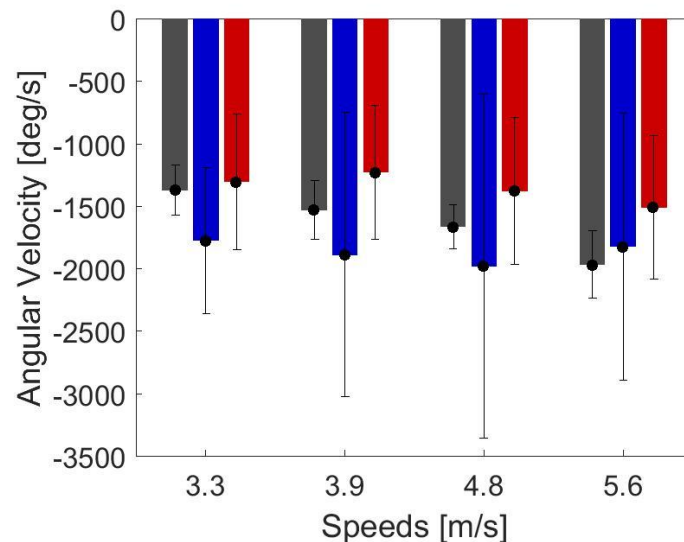


Figure 79 - Mean and standard deviations of the experimental vs. optimised knee angular velocities [deg/s] used when simulating the SK models. The dark grey bar represents the experimental data, the blue the *SKlinear* model and the red the *SKtorsional* model.

8.3.7. Linear stiffness vs. experimental limb stiffness

In the *SKlinear* model, a *PointToPoint* spring connected the point mass to the fixed contact point (Figure 68). The model stiffness values were compared to the lower limb stiffness values, previously derived from the force-length curves (Chapter 5.3.2; Page 107; Table 18 – PC method). The optimised lower limb stiffness values were significantly different from the experimental lower limb stiffness values at speed 1 only (Figure 80). Furthermore, the percentage differences between the model and experimental values were -17.5 (17.1), -6.1 (19.5), 1.6 (22.6) and 17.8 (15.9) at speeds 1 to 4, respectively.

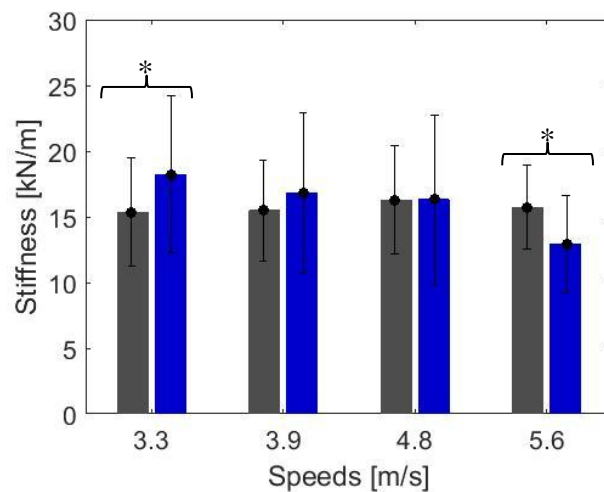


Figure 80 - Mean and standard deviations of experimental and optimised lower limb stiffness values [kN/m]. The dark grey bar represents the experimental data and the blue represents the *SKlinear* model.* - indicates optimised and experimental values are significantly different ($p \leq 0.013$) at that speed.

8.3.8. Knee joint stiffness / joint torques

In the *SKtorsional* model, a *SpringGeneralizedForce* acted as a torsional spring at the intersegmental joint (Figure 68). The optimised values found here were not significantly different from the experimental knee joint stiffness values at any speed (Figure 81).

Furthermore, the percentage differences between the model and experimental values were (-22.6 (38.9), -0.3 (29.1), 5.4 (38.5) and 8.4 (33.8) at speed 1-4, respectively.

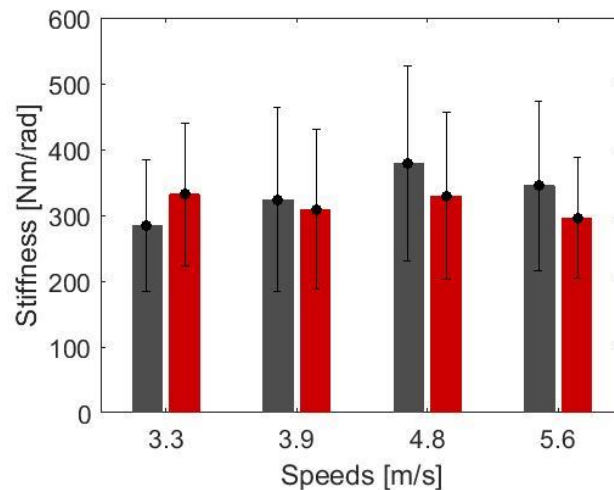


Figure 81 - Mean and standard deviations of experimental and optimised knee joint stiffness values [Nm/rad]. The dark grey bar represents the experimental data and the red represents the *SKtorsional* model.

8.4.Discussion

The aim of this chapter was to develop a two-segment model in OpenSim and compare it to experimental data. Previous two-segment models of running aimed to investigate the stability of such a model and compared simulations to outputs from the spring mass model (Rummel et al. 2008, Phan et al. 2017). Although these studies argued that the stable parameter range of their models was biologically relevant for human locomotion, the results were not directly compared to experimental data. Therefore, this chapter aimed to determine the individual contributions of adding segments, with finite mass, and a knee joint to the movement characteristics of the spring mass model and directly compare the simulations to experimental data. With this model it was not possible to model early and late stance, however there was reasonable kinematic agreement with experimental data during the middle 60 % (approximately) of stance.

The previous chapter showed that the CoM trajectory simulated by the spring mass model generally matched the experimental trajectory during early stance, but deviated from midstance to late stance (Chapter 7.3.2). In addition, the vertical displacement of the CoM is generally overestimated by the spring mass model (Chapter 7.3.2). Therefore, it was argued that the spring mass model was too simple to model normal running, and complexity was needed in order to get a better match with experimental data. Therefore, two versions of a sprung knee model were developed, the first the *SKlinear* model, introduced rigid segments, with finite mass, while the second, the *SKtorsional* model, replaced the linear spring with a torsional spring at the intersegmental joint. This allowed investigation of the individual contributions of segments, with fixed inertial properties, and a torsional spring.

Geometry restrictions with the SK models meant that it was not possible to model early and late stance using these models. This was because the model “shank” segment combined the anatomical shank and foot, and thus the model segment length was estimated as the mean distance between the knee joint and the average CoP during stance.

Simulations using both the *SKlinear* and the *SKtorsional* models show good qualitative agreement between the middle portions of stance, however the RMSD between the experimental and simulated CoM trajectories is approximately 19 to 38 % of the vertical displacement, which suggests the match is quantitatively not that good. Furthermore, it should be reiterated that the SK models were only able to model the middle portion of stance, and that if the spring mass model was used to model the same period its results would have been closer to the results of the SK models.

Figure 82 shows the differences in a typical CoM trajectory produced by the spring mass model and the SK models compared to experimental data. From this it is evident that during midstance there is much closer agreement between the SK models and the experimental data than between the spring mass model and the experimental data. The *SKlinear* model presented here is similar to the spring mass model of the previous chapter, however now the model includes rigid segments with finite mass. Although the improved agreement between model and experimental data may be due to SK model modelling a smaller portion of stance, these results suggest that the lower limb acts similar to a passive spring during the middle portion of stance.

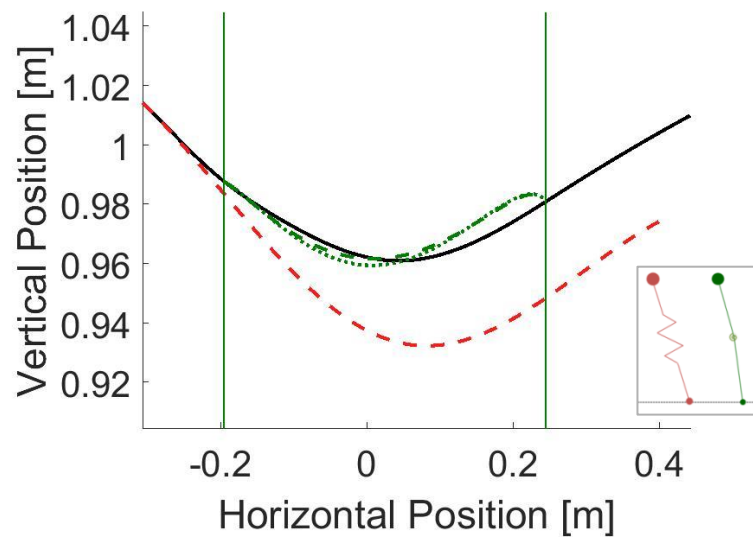


Figure 82 - Example of the difference in the simulated CoM trajectories from the spring mass model (red dashed line), the *SKlinear* SK model (dotted green line), the *SKtorsional* model (dashed green line) and the experimental data (solid black line) for one subject at speed 1 [3.3 m/s].

Comparison of the kinetics produced by the SK model suggests less agreement with the experimental data than the spring mass model. Excessively large values for the AP and negative values for the vertical GRFs occur for approximately the first 3 % and the last 5 % of the simulated stance phase. These large values coincide with high loading rates, resulting in a squarer shaped vertical GRF rather than the expected sinusoidal curve evident in the spring mass model and the experimental data (bottom right of Figure 83). This square vertical GRF profile was also produced by the two-segment model present by Rummel et al. (2008), who argued that since the two-segment model produces a non-linear force length curve, assuming constant joint stiffness (joint torque proportional to joint flexion) results in high force rates in early stance.

These errors in the initial and final forces could be attributed to a number of things. For example, the fixed contact point or errors in the estimated resting length/angle of the springs. The resting length for the linear spring was estimated as the distance between the hip joint centre of the average CoP at initial contact, and the resting angle of the torsional spring was estimated as 0° . Because of the geometry restrictions of the model, the actual

equivalent angle at initial contact could not be calculated, thus it is possible that this estimated value resulted in a pre-load in the spring, which could affect the GRFs. Furthermore, having a fixed contact point instead of an ankle and foot means that towards the end of stance the point mass is “pulled down” towards the contact point rather than extending and preparing for flight (Figure 83). It is possible that this contributes to the large errors in the GRFs during late stance. In addition, this suggests that another layer of complexity, that introduces an ankle joint, is necessary before the GRFs can be accurately modelled.

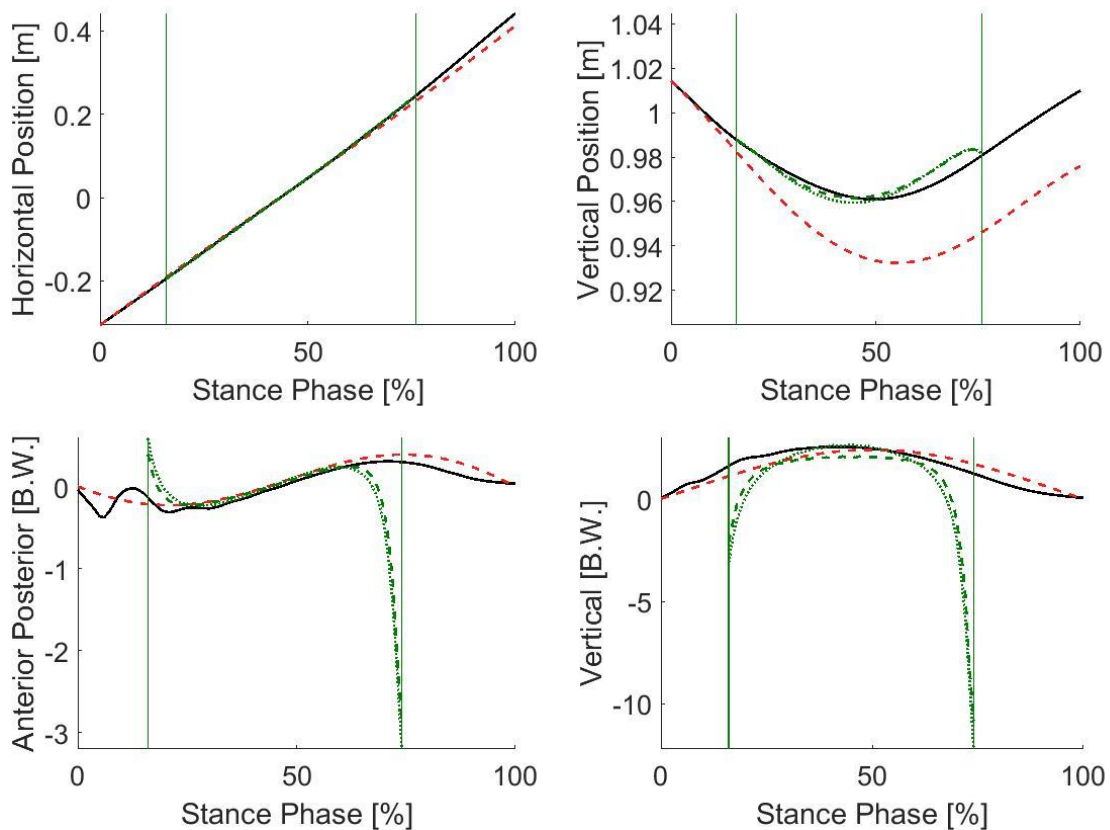


Figure 83 – Horizontal and vertical CoM movement and GRFs from the spring mass model (red dashed line), the *SKlinear* SK model (dotted green line), the *SKtorsional* model (dashed green line) and the experimemtal data (solid black line) for one subject at speed 1 [3.3 m/s].

It is unsurprising that the model joint angles and joint trajectories did not match closely with the experimental joint angles or trajectories. Combining the anatomical shank and foot into a single model “shank” segment fundamentally changed the geometry of the system. This meant that the model “hip” and “knee” joint needed to take on a configuration that was inherently different from the anatomical configuration. The lack of ankle joint also meant the model “knee” was more extended at initial contact than the anatomical knee would have been. Furthermore, in order to follow a similar CoM trajectory to the experimental data, the hip and knee would need to flex more to compensate for the lack of ankle flexion. This explains why both the peak hip and knee joint flexions were considerably higher in both the *SKlinear* and *SKtorsional* model simulations than in the experimental data. The published two-segment models do not present or compare the intersegment joint angles produced to experimental data, so it is not possible to compare the results from this investigation to those other studies. However, Rummel et al. (2008) reported stable running with approach angle between 150 and 170 ° of knee extension, which is similar to the initial angles used for simulating the SK models (approximately 10 ° flexion).

The initial conditions for both the *SKlinear* and *SKtorsional* models were determined from the experimental data. However, the angular velocities and the spring stiffness were determined from the optimisation. These optimised values were statistically different to the experimental values for the hip angular velocities, but not for the knee angular velocities. Furthermore, the optimised knee angular velocities from both the *SKlinear* and *SKtorsional* models were approximately 5 times larger than knee angular velocities published in literature for running at similar speeds (De Wit et al. 2000). However, since the “shank” in the two-segment model combined the anatomical shank and foot it is likely that these angular velocities do not directly relate to the experimental values.

Interestingly, the optimised stiffness values were statistically similar to the derived experimental values. Experimental knee joint stiffness, calculated using the ratio of the knee joint moment to the knee joint angular displacement, has been shown to increase as speed increases (Arampatzis et al. 1999, Günther et al. 2002, Kuitunen et al. 2002). The derived experimental values presented here appear to follow a similar trend, but the optimised joint stiffness values from the *SKtorsional* model do not. Additionally, in agreement with literature (He et al. 1991, Morin et al. 2005, Brughelli et al. 2008a), the

derived lower limb stiffness values (Chapter 5.3) appear to remain relatively constant with speed, however the linear stiffness values from the *SKlinear* model are larger at the slower speeds than at the faster speeds. However, because the number of participants in each group changed with speed, it is not possible to conclude about how these stiffness values relate to speed.

There is close agreement between the SK models and the experimental CoM trajectories during the middle portion of stance. This may suggest that the linear passive spring analogy, that forms the basis of using spring mass models for studying running, at least has some merit during midstance. However, the RMSD between the SK models and the experimental CoM trajectories was larger at the faster speeds compared to the slower speeds. As speed increases, the knee is required to attenuate higher loads while controlling the amount of joint flexion. Thus, the larger errors at the faster speed suggest a purely passive joint may be insufficient for preventing knee collapse at these higher speeds. On the other hand, at slower speeds where there is relative good agreement between model and experiment, it might suggest that during running the body aims to utilise the passive structures acting about the knee as a method for controlling joint movement during loading.

The close agreement between the *SKtorsional* model and the experimental CoM trajectories suggest this passive spring behaviour exhibited by the knee joint suggests the muscles acting about the knee joint do so in a way that is similar to a passive torsional spring. Finally, the nearly identical CoM movement produced by the *SKlinear* and *SKtorsional* models further suggests that the knee joint stiffness may be largely responsible for the overall lower limb stiffness during running, something that has previously been suggested in literature (Farley et al. 1998, Günther et al. 2002).

A major limitation of the SK models presented here is the effect of combining the anatomical shank and foot into a single “shank” segment. This meant that due to the geometry restrictions it was not possible to model early and late stance, and thus the SK model was modelling a smaller portion of stance than the spring mass model in chapter 7. It is possible that if the spring mass model was optimised for the same period as the SK model it would perform just as well. However, apart from better agreement during midstance, the spring mass model still wouldn't be able to provide any more information than it already does.

Another limitation of the SK model is the fixed contact point. During running there is a net distal-to-proximal translation of the CoP under the foot. By including a fixed contact point in the model, it eliminates this movement, and this likely restricts the ability of the model. At approximately midstance the CoP is below the CoM and the fixed contact point likely has little effect, however during loading and unloading the fixed contact point will be either anterior or posterior to the actual CoP and this is likely to contribute to the errors in the AP GRFs. The fixed contact point and missing ankle also mean that prior to the end of the simulation the point mass is being pulled down towards the fixed contact point, and this likely contributes to the errors in the GRFs.

The results of this chapter show that a two-segment model is insufficient for modelling the stance phase of running. Although the agreement during midstance is reasonable, the two-segment model presented here is incapable of modelling early and late stance, due to the shank/foot segment having a single length for the whole stance phase. Therefore, more complexity is needed. The next chapter will introduce the next layer of complexity, an ankle joint and foot segment, and discuss how this affects the ability of the model at replicating normal distance running. The addition of an ankle joint and foot segment seemed a reasonable next step in the sequential modelling as it would presumably eliminate the geometrical restrictions that prevent the two-segment modelling early and late stance.

9. ... adding an ankle joint

9.1. Introduction

The results of the previous chapter show that more complexity is needed to model the entire stance phase during running. The sprung knee (SK) models (Chapter 8) do well to replicate approximately the middle 60 % of stance, but geometric restrictions mean it is not possible to model both early and late stance with the same segment lengths. Therefore, the next phase of this PhD was to add an additional layer of complexity, in the form of an ankle joint and foot segment. This layer of complexity would potentially determine the phases of stance during which the ankle is most important. It is hypothesized that the introduction of an ankle joint will allow for successful simulation of the full stance phase.

During early stance to midstance the ankle dorsiflexes until the CoM passes over the CoP and begins to accelerate upwards (Ferber et al. 2014). It is therefore expected that the ankle stiffness will play a pivotal role in controlling the rate of dorsiflexion and allow for a smooth CoP trajectory. A similar argument can be used for the importance of the ankle during late stance. During this phase the knee is extending and the ankle plantar flexes, presumably preparing the system for flight. Therefore, it is expected that the ankle will be essential for fully extending the lower limb and allowing complete rebound of the CoM. However, it is unlikely that a purely passive ankle joint will retain sufficient energy for this to happen. Considering this, it is hypothesized that a certain amount of actuation will be required during late stance in order for the ankle joint to fully plantar flex and propel the CoM upwards.

The biomechanics of the ankle joint are somewhat dependent on the foot strike pattern adopted. The main difference in the ankle joint kinematics between forefoot and rearfoot strikers occurs in the sagittal plane at, and immediately after, initial contact (Figure 84). Forefoot strikers tend to land in a plantar flexed position and then rapidly dorsiflex as the heel comes into (near) contact with the ground (Ahn et al. 2014). In contrast, for rearfoot strikers, the ankle is initially dorsiflexed, then during early stance the ankle quickly plantar flexes to a foot-flat position (Ahn et al. 2014). In the frontal and transverse planes, the ankle is inverted and internally rotated (Adelaar 1986, Ferber et al. 2014, Farris et al.

2017) (Figure 85). From approximately 20 % of stance the ankle kinematics for rearfoot and forefoot strike patterns are similar (Kulmala et al. 2013). As the shank moves anteriorly over the foot, the ankle dorsiflexes again, lifting the heel off the ground. At the same time, the foot everts and internally rotates from initial contact to midstance (Ferber et al. 2014).

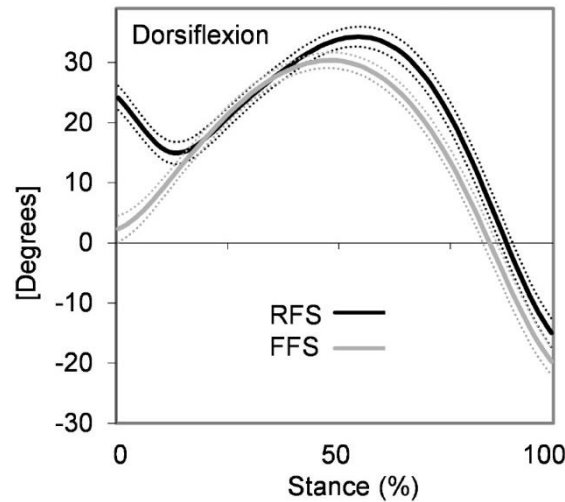


Figure 84 - Sagittal plane angle kinematics for habitual forefoot and rearfoot strikers running at 4 m/s (Kulmala et al. 2013).

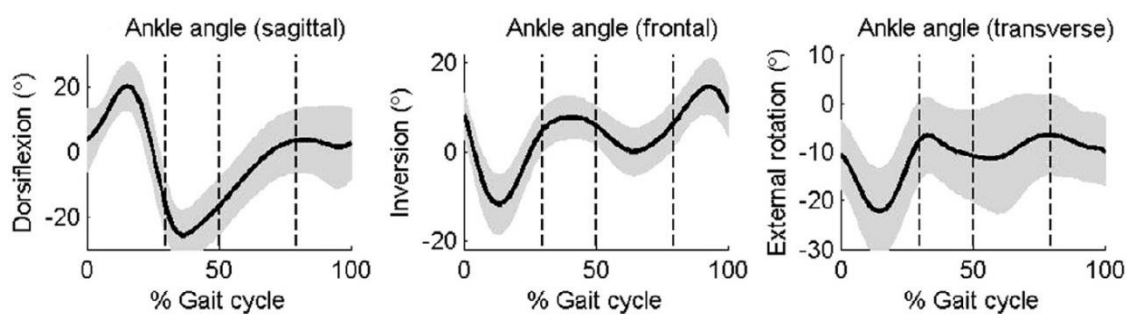


Figure 85 - Ankle kinematics during running (with a rearfoot strike pattern) (Preece et al. 2016). Positive degree changes imply dorsiflexion, inversion and external rotation. The gait cycle begins and ends with right foot initial contact and the vertical lines represent right foot toe off, left foot initial contact and left foot toe off, respectively.

Differences in the ankle joint kinetics are evident between forefoot and rearfoot strikers. For example, rearfoot strikers tend to have greater peak ankle dorsiflexor moments than forefoot strikers, while forefoot strikers tend to have greater peak plantar flexor moments than rearfoot strikers (Figure 86). This increased plantar flexor moment in forefoot strikers is due to a larger peak vertical GRF and a more anterior CoP location (Kuhman et al. 2016). Furthermore, the peak ankle eccentric plantar flexor power is greater in forefoot strikers than rearfoot strikers. This suggests greater loads are placed on the ankle joint and there is increased plantar flexor involvement in forefoot running compared to rearfoot running (Kuhman et al. 2016).

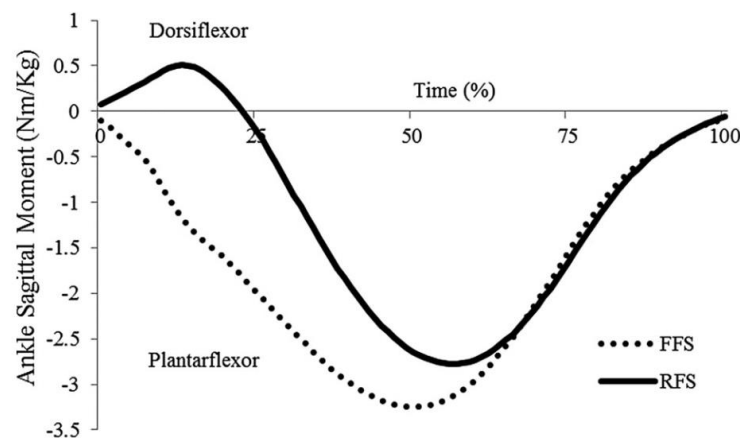


Figure 86 - Normalised sagittal plane ankle kinetics (internal joint moments) for habitual rearfoot and imposed forefoot strike patterns (Kuhman et al. 2016).

Achilles tendon related injuries are prevalent in runners (Lyght et al. 2016). It has been shown that rearfoot strikers tend to have lower peak Achilles tendon stress, strain and a reduced strain rate compared to forefoot strikers (Lyght et al. 2016). The increased stress, strain and strain rate associated with forefoot running may be attributed to the plantar flexed position of the ankle joint at initial contact and the higher plantar flexor moment described above. The plantar flexed position at initial contact orientates the GRF vector anterior to the ankle; therefore, to control the lowering of the heel during early stance the triceps surae must produce a higher plantar flexor moment which results in a larger force being transmitted through the Achilles tendon as it is stretched (Lyght et al. 2016).

Joint stiffness can be approximated using the perturbation method; the ratio of the joint moment to the angular displacement of the joint (see chapter 8 pages 162-163; Farley et al. 1998, Günther et al. 2002, Brughelli et al. 2008a). Using this method it has been shown that the ankle joint tends to be less stiff than the knee joint and that as running velocity increases knee joint stiffness also increases, but ankle joint stiffness remains constant (Arampatzis et al. 1999, Günther et al. 2002, Kuitunen et al. 2002). However, it has more recently been shown that joint stiffness may be partly dependent on the foot strike pattern adopted (Hamill et al. 2014). Hamill et al. (2014) found that in a group of forty runners (20 forefoot strikers and 20 rearfoot strikers) the knee joint stiffness was higher than the ankle joint stiffness when participants were asked to forefoot strike, and the opposite was true when they were asked to rearfoot strike; regardless of the natural foot strike pattern of the participants. Interestingly, it has also been shown that there is a greater ankle stiffness associated with more structured footwear (conventional and structured barefoot-inspired running shoes) compared to barefoot running and minimalist bare-foot inspired running shoes (Sinclair et al. 2016), and those running in conventional footwear tend to adopt a rearfoot strike pattern. However, these results have all been determined using the perturbation method of calculating joint stiffness, and it has yet to be determined how appropriate the assumption of a passive system is for the ankle joint during running.

Few running models that incorporate an ankle joint exist in the literature (Seyfarth et al. 2001, Seyfarth et al. 2006, Qiao et al. 2017). However it has been argued that exploring the spring-like behaviour of a segmented leg has the potential to provide information about the architecture and function of biological legs (Seyfarth et al. 2006). For example, a simple three-segment model was developed by Seyfarth et al. (2001) to investigate the segmental configuration of the leg (Figure 87). Such a model was used to explore the kinematic redundancy problem associated with multi-segment (minimum of three) models. A similar model was used by Seyfarth et al. (2006) to explore the extent to which spring like behaviour could be used in combining walking and running models.

The control of joint torques, torsional stiffness adjustment and the effects of segment length and orientation were used as a means of testing the stability and predictability of leg operation (Seyfarth et al. 2001). The authors showed that a model configuration characteristic of the human leg resulted in a maximum working range of joint stiffness values (Seyfarth et al. 2001). They also showed that having a small foot relative to the

length of the shank allows for large knee extensions, and a small foot relative to the length of the thigh requires a lower ankle joint stiffness than knee joint stiffness. These results are similar to published experimental data and characteristic of a human leg configuration, suggesting such a model could predict kinematics and kinetics characteristics of running. However, although the authors stated that the forces predicted by their three-segment model were similar to those observed in experimental data of fast types of locomotion (i.e. running), the fundamental purpose of the study was to investigate stability and not quantitatively compare model outputs with experimental data.

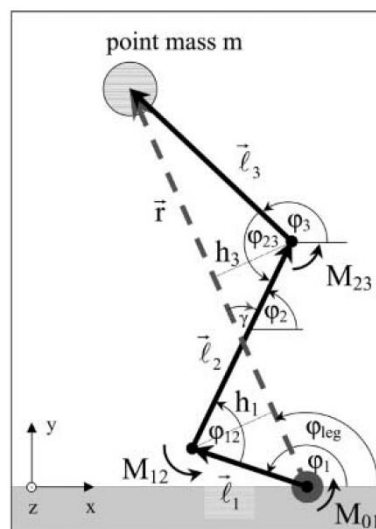


Figure 87 - Three-segment planar model used by Seyfarth et al. (2001). The configuration of the leg is defined by the ankle (ϕ_{12}) and knee (ϕ_{23}) angles and M_{01} , M_{12} and M_{23} represent the joint torques at the ball, ankle and knee joints, respectively.

Using a three-segment leg Seyfarth et al. (2006) aimed to explore the internal segmentation and elastic stability of the leg. The segments were assumed to have equal geometry (lengths and initial joint angles), and the joints to be equally stiff. Stability analysis showed that different solutions exist to avoid instability and that stable leg operation is not guaranteed by elastic joint behaviour during stance (Seyfarth et al. 2006). Although such results reinforce the idea that understanding the operation of spring-like legs could provide further insights into the architecture and function of biological legs, the

assumption of equal segment length and equal joint stiffness used in this model is inherently uncharacteristic of humans.

From a slightly different perspective, the motor-damper-spring (MDS) model (Figure 88) used by Qiao et al. (2017) is based on the simple spring loaded inverted pendulum (SLIP) model (Holmes et al. 2006). The three segment planar model incorporated a proximal motor equivalent to the hip joint, a spring and damper in parallel representative of the knee, and a distal spring corresponding to the ankle and foot. The segment masses are based on anthropometric data, and model parameters (stiffness, k_{MDS} , spring resting length, l_0 , damping coefficient, d_{MDS} , and the constant motor force, F_{motor}) were estimated from experimentally measured GRFs and the CoM trajectory using multiple linear regressions (Qiao et al. 2017). Finally, the location of the foot was defined as the average CoP at midstance, the initial conditions (CoM position and velocity) were taken as the experimental values at initial contact, and the conditions at take-off as the objective of the cost function (Qiao et al. 2017).

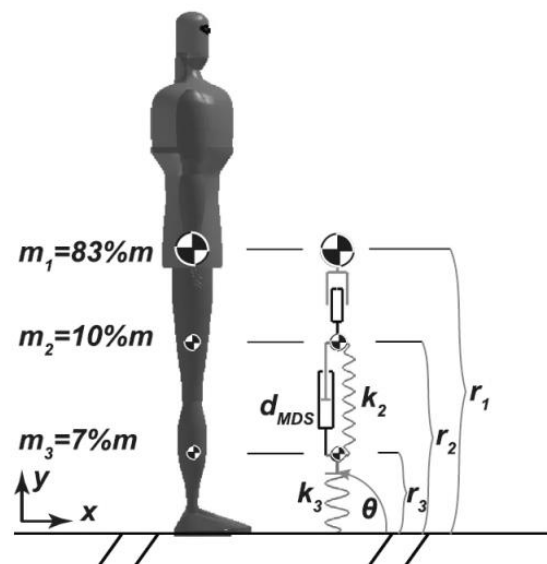


Figure 88 - Motor-damper-spring (MDS) model used by Qiao et al. (2017). The proximal mass incorporates the head, trunk, arms, and the lower limb in swing. The middle mass represents the thigh, and the lower mass the shank and foot. The segment resting lengths are $r_1 = l_{0,MDS}$, $r_2 = 67\%l_{0,MDS}$ ($67\% = \text{CoM}_{y,\text{upper leg}}/\text{CoM}_{y,\text{human body}}$), and $r_3 = 27\%l_{0,MDS}$ ($27\% = \text{CoM}_{y,\text{lower leg+foot}}/\text{CoM}_{y,\text{human body}}$).

The MDS model (Figure 88) was used to test the hypotheses about the principle functions of the lower limb joints. The authors hypothesised that the hip functions as a ‘motor’, actively generating or absorbing energy; the knee as a ‘strut’, passively transferring energy between joints; and the ankle as a torsional ‘spring’, storing and returning elastic energy. The results showed that fundamentally humans may not only optimise for dynamic stability, but that they also potentially choose mechanical and behavioural parameters that are specifically tailored for the task (e.g. constant-average-velocity locomotion and stepping manoeuvres). Furthermore, the authors found that consistent with the hypotheses the hip and ankle function as a motor and spring, respectively, but contrary to their hypothesis the knee acts more like a damper than a strut. Again this study did not quantify how well the model predicted running kinematics, but instead focused on stability. However, it does reinforce the idea that understanding joint-level mechanical function is essential for understanding whole-body performance during locomotion.

Aims

The aim of this chapter is to develop a three-segment model in OpenSim and compare it to experimental data. The chapter aims to determine the contributions of adding an ankle joint and foot segment to the movement characteristics of the spring mass (Chapter 7) and sprung knee (Chapter 8) models presented earlier. Again, the effect of this added layer of complexity will be explored with respect to the biomechanical characteristics of normal distance running, with the aim of establishing how the mechanical properties of the ankle joint contribute to how and why people run the way they do. It has been argued that the greater demand on the ankle extensors, compared to the knee extensors, may be a key biomechanical factor that influence the way we move (Kulmala et al. 2016), therefore it is hypothesised the ankle joint stiffness, and the amount of actuation required at the ankle, will be important during the whole stance phase, but particularly influential for accurately modelling the propulsive phase as the ankle plantar flexes for push off.

9.2. Methods

9.2.1. The Model

The sprung knee and ankle (SKA) model added an additional layer of complexity to the sprung knee model (presented in the previous chapter). This SKA model consisted of five parts (point mass, thigh, shank, foot and contact point). Again, the point mass and the contact point were equivalent to the spring mass and the sprung knee models; however, they were now connected via three rigid segments representing the anatomical thigh, shank and foot. Similar to the spring knee model, the segments had finite mass; based on an anatomical distribution (Figure 89), with the combined mass of the head, arms, torso and swing leg included in the point mass. The point mass was connected to the thigh segment via a weld joint (see chapter 6.3), the thigh to the shank and the shank to the foot via a pin joints (see chapter 6.3). Finally, for visual clarity the contact point was modelled using a massless sphere which was connected to the foot via a weld joint. How this contact point interacted with the ground will be described below.

Three versions of this model were developed; these will be referred to as *SKAconstraint*, *SKAcontact* and *SKAactuator*. This meant it was possible to explore the effects of gradual increases in model complexity. The *SKAconstraint* and *SKAcontact* models incorporated two torsional springs at the intersegmental joints, i.e. the knee and ankle. These torsional springs were modelled using a *SpringGeneralizedForce*. In the *SKAconstraint* model, the contact point was connected to the ground via a point constraint, while in the *SKAcontact* model the point constraint was removed and a *HuntCrossleyForce* contact model added. Finally, for the *SKAactuator* model, the ankle spring was replaced by an actuator and the foot-ground interaction was again modelled using a *HuntCrossleyForce* contact model.

The *HuntCrossleyForce* used in the contact model is based on Hertz contact theory (Hertz 1881). This method is a built-in functionality in OpenSim and uses the linear elasticity foundation theory to analytically determine the forces and deformations in the contact geometries (Delp et al. 2007, Seth et al. 2011). This method is limited to simple geometric objects, such as spheres, ellipsoids and planes, thus the choice to define the contact element on the model as a sphere, and the contact element on the ground as a plane. Hertz contact theory is applied between two linearly elastic materials in non-conforming contact, the *ContactSphere* and *ContactHalfSpace* in this case, where the contact patch dimensions

are small compared to both the curvature and the overall object dimensions (Delp et al. 2007, Seth et al. 2011).

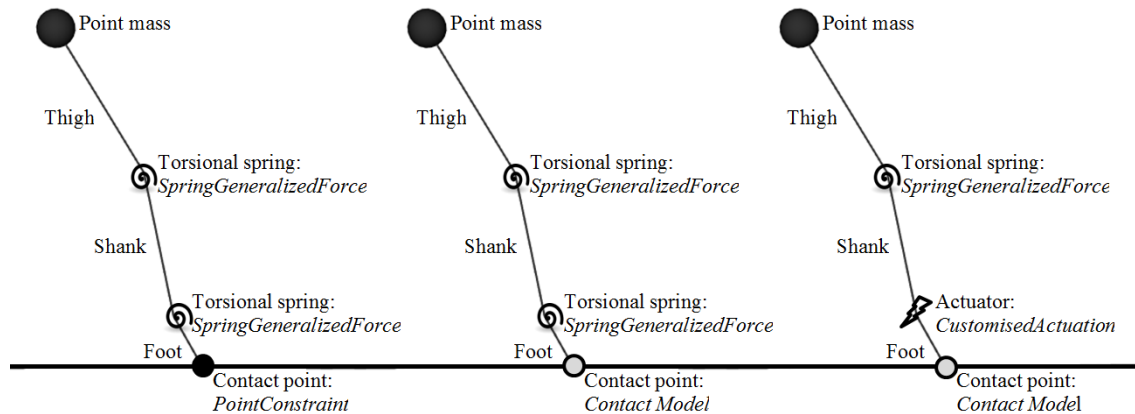


Figure 89 - OpenSim SKA models (left *SKAconstraint*, middle: *SKAcontact* and right: *SKAactuator*). Segment lengths, l , were determined from subject-specific anatomical data, where the point mass account for the combined weight of the head, arms, trunk and swing leg ($m_{\text{point mass}} = 0.845 \cdot \text{total body mass}$). The model segment masses, m , and moments of inertia, I , were approximated used data from Dempster (1955). The model “thigh” and “shank” segments approximated the anatomical thigh and shank ($m_{\text{thigh}} = 0.096 \cdot \text{total body mass}$; $I_{\text{thigh}} = m_{\text{thigh}} \cdot (0.323 \cdot l_{\text{thigh}})^2$ and $m_{\text{shank}} = 0.045 \cdot \text{total body mass}$; $I_{\text{shank}} = m_{\text{shank}} \cdot (0.302 \cdot l_{\text{shank}})^2$, respectively). The model “foot” segment represented the anatomical foot ($m_{\text{foot}} = 0.014 \cdot \text{total body mass}$; $I_{\text{foot}} = m_{\text{foot}} \cdot (0.475 \cdot l_{\text{foot}})^2$), and its length was estimated as the mean distance from the ankle joint to the average CoP.

In these models, the thigh and shank segments were defined in the same way as the experimental segments (Chapter 6.5), i.e. as the average distance between the proximal and distal joint centres. On the other hand, the “*foot*” segment was defined as the average distance between the ankle joint centre and the average CoP during stance. There was substantial variation in the length of the model “*foot*” segment because this “*foot*” segment neglected the translation of the CoP and as it was defined using the distal end of the shank it neglects movement between the tibia and ankle that exists in the visual3D model and an

anatomical joint (Figure 90). Therefore, similar to with the SK models, the segment length was too short to model the first and last 5 % (approximately) of stance.

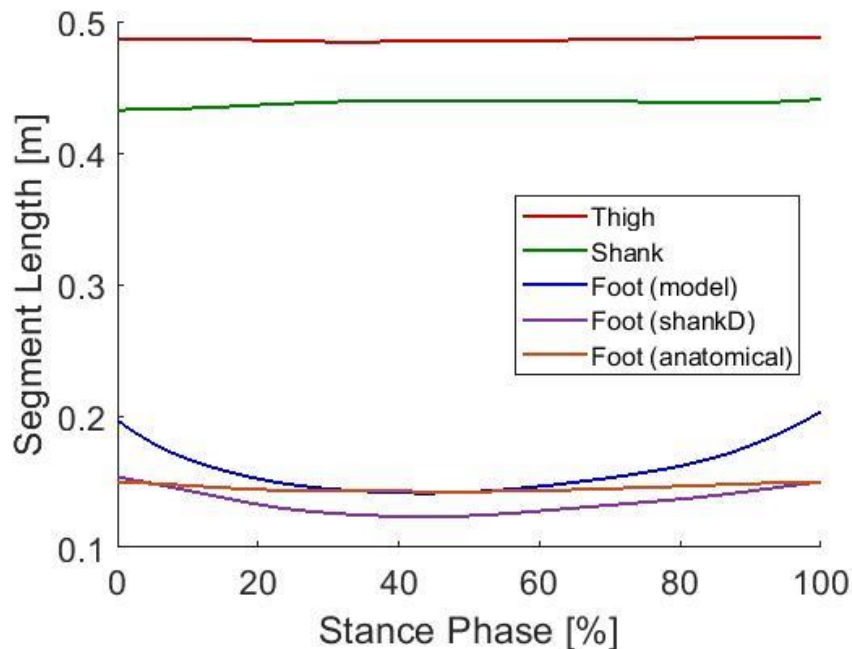


Figure 90 - Example experimental segment length changes during the stance phase of running. The segments are defined as follows: red - thigh, green - shank, blue – modelled foot, purple – foot segment defined using the distal end of the Visual3D shank and the proximal end of the Visual3D foot, and orange – anatomical foot (defined as the distance between the proximal and distal ends of the Visual3D foot). The Visual3D foot segment was defined using the ankle malleoli and the first and fifth metatarsal markers (Mason et al.).

9.2.2. Joint angle calculations

In the SKA model the foot was approximated as a rigid segment connecting the ankle joint centre to the average CoP during stance. Therefore, the model joint angle calculations (Table 47) are slightly different to those used to calculate the experimental joint angles (Table 21 – Chapter 6.5). Again, zero degrees (0°) of flexion was defined as vertical for the hip and fully extended for the knee, and perpendicular (90°) to the shank for the ankle.

Table 47 - Equations for determining the SKA model joint angles.

Hip angle: $\alpha = -\sin^{-1}\left(\frac{thigh_x}{thigh_l}\right)$

$knee_x = hip_x - thigh_x$

$knee_y = hip_y - (thigh_l \cdot \cos(\alpha))$

$knee_l = \sqrt{knee_x^2 + knee_y^2}$

Knee angle: $\beta = -\sin^{-1}\left(\frac{knee_x}{knee_l}\right)$

$\gamma = \cos^{-1}\left(\frac{shank_l^2 + knee_l^2 - foot_l^2}{2 \cdot shank_l \cdot knee_l}\right)$

$\delta = \cos^{-1}\left(\frac{foot_l^2 + shank_l^2 - knee_l^2}{2 \cdot foot_l \cdot shank_l}\right)$

Ankle angle: $\varepsilon = \pi - \delta$

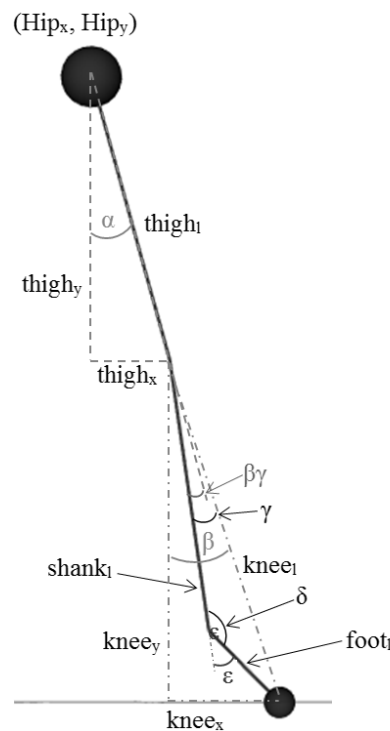


Figure 91 - OpenSim SKA model configuration.

9.2.3. *Initial conditions, optimisation and simulation*

Depending on the model used, there were slight differences in the initial conditions which were either explicitly defined or were allowed to vary in the optimisation. For all three models, the initial position of the CoM and the corresponding linear velocities were taken from experimental data, and the joint angles were calculated using the equations in Table 47.

Similar to the SK model, the start and endpoints of the simulation had to be determined prior to optimisation. The start point, i , was defined as the first point in the stance phase where the calculated joint angles were real numbers. Similarly, the end point was then defined as the last point, i , in the stance phase where the calculated joint angles were real numbers. Again, based on an initial inspection of the results, a further condition that the knee angle must be greater than 10° of flexion was added for determining the start point. As stated previously, the choice of 10° of flexion was because most runners tend to land with a knee flexion angle between 10 and 20° (Nicola et al. 2012). This changed the start point by $2.1 \pm 2.5\%$.

As with the spring mass model (Chapter 7) and the SK models (Chapter 8) the equations of motion for all three SKA models were determined within OpenSim. Based on the mass and inertia properties of the model segments the equations were automatically generated. For each of the models the simulation cut-off was defined using the spring torque. The first minimum in the knee torque and the first maximum in the ankle torque were identified and the cut-off point set as whichever occurred first. A further check was then added to make sure that the joint angles did not exceed 0° or 180° flexion for the knee and 90° dorsiflexion or plantar flexion for the ankle. In addition, for each of the models the optimisations were also run using two other guesses to reduce the possibility of the optimiser getting stuck in a local minimum. Finally, the cost function associated with the optimisation was the same as for the spring mass model and the SK models, the RMSD between the experimental and simulated CoM trajectories (Chapter 6.4).

For the *SKAconstraint* model both the knee and ankle spring stiffness and the initial angular velocities were allowed to vary in the optimiser. The initial angular velocities were allowed to vary as the model joints did not directly correspond to the anatomical joints, and thus the corresponding angular velocities might have been erroneous. The

ForwardTool was used to integrate the equations of motion forward in time and the initial guesses for the optimisation were taken from the experimental angular velocities in the model configuration (foot estimated as the distance between the ankle joint centre and the average CoP).

To create a customised control function for the actuator, in OpenSim, the simulation had to be integrated using a customised code. However, with this custom code, the *PointConstraint* was ignored by the integrator. Therefore, in the *SKAcontact* model the *PointConstraint* was replaced with a contact model. To determine the appropriate parameters for the contact model, the optimisation now included the knee and ankle stiffness, the angular velocities, as well as the contact parameters for the contact model (the sphere radius and the contact stiffness). The initial guesses for the stiffness values and angular velocities were taken as the optimised values from *SKAconstraint* model, and the initial guesses for the contact parameters were based on the recommendations from OpenSim (0.05 m for the contact sphere and $5E7$ N/m for the stiffness). Again the *ForwardTool* was used to integrate the equations of motion forward in time, however an additional condition was included where the simulation was cut-off if the vertical contact force was equal to or less than zero, or if the contact point moved more than 1 mm in one integration step. In addition, a penalty of the maximum distance moved by the contact point was added to the cost function. This penalty was included in an attempt to get optimised parameters that would result in a CoM trajectory similar to the experimental data, while maintain as close to fixed contact point as possible.

Finally for the *SKAactuator* model the customised control function combined the spring force from the optimised *SKAcontact* model with a Gaussian function (Figure 92). For this model a Gaussian function was chosen as an approximation of experimental EMG data; which tends to show smooth ramping in activity, to a maximum value, then smooth reduction to zero. When simulating the *SKAactuator* model, only the Gaussian function coefficients were allowed to vary in the optimiser. This was because the purpose of this model was to determine how actuation at the ankle affect the ability of the model, thus all other parameters needed to be the same as the *SKAcontact* model. Initial guesses for the control function were based on the maximum spring force at the ankle and the contact time of the simulation. As mentioned previously, a custom code had to be used for the integration. This code was based on the OpenSim dynamic walker challenge (Seth et al.

2010, Sherman et al. 2011, OpenSim 2012), where the function determines the current state of the model, integrates the state using the built-in MATLAB ode45 solver, stores the new state values, and repeats for a specified time.

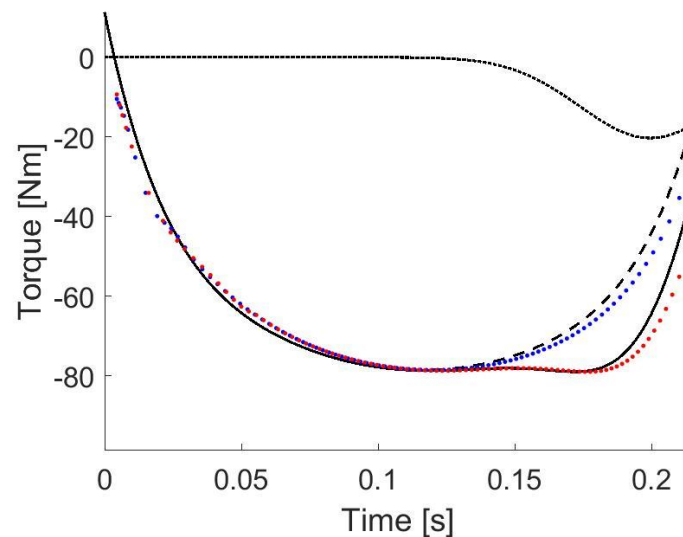


Figure 92 - Example of the control function used for the ankle actuator in the *SKAactuator* model for a single participant (who had the lowest RMSD between simulated and experimental CoM trajectories) at speed 1 [3.3 m/s].

9.2.4. Ground reaction force calculations

For all three SKA models the built-in OpenSim *ForceReporter* was used to determine the torque in the torsional springs and the actuator. Again, the GRFs were manually determined using MATLAB, based on the mass and accelerations of the segments. Using the segment ratios detailed in Dempster (1955), the segment CoM positions were calculated, and the accelerations determined by double differentiating the segment CoM positions. Finally, the sum of the forces, due to each component, in each direction determined the total anterior-posterior and vertical forces (Table 48 & Figure 72).

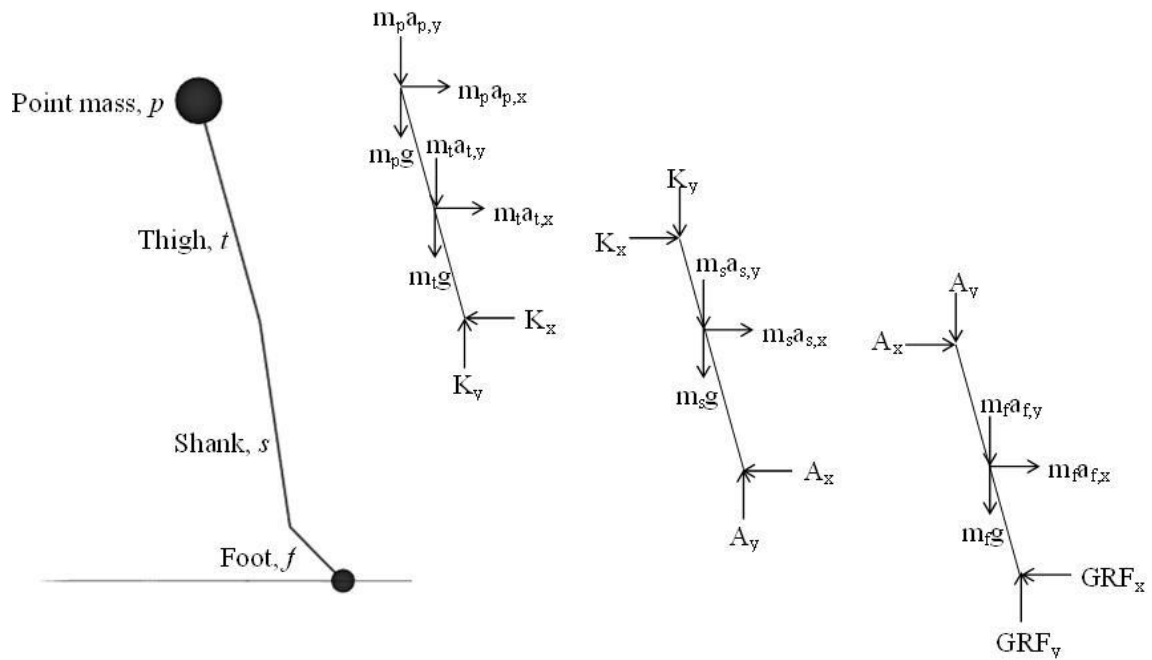


Figure 93 - Force diagram of the SKA model.

Table 48 - Equations for calculating the GRFs

$$\sum F_x = ma_x$$

$$K_x = m_p a_{p,x} + m_t a_{t,x}$$

$$A_x = K_x + m_s a_{s,x}$$

$$GRF_x = A_x + m_f a_{f,x}$$

$$\sum F_y = ma_y$$

$$K_y = m_p a_{p,y} + m_p g + m_t a_{t,y} + m_t g$$

$$A_y = K_y + m_s a_{s,y} + m_s g$$

$$GRF_y = A_y + m_f a_{f,y} + m_f g$$

9.2.5. Comparing solutions & Statistics

Solutions from the three SKA models were compared to the experimental data. A solution was deemed a failure if the CoM failed to rebound during the second half of stance. Those participants whose solutions failed were excluded from analysis. In the same way as the spring mass and SK models, the cost function was defined as the root mean square difference (RMSD) between the simulated and experimental CoM trajectories (see Chapter 6.4 for details). This RMSD was again the primary indicator of accuracy between the experimental and simulated CoM trajectories. Again, the maximum vertical CoM displacement for each model was then calculated and compared to the experimental data; this displacement was calculated as the difference between the maximum and minimum vertical CoM positions, during the simulation. Using paired t-tests the maximum vertical displacements from the three models were individually compared to the experimental values. Paired t-tests were used instead of an ANOVA as the aim was to determine how the layers of complexity affected the ability of the model at replicating experimental data; how the models compared to each other did not seem important. The percentage difference was also calculated in the same way as before (Eq. 28).

Similar to the spring mass and SK models, the RMSD between the GRFs were also determined, and the difference in the GRFs peak amplitudes calculated and compared. In addition, since these SKA models included two intersegmental joints, representing the knee and ankle, the simulated joint trajectories were also compared to the experimental joint trajectories using a RMSD. Again, as well as determining the RMSD, the CoM and joint trajectories and the GRF profiles were correlated between the model simulations and the experimental data in order to assess the type and strength of the relationship (Gutierrez-Farewik et al. 2006). A correlation was considered strong if r greater than 0.7, moderate if r was greater than 0.5 and weak if r was greater than 0.3.

As with the SK models, the optimised angular velocities were compared to the experimental values using a paired t-test and the percentage difference (Eq. 28). Finally, the ankle and knee joint stiffness, for the three SKA models individually, were compared to the experimental values using paired t-tests. The experimental joint stiffness values were calculated using the peak joint moments and the maximum change in joint angles, during the stance phase, where the joint angles and the net joint moments were determined using Visual3D (Chapter 3.3).

9.3. Results

Initial inspection of the results revealed that when the contact model was introduced the solutions failed for a number of people (Figure 94, Table 49). It should be reiterated that because of the changing number of participants, firstly due to the number of forefoot strikers at each speed, $n = 11, 12, 13$ and 19 at speeds 1 – 4, and secondly due to the number of failed solutions (Table 49), individual t-tests were determined for each speed; resulting in a new significance level of 0.013 . Therefore, analysis was completed on $n = 11, 11, 12$ and 13 participants at speeds 1 – 4, respectively. Removing participants whose solutions failed was necessary to compare between the different models. The possible reasons why the models failed will be discussed later.

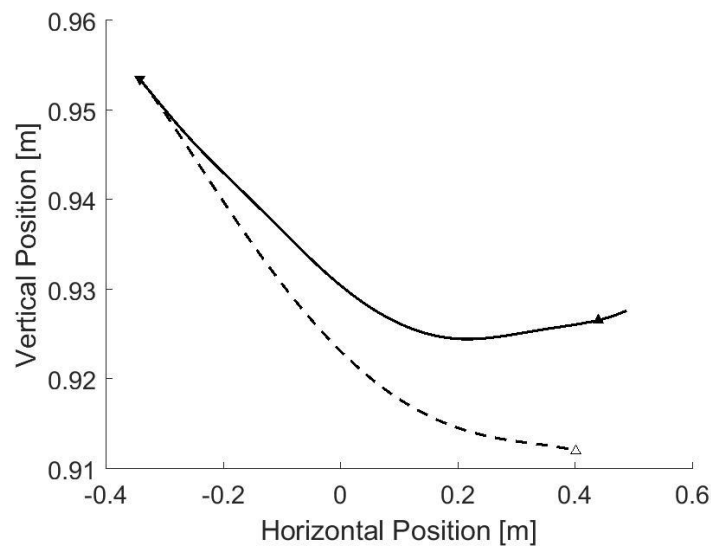


Figure 94 – Example of a failed simulation of the *SKAcontact* model

Table 49 - Number of failed solutions using the contact model.

	Speed 1	Speed 2	Speed 3	Speed 4
No. failed	0	1	1	6
Success rate [%]	100	92	92	68

9.3.1. CoM trajectory curves

The root mean square differences (RMSD) between the experimental and simulated CoM trajectories were lowest for the *SKAconstraint* model (Table 50). However, the RMSD for the *SKAactuator* model was lower than that for the *SKAcontact* model, at all four speeds. The horizontal components of the CoM trajectories from the three different SKA models were significantly and highly correlated with those from the experimental data ($r > 0.991$; $p \leq 0.013$) at all four speeds for all participants. In contrast, the correlation coefficients relating the vertical components of the CoM trajectories varied between the three different SKA models, however all were significant at the four speeds considered (Table 51). The *SKAconstraint* model consistently had the highest correlation coefficients, while the *SKAcontact* model consistently had the lowest (Table 50). Figure 95 shows examples of the simulated CoM trajectories compared to the experimental data.

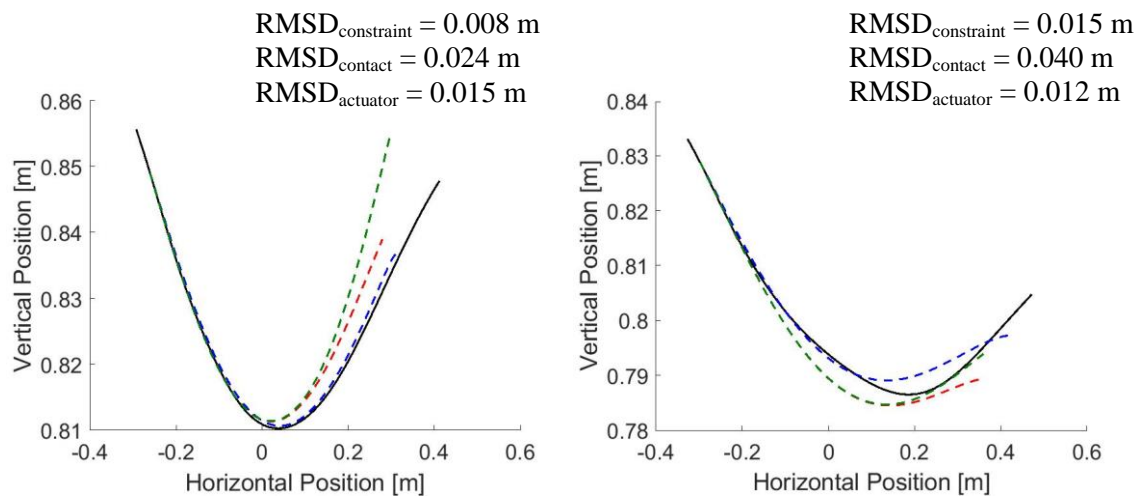


Figure 95 – Example of typical simulated CoM trajectories of the *SKAconstraint* (blue dashed), *SKAcontact* (red dashed) and *SKAactuator* (green dashed) compared to the experimental CoM trajectory (black solid) at speed 1 [3.3 m/s] (left) and speed 4 [5.6 m/s] (right).

Table 50 - Mean (SD) of the RMSD [m] between the simulated and experimental CoM trajectories.

	Speed 1	Speed 2	Speed 3	Speed 4
SKAconstraint	0.008 (0.003)	0.009 (0.004)	0.010 (0.004)	0.014 (0.005)
SKAcontact	0.027 (0.009)	0.030 (0.008)	0.031 (0.008)	0.039 (0.007)
SKAactuator	0.012 (0.005)	0.013 (0.004)	0.015 (0.005)	0.020 (0.009)

Table 51 - Mean (SD) correlation coefficients between the simulated and experimental vertical CoM trajectories. Correlations for all participants were significant ($p \leq 0.013$).

	Speed 1	Speed 2	Speed 3	Speed 4
SKAconstraint	0.991 (0.007)	0.988 (0.011)	0.949 (0.074)	0.867 (0.146)
SKAcontact	0.915 (0.079)	0.937 (0.062)	0.909 (0.108)	0.957 (0.034)
SKAactuator	0.953 (0.054)	0.953 (0.064)	0.917 (0.119)	0.946 (0.048)

9.3.2. Maximum vertical displacement

The maximum vertical displacements relate only to the period being simulated (approximately 5 - 90 % of stance). However, this includes the period during which the maximum vertical displacement occurs, since the maximum vertical displacement generally occurs at midstance during running. The simulated vertical CoM displacements appear different to the experimental values (Table 52), with significant differences found at speeds 2-4 for the *SKAconstraint* and *SKAactuator* models and at speed 3 and 4 for the *SKAcontact* model. The percentage difference between the vertical CoM displacement from the *SKAactuator* model compared to those from the experimental data were the largest of the three models (-11.3 (15.5), -23.8 (15.3), -22.7 (23.6) and -25.5 (26.1) at speed 1 – 4, respectively). Unsurprisingly, the percentage difference between vertical CoM displacements from the *SKAconstraint* model compare to those from the experimental data

were the smallest (-3.8 (23.3), -10.4 (13.7), -17.0 (21.8) and -17.8 (15.5) at speed 1 – 4, respectively).

Table 52 - Mean (SD) of the maximum vertical displacement [m] of the experimental data and simulations. * indicates a significant difference between the simulated and experimental values ($p \leq 0.013$).

	Speed 1	Speed 2	Speed 3	Speed 4
Experimental	0.045 (0.004)	0.042 (0.007)	0.036 (0.008)	0.035 (0.009)
SKAconstraint	0.047 (0.012)	0.047 (0.010)*	0.041 (0.007)*	0.041 (0.010)*
SKAcontact	0.049 (0.009)	0.050 (0.010)	0.044 (0.012)*	0.044 (0.013)*
SKAactuator	0.050 (0.008)	0.052 (0.012)*	0.044 (0.012)*	0.043 (0.013)*

9.3.3. GRF curves

The simulated AP and vertical GRFs profiles from the *SKAconstraint* model was observed to have a very similar shape to the experimental data (Figure 96). However, with the *SKAcontact* and *SKAactuator* models, during the first and last 5 % (approximately) of the simulation there were periods of high loading and unloading rates in both the AP and the vertical GRFs. These high loading rates result in a squarer shape for the vertical GRF, and a further underestimation of the peak vertical GRF (Figure 96). These differences are evident in the somewhat large RMSD between the simulated and experimental GRF profiles (Table 53 and Table 54). However, it should be noted that the RMSD for the *SKAactuator* was consistently the lowest, and the RMSD for the *SKA constraint* model consistently the highest.

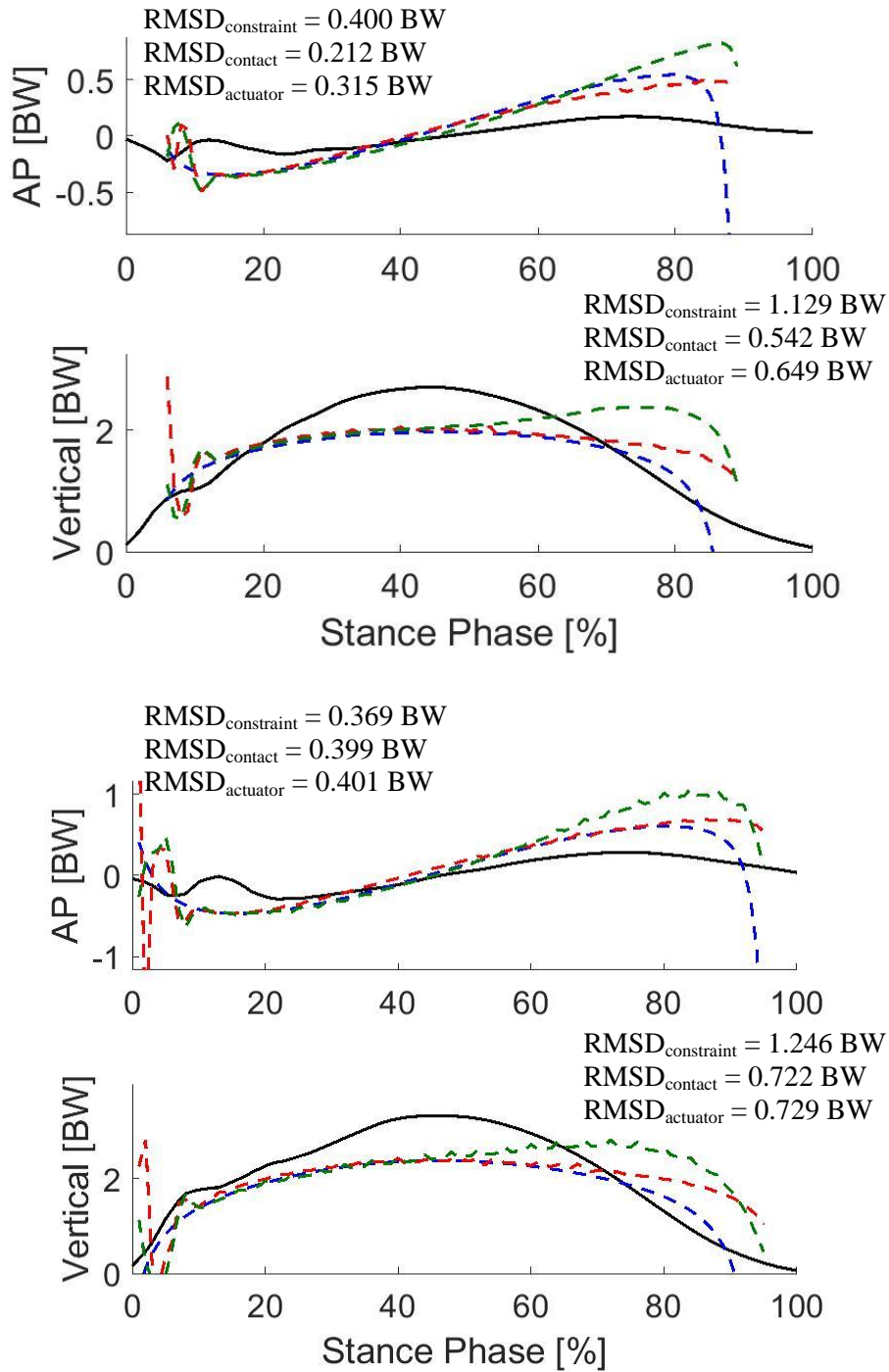


Figure 96 – Example of typical experimental (black solid) and simulated (SKAconstraint: blue dashed; SKAcontact: red dashed; SKAactuator: green dashed) GRF profiles at speed 1 [3.3 m/s] (top) and speed 4 [5.6 m/s] (bottom).

Table 53 - Mean (SD) of the RMSD [BW] between the simulated and experimental anterior-posterior (AP) GRF profiles.

	Speed 1	Speed 2	Speed 3	Speed 4
SKAconstraint	0.306 (0.393)	0.262 (0.118)	0.454 (0.179)	0.757 (0.629)
SKAcontact	0.296 (0.161)	0.322 (0.206)	0.562 (0.468)	0.675 (0.626)
SKAactuator	0.233 (0.048)	0.245 (0.052)	0.319 (0.083)	0.353 (0.105)

Table 54 - Mean (SD) of the RMSD [BW] between the simulated and experimental vertical GRF profile.

	Speed 1	Speed 2	Speed 3	Speed 4
SKAconstraint	1.086 (1.053)	0.796 (0.170)	1.187 (0.361)	1.903 (1.550)
SKAcontact	0.716 (0.258)	0.846 (0.436)	1.208 (0.623)	1.311 (0.883)
SKAactuator	0.639 (0.111)	0.652 (0.129)	0.842 (0.156)	0.898 (0.219)

The correlation analysis showed a significant relationship between the AP GRFs from the three SKA models and the experimental data at all four speeds (Table 55). However, for the AP GRFs the correlation coefficients indicates only a moderate relationship for the *SKAconstraint* model, but a strong relationship for both the *SKAcontact* and *SKAactuator* models. In contrast, the correlation analysis revealed significant relationships between the vertical GRFs (Table 56). Furthermore, the correlation coefficients for the vertical GRFs were generally lower than those for the AP GRFs. In addition, opposite to the AP GRFs, the correlation coefficients for the vertical GRFs from the *SKAconstraint* model were consistently the highest.

Table 55 - Mean (SD) of the correlation coefficients between the simulated and experimental anterior-posterior (AP) GRF profile. * indicates the correlation was significant ($p \leq 0.013$).

	Speed 1	Speed 2	Speed 3	Speed 4
SKAconstraint	0.696 (0.252)	0.787 (0.184)*	0.575 (0.209)*	0.477 (0.296)
SKAcontact	0.737 (0.178)*	0.743 (0.133)*	0.641 (0.200)*	0.643 (0.189)*
SKAactuator	0.870 (0.050)*	0.871 (0.075)*	0.808 (0.095)*	0.795 (0.131)*

Table 56 - Mean (SD) of the correlation coefficients between the simulated and experimental vertical GRF profile. * indicates the correlation was significant ($p \leq 0.013$).

	Speed 1	Speed 2	Speed 3	Speed 4
SKAconstraint	0.743 (0.182)*	0.791 (0.049)*	0.701 (0.114)*	0.707 (0.113)*
SKAcontact	0.534 (0.383)	0.510 (0.356)	0.300 (0.480)	0.350 (0.456)
SKAactuator	0.560 (0.213)*	0.637 (0.214)*	0.526 (0.261)	0.527 (0.304)

Comparison of the peak/trough GRF values indicates significant differences between the SKA models and the experimental data (Table 57, Table 58 and Table 59). The AP troughs were statistically similar between the three SKA models and the experimental data at all four speeds considered (Table 57). The peak AP GRFs were consistently overestimated while the peak vertical GRFs were consistently underestimated by the three SKA models (Table 58, Figure 96). Furthermore, the peak vertical GRFs were statistically similar between the *SKAconstraint* model and the experimental values at speeds 3 and 4 (Table 59). However, the peak AP and peak vertical GRFs were significantly different from the experimental data for both the *SKAcontact* and *SKAactuator* models, at all four speeds considered (Table 58 and Table 59).

Table 57 - Mean (SD) of the trough AP GRF force values [BW] of the experimental data and simulations.

	Speed 1	Speed 2	Speed 3	Speed 4
Experimental	-0.324 (0.165)	-0.380 (0.170)	-0.404 (0.189)	-0.460 (0.227)
SKAconstraint	-0.304 (0.068)	-0.397 (0.107)	-0.405 (0.105)	-0.446 (0.065)
SKAcontact	-0.664 (0.482)	-1.097 (1.768)	-1.876 (2.293)	-2.911 (3.991)
SKAactuator	-0.438 (0.096)	-0.531 (0.110)	-0.551 (0.103)	-0.539 (0.092)

Table 58 - Mean (SD) of the peak AP GRF force values [BW] of the experimental data and simulations. All simulated values were significantly different from the experimental value ($p \leq 0.013$).

	Speed 1	Speed 2	Speed 3	Speed 4
Experimental	0.249 (0.085)	0.327 (0.119)	0.388 (0.134)	0.445 (0.166)
SKAconstraint	0.391 (0.095)	0.532 (0.143)	0.609 (0.123)	0.694 (0.177)
SKAcontact	0.438 (0.072)	0.512 (0.063)	0.608 (0.072)	0.705 (0.121)
SKAactuator	0.650 (0.124)	0.704 (0.134)	0.804 (0.143)	0.856 (0.169)

Table 59 - Mean (SD) of the peak vertical GRF force values [BW] of the experimental data and simulations. * indicates simulated values were significantly different from the experimental value ($p \leq 0.013$).

	Speed 1	Speed 2	Speed 3	Speed 4
Experimental	2.717 (0.123)	2.904 (0.155)	3.060 (0.204)	3.201 (0.217)
SKAconstraint	1.803 (0.257)*	2.083 (0.405)*	2.110 (0.290)	2.263 (0.306)
SKAcontact	2.052 (0.274)*	2.095 (0.319)*	2.420 (1.116)*	2.309 (0.598)*
SKAactuator	2.141 (0.182)*	2.239 (0.334)*	2.167 (0.372)*	2.324 (0.430)*

9.3.4. Hip joint angles

The simulated hip joints angles, from the three SKA models, followed a similar pattern to the experimental values (Table 60 and Figure 97). The initial joint angles were set using the experimental values; however, during the simulation hip joint angle were underestimated compared to the experimental values.

Table 60 - Mean (SD) of the RMSD [deg] between the simulated and experimental hip joint angles.

	Speed 1	Speed 2	Speed 3	Speed 4
SKAconstraint	3.66 (1.03)	3.36 (1.66)	3.56 (1.33)	4.01 (1.23)
SKAcontact	3.92 (2.23)	4.81 (2.01)	4.94 (1.84)	5.58 (1.59)
SKAactuator	3.41 (1.97)	3.90 (1.76)	4.44 (1.31)	4.55 (2.19)

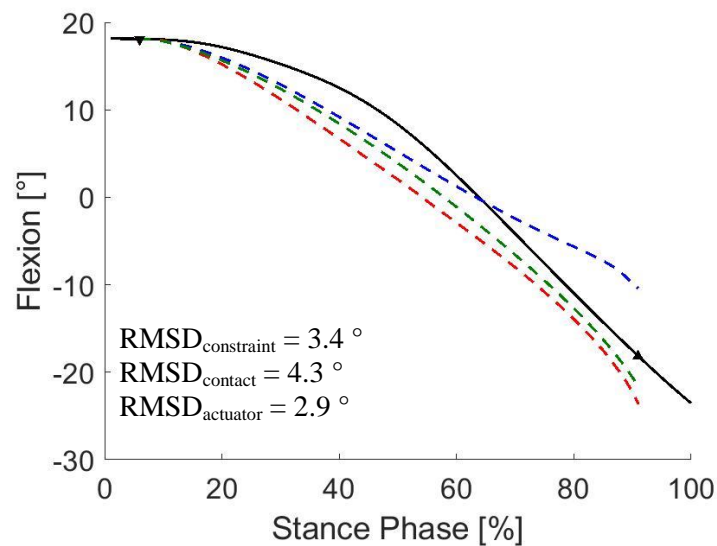


Figure 97 – Example of typical experimental (black solid) and simulated (SKAconstraint: blue dashed; SKAcontact: red dashed; SKAactuator: green dashed) hip joint angle profiles at speed 1 [3.3 m/s].

9.3.5. Knee kinematics

The simulated knee joint trajectories were similar in shape to the experimental trajectories (Figure 98). However, the maximum vertical displacement was, in general, overestimated and offset by the SKA models (Figure 98). The RMSD between the trajectories were relatively small compared to the range of motion (Table 61), and the correlation coefficients indicate a strong correlation between the horizontal component of the simulated and experimental knee trajectories, at all four speeds (Table 62). In contrast, the correlation coefficients for the vertical component indicate negative, weak and insignificant correlations for all three SKA models, at all four speeds (Table 62).

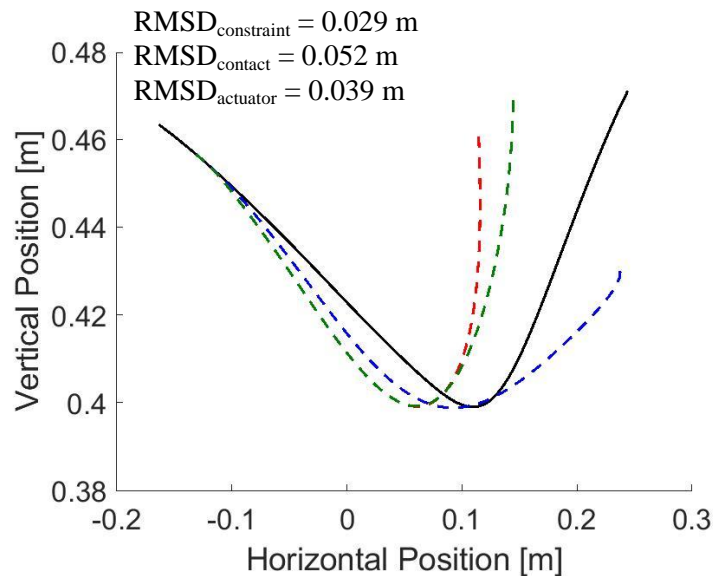


Figure 98 – Example of typical experimental (black solid) and simulated (SKAconstraint: blue dashed; SKAcontact: red dashed; SKAactuator: green dashed) knee trajectories at speed 1 [3.3 m/s].

Table 61 - Mean (SD) of the RMSD [m] between the simulated and experimental knee trajectories.

	Speed 1	Speed 2	Speed 3	Speed 4
SKAconstraint	0.027 (0.009)	0.024 (0.011)	0.025 (0.008)	0.028 (0.007)
SKAcontact	0.034 (0.009)	0.043 (0.014)	0.042 (0.013)	0.045 (0.015)
SKAactuator	0.028 (0.012)	0.035 (0.013)	0.038 (0.013)	0.040 (0.015)

Table 62 - Mean (SD) correlation coefficients between the simulated and experimental knee trajectories. * indicates correlation was significant ($p \leq 0.013$).

Speed	SKAconstraint		SKAcontact		SKAactuator	
	x	y	x	y	x	y
1	0.993*	-0.341	0.982*	-0.452	0.989*	-0.367
	(0.006)	(0.328)	(0.010)	(0.270)	(0.016)	(0.321)
2	0.993*	-0.458	0.985	-0.576*	0.994*	-0.492*
	(0.004)	(0.189)	(0.010)	(0.160)	(0.007)	(0.200)
3	0.994*	-0.622	0.981*	-0.676*	0.988*	-0.629*
	(0.004)	(0.217)	(0.022)	(0.211)	(0.020)	(0.228)
4	0.994*	-0.642*	0.982*	-0.675*	0.990*	-0.630*
	(0.005)	(0.172)	(0.017)	(0.226)	(0.014)	(0.243)

The discrepancies in the knee trajectories are highlighted by the difference between the knee joint angle profiles (Figure 99 and Table 63). The initial and peak knee joint angles were consistently underestimated by the three SKA models. Furthermore, the RMSD between the joint angle profiles was largest for the *SKAcontact* model and smallest for the *SKAconstraint* model (Table 63).

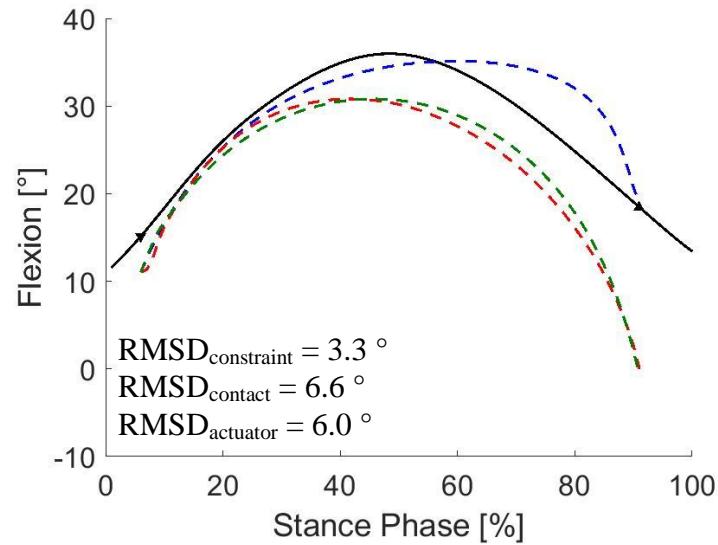


Figure 99 - Example of typical experimental (black solid) and simulated (*SKAconstraint*: blue dashed; *SKAcontact*: red dashed; *SKAactuator*: green dashed) knee joint angles at speed 1 [3.3 m/s].

Table 63 - Mean (SD) of the RMSD [deg] between the simulated and experimental knee joint angles.

	Speed 1	Speed 2	Speed 3	Speed 4
SKAconstraint	5.45 (1.68)	5.42 (2.18)	5.18 (1.48)	5.43 (1.49)
SKAcontact	6.26 (3.06)	7.25 (2.53)	8.30 (2.62)	8.55 (3.26)
SKAactuator	6.31 (2.98)	6.76 (2.24)	8.00 (2.23)	7.81 (3.41)

9.3.6. Ankle kinematics

The simulated ankle joint trajectories showed a very different shape to the experimental trajectories (Figure 100). The experimental trajectory followed a similar shape to both the knee and CoM trajectories; in contrast, the simulated trajectories followed a trajectory more similar to an inverted pendulum. The RMSD between the trajectories still appear small (Table 64), however the range of motion of the ankle is considerably smaller than that of the knee. Somewhat surprisingly, the correlation coefficients indicate significant

and strong correlations between both the horizontal and vertical components of the simulated and experimental ankle trajectories, for all three SKA models, at all four speeds (Table 65).

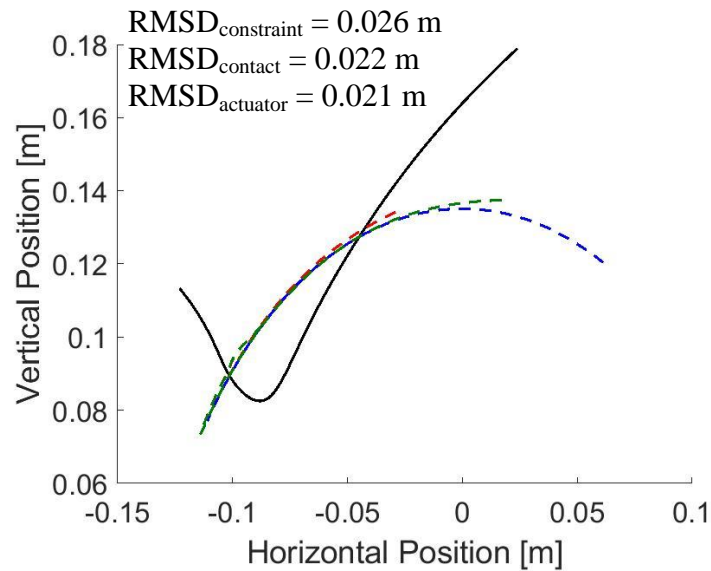


Figure 100 – Example of typical experimental (black solid) and simulated (*SKAconstraint*: blue dashed; *SKAcontact*: red dashed; *SKAactuator*: green dashed) ankle trajectories at speed 1 [3.3 m/s].

Table 64 - Mean (SD) of the RMSD [m] between the simulated and experimental ankle trajectories.

	Speed 1	Speed 2	Speed 3	Speed 4
SKAconstraint	0.025 (0.009)	0.024 (0.009)	0.027 (0.008)	0.030 (0.009)
SKAcontact	0.025 (0.006)	0.031 (0.011)	0.030 (0.011)	0.033 (0.009)
SKAactuator	0.022 (0.006)	0.028 (0.008)	0.028 (0.008)	0.031 (0.008)

Table 65 - Mean (SD) correlation coefficients between the simulated and experimental ankle trajectories. All correlations were significant ($p \leq 0.013$).

Speed	SKAconstraint		SKAcontact		SKAactuator	
	x	y	x	y	x	y
1	0.914 (0.048)	0.838 (0.075)	0.892 (0.090)	0.829 (0.102)	0.914 (0.058)	0.849 (0.091)
2	0.902 (0.051)	0.814 (0.078)	0.816 (0.136)	0.760 (0.112)	0.877 (0.075)	0.800 (0.075)
3	0.896 (0.044)	0.767 (0.056)	0.826 (0.114)	0.781 (0.096)	0.883 (0.062)	0.815 (0.071)
4	0.896 (0.063)	0.754 (0.100)	0.838 (0.139)	0.763 (0.139)	0.874 (0.123)	0.784 (0.137)

The discrepancies in the ankle trajectories are further highlighted by the differences between the ankle joint angle profiles (Table 66 and Figure 101). Similar to the knee joint angles, the initial ankle joint angles were consistently underestimated by the three SKA models. However, in contrast to the knee joint angle, the peak ankle joint angles were consistently overestimated by the three SKA models. In contrast with the RMSD between the trajectories, the RMSD between the joint angle profiles was smallest for the *SKAactuator* model and largest for the *SKAconstraint* model (Table 66).

Table 66 - Mean (SD) of the RMSD [deg] between the simulated and experimental ankle joint angles.

	Speed 1	Speed 2	Speed 3	Speed 4
SKAconstraint	11.77 (4.07)	11.83 (3.39)	14.36 (3.47)	15.53 (3.53)
SKAcontact	8.70 (3.95)	12.37 (3.26)	10.40 (3.54)	13.23 (4.50)
SKAactuator	10.13 (3.19)	12.27 (3.89)	10.11 (2.85)	12.94 (4.46)

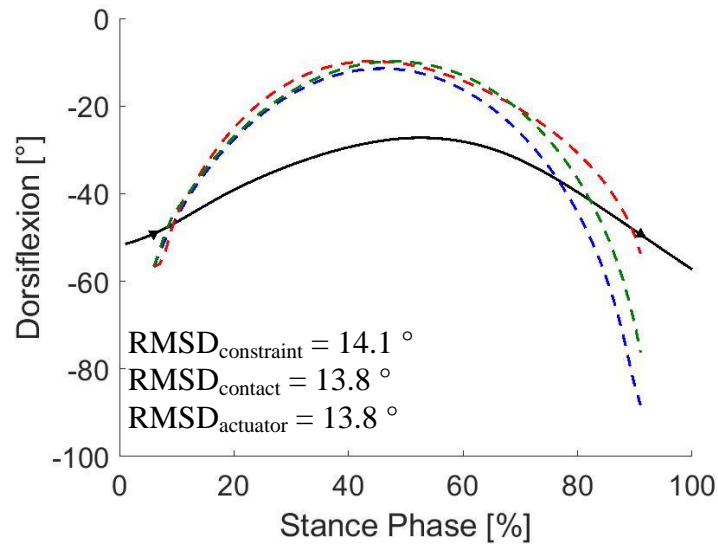


Figure 101 - Example of typical experimental (black solid) and simulated (*SKAconstraint*: blue dashed; *SKAcontact*: red dashed; *SKAactuator*: green dashed) ankle joint angles at speed 1 [3.3 m/s].

9.3.7. Initial conditions vs. Experimental data

The optimised values for the hip, knee and ankle angular velocities were similar to the experimental values at all four speeds (Figure 102 - Figure 104). Paired t-tests showed significant differences for the initial ankle angular velocities between *SKAcontact* and model when compared to the experimental values at all four speeds. A significant difference was found for initial ankle angular velocities between the *SKAconstraint* model and the experimental values at speed 1 only (Figure 104). However, the large error bars indicate the considerable inter-subject variability, especially in the hip angular velocities (Figure 102 - Figure 104). It should be reiterated that the optimised stiffness values and angular velocities for the *SKAcontact* model were used for the *SKAactuator* model.

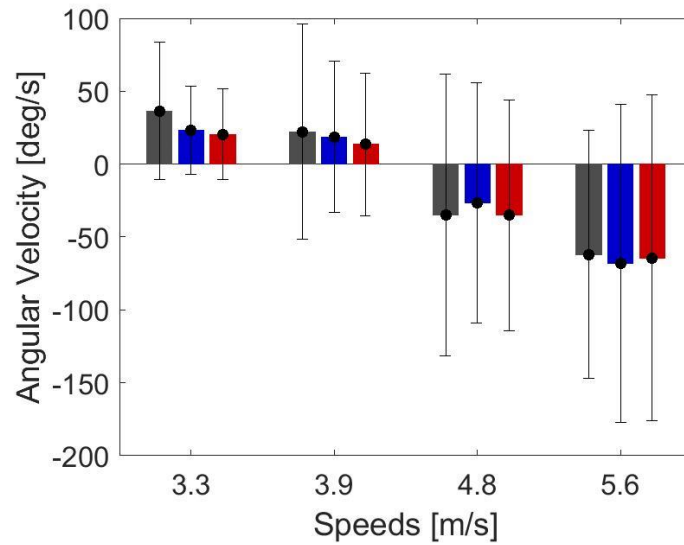


Figure 102 - Mean and standard deviations of the experimental vs. optimised hip angular velocities [deg/s] used when simulating the SKA models. The dark grey bar represents the experimental data, the blue the *SKAconstraint* model and the red the *SKAcontact* model.

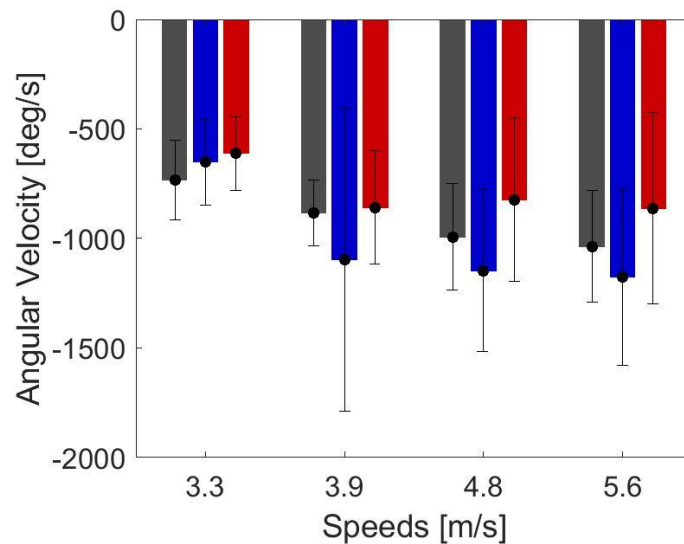


Figure 103 - Mean and standard deviations of the experimental vs. optimised knee angular velocities [deg/s] used when simulating the SKA models. The dark grey bar represents the experimental data, the blue the *SKAconstraint* model and the red the *SKAcontact* model.

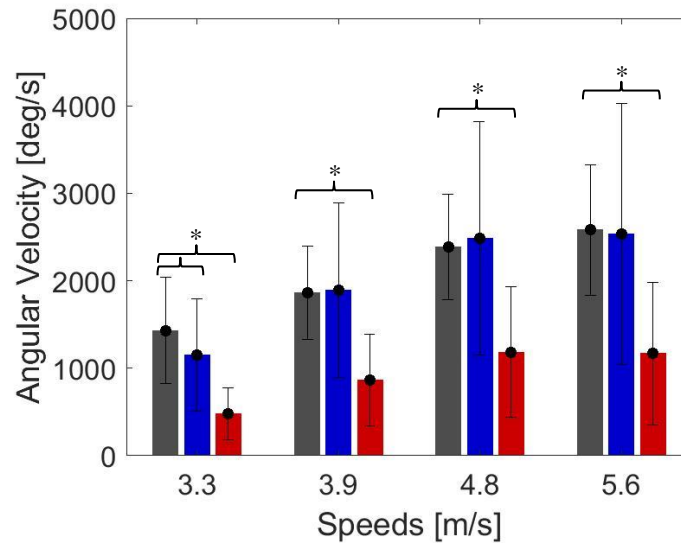


Figure 104 - Mean and standard deviations of the experimental vs. optimised ankle angular velocities [deg/s] used when simulating the SKA models. The dark grey bar represents the experimental data, the blue the *SKAconstraint* model and the red the *SKAcontact* model.

9.3.8. Joint stiffness / joint torques

In the SKA models, a *SpringGeneralizedForce* acted as a torsional spring at the intersegmental “knee” joint (Figure 89). The optimised knee stiffness values from *SKAconstraint* and *SKAcontact* models were significantly different from the experimental values, calculated using the ratio of the peak knee joint moment to peak angular displacement of the knee from Visual3D, at all four speeds considered (Figure 105).

Again, the optimised values from the *SKAcontact* model were used for the *SKAactuator* model. Furthermore, the percentage differences between the model and experimental values were (57.2 (11.4), 48.0 (18.6), 42.3 (30.0) and 46.5 (16.6) for the *SKAconstraint* model and 47.8 (16.2), 46.3 (15.9), 39.1 (30.4) and 38.6 (25.4) for the *SKAcontact* model at speed 1-4, respectively).

Similar to the knee stiffness, the optimised ankle stiffness values from *SKAconstraint* and *SKAcontact* models were significantly different from the experimental values, calculated using the ratio of the peak ankle joint moment to peak angular displacement of the ankle from Visual3D, at all four speeds considered (Figure 105). Furthermore, the percentage

differences between the model and experimental values were (57.6 (11.3), 57.4 (12.4), 58.9 (10.8) and 62.7 (6.0) for the *SKAconstraint* model and 53.7 (13.4), 58.5 (12.9), 62.2 (11.0) and 64.8 (8.0) for the *SKAcontact* model at speed 1-4, respectively).

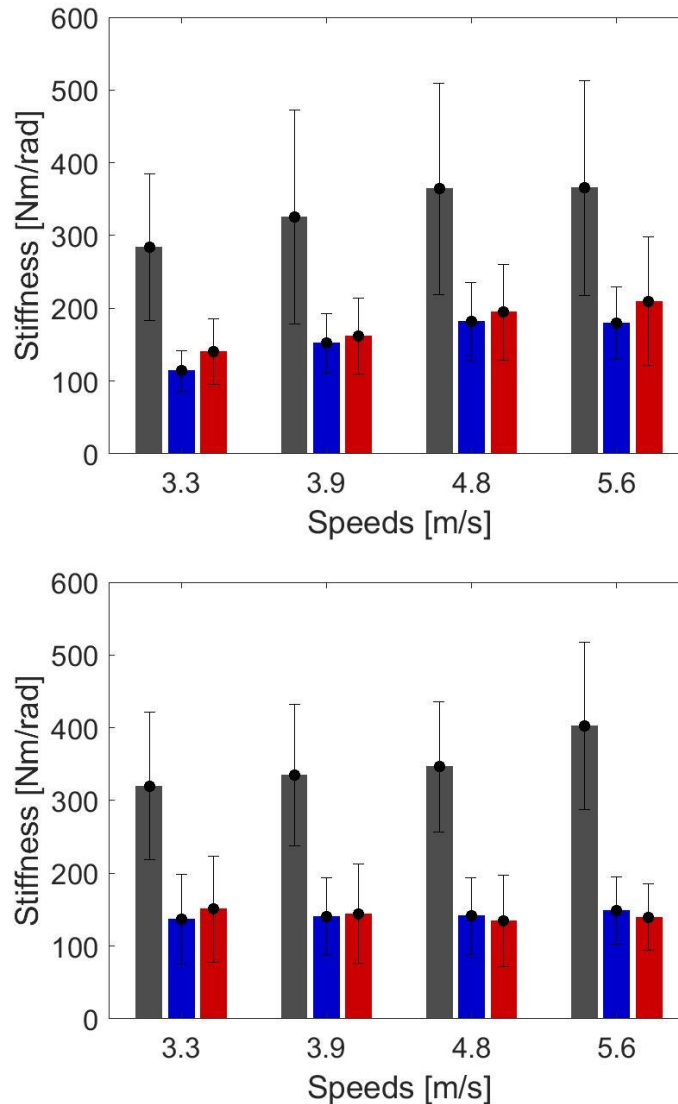


Figure 105 - Mean and standard deviations of experimental and optimised knee (top) and ankle (bottom) joint stiffness values [Nm/rad]. The dark grey bar represents the experimental data, the red the *SKAconstraint* model, and the red the *SKAcontact* model. All optimised stiffness values were significantly different from the experimental values.

9.4. Discussion

The aim of this chapter was to develop a three-segment model of human running in OpenSim and compare it to experimental data. A few three-segment models have been presented in literature (Seyfarth et al. 2001, Seyfarth et al. 2006, Qiao et al. 2017). However these studies tended to focus of model segment orientation, dynamic stability and leg joint function rather than assessing how well these models can reproduce normal running kinematics and kinetics. These previous studies highlighted the benefits for understanding the spring-like behaviour of segmented lower limbs and proposed that this could contribute to a better understanding of biological lower limbs, but they were limited in how they compared results to real world experimental data. Therefore, this chapter aimed to determine the individual contributions of adding an ankle joint and foot segment with fixed inertial properties. The models presented in this chapter show good kinematic and kinetic agreement with experimental data during the first 90 % (approximately) of stance.

Chapters 7 and 8 showed the strengths and limitations of the spring mass model and two sprung knee (SK) models. The spring mass model produced a sinusoidal CoM trajectory, but overestimated the vertical CoM displacement and did not rebound during mid to late stance. On the other hand, the SK models showed closer kinematic agreement during the middle 60 % (approximately) of stance. However, geometry restrictions meant it was not possible to model early or late stance with these models. Therefore, by adding an ankle joint and foot segment it was hoped that the SKA models would be able to model both early and late stance with better kinematic and kinetic agreement.

Similar to the SK models, geometry restrictions meant it was not possible to model the first 5 % and last 10% (approximately) of stance. This was because the foot segment length was approximated as the mean distance from the ankle joint centre to the average CoP during stance, and therefore the foot length was underestimated during the first 5 % and last 10% (approximately) of stance. However, simulations using all three SKA models (*SKAconstraint*, *SKAcontact* and *SKAactuator*) generally showed close kinematic agreement during the first 90 % (approximately) of stance. This close agreement was highlighted by the small RMSD between the simulated and experimental CoM trajectories,

and the similar vertical CoM displacements from the simulations compared to the experimental values.

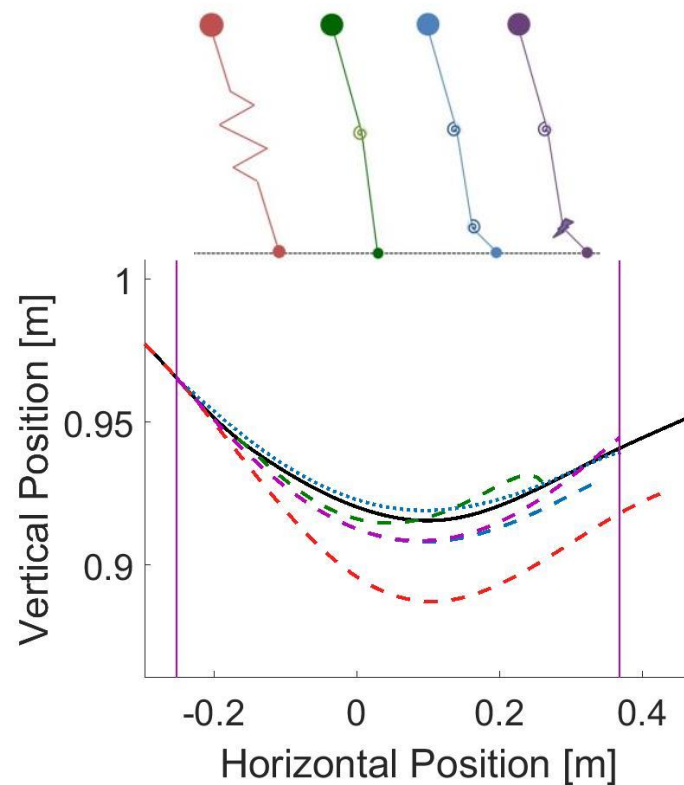


Figure 106 - Example of the difference in the simulated CoM trajectories from the experimntal data (solid black line), spring mass model (red dased line), *SKA torsional* model (dashed green line) *SKA constraint* model (dotted blue line), *SKAcontact* (dashed blue line) and *SKAactuator* model (dashed purple line) for one subject at speed 1 [3.3 m/s].

Figure 106 shows the general increase in agreement between simulation and experiment data as the overall model complexity increases (spring mass model (red dashed) shows the lowest agreement; *SKAconstraint* model (blue dotted) shows the highest agreement). The close agreement between the *SKAconstraint* model, and the apparent decrease in agreement with the *SKAcontact* and *SKAconstraint* models, suggests that a purely passive system is sufficient for modelling the first 90 % (approximately) of forefoot running. The RMSD values were higher for the *SKAcontact* model and experimental CoM trajectories

than those between the *SKAconstraint* model and the experimental CoM trajectories (Table 50). Furthermore, by replacing the spring with an actuator the kinematic agreement between the simulated and experimental CoM trajectories increased compared to the *SKAcontact* model (Figure 106); the mean RMSD for the *SKAactuator* model was approximate half that of the *SKAcontact* model at all four speeds (Table 50). However, the values were still higher than those for the *SKAconstraint* model. This result suggests that, at least for forefoot strikers, introducing a small amount of energy during late stance does not increase the ability of the model, and that a passive system with two torsional springs at the knee and ankle joints, *SKAconstraint* model, may be sufficiently complex.

Although the agreement between the CoM trajectories was highest between the *SKAconstraint* model and the experimental data, the *SKAactuator* model consistently had closer agreement with the experimental ankle joint kinematics than the *SKAconstraint* model. Furthermore, the *SKAactuator* model had smaller RMSD values between the GRF profiles than the *SKAconstraint* model. Across all these parameters the *SKAcontact* model had the lowest agreement with the experimental data. These results suggest that although there are difficulties associated with adding an actuator, namely in tuning the contact model, introducing a small amount of energy in late stance provides a closer match between the simulated and experimental ankle joint kinematics. Furthermore, the underestimated vertical GRFs using all three SKA models suggest that these models fail to generate enough vertical GRF in midstance, thus requiring increased GRF in late stance. It is possible that replacing the knee spring with an actuator would further increase the agreement in the kinetics and improved the agreement between the simulated and experimental knee joint angles.

A limitation of OpenSim meant the *PointConstraint*, representing the fixed contact point between the model and ground, was ignored in the customised control function of the actuator. Therefore the *PointConstraint* had to be replaced with a contact model so that the torsional spring at the ankle could then be replaced with a custom controlled actuator. This *SKAcontact* model “failed” for a number of participants (Table 49) and it is difficult to say why this model failed for these participants. However, it is important to note that it is unclear what contact parameters (stiffness and contact radius) should be used to model the foot-ground interaction during running; and it was recommended by OpenSim that the contact parameters be included in the optimisation. Therefore, in an effort to get a

successful solution I tried a number of different optimisations of the contact parameters and initial angular velocities; however I could not solve the problem. The number of failed solutions and the higher RMSD for the *SKAcontact* and *SKAactuator* models suggest that the optimised values used here may not be the most appropriate for running and that a different, and more robust, method for determining the contact model parameters needs to be investigated.

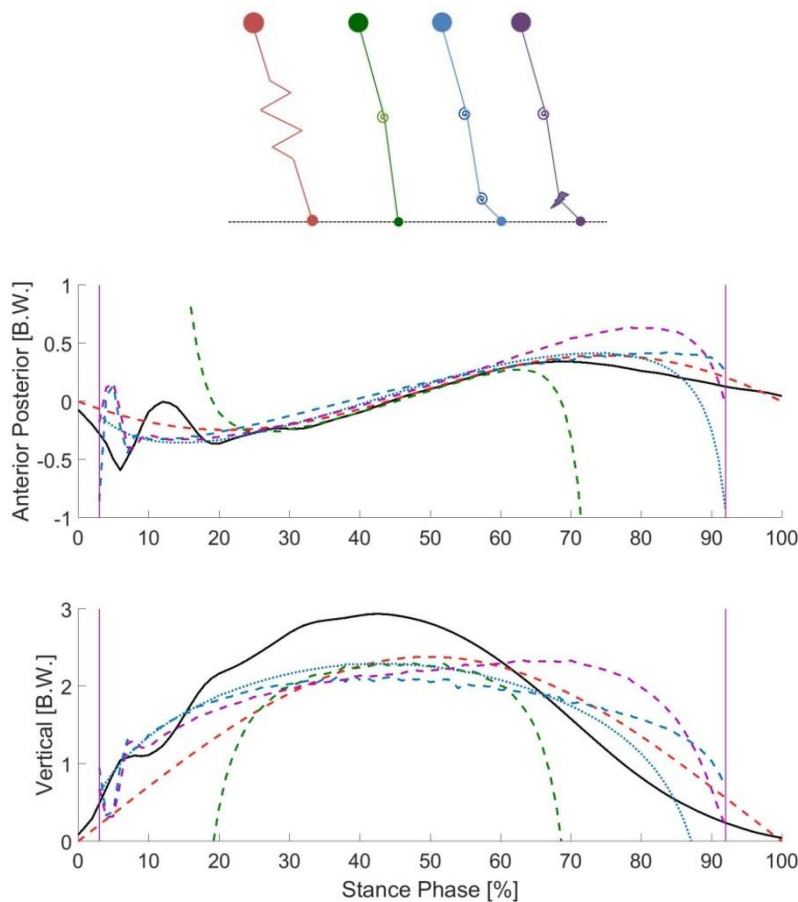


Figure 107 - Example of the difference in the simulated CoM trajectories from the experiemntal data (solid black line), spring mass model (red dased line), *SKtorsional* model (dashed green line) SKA constraint model (dotted blue line), *SKAcontact* (dashed blue line) and *SKAactuator* model (dashed purple line) for one subject at speed 1 [3.3 m/s].

The predominant difference between the GRFs from the contact model (*SKAcontact* and *SKAactuator*) versus the fixed contact point (*SKAconstraint*) is the shape of the vertical GRF profile (Figure 107). When a contact model is used instead of a *PointConstraint* the vertical GRF becomes squarer, with periods of high loading during early and late stance. However, somewhat surprisingly these GRF profiles resulted in lower RMSD values compared to the *SKAconstraint* model (Table 53 and Table 54). These high loading rates are likely a consequence of inappropriately tuned contact parameters. Modelling the foot-ground interaction using a single viscoelastic sphere is a considerable simplification of how a real foot interacts with the ground, and likely introduced larger errors for those participants who have a relatively larger range-of-motion of the CoP. It is accepted that accurately modelling the foot-ground interaction during locomotion is very complex (Naemi et al. 2013, Uchida et al. 2015, Jackson et al. 2016), and it remains unclear how best to determine the contact parameters of viscoelastic elements used in many of these models. Furthermore, the square vertical GRF profile was also produced by the SK models presented in the previous chapter, and by another two-segment model presented in the literature (Rummel et al. 2008). Rummel et al. (2008) attributed the high loading rates to constant joint stiffness, however our results show a sinusoidal GRF profile can be produced using a model with two passive joints with constant stiffness (*SKAconstraint model*). Thus the high loading rates produced using the *SKAcontact* and *SKAactuator* models are likely a consequence of the contact model, and not the constant joint stiffness.

The results presented here showed significant differences between optimised knee and ankle joint stiffness compared to experimental values. However it has been shown that using the simple approximation of the ratio of maximum joint moment to maximum change in joint angle overestimates the ankle stiffness by approximate 40 % (Günther et al. 2002). Furthermore, joint stiffness incorporates multiple different factors, including muscle activation, co-contraction, and reflexes as well as joint moment and joint angle (Farley et al. 1998), therefore the “real” joint stiffness values may be different to those calculated using the perturbation method. In contrast to the results presented here, Qiao et al. (2017) compared the parameters of a three-segment MDS model to experimental data and found a direct correlation with the lower limb stiffness and lower limb length measured for their participants despite the model initial conditions being optimised to match human kinematics. Furthermore, they found no significant differences between the mechanical work at the hip, knee and ankle between the MDS model and the experimental

data during level running (Qiao et al. 2017). This suggests this MDS model captures some of the important mechanical functions of the lower limb. However the model presented by Qiao et al. (2017) included a functional hip joint, which acted primarily as a motor, whereas the SKA models presented here did not model hip function. Furthermore, their model did not include rigid segments, but modelled the lower limb as a motor-damper-spring system.

In contrast to published research, the result of the SKA models show similar values for knee and ankle joint stiffness, at each of the four speeds considered. It has been reported that the knee joint is, in general, more stiff than the ankle (Günther et al. 2002), and that there is a greater demand on the ankle extensors than the knee extensors during locomotion (Kulmala et al. 2016). This greater demand on the ankle has been suggested as a key influence in the way humans move. Our finding that the ankle may not act as a purely passive spring is in agreement with this, suggesting that the control of the ankle joint is important for optimal running biomechanics. However, in contrast to the results presented here, some research has suggested that the primary function of the ankle during running is as a spring (Farris et al. , Qiao et al. 2017). However, neither of these studies commented on the ability level or foot strike pattern adopted by their participants.

The changing number of participants at each speed meant direct comparisons about how well these models performed could not be made across the speeds. However, modelling studies often focus on a single participant and/or a single speed, so although direct comparisons cannot be made, the results of this chapter show that this model can be used to investigate a range of participants at a range of speeds. It should be noted that the *SKAconstraint* model “failed” for two participants (at speed 4), suggesting that at this faster speed it may not be possible for the passive system to store enough energy for the CoM to rebound during late stance, and that adding a small amount of actuation at the knee or ankle might overcome this. However, difficulties in determining the contact parameters of the *SKAcontact* model prevented this from being confirmed.

Another limitation of the SKA models presented here is the way in which the contact parameters were defined. During running there is a net distal-to-proximal translation of the CoP under the foot, therefore modelling the foot-ground interaction using either a fixed point, or using a single viscoelastic sphere, neglects this net CoP movement. These simplifications are likely to contribute to the errors in both the AP and vertical GRFs. The

fixed contact point also means that, in the *SKAconstraint* model, prior to the end of the simulation the point mass is being pulled down towards the fixed contact point, and this likely contributes to the errors in the vertical GRFs. Furthermore, the length of the foot segment was underestimated in the SKA models. This meant that in all three SKA models, the simulation was terminated before the anatomical foot would have left the ground, and as mentioned previously, is likely the reason why the SKA models could not model the last 10 % of stance. However during the last 10 % of stance the body is preparing for flight and lower limb muscle activation is low, suggesting this approach is an appropriate step in modelling running, and gives insight into the fundamental mechanisms that characterise the stance phase of running.

The results of this chapter show that a passive three-segment model, with two torsional springs at the knee and ankle may be sufficient for modelling the CoM trajectory during the stance phase of running. However, the increased agreement in the joint kinematics and the GRFs when the ankle spring is replaced with an actuator suggests that introducing a small amount of energy at the ankle results in joint coordination more similar to normal running. Therefore, more investigation is needed. Firstly, it might be worth exploring the effect of different control functions to determine if increased agreement in the CoM trajectories can also be achieved with the *SKAactuator* model. In addition, developing this model by adapting the contact model and introducing a more anatomically accurate foot could potentially allow for modelling of rearfoot running as well as forefoot running.

10. General Discussion

10.1. Introduction

Despite substantial previous research into running, relatively little is known about the fundamental principles which underlie and explain why people run the way they do. Mathematical models can provide a useful method for investigating some of the unknown aspects about how and why people run the way they do. However, there is a large gap in complexity between the existing models of running.

Current models of running can generally be categorised as simple or complex. The simple models have often been used to investigate simple mechanical relationships, and the complex models are often used to investigate individual muscular functions. However, a broader understanding of the mechanisms that determine why people run the way they do remains unclear. By first considering the simplest model of running, the spring mass model, and its fundamental assumptions, this thesis aimed to highlight some the major limitations of the spring mass model and thus provide a starting point for subsequent work which was aimed at gradually developing the complexity of the model. By sequentially adding complexity it is possible to investigate the effects of each additional layer of complexity, and thus identify possible mechanical characteristics that contribute to how and why humans run the way they do.

The spring mass model is the simplest and most common model used to investigate running. It has been claimed that this model is capable of replicating certain characteristics of the normal running (Bullimore et al. 2007). However, the results of this PhD show that when compared to experimental data of forefoot strikers (those who are most likely to obey the assumptions of the spring mass model) this model is too simple and cannot accurately replicate the biomechanics of normal running. Two (Rummel et al. 2008, Phan et al. 2017) and three (Seyfarth et al. 2001, Seyfarth et al. 2006, Qiao et al. 2017) segment models have been developed from the spring mass model, however these models have, in general, primarily been used to investigate dynamic stability and their simulations have not been directly compared to experimental data. Therefore, this PhD is the first investigation

that has sequentially added complexity to the spring mass model and quantitatively compared the simulations to real world experimental data.

Following a general introduction, this thesis discussed the existing simple and complex models of running (Chapter 2). This literature review highlighted the strengths and weaknesses of the existing models, and identified areas of running biomechanics that have not yet been explored or remain relatively misunderstood.

Chapter 4 then discussed the fundamental assumption of the spring mass model (that the body acts similar to a massless linear spring of constant stiffness). The validity of this assumption was explored for a range of foot strike patterns and running speeds. Chapter 5 investigated the range of methods of calculating lower limb stiffness (assumed to be equivalent to the spring stiffness in the spring mass model) and compared these to the most physically consistent definition.

Chapters 7, 8 and 9 outlined the spring mass model, the sprung knee (SK) models and the sprung knee and ankle (SKA) models. Chapter 7 assessed the ability of the spring mass model using a dataset of nineteen forefoot strikers (the experimental data was described in Chapter 3). The first layers of complexity added to the spring mass model were rigid segments, with finite mass, and a torsional spring at the intersegmental joint (Chapter 8). Then an additional foot segment and another torsional spring were added to model the ankle joint (Chapter 9). The effects of these additional layers of complexity were continuously assessed by quantifying the agreement between model simulations and the experimental data.

This final chapter will form a general discussion of the PhD. It will include a recap of the findings and a discussion of the extent to which the research questions were answered. Furthermore, the chapter will discuss some of the general limitations of the methods and outline potential future avenues of research.

10.2. *Research Question 1*

Is the spring mass model appropriate for modelling running?

Chapter 4 investigated this research question. The simplest model of running is the spring mass model, and it was developed to investigate the fundamental relationships between running parameters and the mechanical variables. The spring mass model assumes that, during running, the human body acts in a similar way to a point mass bouncing on a massless linear spring of constant stiffness. Therefore, this chapter compared the force-length relationships of 28 participants ranging in ability level and natural foot strike pattern, and found the assumption of linearity to be valid only for forefoot strikers. Rearfoot strikers consistently exhibit a non-linear force-length relationship, with three distinct phases of stance. Therefore, from the findings of this chapter, it appears that the spring mass model may be appropriate for modelling forefoot running, but cannot be for rearfoot running, as rearfoot runners do not adhere to the assumption of linearity.

10.3. *Research Question 2*

Do the commonly used methods for determining stiffness, during running, have a clear mechanical (physics) basis?

Use of the spring mass model, and the assumption of a massless linear spring, introduces the concept of lower limb stiffness. In physics, linear stiffness has a clear definition based on Hooke's law, where the amount the spring is deformed is directly proportional to the applied force. However, in running literature, a range of methods of calculating lower limb stiffness have been used. To address this research question, chapter 5 compared four methods of calculating lower limb stiffness to the most physically consistent definition. The results of the chapter showed significant differences between physically consistent definition and the four methods presented in literature. Furthermore, a regression analysis showed varying relationships between the different methods and the physically consistent method. Therefore, although these other methods are based on physics, the assumptions made when applying them to real world data make them physically inconsistent, and therefore I recommend that an effort should be made by researchers to use the physically

consistent definition when calculating lower limb stiffness in the future. The results of this chapter show that when different methods are used to calculate limb stiffness the results can be very different. Therefore, while these alternative methods are being used in research the results cannot be compared across studies.

10.4. Research Question 3

What level of model complexity is required to accurately describe the kinematics and kinetics of distance running?

This PhD aimed to develop an “appropriately” complex biomechanical model of normal distance running. By embracing the idea of the “simpler the better” and sequentially adding complexity to the spring mass model the aim was to determine the effect of the different layers of complexity would have on the biomechanical characteristics of running. First, the spring mass model was assessed using a cohort of 19 forefoot strikers. The analysis was restricted to forefoot strikers based on the findings of Chapter 4. Comparing the simulated kinematics and kinetics to the experimental data showed that this model consistently overestimated the vertical CoM displacement, underestimated the GRF peaks and also showed that there was insufficient energy for the CoM to rebound fully from mid to late stance. Taken together, these findings suggest that the spring mass model is too simple for accurately modelling the stance phase of running.

The sprung knee (SK) models were then developed. The *SKlinear* model was identical to the spring mass model, except now two rigid segments (representing the thigh and shank) were included. The *SKtorsional* model was a further development on this model by which the linear spring was replaced with a torsional spring at the intersegmental joint, representing the “knee”. Geometry restrictions with these models meant it was not possible to model early or late stance, however there was good kinematic agreement between the SK models and the experimental data during the middle 60 % (approximately) of stance. Considering only the middle portion of stance could be modelled using these SK models, they are deemed too simple for modelling the stance phase of running.

Finally, the sprung knee and ankle (SKA) models were then developed by adding an additional segment to represent the foot and ankle. Three versions of these SKA models

were developed and an initial inspection of the results revealed that the model failed for a number of participants (Table 49, Chapter 9.3, page195); where a solution was deemed a failure if the CoM failed to rebound during late stance (Figure 108). Although the majority of failed solutions occurred once the contact model was introduced, and are likely a result of incorrect contact parameters, the *SKAconstraint* model failed to find a solution for two participants at speed 4. This suggests that at faster speeds, some participants require active generation of energy at the knee and/or ankle, and that the *SKAconstraint* model is too simple to capture the CoM movement. This idea is reinforced when considering the GRFs and joint angles. The *SKAconstraint* model fails to generate enough vertical GRF in midstance, and thus requires increased GRF in late stance (Figure 96), suggesting that some actuation is required and that a purely passive system has its limitations.

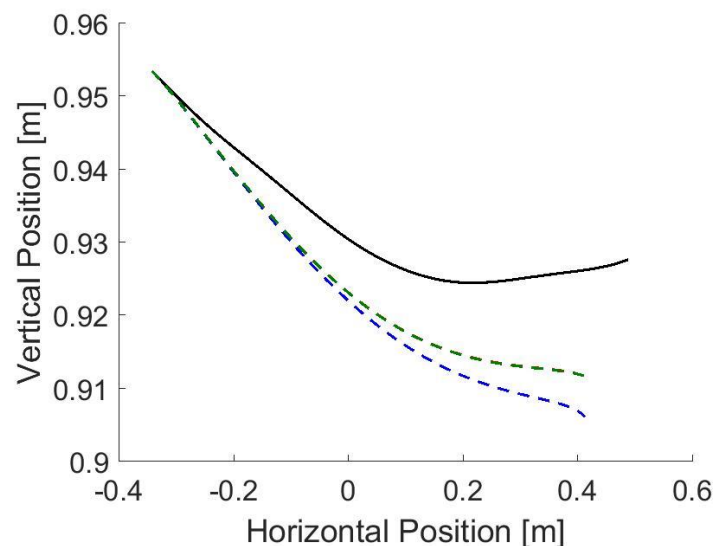


Figure 108 - Failed simulation using the SKA models.

The *SKAconstraint* model was similar to the *SKtorsional* model, but included the additional foot segment and an additional torsional spring at the intersegmental joint, representing the “ankle”. This model showed good kinematic and kinetic agreement with the experimental data, but again due to geometry restrictions it was not possible to model the first and last 5 – 10 % of stance using the same segment lengths. Furthermore, with this model, the fixed contact point meant the CoM was being pulled “down and back” at the

end of the simulation. The *SKAcontact* model was the same as the *SKAconstraint* model, however now the fixed contact point was replaced with a contact model. This contact model consisted of a contact sphere at the distal end of the foot segment that interacted with a contact half space on the ground.

A limitation of OpenSim meant that the *PointConstraint* was ignored by the customised controller code. Therefore, the *SKAcontact* model was developed as a stepping stone to replacing the ankle spring with a custom controlled actuator. Interestingly, the kinematic and kinetic agreement between the experimental data and the *SKAcontact* model was much lower compared to the *SKAconstraint* model. This lower agreement was likely due to incorrect tuning of the contact parameters. However, it is unclear what contact parameters are appropriate for running, and there are no clear guidelines for choosing these parameters. Therefore the contact parameters were built into the optimisation and the best-fit determined for each participant.

In the *SKAactuator* model, the torsional spring at the ankle was replaced with a custom controlled actuator. The control function of the actuator combined a Gaussian function with the spring function from the *SKAcontact* model. The initial conditions and “knee” spring stiffness were set to those from the *SKAcontact* model, and only the coefficients of the Gaussian function optimised. The RMSD values between the experimental data and simulations of *SKAactuator* model were higher for CoM trajectories and there were larger differences in the AP GRF peaks/troughs, compared to simulations of the *SKAconstraint* model. However, the RMSD values between the experimental and simulated joint kinematics and GRF profiles were lower for the *SKAactuator* model, but only slightly compare to the *SKAconstraint* model.

The aim of this chapter was to determine: **What level of model complexity is required to accurately describe the kinematics and kinetics of distance running?** This PhD has shown that the simple spring mass model is insufficient for modelling normal distance running. However, the fact that some of the basic biomechanical characteristics are predicted by this model suggests that, in part at least, there is some spring-like behaviour occurring during running. The close agreement between the kinematics of the SK models and the experimental data suggests that a passive torsional spring at the knee is sufficient for modelling midstance of forefoot running. This further suggests that during this phase the knee joint, and thus the net effect of the muscles crossing the knee joint, acts to

function similar to a passive torsional spring controlling the amount of knee flexion in response to the forces applied during loading.

The close kinematic agreement between the *SKAconstraint* model and the experimental data suggests that a passive system, with two torsional springs at the knee and ankle, is sufficient for modelling the first 90 % (approximately) of stance. Due to the geometry restrictions in the way the foot segment was defined, discussed earlier (Chapter 9.2.1), the last 10 % of stance cannot be modelled here. Furthermore, the lower agreement between the experimental and simulated CoM trajectories for the *SKAactuator* model compared to the *SKAconstraint* model suggests that forefoot strikers efficiently utilise the elastic properties of the musculoskeletal system, and particularly of the knee extensors and ankle plantarflexors, and hence forefoot running can be modelled using a passive system. It is likely that correct tuning of the contact parameters, or development of the contact model, is required before the model can be used to investigate rearfoot runners. Possible avenues of future research will be discussed in more detail below.

10.5. General Limitations

There are a number of limitations associated with this PhD. Firstly the data used for these investigations were originally collected for a study comparing the biomechanical characteristics of elite and recreational runners. Distinct differences between the biomechanics of forefoot and rearfoot strikers have been reported in literature (Dicharry 2010, Lieberman et al. 2010, Williams et al. 2012, Almeida et al. 2015, Thompson et al. 2015, Kuhman et al. 2016, Gruber et al. 2017), therefore for this PhD participants were classified based on their foot strike index. However, there appears to be an inter-relationship between foot strike pattern and athlete ability. A forefoot strike pattern is more common among elite runners while recreational runners tend to exhibit a rearfoot strike pattern. Considering this, it is possible that athlete ability could influence the linearity of the force-length curve. However, an impact transient in the vertical GRF profile is a fundamental biomechanical characteristic of rearfoot running (Dicharry 2010, Lieberman et al. 2010, Almeida et al. 2015, Thompson et al. 2015, Gruber et al. 2017), and the results of chapter 4 suggest that this impact peak is the primary contributor to the non-linearity in the force-length curves of rearfoot runners. Therefore, if a cohort of rearfoot and forefoot

runners of equal ability were used for this investigation the results would likely be the same.

A limitation of the models presented here is that they are all 2D (sagittal plane only). However, during running the majority of joint movement occurs in the sagittal plane, therefore subtleties in joint rotations (which would be ignored by these models) are unlikely to have a significant effect on such simple models. Furthermore, the hip joint function was not modelled here, and it has been shown that the hip functions primarily as a motor (energy producer) during running (Farris et al. 2017, Qiao et al. 2017). It is possible that modelling the hip as a motor would affect the mechanical function of the more distal joints, and thus, since the lower limb is a linked chain change the outcome of the model and the simulated biomechanics of the participant. However, a choice had to be made as to which layers of complexity should be introduced to the spring mass model first; and it seemed reasonable to first introduce a knee joint as it has the largest range of motion during running. The resulting agreement between the SK model simulations and experimental data, for the middle 60 % of stance, suggest this was the right choice to make. Furthermore, the results of these SK models then suggested that the ankle should be introduced next as it would address the issues of not being able to model early and late stance. Therefore, the effects of an actuated hip joint would be a future step in the development of these models.

A limitation associated with the *SKAcontact* and *SKAactuator* models is the choice of contact model. Accurately modelling the foot-ground interaction during locomotion is difficult (Naemi et al. 2013, Uchida et al. 2015, Jackson et al. 2016). Various models have been presented in literature, ranging from a rolling constraint (Hamner et al. 2013) to a series of viscoelastic spheres (Gilchrist et al. 1996, Cenk Güler et al. 1998, Naemi et al. 2013). However how to choose the properties of these spheres remains unclear. Furthermore, the choice of these properties is likely subject-specific and potentially influenced by their choice of shoes. For this PhD, a contact model had to be introduced as the *PointConstraint* was ignored by OpenSim when ankle spring was replaced with a customised controlled actuator. Therefore, to explore how actuation at the ankle would affect the ability of the model, a contact model had to be developed. Efforts were made to tune the parameters of the contact model, however for a number of participants (Table 49), successful solutions could not be found. Therefore, correctly modelling the foot-ground

interaction during running is an essential next step in modelling if the biomechanics of running are to be accurately reproduced.

10.6. A note on OpenSim

OpenSim is open source musculoskeletal modelling software that has gained considerable popularity in biomechanics over the last few years. It is generally used to do complex musculoskeletal modelling, incorporating multiple segments, joints, and musculotendinous units. This software is rarely used to investigate simple mechanical systems, however a preliminary investigation showed it produced nearly identical results to equations of motion derived using Lagrangian mechanics, implemented in MATLAB (see appendix AI). The rationale behind using OpenSim instead of manually deriving equations of motion was twofold: firstly, it would minimise the potential for human error in deriving equations of motion as the models got more complex, and, in theory, save time. Secondly, it would provide a means of sequentially adding complexity to a model, bridging the gap between the simple and complex, within the same software, eliminating discrepancies due to implementation. However, although OpenSim generally allows modelling which would be laborious otherwise, it is somewhat restrictive in how models can be set up and simulated. In addition, there have been times throughout this PhD where I have found it is just not possible to do certain things in OpenSim (for example adding an actuator to the *SKAconstraint* model). As OpenSim relies on user contribution it is likely that it will improve and become more adaptable overtime. In addition, after attending an OpenSim workshop at TGCS 2017 where the new release (OpenSim 4.0) was demonstrated, it already appears more users friendly and functionality with MATLAB has been expanded and improved. Therefore, although it may not be as simple as originally expected, I think it is worthwhile using OpenSim for developing these kinds of models.

10.7. Future Work

This PhD has outlined the strengths and weakness of existing models of running. Throughout the PhD the limitations of the different models have also been discussed. From these some possible avenues of future research will now be discussed.

The next phase of modelling should concentrate of the foot-ground interaction. This could take a number of avenues. Firstly, developing a more robust optimisation method for determining the appropriate contact parameters of a single viscoelastic sphere could potentially increase the agreement between the *SKAconstraint* and *SKAcontact* models. However, a single contact point is an oversimplification of the foot-ground interaction during running. Therefore it might be more appropriate to develop a deformable foot segment, with viscoelastic spheres placed at significant points on the bottom of the foot. For example a two segment foot, with a pin joint in line with the ball of the foot, and viscoelastic spheres at the heel, the ball of the foot and the toes. Such a model could also allow modelling of rearfoot strikers, as the heel could make initial contact with the ground then, as the CoP travels distally the foot could bend at the pin joint and push off using the toes.

An alternative next layer of complexity would be to extend the CoM and model a functional hip joint. In walking the hip has been shown to be important in controlling trunk motion (McGrath et al. 2015), it is possible it has a similar function in running. However, it has also been suggested that the hip acts primarily as a motor (energy producer) during running (Farris et al. 2017, Qiao et al. 2017). Therefore it is possible that including a functional hip joint might influence the mechanical function of the more distal joints and thus provide a closer kinematic match between the simulated and experimental CoM trajectories; while maintaining the closer agreement in the joint kinematics seen with the *SKAactuator* model.

Finally, it would be interesting to see how well this passive three-segment model (*SKAconstraint*) does at modelling sprinting. Sprinters tend to land with their forefoot, and the CoP likely has a smaller range of motion than in normal distance running. Therefore it is possible that these simple models, with fixed contact points, might be sufficient for modelling sprinting. However, during sprinting athletes tended to have a greater forward lean, thus it is possible an extended CoM and hip joint would be needed to appropriately

model sprinting. In addition, during sprinting the majority of the event is spent either accelerating or decelerating, therefore the GRFs would be asymmetrical and it would be interesting to see how well the passive joints of the *SKAconstraint* model deal with this biomechanical characteristic.

10.8. Conclusions

- The assumption of a linear-force length relationship is not appropriate for rearfoot running, and thus use of the spring mass model should be restricted to investigating forefoot runners. Furthermore, authors should be clear about the foot strike patterns adopted by the participants included in modelling investigations.
- There are significant differences in lower limb stiffness calculated using the methods presented in literature compared to the most physically consistent definition. Therefore authors should aim to use the physically consistent definition when calculating lower limb stiffness so results can be compared across studies.
- The spring mass model is too simple, and thus insufficient for modelling even forefoot running.
- The sprung knee (SK) models are sufficient for modelling the middle portion of stance, but geometry restrictions mean they cannot be used to model early or late stance.
- The sprung knee and ankle (SKA) models show a passive three-segment model is sufficient for modelling CoM movement during forefoot running.
- A better match with experimental kinetics and joint trajectories can likely be achieved by including additional actuation, but technical problems in modelling this within OpenSim have prevented this from being fully confirmed.

Appendices

AI. *OpenSim Validation*

Introduction

OpenSim is open-source musculoskeletal modelling software that lets users to develop models and generate dynamic simulations of musculoskeletal systems and their movements (Delp et al. 2007). Generally, OpenSim is used to develop complex models incorporating multiple muscles; however the spring mass model is a simple mechanical system incorporating a single linear spring. Therefore, to gauge the appropriateness of using OpenSim for such a simple mechanical system, solutions from OpenSim were compared to solutions from equations of motion derived using Lagrangian mechanics, implemented in MATLAB.

MATLAB implementation

Equations of motion for simple systems are often determined using Newton's laws of motions. However, the maths gets considerably more complicated as the system is made more complex. Therefore, when considering multi-link systems it can often be more appropriate to use Lagrange Mechanics to determine the relevant equations of motion. Lagrange Mechanics is essentially a more general form of Newton's Second Law, but instead of accelerations, mechanical energies are used to describe the system. The linear form of Lagrange's equation of motion is:

$$\frac{d}{dt} \frac{\partial KE}{\partial V_i} - \frac{\partial KE}{\partial Y_i} + \frac{\partial PE}{\partial Y_i} = F_i \quad 29$$

where KE and PE are the total kinetic and potential energies of the system, V_i and Y_i are the velocity and position for the i^{th} component of the system (in the y (vertical) direction), and F_i is the external force acting on the i^{th} component. On the other hand, the angular form of Lagrange's equation of motion is:

$$\frac{d}{dt} \frac{\partial KE}{\partial \omega_i} - \frac{\partial KE}{\partial \theta_i} + \frac{\partial PE}{\partial \theta_i} = M_i \quad 30$$

where ω and θ are the angular velocity and position, and M_i is the moment (D. Gordon E. Robertson et al. 2013). Therefore, the resulting equations of motion for the simple spring mass model being implemented in MATLAB were then:

$$T = \text{kinetic energy} = \frac{1}{2}mv^2 = \frac{1}{2}m(l^2\dot{\theta}^2 + \dot{l}^2) \quad 31$$

$$V = \text{potential energy} = mgh + \frac{1}{2}k\Delta l^2 = mgl\sin\theta + \frac{1}{2}k(l - l_0)^2 \quad 32$$

$$L = \text{lagrangian} = \frac{1}{2}m(l^2\dot{\theta}^2 + \dot{l}^2) - mgl\sin\theta - \frac{1}{2}k(l - l_0)^2 \quad 33$$

$$\ddot{l} = l\dot{\theta}^2 - g\sin\theta - \omega^2(l - l_0); \quad \omega = \sqrt{\frac{k}{m}} \quad 34$$

$$\ddot{\theta} = \frac{-g\cos\theta - 2l\dot{\theta}}{l} \quad 35$$

Model simulation

The initial conditions for the MATLAB implementation were taken from the best-fitting OpenSim solutions (Chapter 7). The above equations of motion were then integrated forward in time using the built-in MATLAB ode45 solver. This solver integrates the differential equations over a defined timespan using designated initial conditions. As the experimental data is in Cartesian coordinates, but these equations of motion are determined in polar coordinates, the initial conditions first had to be transformed into polar coordinates. The integrator time-step was also set to 1e-3 s. Finally, the ground reaction forces (GRFs) were calculated using Hooke's Law, i.e. using the spring stiffness and the change in spring length (Table 67). This spring force was then resolved into the horizontal and vertical components based on the angle.

Table 67 - Equations for calculating the GRFs

$$F_{spring} = k * \Delta l$$

$$GRF_x = F_{spring} \cos(\theta)$$

$$GRF_z = F_{spring} \sin(\theta)$$

Comparing solutions and statistics

The solutions from OpenSim and MATLAB were compared to each other using a root mean square difference (RMSD) between the CoM trajectories and the GRFs.

Additionally, the percentage difference in the contact time, peak CoM displacement, and the peak amplitude of the GRFs were also computed and compared between MATLAB and OpenSim, calculated as the follows:

$$\left(\frac{\text{OpenSim value} - \text{MATLAB value}}{\text{OpenSim value}} \right) * 100 \quad 36$$

Statistically the experimental and simulated CoM and GRF waveforms were compared using a correlation coefficient (Gutierrez-Farewik et al. 2006). A correlation was considered strong if r great than 0.7, moderate if r was greater than 0.5 and weak if r was greater than 0.3.

Results

The RMSD between the OpenSim and MATLAB CoM trajectories and GRFs profiles show that the two solutions were nearly identical (Table 68, Figure 109 - Figure 111). Correlation analysis also showed the OpenSim and MATLAB CoM trajectories and the GRF profiles were highly and significantly correlated ($r > 0.999$; $p < 0.001$).

Table 68 - Mean and standard deviation RMSD between simulated and experimental CoM trajectories [m] and GRF profiles [BW] for n=11, 12, 13 and 19 participants at speeds 1 to 4, respectively.

	CoMx	CoMy	GRFx	GRFy
Speed 1	0.002 (<0.001)	0.000 (<0.001)	0.004 (0.001)	0.013 (0.001)
Speed 2	0.002 (<0.001)	0.000 (<0.001)	0.005 (0.001)	0.014 (0.002)
Speed 3	0.002 (<0.001)	0.000 (<0.001)	0.006 (0.001)	0.016 (0.002)
Speed 4	0.003 (<0.001)	0.000 (<0.001)	0.006 (0.001)	0.016 (0.002)

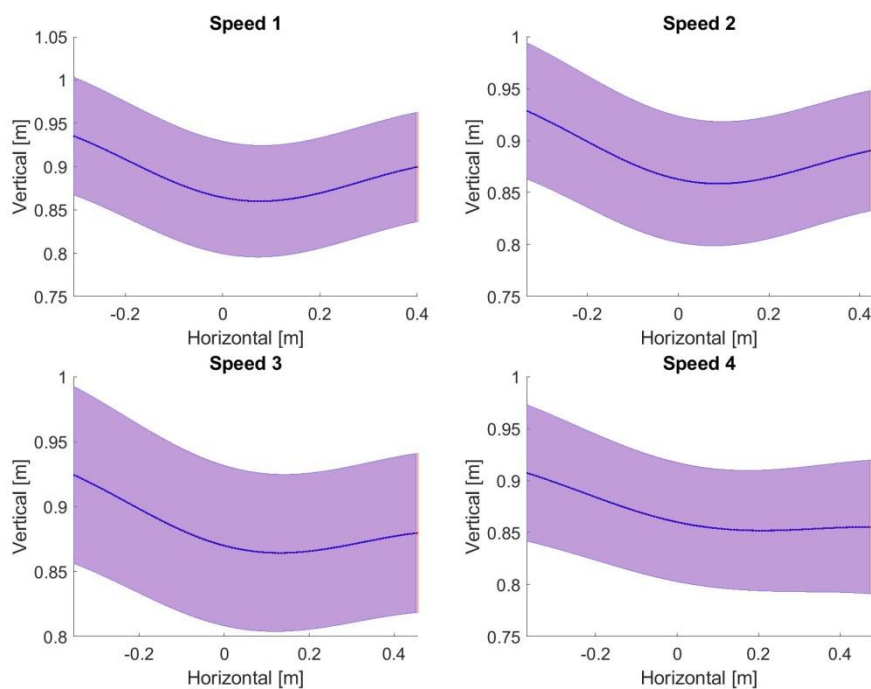


Figure 109 – Comparison of ensemble averages (n = 11, 12, 13 and 19) of the OpenSim (red) and MATLAB (blue) CoM trajectories at speeds 1-4 [3.3, 3.9, 4.8, 5.6 m/s], respectively.

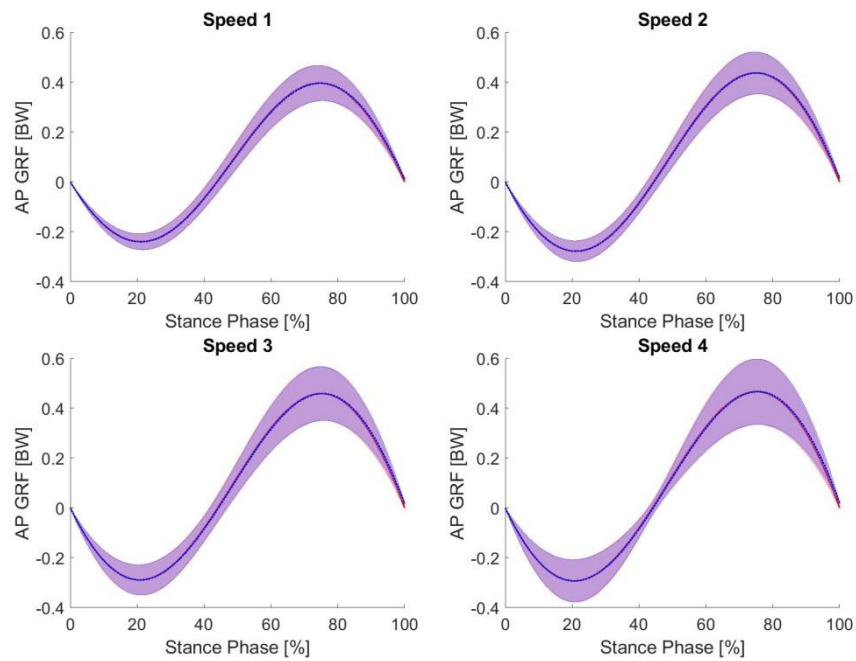


Figure 110 – Comparison of ensemble averages (n = 11, 12, 13 and 19) of the OpenSim (red) and MATLAB (blue) AP GRFs at speeds 1-4 [3.3, 3.9, 4.8, 5.6 m/s], respectively.

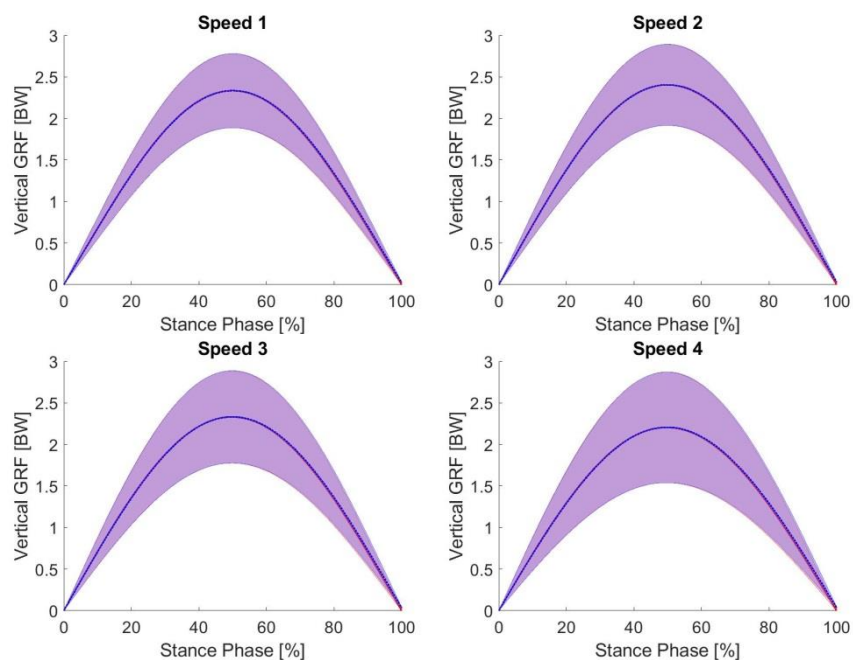


Figure 111 – Comparison of ensemble averages (n = 11, 12, 13 and 19) of the OpenSim (red) and MATLAB (blue) vertical GRFs at speeds 1-4 [3.3, 3.9, 4.8, 5.6 m/s], respectively.

Table 69 - Comparison of the mean (SD) GRF trough/peaks from the OpenSim and MATLAB solutions.

		OpenSim	MATLAB	Percentage Difference
AP GRF (trough) [BW]	Speed 1	0.247 (0.057)	0.247 (0.057)	-0.079 (0.014)
	Speed 2	0.285 (0.058)	0.285 (0.058)	-0.076 (0.023)
	Speed 3	0.292 (0.068)	0.292 (0.068)	-0.038 (0.029)
	Speed 4	0.286 (0.055)	0.286 (0.055)	-0.004 (0.019)
AP GRF (peak) [BW]	Speed 1	0.400 (0.045)	0.400 (0.045)	0.060 (0.020)
	Speed 2	0.439 (0.042)	0.438 (0.042)	0.061 (0.018)
	Speed 3	0.454 (0.058)	0.454 (0.058)	0.009 (0.023)
	Speed 4	0.454 (0.073)	0.454 (0.073)	-0.020 (0.023)
Vert. GRF (peak) [BW]	Speed 1	2.339 (0.178)	2.339 (0.178)	-0.015 (0.004)
	Speed 2	2.407 (0.258)	2.408 (0.258)	-0.027 (0.019)
	Speed 3	2.304 (0.323)	2.306 (0.323)	-0.072 (0.038)
	Speed 4	2.137 (0.381)	2.140 (0.381)	-0.107 (0.061)

The maximum vertical CoM displacement and contact time appear identical between the MATLAB and OpenSim solutions (Table 70). The percentage difference ranged from -0.02 (0.00) to 0.62 (0.30) % indicating close agreement between the two solutions. Furthermore, mean (SD) peaks and troughs of the AP GRF appear identical (Table 69) with the percentage difference ranging between -0.08 (0.01) to 0.06 (0.03) %. Slight difference exist in the vertical GRFs (Table 69) with the percentage difference ranging between -0.11 (0.00) to -0.02 (0.06) %. However, these differences are small and are likely due to slight differences in the integration time steps causing rounding errors towards the end of the simulation.

Table 70 - Comparison of the mean (SD) maximum vertical CoM displacements and contact times from the OpenSim and MATLAB solutions.

		OpenSim	MATLAB	Percentage Difference
Vertical CoM displacement [m]	Speed 1	0.076 (0.012)	0.076 (0.012)	-0.022 (0.004)
	Speed 2	0.070 (0.013)	0.070 (0.013)	-0.016 (0.007)
	Speed 3	0.062 (0.012)	0.062 (0.012)	0.070 (0.235)
	Speed 4	0.059 (0.012)	0.059 (0.012)	0.171 (0.297)
Contact time [s]	Speed 1	0.230 (0.014)	0.229 (0.014)	0.436 (0.026)
	Speed 2	0.209 (0.015)	0.208 (0.015)	0.482 (0.035)
	Speed 3	0.182 (0.013)	0.181 (0.013)	0.553 (0.041)
	Speed 4	0.163 (0.013)	0.162 (0.013)	0.617 (0.053)

Discussion

This investigation aimed to validate the use of OpenSim for modelling a simple mechanical system, the spring mass model. The OpenSim simulations of the spring mass model were compared to manually derived equations of motion implemented in MATLAB, at a range of speeds. Comparing the CoM trajectories, GRF profiles, maximum vertical CoM displacements and troughs/peaks of the AP and vertical GRFs show that the OpenSim and MATLAB solutions are essentially identical. Slight differences exist in the vertical GRF peaks, however it is likely these differences are due to round errors in the integration (the OpenSim *ForwardTool* use a variable integrator (Chapter 6) while MATLAB had a fixed time-step). Furthermore, the GRFs in MATLAB were calculated manually while the OpenSim GRFs were determined using a built-in OpenSim *ForceReporter* which again could have introduced rounding errors. Despite these very slight differences, the similarity between the MATLAB and OpenSim solutions suggest OpenSim can confidently be used for modelling simple mechanical systems.

AII. Extra Figures

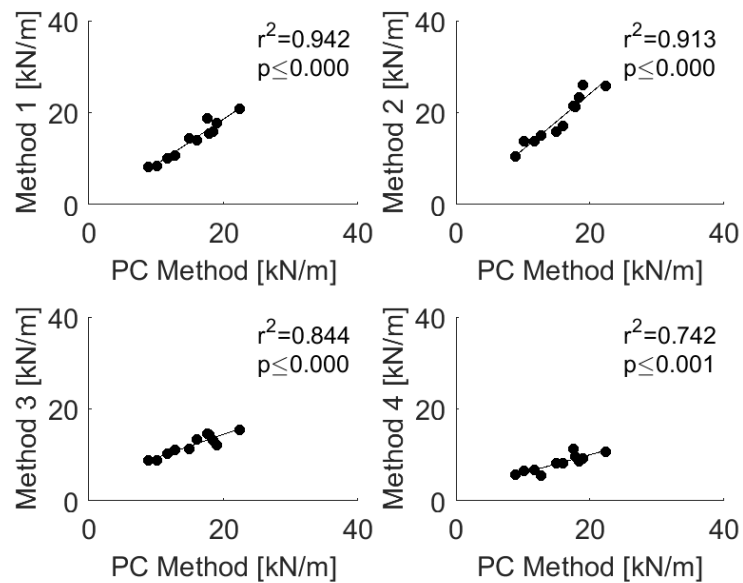


Figure 112 - Relationships between the PC method and the other methods of calculating lower limb stiffness at speed 1 (3.3 m/s)

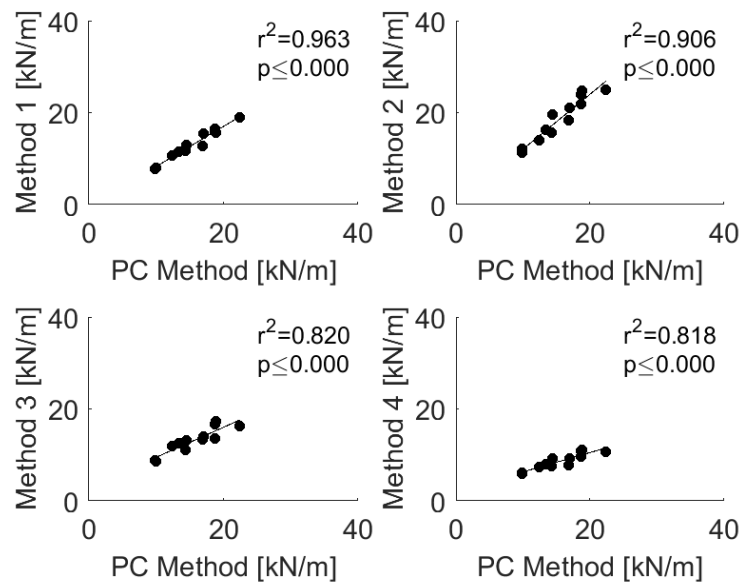


Figure 113 - Relationships between the PC method and the other methods of calculating lower limb stiffness at speed 2 (3.9 m/s)

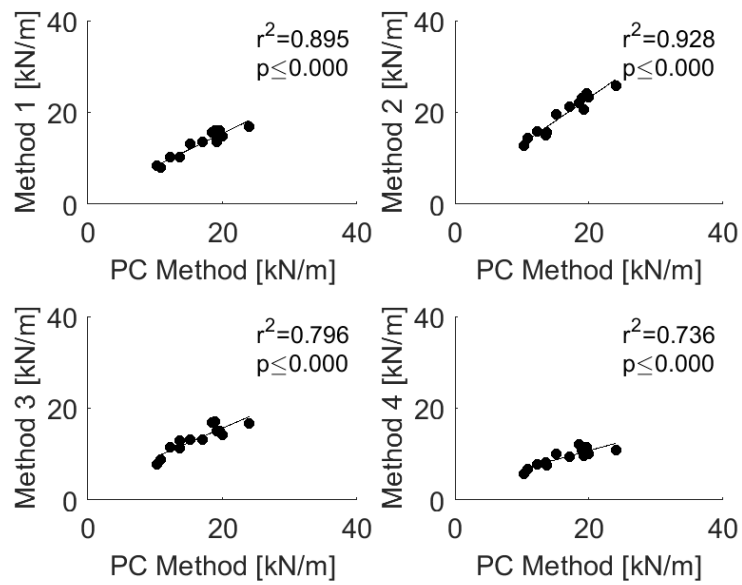


Figure 114 - Relationships between the PC method and the other methods of calculating lower limb stiffness at speed 3 (4.8 m/s)

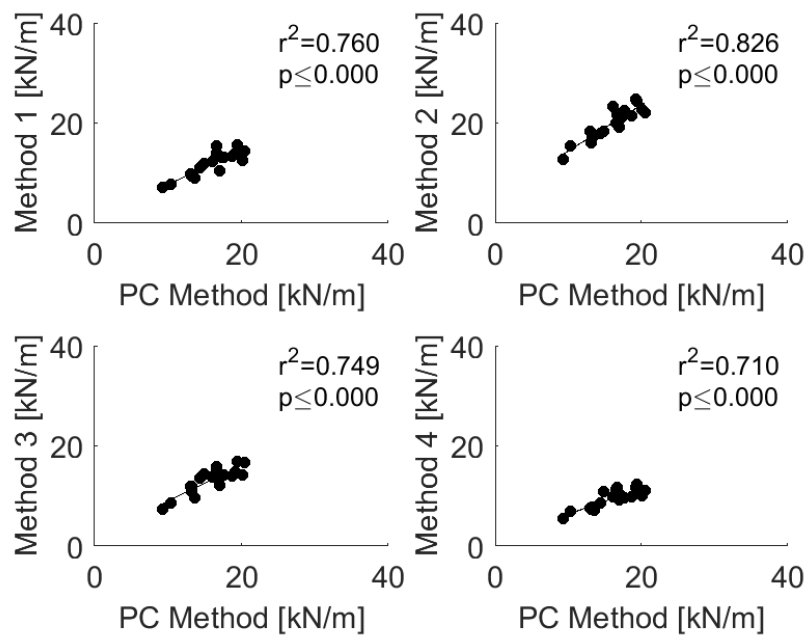


Figure 115 - Relationships between the PC method and the other methods of calculating lower limb stiffness at speed 4 (5.6 m/s)

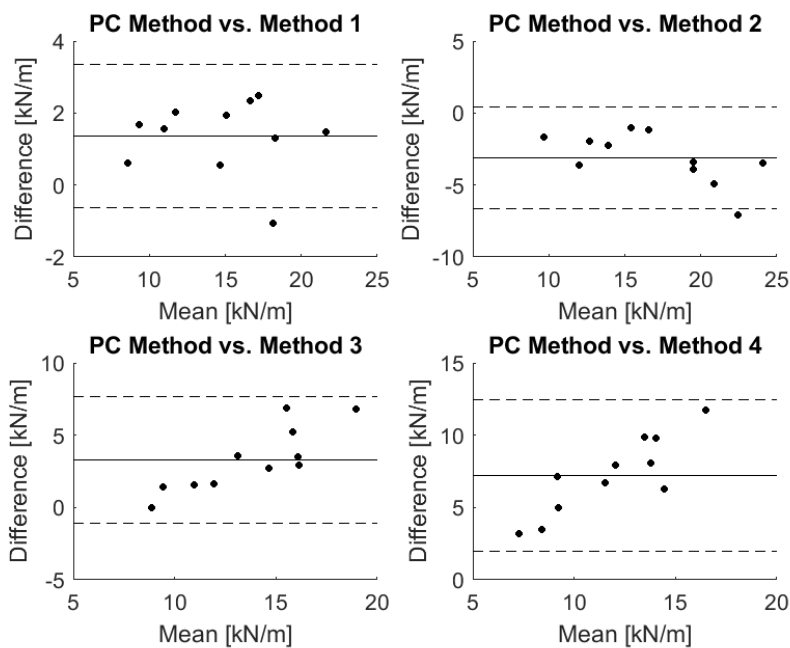


Figure 116 – Bland-Altman analysis comparing the PC method and the other methods of calculating lower limb stiffness at speed 1(3.3 m/s)

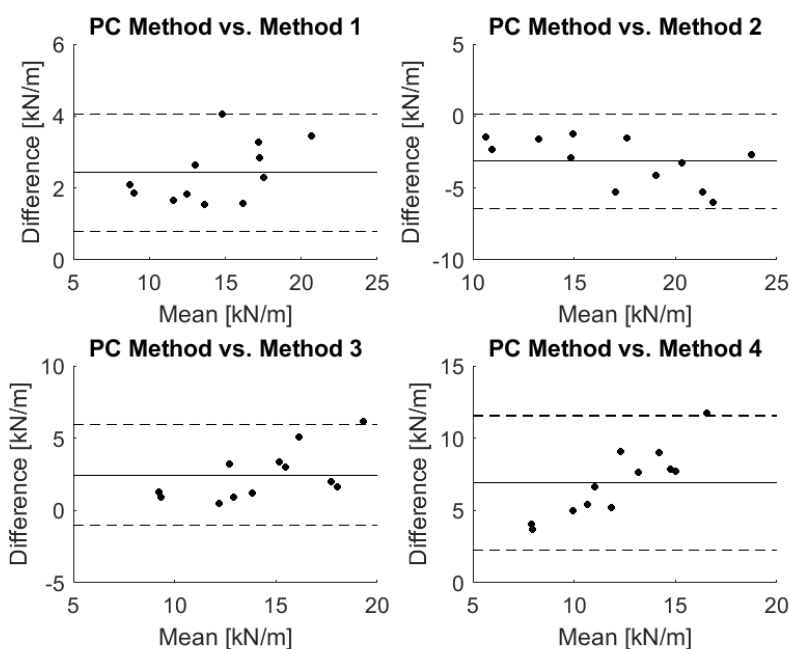


Figure 117 – Bland-Altman analysis comparing the PC method and the other methods of calculating lower limb stiffness at speed 2 (3.9 m/s)

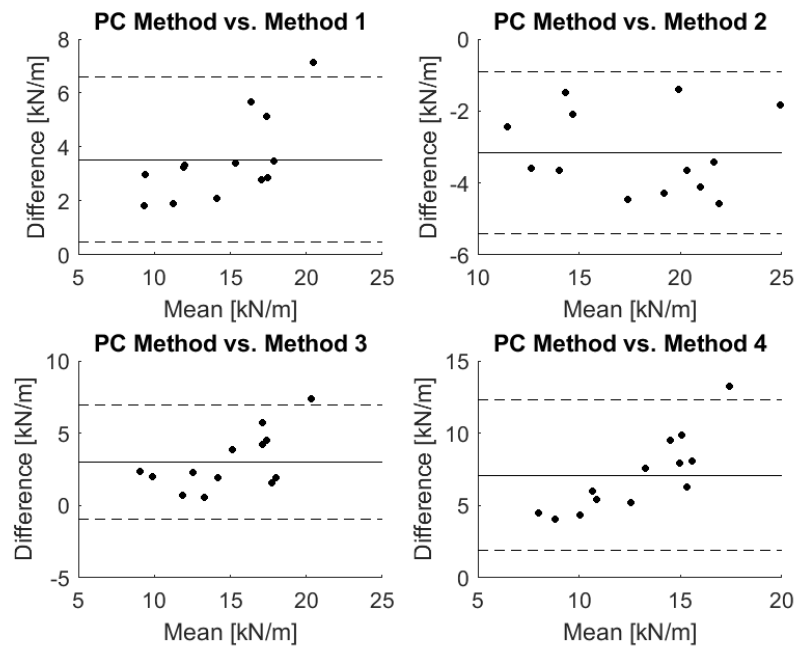


Figure 118 – Bland-Altman analysis comparing the PC method and the other methods of calculating lower limb stiffness at speed 3 (4.8 m/s)

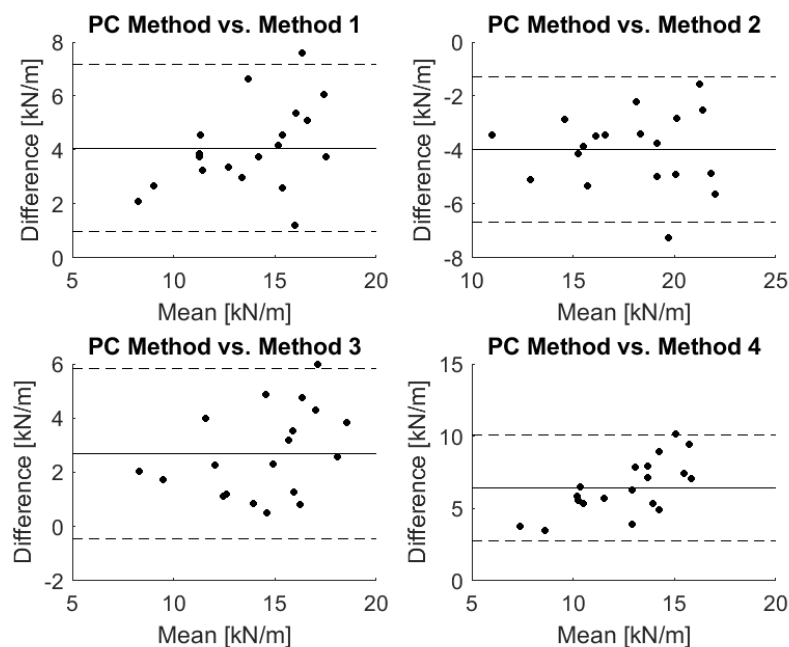
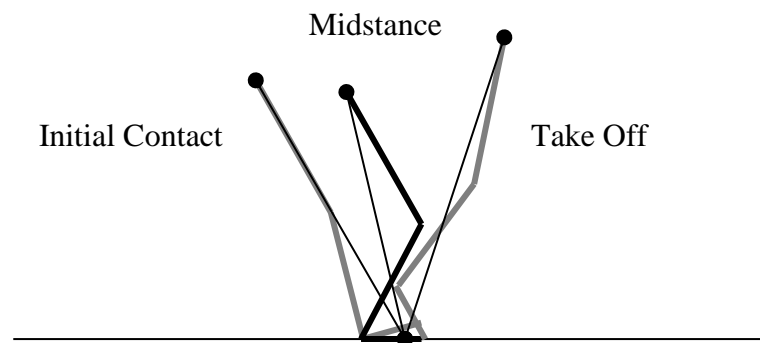


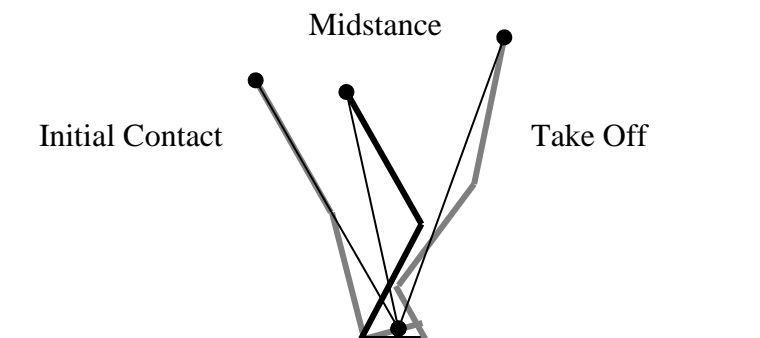
Figure 119 – Bland-Altman analysis comparing the PC method and the other methods of calculating lower limb stiffness at speed 4 (5.6 m/s)

AIII. Different lower limb length definitions in rearfoot strikers

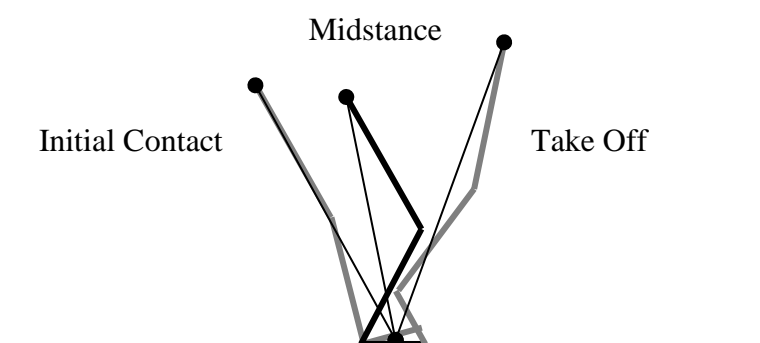
1. Hip to ball of foot at midstance



2. Hip to ball of foot at initial contact



3. Hip to average CoP



AIV. Are The Arms and Head Required To Accurately Estimate Centre Of Mass Motion During Running?

Niamh Gill, Stephen J. Preece, Samantha Young, Christopher Bramah, *Are the arms and head required to accurately estimate centre of mass motion during running?*, *Gait & Posture*, Volume 51, January 2017, Pages 281-283, ISSN 0966-6362, <http://dx.doi.org/10.1016/j.gaitpost.2016.11.001>.

(<http://www.sciencedirect.com/science/article/pii/S0966636216306270>)

Abstract

Accurate measurement of centre of mass (CoM) motion can provide valuable insight into the biomechanics of human running. However, full-body kinematic measurement protocols can be time consuming and difficult to implement. Therefore, this study was performed to understand whether CoM motion during running could be estimated from a model incorporating only lower extremity, pelvic and trunk segments. Full-body kinematic data was collected whilst (n=12) participants ran on a treadmill at two speeds (3.1 and 3.9 m/s). CoM trajectories from a full-body model (16-segments) were compared to those estimated from a reduced model (excluding the head and arms). The data showed that, provided an offset was included, it was possible to accurately estimate CoM trajectory in both the anterior-posterior and vertical direction, with root mean square errors of 5mm in both directions and close matches in waveform similarity ($r=0.975-1.000$). However, in the ML direction, there was a considerable difference in the CoM trajectories of the two models ($r=0.774-0.767$). This finding suggests that a full-body model is required if CoM motions are to be measured in the ML direction. The mismatch between the reduced and full-body model highlights the important contribution of the arms to CoM motion in the ML direction. We suggest that this control strategy, of using the arms rather than the heavier trunk segments to generate CoM motion, may lead to less variability in CoM motion in the ML direction and subsequently less variability in step width during human running.

Keywords: Centre of Mass; Running; Full-Body Gait; Arm Motion

Introduction

Precise measurement of centre of mass (CoM) motion is essential for understanding different aspects of running gait, such as energy fluctuations (Lee et al. 1998) and gait asymmetry (Lee et al. 2010). CoM motion is typically calculated either from a weighted sum of individual segment centroids, or by using a simplified model that assumes CoM motion can be derived using a reduced set of markers (Gullstrand et al. 2009, Halvorsen et al. 2009). However, these simplified models have been associated with errors of up to 1-2 cm (Gullstrand et al. 2009, Halvorsen et al. 2009) and therefore may not be appropriate for running-related research. However, it is common practice to collect data from only the pelvis and lower limbs during running (Franz et al. 2009, Smith et al. 2015). With this set up, it would be relatively straightforward to add a trunk segment to this model. Depending on the precise contribution of the arms to CoM motion, such a model may prove an accurate method of estimating CoM during running, and therefore be of considerable practical benefit.

To date, there has been limited study of the biomechanical function of the arms during human running. Although it is accepted that the arms acts to counteract the angular momentum generated by the lower limbs, about the vertical axis (Hamner et al. 2010), the contribution of the arms and head to linear CoM motion, in each plane, is not clear. Such insight may improve our understanding of the biomechanical mechanisms that facilitate mediolateral CoM motion during running. Given this limitation in the current knowledge and the potential practical benefit identified above, we carried out a study to determine the effect of excluding the arms and head on CoM trajectory during human running.

Methods

Twelve participants (age 41(8)years, height 1.75(0.10)m and body mass 73(13)kg), familiar with treadmill-running, participated in this investigation. Informed consent was obtained and ethical approval provided by the Local Ethics Committee. Full body (upper limbs, head, thoracic and lumbar spine, pelvis, and lower limbs) kinematic data were collected for each participant whilst running on a treadmill at two speeds (3.1 and 3.9 m/s), representative of average recreational running speeds (Cavanagh et al. 1989).

Twelve Qualisys Oqus 3D cameras (240Hz) were used for kinematic data collection. Lower limb, pelvis and trunk segments were modelled and tracked using the approach described in Preece et al. (2016). In addition, markers were placed on the acromion processes, lateral shoulders, medial and lateral epicondyles of the humeri, styloid processes of the ulnae and radii, as well as on the 2nd and 5th metacarpal heads. Head markers were placed bilaterally in anterior and posterior positions. Data from Dempster (1955) were used to define segment masses and inertial properties were then calculated from marker positions, assuming the head to be an ellipsoid, the upper arms and forearms to be frusta of cones, and the hands to be spheres.

To understand the effect of excluding the arms and head on CoM motion, two models were defined. The reduced model consisted of nine segments: the feet, shanks, thighs, pelvis, and lumbar and thoracic spine. The full-body model comprised of 16 segments, those in the reduced model, as well as the upper arms, forearms, hands and head. Data processing methods as outlined in Preece et al. (2016) were used, in which raw marker data were first low pass filtered (10Hz). A kinematic approach (2010) was then used to define gait events for 10 consecutive gait cycles and CoM trajectories calculated using the Visual3D software. With this approach the CoM for each model was obtained for each subject at both running speeds.

Including the head and arms may result in a systematic shift in CoM trajectory in the AP (anterior-posterior) and vertical directions. Therefore, a correction factor was determined, in both planes, and expressed as a percentage of participant height. The difference between the reduced and full model, with/without correction, was then characterised using a number of statistics. Firstly, root mean square error (RMSE) was calculated for both position and velocity from individual ensemble average data and then averaged across all participants. RMSE in the range of movement (RoM) over the 10 gait cycles was also calculated and averaged across participants. Finally, a correlation coefficient was used to compare curve similarity (Gutierrez-Farewik et al. 2006) between ensemble average trajectories which was also averaged across participants.

Results

There was minimal variation in the vertical and AP correction factors with speed. Therefore a consistent 0.3% correction was applied to all AP data, which lead to a mean

RMSE of 5mm in position and mean RMSE of 2mm in RoM (Table 71). In this plane, there was a close match in waveform similarity between the two models (Figure 120) with mean correlations of $r=0.975-0.978$ (Table 71). However, in the ML direction, there was less similarity in CoM trajectories (Figure 120) resulting in lower correlation coefficients (Table 71). In this plane, the reduced model appeared to underestimate the full-body RoM and although the RMSE in position/RoM was only 3/4mm (Table 71), this was comparable with the overall RoM of approximately 10mm (Figure 120).

In the vertical direction, a correction of 4.5% was applied to the data from both speeds. With this correction, there was a very close match in the CoM trajectory of the two models (Figure 120), with correlation coefficients of 0.999-1.000 (Table 71). Moreover, the mean RMSE for position was only 5-6mm with a similar error in the RoM estimation (Table 71).

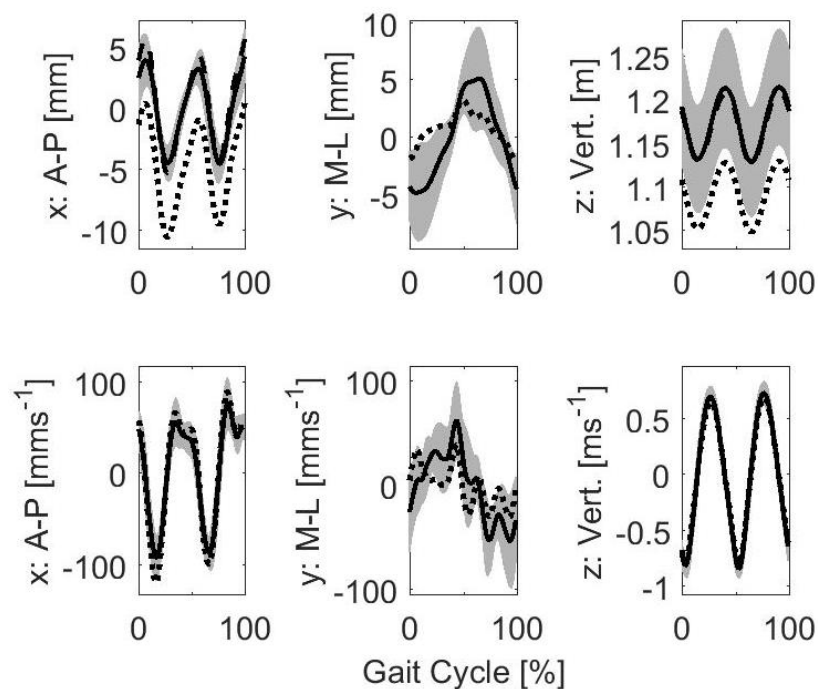


Figure 120 - Ensemble averages of CoM position (top) and velocity (bottom) from the reduced model (dotted), reduced model including offset (dashed) and full-body model (solid) at speed 1. The grey outline represents the standard deviation of the full-body model, and therefore the variability in CoM motion across participants not the difference between the two models. Positive x represents forward movement, while positive y represents motion towards the contralateral side. Note, data is plotted from right initial contact (RIC) to the following RIC and for plotting purposes the CoM position data (AP and ML) were referenced to mean position of the full-body model.

Table 71 - Root mean square error (mean (SD)) between the full-body and reduced model for the CoM position, velocity and the RoM, as well as the correlation coefficient (mean (SD)) indicating waveform similarity between the full-body and reduced model. * indicates correlation was significant ($p < 0.005$) for all participants.

Anatomical Plane	Speed	Position [mm]	RMSE		Correlation Coefficient
			Velocity [mm/s]	RoM [mm]	
AP	1	6 (5)	19 (5)	2 (1)	0.975 (0.016) *
	2	6 (5)	22 (7)	3 (1)	0.978 (0.013) *
AP – incl. 0.3 % offset	1	5 (3)	19 (5)	2 (1)	0.975 (0.016) *
	2	5 (2)	22 (7)	3 (1)	0.978 (0.013) *
ML	1	3 (1)	27 (6)	4 (2)	0.774 (0.218)
	2	3 (1)	30 (8)	4 (3)	0.767 (0.223) *
Vert.	1	84 (6)	38 (11)	6 (1)	1.000 (<0.001) *
	2	83 (7)	42 (13)	6 (2)	0.999 (<0.001) *
Vert. – incl. 5 % offset	1	6 (3)	38 (11)	6 (1)	1.000 (<0.001) *
	2	5 (2)	42 (13)	6 (2)	0.999 (<0.001) *

Discussion

This study sought to establish the possibility of estimating both CoM position and velocity, at two running speeds, from a model incorporating only lower extremity and trunk segments. The data showed a good match in waveform similarity between the reduced and

full-body model in both the AP and vertical directions but not in the ML direction. If the RMSE in the CoM position is compared with the corresponding RoM during over ground running (Preece et al. 2016), it appears small in the AP (0.2%) and vertical (7%) directions, but substantial in the ML (40%) direction. Thus, it would appear that the reduced model may only be appropriate for estimating AP and vertical CoM trajectory and velocity and that a full-body model would be required for estimating ML motions.

The mismatch between the full-body and reduced model, at both running speeds, provides insight into the relative contribution of the arms to CoM motion in the ML direction. Previous research has shown that humans will adopt a small, but non-zero, step width during unconstrained treadmill running, typically about 2-4cm (Meardon et al. 2012, Voloshina et al. 2015). Running with a non-zero step width will require a displacement between the CoM and the stance foot in order to generate the moment, about the base of support, required to transition onto the contralateral foot. Figure 120 illustrates this idea, showing that the CoM moves away from the stance foot from late stance until contralateral foot contact. Interestingly, this pattern is not evident in the reduced model (Figure 120). It would therefore appear that the ML motion of the CoM is primarily generated by the motion of the arms and is not the result of motion of the heavier trunk segments. Given the small ML RoM of the CoM and the more challenging task of achieving these small changes with the heavier trunk segments, this strategy may lead to less variability in ML CoM motions. This idea is consistent with previous research which has suggested that the arms may function to minimise step width variability (Arellano et al. 2011) and so minimise the energetic cost of running. However, further research is required to fully confirm this idea.

Conflict of Interest

Conflict of interest: none

References

[1] Lee CR, Farley CT. Determinants of the center of mass trajectory in human walking and running. *Journal of Experimental Biology*. 1998;201:2935-44.

- [2] Lee JB, Sutter KJ, Askew CD, Burkett BJ. Identifying symmetry in running gait using a single inertial sensor. *Journal of Science and Medicine in Sport*. 2010;13:559-63.
- [3] Halvorsen K, Eriksson M, Gullstrand L, Tinmark F, Nilsson J. Minimal marker set for center of mass estimation in running. *Gait & Posture*. 2009;30:552-5.
- [4] Gullstrand L, Halvorsen K, Tinmark F, Eriksson M, Nilsson J. Measurements of vertical displacement in running, a methodological comparison. *Gait & Posture*. 2009;30:71-5.
- [5] Smith L, Preece S, Mason D, Bramah C. A comparison of kinematic algorithms to estimate gait events during overground running. *Gait & Posture*. 2015;41:39-43.
- [6] Franz JR, Paylo KW, Dicharry J, Riley PO, Kerrigan DC. Changes in the coordination of hip and pelvis kinematics with mode of locomotion. *Gait & Posture*. 2009;29:494-8.
- [7] Hamner SR, Seth A, Delp SL. Muscle contributions to propulsion and support during running. *Journal of Biomechanics*. 2010;43:2709-16.
- [8] Cavanagh PR, Kram R. Stride length in distance running: velocity, body dimensions, and added mass effects. *Medicine & Science in Sports & Exercise*. 1989;21:467-79.
- [9] Preece SJ, Mason D, Bramah C. The coordinated movement of the spine and pelvis during running. *Human Movement Science*. 2016;45:110-8.
- [10] Dempster WT. Space requirements of the seated operator: geometrical, kinematic, and mechanical aspects of the body, with special reference to the limbs. Dayton (OH), USA: Wright-Patterson Air Force Base; 1955.
- [11] Fellin RE, Rose WC, Royer TD, Davis IS. Comparison of methods for kinematic identification of footstrike and toe off during overground and treadmill running. *Journal of Science and Medicine in Sport*. 2010;13:646-50.
- [12] Gutierrez-Farewik EM, Bartonek Å, Saraste H. Comparison and evaluation of two common methods to measure center of mass displacement in three dimensions during gait. *Human Movement Science*. 2006;25:238-56.

[13] Meardon SA, Campbell S, Derrick TR. Step width alters iliotibial band strain during running. *Sports Biomechanics*. 2012;11:464-72.

[14] Voloshina AS, Ferris DP. Biomechanics and energetics of running on uneven terrain. *Journal of Experimental Biology*. 2015;218:711-9.

[15] Arellano CJ, Kram R. The effects of step width and arm swing on energetic cost and lateral balance during running. *Journal of Biomechanics*. 2011;44:1291-5.

References

Addison, B. J. and D. E. Lieberman (2015). "Tradeoffs between impact loading rate, vertical impulse and effective mass for walkers and heel strike runners wearing footwear of varying stiffness." Journal of Biomechanics **48**(7): 1318-1324.

Adelaar, R. S. (1986). "The practical biomechanics of running." The American Journal of Sports Medicine **14**(6): 497-500.

Ahn, A. N., C. Brayton, T. Bhatia and P. Martin (2014). "Muscle activity and kinematics of forefoot and rearfoot strike runners." Journal of Sport and Health Science **3**(2): 102-112.

Alexander, R. M. (2003a). "Modelling approaches in biomechanics." Philosophical Transactions of the Royal Society of London Series B-Biological Sciences **358**(1437): 1429-1435.

Almeida, M. O., I. S. Davis and A. D. Lopes (2015). "Biomechanical Differences of Foot-Strike Patterns During Running: A Systematic Review With Meta-analysis." Journal of Orthopedic & Sports Physical Therapy **45**(10): 738-755.

Altman, A. R. and I. S. Davis (2012). "A Kinematic Method for Footstrike Pattern Detection in Barefoot and Shod Runners." Gait & Posture **35**(2): 298-300.

Altman, D. G. and J. M. Bland (1983). "Measurement in medicine: the analysis of method comparison studies." The statistician: 307-317.

Anderson, A. E., B. J. Ellis and J. A. Weiss (2007). "Verification, validation and sensitivity studies in computational biomechanics." Computer Methods in Biomechanics and Biomedical Engineering **10**(3): 171-184.

Arampatzis, A., G. P. Brüggemann and V. Metzler (1999). "The effect of speed on leg stiffness and joint kinetics in human running." Journal of Biomechanics **32**(12): 1349-1353.

Arellano, C. J. and R. Kram (2011). "The effects of step width and arm swing on energetic cost and lateral balance during running." Journal of Biomechanics **44**(7): 1291-1295.

Arellano, C. J. and R. Kram (2014). "Partitioning the Metabolic Cost of Human Running: A Task-by-Task Approach." Integrative and Comparative Biology **54**(6): 1084-1098.

Bland, J. M. and D. G. Altman (1986). "Statistical methods for assessing agreement between two methods of clinical measurement." The Lancet **327**(8476): 307-310.

Blickhan, R. (1989). "The spring-mass model for running and hopping." Journal of Biomechanics **22**(11-12): 1217-1227.

Blum, Y., S. W. Lipfert and A. Seyfarth (2009). "Effective leg stiffness in running." Journal of Biomechanics **42**(14): 2400-2405.

Bret, C., A. Rahmani, A. B. Dufour, L. Messonnier and J. R. Lacour (2002). "Leg strength and stiffness as ability factors in 100m sprint running." Journal of Sports Medicine and Physical Fitness **42**(3): 274-281.

Brughelli, M. and J. Cronin (2008a). "Influence of running velocity on vertical, leg and joint stiffness : modelling and recommendations for future research." Sports Medicine **38**(8): 647-657.

Brughelli, M. and J. Cronin (2008b). "A review of research on the mechanical stiffness in running and jumping: Methodology and implications." Scandinavian Journal of Medicine and Science in Sports **18**(4): 417-426.

Brughelli, M., J. Cronin and A. Chaouachi (2011). "Effects of Running Velocity on Running Kinetics and Kinematics." The Journal of Strength & Conditioning Research **25**(4): 933-939.

Bullimore, S. R. and J. F. Burn (2006). "Consequences of forward translation of the point of force application for the mechanics of running." Journal of Theoretical Biology **238**(1): 211-219.

Bullimore, S. R. and J. F. Burn (2007). "Ability of the planar spring-mass model to predict mechanical parameters in running humans." Journal of Theoretical Biology **248**(4): 686-695.

Butler, R. J., H. P. Crowell iii and I. M. Davis (2003). "Lower extremity stiffness: implications for performance and injury." Clinical Biomechanics **18**(6): 511-517.

Cavagna, G. A., P. Franzetti, N. C. Heglund and P. Willems (1988). "The determinants of the step frequency in running, trotting and hopping in man and other vertebrates." Journal of Physiology **399**: 81-92.

Cavagna, G. A., N. C. Heglund and C. R. Taylor (1977). Mechanical work in terrestrial locomotion: two basic mechanisms for minimizing energy expenditure.

Cavagna, G. A., H. Thys and A. Zamboni (1976). "The sources of external work in level walking and running." Journal of Physiology **262**(3): 639-657.

Cavanagh, P. R. (1990). Biomechanics of Distance Running, Human Kinetics Books.

Cavanagh, P. R. and R. Kram (1989). "Stride length in distance running: velocity, body dimensions, and added mass effects." Medicine & Science in Sports & Exercise **21**(4): 467-479.

Cavanagh, P. R. and M. A. LaFortune (1980). "Ground reaction forces in distance running." Journal of Biomechanics **13**(5): 397-406.

Cenk Güler, H., N. Berme and S. R. Simon (1998). "A viscoelastic sphere model for the representation of plantar soft tissue during simulations." Journal of Biomechanics **31**(9): 847-853.

Clark, K. P. and P. G. Weyand (2014). "Are running speeds maximized with simple-spring stance mechanics?" Journal of Applied Physiology **117**(6): 604-615.

Cole, G. K., B. M. Nigg, A. J. van den Bogert and K. G. M. Gerritsen (1996). "Lower extremity joint loading during impact in running." Clinical Biomechanics **11**(4): 181-193.

Coleman, D. R., D. Cannavan, S. Horne and A. J. Blazeovich (2012). "Leg stiffness in human running: Comparison of estimates derived from previously published models to direct kinematic-kinetic measures." Journal of Biomechanics **45**(11): 1987-1991.

Cook, D. D. and D. J. Robertson (2016). "The generic modeling fallacy: Average biomechanical models often produce non-average results!" Journal of Biomechanics **49**(15): 3609-3615.

-
- D. Gordon E. Robertson, G. E. C., Joseph Hamill, Gary Kamen and S. N. Whittlesey (2013). Research Methods in Biomechanics-2nd Edition, Human Kinetics.
- Daintith, J. and E. A. Martin (2010). A Dictionary of Science, Oxford University Press.
- Dalleau, G., A. Belli, M. Bourdin and J. R. Lacour (1998). "The spring-mass model and the energy cost of treadmill running." European Journal of Applied Physiology and Occupational Physiology **77**(3): 257-263.
- De Wit, B., D. De Clercq and P. Aerts (2000). "Biomechanical analysis of the stance phase during barefoot and shod running." Journal of Biomechanics **33**(3): 269-278.
- Delp, S. L., F. C. Anderson, A. S. Arnold, P. Loan, A. Habib, C. T. John, E. Guendelman and D. G. Thelen (2007). "OpenSim: open-source software to create and analyze dynamic simulations of movement." IEEE Trans Biomed Eng **54**(11): 1940-1950.
- Dempster, W. T. (1955). Space requirements of the seated operator: geometrical, kinematic, and mechanical aspects of the body, with special reference to the limbs. Dayton (OH), USA, Wright-Patterson Air Force Base.
- Derrick, T. R., G. E. Caldwell and J. Hamill (2000). "Modeling the stiffness characteristics of the human body while running with various stride lengths." Journal of Applied Biomechanics **16**(1): 36-51.
- Dicharry, J. (2010). "Kinematics and kinetics of gait: from lab to clinic." Clinics in Sports Medicine **29**(3): 347-364.
- Divert, C., G. Mornieux, H. Baur, F. Mayer and A. Belli (2005). "Mechanical comparison of barefoot and shod running." International Journal of Sports Medicine **26**(7): 593-598.
- Donelan, J. M. and R. Kram (2000). "Exploring dynamic similarity in human running using simulated reduced gravity." Journal of Experimental Biology **203**(16): 2405-2415.

-
- Dorn, T. W., A. G. Schache and M. G. Pandy (2012). "Muscular strategy shift in human running: dependence of running speed on hip and ankle muscle performance." J Exp Biol **215**(Pt 11): 1944-1956.
- Dugan, S. A. and K. P. Bhat (2005). "Biomechanics and analysis of running gait." Physical Medicine & Rehabilitation Clinics of North America **16**(3): 603-621.
- Farley, C. T. and D. P. Ferris (1998). "Biomechanics of walking and running: Center of mass movements to muscle action." Exercise and Sport Sciences Reviews, Volume 28, 1998 **26**: 253-285.
- Farley, C. T., J. Glasheen and T. A. McMahon (1993). "Running springs: speed and animal size." Journal of Experimental Biology **185**(1): 71-86.
- Farley, C. T. and O. Gonzalez (1996). "Leg stiffness and stride frequency in human running." Journal of Biomechanics **29**(2): 181-186.
- Farley, C. T., H. H. P. Houdijk, C. Van Strien and M. Louie (1998). "Mechanism of leg stiffness adjustment for hopping on surfaces of different stiffnesses." Journal of Applied Physiology **85**(3): 1044-1055.
- Farley, C. T. and D. C. Morgenroth (1999). "Leg stiffness primarily depends on ankle stiffness during human hopping." Journal of Biomechanics **32**(3): 267-273.
- Farris, D. J. and B. J. Raiteri (2017). "Modulation of leg joint function to produce emulated acceleration during walking and running in humans." Royal Society Open Science **4**(3).
- Faul, F., E. Erdfelder, A.-G. Lang and A. Buchner (2007). "G*Power 3: A flexible statistical power analysis program for the social, behavioral, and biomedical sciences." Behavior Research Methods **39**(2): 175-191.
- Fellin, R. E., W. C. Rose, T. D. Royer and I. S. Davis (2010). "Comparison of methods for kinematic identification of footstrike and toe-off during overground and treadmill running." Journal of Science and Medicine in Sport **13**(6): 646-650.
- Ferber, R. and S. Macdonald (2014). Running mechanics and gait analysis, Human Kinetics.

Ferris, D. P. and C. T. Farley (1997). "Interaction of leg stiffness and surface stiffness during human hopping." Journal of Applied Physiology **82**(1): 15-22.

Ferris, D. P., M. Louie and C. T. Farley (1998). "Running in the real world: adjusting leg stiffness for different surfaces." Proceedings of the Royal Society of London B: Biological Sciences **265**(1400): 989-994.

Field, A. P. (2009). Discovering Statistics Using SPSS: (and Sex and Drugs and Rock 'n' Roll), SAGE.

Franz, J. R., K. W. Paylo, J. Dicharry, P. O. Riley and D. C. Kerrigan (2009). "Changes in the coordination of hip and pelvis kinematics with mode of locomotion." Gait & Posture **29**(3): 494-498.

Fukuchi, R. K., C. A. Fukuchi and M. Duarte (2017). "A public dataset of running biomechanics and the effects of running speed on lower extremity kinematics and kinetics." PeerJ **5**: e3298.

Gerritsen, K. G. M., A. J. Vandenbogert and B. M. Nigg (1995). "Direct dynamics simulation of the impact phase in heel - toe running." Journal of Biomechanics **28**(6): 661-668.

Gilchrist, L. A. and D. A. Winter (1996). "A two-part, viscoelastic foot model for use in gait simulations." Journal of Biomechanics **29**(6): 795-798.

Gill, N., S. J. Preece, S. Young and C. Bramah (2017). "Are the arms and head required to accurately estimate centre of mass motion during running?" Gait & Posture **51**: 281-283.

Gross, D. L. and M. T. Gross (2013). "A Comparison of Negative Joint Work and Vertical Ground Reaction Force Loading Rates in Chi Runners and Rearfoot-Striking Runners." Journal of Orthopaedic & Sports Physical Therapy **43**(10): 685-692.

Gruber, A. H., W. B. Edwards, J. Hamill, T. R. Derrick and K. A. Boyer (2017). "A comparison of the ground reaction force frequency content during rearfoot and non-rearfoot running patterns." Gait & Posture **56**: 54-59.

Gruber, A. H., B. R. Umberger, B. Braun and J. Hamill (2013). "Economy and rate of carbohydrate oxidation during running with rearfoot and forefoot strike patterns." Journal of Applied Physiology **115**(2): 194-201.

-
- Gullstrand, L., K. Halvorsen, F. Tinmark, M. Eriksson and J. Nilsson (2009). "Measurements of vertical displacement in running, a methodological comparison." Gait & Posture **30**(1): 71-75.
- Günther, M. and R. Blickhan (2002). "Joint stiffness of the ankle and the knee in running." Journal of Biomechanics **35**(11): 1459-1474.
- Gutierrez-Farewik, E. M., Å. Bartonek and H. Saraste (2006). "Comparison and evaluation of two common methods to measure center of mass displacement in three dimensions during gait." Human Movement Science **25**(2): 238-256.
- Halvorsen, K., M. Eriksson, L. Gullstrand, F. Tinmark and J. Nilsson (2009). "Minimal marker set for center of mass estimation in running." Gait & Posture **30**(4): 552-555.
- Hamill, J., A. H. Gruber and T. R. Derrick (2014). "Lower extremity joint stiffness characteristics during running with different footfall patterns." European Journal of Sport Science **14**(2): 130-136.
- Hamner, S. R., A. Seth and S. L. Delp (2010). "Muscle contributions to propulsion and support during running." Journal of Biomechanics **43**(14): 2709-2716.
- Hamner, S. R., A. Seth, K. M. Steele and S. L. Delp (2013). "A rolling constraint reproduces ground reaction forces and moments in dynamic simulations of walking, running, and crouch gait." Journal of Biomechanics **46**(10): 1772-1776.
- He, J. P., R. Kram and T. A. McMahon (1991). "Mechanics of running under simulated low gravity." Journal of Applied Physiology **71**(3): 863-870.
- Henninger, H. B., S. P. Reese, A. E. Anderson and J. A. Weiss (2010). "Validation of computational models in biomechanics." Proceedings of the Institution of Mechanical Engineers Part H-Journal of Engineering in Medicine **224**(H7): 801-812.
- Hertz, H. (1881). "On the contact of elastic solids." Journal für die reine und angewandte Mathematik **92**(110): 156-171.
- Hicks, J. L., T. K. Uchida, A. Seth, A. Rajagopal and S. L. Delp (2015). "Is My Model Good Enough? Best Practices for Verification and Validation of

-
- Musculoskeletal Models and Simulations of Movement." Journal of Biomechanical Engineering **137**(2): 020905-020905.
- Hill, A. V. (1938). The Heat of Shortening and the Dynamic Constants of Muscle.
- Hobara, H., K. Inoue, K. Gomi, M. Sakamoto, T. Muraoka, S. Iso and K. Kanosue (2010). "Continuous change in spring-mass characteristics during a 400 m sprint." Journal of Science and Medicine in Sport **13**(2): 256-261.
- Holmes, P., R. J. Full, D. Koditschek and J. Guckenheimer (2006). "The dynamics of legged locomotion: Models, analyses, and challenges." Siam Review **48**(2): 207-304.
- Hunter, I. (2003). "A new approach to modeling vertical stiffness in heel-toe distance runners." Journal of Sports Science & Medicine **2**(4): 139-143.
- Iida, F., J. Rummel and A. Seyfarth (2008). "Bipedal walking and running with spring-like biarticular muscles." Journal of Biomechanics **41**(3): 656-667.
- Jackson, J. N., C. J. Hass and B. J. Fregly (2016). "Development of a Subject-Specific Foot-Ground Contact Model for Walking." Journal of Biomechanical Engineering **138**(9): 091002-091002-091012.
- Jenkins, D. W. and D. J. Cauthon (2011). "Barefoot Running Claims and Controversies." Journal of the American Podiatric Medical Association **101**(3): 231-246.
- Jones, A. M. and J. H. Doust (1996). "A 1% treadmill grade most accurately reflects the energetic cost of outdoor running." Journal of Sports Sciences **14**(4): 321-327.
- Kehler, A. L., E. Hajkova, H. C. Holmberg and R. Kram (2014). "Forces and mechanical energy fluctuations during diagonal stride roller skiing; running on wheels?" Journal of Experimental Biology **217**(21): 3779-3785.
- Kerdok, A. E., A. A. Biewener, T. A. McMahon, P. G. Weyand and H. M. Herr (2002). "Energetics and mechanics of human running on surfaces of different stiffnesses." Journal of Applied Physiology **92**(2): 469-478.
- Kim, W., A. S. Voloshin and S. H. Johnson (1994). "Modeling of heel strike transients during running." Human Movement Science **13**(2): 221-244.

Kubo, K., H. Kanehisa and T. Fukunaga (2005). "Effects of viscoelastic properties of tendon structures on stretch-shortening cycle exercise in vivo." Journal of Sports Sciences **23**(8): 851-860.

Kubo, K., T. Tabata, T. Ikebukuro, K. Igarashi and N. Tsunoda (2010). "A longitudinal assessment of running economy and tendon properties in long-distance runners." Journal of Strength & Conditioning Research **24**(7): 1724-1731.

Kuhman, D., D. A. Melcher and M. R. Paquette (2016). "Ankle and knee kinetics between strike patterns at common training speeds in competitive male runners." European Journal of Sport Science **16**(4): 433-440.

Kuitunen, S., P. V. Komi and H. Kyröläinen (2002). "Knee and ankle joint stiffness in sprint running." Medicine & Science in Sports & Exercise **34**(1): 166-173.

Kulmala, J. P., J. Avela, K. Pasanen and J. Parkkari (2013). "Forefoot strikers exhibit lower running-induced knee loading than rearfoot strikers." Medicine & Science in Sports & Exercise **45**(12): 2306-2313.

Kulmala, J. P., M. T. Korhonen, L. Ruggiero, S. Kuitunen, H. Suominen, A. Heinonen, A. Mikkola and J. Avela (2016). "Walking and Running Require Greater Effort from Ankle than Knee Extensor Muscles." Medicine & Science in Sports & Exercise **48**(11): 2181-2189.

Kyröläinen, H., A. Belli and P. V. Komi (2001). "Biomechanical factors affecting running economy." Medicine & Science in Sports & Exercise **33**(8): 1330-1337.

Lacour, J. R. and M. Bourdin (2015). "Factors affecting the energy cost of level running at submaximal speed." European Journal of Applied Physiology **115**(4): 651-673.

Lee, C. R. and C. T. Farley (1998). "Determinants of the center of mass trajectory in human walking and running." Journal of Experimental Biology **201**(21): 2935-2944.

Lee, J. B., K. J. Sutter, C. D. Askew and B. J. Burkett (2010). "Identifying symmetry in running gait using a single inertial sensor." Journal of Science and Medicine in Sport **13**(5): 559-563.

-
- Lieberman, D. E., M. Venkadesan, W. A. Werbel, A. I. Daoud, S. D'Andrea, I. S. Davis, R. O. Mang'Eni and Y. Pitsiladis (2010). "Foot strike patterns and collision forces in habitually barefoot versus shod runners." Nature **463**(7280): 531-535.
- Lipfert, S. W., M. Gunther, D. Renjewski, S. Grimmer and A. Seyfarth (2012). "A model-experiment comparison of system dynamics for human walking and running." Journal of Theoretical Biology **292**: 11-17.
- Liu, W. and B. M. Nigg (2000). "A mechanical model to determine the influence of masses and mass distribution on the impact force during running." Journal of Biomechanics **33**(2): 219-224.
- Lopes, A. D., L. C. Hespanhol, S. S. Yeung and L. O. P. Costa (2012). "What are the Main Running-Related Musculoskeletal Injuries?" Sports Medicine **42**(10): 891-905.
- Lund, M. E., M. de Zee, M. S. Andersen and J. Rasmussen (2012). "On validation of multibody musculoskeletal models." Proceedings of the Institution of Mechanical Engineers Part H-Journal of Engineering in Medicine **226**(H2): 82-94.
- Ly, Q. H., A. Alaoui, S. Erlicher and L. Baly (2010). "Towards a footwear design tool: Influence of shoe midsole properties and ground stiffness on the impact force during running." Journal of Biomechanics **43**(2): 310-317.
- Lyght, M., M. Nockerts, T. W. Kernozek and R. Ragan (2016). "Effects of Foot Strike and Step Frequency on Achilles Tendon Stress During Running." Journal of Applied Biomechanics **32**(4): 365-372.
- Mason, D. L., S. J. Preece, C. A. Bramah and L. C. Herrington (2014). "Reproducibility of kinematic measures of the thoracic spine, lumbar spine and pelvis during fast running." Gait & Posture(0).
- Mayhew, J. L. (1977). "Oxygen cost and energy expenditure of running in trained runners." British Journal of Sports Medicine **11**(3): 116-121.
- Maykranz, D., S. Grimmer, S. W. Lipfert and A. Seyfarth (2009). Foot function in spring mass running. Autonome Mobile Systeme 2009, Springer: 81-88.

-
- McGeer, T. (1990). "Passive bipedal running." Proceedings of the Royal Society B-Biological Sciences **240**(1297): 107-134.
- McGrath, M., D. Howard and R. Baker (2015). "The strengths and weaknesses of inverted pendulum models of human walking." Gait & Posture **41**(2): 389-394.
- McMahon, T. A. and G. C. Cheng (1990). "The mechanics of running: How does stiffness couple with speed?" Journal of Biomechanics **23, Supplement 1**(0): 65-78.
- McMahon, T. A., G. Valiant and E. C. Frederick (1987). "Groucho running." Journal of Applied Physiology **62**(6): 2326-2337.
- Meardon, S. A., S. Campbell and T. R. Derrick (2012). "Step width alters iliotibial band strain during running." Sports Biomechanics **11**(4): 464-472.
- Miller, R. H. and J. Hamill (2015). "Optimal footfall patterns for cost minimization in running." Journal of Biomechanics **48**(11): 2858-2864.
- Morin, J. B., G. Dalleau, T. Jeannin and A. Belli (2005). "A simple method for measuring stiffness during running." Journal of Applied Biomechanics **21**(2): 167-180.
- Morin, J. B., P. Samozino, K. Zameziati and A. Belli (2007). "Effects of altered stride frequency and contact time on leg-spring behavior in human running." Journal of Biomechanics **40**(15): 3341-3348.
- Müller, R., A. V. Birn-Jeffery and Y. Blum (2016). "Human and avian running on uneven ground: a model-based comparison." Journal of The Royal Society Interface **13**(122).
- Naemi, R. and N. Chockalingam (2013). "Mathematical Models to Assess Foot-Ground Interaction: An Overview." Medicine & Science in Sports & Exercise **45**(8): 1524-1533.
- Neptune, R. R., S. A. Kautz and F. E. Zajac (2000). "Muscle contributions to specific biomechanical functions do not change in forward versus backward pedaling." Journal of Biomechanics **33**(2): 155-164.
- Nicola, T. L. and D. J. Jewison (2012). "The anatomy and biomechanics of running." Clinics in Sports Medicine **31**(2): 187-+.

- Nigg, B. M. and W. Liu (1999). "The effect of muscle stiffness and damping on simulated impact force peaks during running." Journal of Biomechanics **32**(8): 849-856.
- Nikooyan, A. A. and A. A. Zadpoor (2011). "Mass-spring-damper modelling of the human body to study running and hopping--an overview." Proceedings of the Institution of Mechanical Engineers Part H-Journal of Engineering in Medicine **225**(12): 1121-1135.
- Nordin, M. and V. H. Frankel (2001). Basic Biomechanics of the Musculoskeletal System, Lippincott Williams & Wilkins.
- Novacheck, T. F. (1998). "The biomechanics of running." Gait & Posture **7**(1): 77-95.
- NPD-Group. (2015). "NPD Sports Consumer Panel." from <https://www.npdgroup.co.uk/wps/portal/npd/uk/home/>.
- Ogueta-Alday, A., J. A. Rodriguez-Marroyo and J. Garcia-Lopez (2014). "Rearfoot Striking Runners Are More Economical Than Midfoot Strikers." Medicine & Science in Sports & Exercise **46**(3): 580-585.
- OpenSim. (2007). "How Forward Dynamics Works." 2017, from <http://simtk-confluence.stanford.edu:8080/display/OpenSim/How+Forward+Dynamics+Works>.
- OpenSim. (2012). "From the Group Up: Building a Passive Dynamic Walker Model." 2016, from <https://simtk-confluence.stanford.edu:8443/display/OpenSim/From+the+Ground+Up%3A+Building+a+Passive+Dynamic+Walker+Model>.
- Ounpuu, S. (1994). "The biomechanics of walking and running." Clinics in Sports Medicine **13**(4): 843-863.
- Pandy, M. G. (2001). "Computer modeling and simulation of human movement." Annual Review of Biomedical Engineering **3**(1): 245.
- Pandy, M. G., F. E. Zajac, E. Sim and W. S. Levine (1990). "An optimal control model for maximum-height human jumping." Journal of Biomechanics **23**(12): 1185-1198.

-
- Panjabi, M. (1979). "Validation of mathematical models." Journal of Biomechanics **12**(3): 238.
- Parker, S. P. (2003). McGraw-Hill Dictionary of Scientific and Technical Terms, McGraw-Hill Education.
- Pearson, S. J. and J. McMahon (2012). "Lower limb mechanical properties: determining factors and implications for performance." Sports Medicine **42**(11): 929-940.
- Perl, D. P., A. I. Daoud and D. E. Lieberman (2012). "Effects of Footwear and Strike Type on Running Economy." Medicine & Science in Sports & Exercise **44**(7): 1335-1343.
- Peter, S., S. Grimmer, S. W. Lipfert and A. Seyfarth (2009). Variable joint elasticities in running. Informatik aktuell.
- Pfeifer, S., H. Vallery, M. Hardegger, R. Riener and E. J. Perreault (2012). "Model-based estimation of knee stiffness." IEEE Transactions on Biomedical Engineering **59**(9): 2604-2612.
- Phan, L. T., Y. H. Lee, D. Y. Kim, H. J. Lee and H. R. Choi (2017). "Stable running with a two-segment compliant leg." Intelligent Service Robotics: 1-12.
- Preece, S. J., C. Bramah and D. Mason (2016). "A marker set for measuring the kinematics of the lumbar spine and thoracic spine during running: a technical note." Journal of Human Sport and Exercise **11**(3): 390-396.
- Preece, S. J., D. Mason and C. Bramah (2016). "The coordinated movement of the spine and pelvis during running." Human Movement Science **45**: 110-118.
- Pritsker, A. A. B. (1979). "Compilation of definitions of simulation." Simulation **33**(2): 61-63.
- Qiao, M., J. J. Abbas and D. L. Jindrich (2017). "A model for differential leg joint function during human running." Bioinspiration & Biomimetics **12**(1): 1-17.
- Raabe, M. E. and A. M. W. Chaudhari (2016). "An investigation of jogging biomechanics using the full-body lumbar spine model: Model development and validation." Journal of Biomechanics **49**(7): 1238-1243.

-
- Robilliard, J. J. and A. M. Wilson (2005). "Prediction of kinetics and kinematics of running animals using an analytical approximation to the planar spring-mass system." Journal of Experimental Biology **208**(Pt 23): 4377-4389.
- Rummel, J. and A. Seyfarth (2008). "Stable Running with Segmented Legs." International Journal of Robotics Research **27**(8): 919-934.
- Saunders, P. U., D. B. Pyne, R. D. Telford and J. A. Hawley (2004a). "Factors affecting running economy in trained distance runners." Sports Medicine **34**(7): 465-485.
- Scholz, M. N., M. F. Bobbert, A. J. van Soest, J. R. Clark and J. van Heerden (2008). "Running biomechanics: shorter heels, better economy." Journal of Experimental Biology **211**(20): 3266-3271.
- Serpell, B. G., N. B. Ball, J. M. Scarvell and P. N. Smith (2012). "A review of models of vertical, leg, and knee stiffness in adults for running, jumping or hopping tasks." Journal of Sports Sciences **30**(13): 1347-1363.
- Seth, A., M. Sherman, P. Eastman and S. Delp (2010). "Minimal formulation of joint motion for biomechanisms." Nonlinear Dynamics **62**(1): 291-303.
- Seth, A., M. A. Sherman, J. A. Reinbolt and S. L. Delp (2011). "OpenSim: a musculoskeletal modeling and simulation framework for in silico investigations and exchange." Procedia IUTAM **2**: 212-232.
- Seyfarth, A., H. Geyer, R. Blickhan, S. Lipfert, J. Rummel, Y. Minekawa and F. Iida (2006). Running and Walking with Compliant Legs. Fast Motions in Biomechanics and Robotics: Optimization and Feedback Control. M. Diehl and K. Mombaur. Berlin, Heidelberg, Springer Berlin Heidelberg: 383-401.
- Seyfarth, A., H. Geyer, M. Gunther and R. Blickhan (2002). "A movement criterion for running." Journal of Biomechanics **35**(5): 649-655.
- Seyfarth, A., M. Günther and R. Blickhan (2001). "Stable operation of an elastic three-segment leg." Biological Cybernetics **84**(5): 365-382.
- Shaw, A. J., S. A. Ingham and J. P. Folland (2014). "The valid measurement of running economy in runners." Medicine & Science in Sports & Exercise **46**(10): 1968-1973.

- Shen, Z. and J. Seipel (2015a). "Animals prefer leg stiffness values that may reduce the energetic cost of locomotion." Journal of Theoretical Biology **364**: 433-438.
- Shen, Z. and J. Seipel (2015b). "The leg stiffnesses animals use may improve the stability of locomotion." Journal of Theoretical Biology **377**: 66-74.
- Sherman, M. A., A. Seth and S. L. Delp (2011). "Simbody: multibody dynamics for biomedical research." Procedia IUTAM **2**(0): 241-261.
- Silder, A., T. Besier and S. L. Delp (2015). "Running with a load increases leg stiffness." Journal of Biomechanics(0).
- Sinclair, J., S. Atkins and P. J. Taylor (2016). "The Effects of Barefoot and Shod Running on Limb and Joint Stiffness Characteristics in Recreational Runners." Journal of Motor Behavior **48**(1): 79-85.
- Smith, L., S. Preece, D. Mason and C. Bramah (2015). "A comparison of kinematic algorithms to estimate gait events during overground running." Gait & Posture **41**(1): 39-43.
- SMS-INC. (2014b). "International Running Participation Report 2014." from <http://www.sportmarketingsurveysinc.com/>.
- SMS-INC. (2016). "Core Runners." from <http://www.sportmarketingsurveysinc.com/>.
- Sport-England. (2015). "Sport England's Active People Survey." 2016, from <https://www.sportengland.org/research/who-plays-sport/national-picture/>.
- Sport-England. (2016). "Active Lives Survey." 2017, from <https://www.sportengland.org/media/11498/active-lives-survey-yr-1-report.pdf>.
- Sport-Wales. (2016). "Active Adult Survey 2014: State of the Nation Report." 2016, from http://sport.wales/media/1685965/state_of_the_nation_-_active_adults_survey_2014.pdf.
- Sports-Insight. (2014). "55 % of Runners do at Least a Third of Their Running Outdoors." 2016, from <http://www.sports-insight.co.uk/market-analysis/55-of-runners-do-at-least-a-third-of-their-running-outdoors-on-the-roads-wh>.

-
- Sports-Insight. (2015). "The running shoe market has enjoyed significant increases in sales in recent years." 2016, from <http://www.sports-insight.co.uk/market-analysis/the-running-shoe-market-has-enjoyed-significant-increases-in-sales-in-recen>.
- Sports-Insight. (2016a). "Running Habits - Reasons for Running." 2016, from <http://www.sports-insight.co.uk/market-analysis/running-habits-reasons-for-running>.
- Sports-Insight. (2016b). "Road running is the most popular form of the sport." 2016, from <http://www.sports-insight.co.uk/market-analysis/road-running-is-the-most-popular-form-of-the-sport-with-96>.
- Sprigings, E. J. and D. I. Miller (2004). "Optimal knee in springboard extension timing and platform dives from the reverse group." Journal of Applied Biomechanics **20**(3): 275-290.
- Svedenhag, J. and B. Sjodin (1984). "Maximal and submaximal oxygen uptakes and blood lactate levels in elite male middle-and long-distance runners." International Journal of Sports Medicine **5**(5): 255-261.
- Svedenhag, J. and B. Sjodin (1994). "Body-mass-modified running economy and step length in elite male middle- and long-distance runners." International Journal of Sports Medicine **15**(6): 305-310.
- Thompson, M. A., S. S. Lee, J. Seegmiller and C. P. McGowan (2015). "Kinematic and kinetic comparison of barefoot and shod running in mid/forefoot and rearfoot strike runners." Gait & Posture **41**(4): 957-959.
- Uchida, T. K., M. A. Sherman and S. L. Delp (2015). "Making a meaningful impact: modelling simultaneous frictional collisions in spatial multibody systems." Proceedings of the Royal Society of London A: Mathematical, Physical and Engineering Sciences **471**(2177).
- van Gent, R. N., D. Siem, M. van Middelkoop, A. G. van Os, S. M. Bierma-Zeinstra and B. W. Koes (2007). "Incidence and determinants of lower extremity running injuries in long distance runners: a systematic review." British Journal of Sports Medicine **41**(8): 469-480; discussion 480.
- Voloshina, A. S. and D. P. Ferris (2015). "Biomechanics and energetics of running on uneven terrain." Journal of Experimental Biology **218**(5): 711-719.

- Watkins, J. (2014). Fundamental Biomechanics of Sport and Exercise, Routledge.
- Williams, D. S. B., D. H. Green and B. Wurzinger (2012). "Changes in Lower Extremity Movement and Power Absorption During Forefoot Striking and Barefoot Running." International Journal of Sports Physical Therapy **7**(5): 525-532.
- Williams, K. R. (1985). "Biomechanics of Running." Exercise and Sport Sciences Reviews **13**(1): 389-442.
- Williams, K. R. and P. R. Cavanagh (1987). "Relationship between distance running mechanics, running economy and performance." J Appl Physiol **63**(3): 1236-1245.
- Williams, K. R. and P. R. Cavanagh (1987). "Relationship between distance running mechanics, running economy, and performance." Journal of Applied Physiology **63**(3): 1236-1245.
- Yeadon, M. R. and M. A. King (2007). Computer simulation modelling in sport. Biomechanical Evaluation of Movement in Sport and Exercise: 176.
- Young, H. D., R. A. Freedman and A. L. Ford (2008). Sears and Zemansky's University Physics, Addison-Wesley.
- Zadpoor, A. A. and A. A. Nikooyan (2006). "A mechanical model to determine the influence of masses and mass distribution on the impact force during running - A discussion." Journal of Biomechanics **39**(2): 388-389.
- Zadpoor, A. A. and A. A. Nikooyan (2010). "Modeling muscle activity to study the effects of footwear on the impact forces and vibrations of the human body during running." Journal of Biomechanics **43**(2): 186-193.
- Zadpoor, A. A., A. A. Nikooyan and A. R. Arshi (2007). "A model-based parametric study of impact force during running." Journal of Biomechanics **40**(9): 2012-2021.